Material and Construction Influences on Football Impact Behaviour

by Henry Hanson

A doctoral thesis submitted in partial fulfilment of the requirements for the award of Doctor of Philosophy of Loughborough University

November 2014

© by Henry Hanson 2014

Acknowledgements

To

my friends and family for supporting my decision to move abroad and encouragement throughout,

my fellow researchers for creating a fun and intellectually stimulating environment,

my advisors Andy Harland, Dan Price, Chris Holmes and Tim Lucas for their perspective and expertise

Katherine Boden, Steve Carr, Max Farrand, and Andrew Hallam for making the office and labs efficient and productive places to work.

Thank you!

Contents

Abstract 5
1 Introduction 1
1.1 Development of Game 1
1.2 Football Development and Requirements 3
1.2.1 Football Regulations 4
1.2.2 Football Loading Conditions 5
1.2.3 Current Constructions, Materials, and Manufacturing Methods 5
1.2.4 Recent developments 8
1.3 Research Aims and Objectives 8
2 Literature Review 10
2.1 Football Impact Behaviour 10
2.1.1 Coefficient of Restitution 11
2.1.2 Contact Time and Contact Force 12
2.1.3 Deformation 14
2.2 Materials 15
2.2.1 Material Properties of Interest 15
2.2.2 Material Characterisation for FEA 17
2.2.3 Material Testing for FEA 17
2.3 Football Simulation 20
2.3.1 Aerodynamics 20
2.3.2 Structural Simulation 21
2.3.3 D.O.E. 23
2.4 Ball Impact Acoustics 24
2.5 Summary 26
3 Materials Characterisation for Footballs 28
3.1 Intentions 28
3.2 Basic Test Protocol 28
3.3 Variations in Test Protocol 32
3.3.1 Representative Strain Rate vs. Representative Strain Magnitude 32
3.3.2 Fabric Characterisation 35
3.3.3 Materials Before and After Processing 41
3.3.4 Testing Composite Sections 45
3.4 Temperature-Dependency 47
3.5 Summary 49
4 Finite Element Analysis Models 51
4.1 Intentions 51

4.2 Basic Model 51
4.2.1 Mesh Refinement 53
4.3 Desired Outputs 56
4.4 Surface Deformation Modelling 57
4.5 Simulating Spatial Variation of Internal Pressure 59
4.6 Parametric Model Creation 65
4.7 Boundary Conditions 66
4.8 Validation 67
4.9 Summary 70
5 Impact Behaviour 71
5.1 Intentions 71
5.2 Validation 71
5.2.1 High-Speed Impact Validation Lab Methods 72
5.2.2 High-Speed Video Processing Methods 74
5.2.3 High-Speed Impact Validation Challenges 75
5.2.4 Drop Test Validation Methods 75
5.2.5 Deformation at 0° and 45° Impact Orientations 77
5.3 Patch Carcass Deformation and Rebound Deviation 79
5.4 Impact Size vs. Anisotropic Element Size 82
5.5 Outer Panel Local Deformation 88
5.6 Patch Carcass Case Studies 91
5.6.1 Modified Patch Carcass 91
5.6.2 Novel Carcass Concepts 96
5.6.3 Picasso 102
5.6.4 Tucasa 104
5.6.5 Triakis 105
5.7 Partial Net Carcass Prototype Comparisons 106
5.8 Summary 109
6 Design of Experiments and Optimisation 110
6.1 Intentions 110
6.2 Simple Yarn Orientation Study 111
6.3 DOE: Relative Panel Contribution 114
6.4 DOE: Relative Component Contribution 117
6.5 DOE: Fabric Yarn Offset Angle 121
6.6 Summary 122
7 Acoustics 124
7.1 Intentions 124
7.2 Physical Acoustic Testing 124

7.2.1 Methods 124
7.2.2 Bar Strike Testing 126
7.2.3 Two-Metre Drop Testing 131
7.3 Acoustic Response Modification 136
7.4 Acoustic Simulation 140
7.4.1 Acoustic Model Setup 140
7.4.2 Acoustic Simulation Results 142
7.5 Internal Acoustic Pressure 146
7.6 Summary 150
8 Summary 152
8.1 Materials Testing and Characterisation 152
8.2 FEA Model Development 152
8.3 Impact Behaviour 153
8.4 Design of Experiments and Optimisation 153
8.5 Acoustics 153
8.6 Recommendations for Future Work 154
8.6.1 Materials and Characterisation 154
8.6.2 Model Creation 154
8.6.3 DOE and Optimisation 155
8.6.4 Acoustics 155
9 Appendices 156
9.1 Pentagon Strain 156
9.2 Supplemental Model Definition Data 159
9.2.1 Fluid Material Input Data 159
9.2.2 Solid Material Input Data 159
9.3 Notational Analysis 164
9.4 Notational Analysis Data 170
9.5 Aerodynamic Data 172
9.6 Alternate Acoustic Excitation Methods 173
9.7 Acoustic Data 174
10 Works Cited 176

Abstract

The purpose of this work was to understand the influence of materials and construction on football performance. Two main areas identified as needing further work were post-impact rebound deviation and acoustic response.

To further investigate these areas, football materials were tested in a lab with different loading scenarios and the resulting data was used in various characterisation methods to help define finite element models. The finite element models were used to efficiently explore a variety of material and construction variations. Acoustic data for a range of balls was collected in an anechoic chamber and advanced coupled Eulerian-Lagrangian simulations were developed to visualise the mode shapes of internal resonances.

In addition to supplying the finite element models with information, the material testing also revealed strong temperature dependence with all of the football materials, extreme anisotropy in the carcass fabric, and a substantial difference in football materials before and after processing and assembly. Lab testing of football carcasses supported the results obtained from a series of simulations investigating the effect of fabric anisotropy and football inhomogeneity on rebound deviation. Off-centre forces induced by asymmetric deformation were observed to cause a rotation during the contact phase that resulted in an angled rebound trajectory.

As a way to check theories and apply knowledge from the observations of carcass labwork and simulation, novel carcass concepts were created and tested. Each carcass prototype showed a smaller average rebound deviation than the current football carcass in simulations.

Acoustic testing highlighted a relationship between ball characteristics and post-impact ring qualities. Greater mass and a smoother internal surface contributed to a longer ring and a greater diameter ball produced a lower frequency. The energy at different frequencies was visualised with an advanced coupled Eulerian-Lagrangian simulation.

1 Introduction

Football, 'The Beautiful Game', is the most popular game in the world (Maguire et al. 1996). It is a combination of endurance athleticism and careful strategy accented with explosive bouts of speed and agility. The game transcends cultural borders and has the power to unite and divide peoples. The large industry surrounding the sport at professional and recreational levels provides an increasingly discerning market for high quality products. Commercial advancements stem from fundamental investigations into the scientific phenomena present in the sport. This first chapter provides large-scale context for the following technical chapters, describing both the game and the football.

1.1 Development of Game

The game of football known today has been officially recognised since 1864 but simple ball games can be seen throughout history. The Chinese province Shan Xi had a stone ball game in the Neolithic age and the South American indigenous tribes in the Amazon had ball games documented in 1500BC. Romans and Greeks had ball games called *harpastum* and *episcyros*, respectively, and Native American peoples played *pasuckquakkohowog* with a ball. As history went forward and more events were recorded, specific ball games popped up in Chile (*pilimatun*), Patagonia (*tchoekah*), and with Celtic peoples in the British Isles (*Cad*) (Giulianotti 1999).

The games were often part of ceremonies and celebrations but they were also past times for warriors looking to stay fit with friendly competition (Murray 1994). The game was a leisure activity - something popular that people did for fun and exercise. The popularity of ball games (and their tendency to replace more productive, mundane tasks) led to abolishment in several civilisations. The Ming Dynasty banned their ball game in 1389 and Edward II banned the games in England to keep his archers on task and prevent avoidable injuries (Orejan 2011).

The independent development of such ball games indicates fundamental human tendencies toward a certain type of competition. *The Soccer Tribe* by Desmond Morris (Morris 1981) depicts modern-day football as an explorer would characterise a newly discovered tribe. The parallels that can be drawn between early civilizations and modern football point to aspects of the game that fulfil human needs. The sense of a community gathering together to accomplish a common 'goal', an outlet for aggression, adherence to abstract rules akin to morality, and the creation of heroes in the community are good examples of societal building blocks provided by the sport.

The popularity of ball sports in cultures around the globe may have prepared the indigenous people for the assimilation of football as introduced by European explorers. Without the European values that were rejected in other inter-cultural interactions, football provided a common ground with the locals by means of focus on the general appeal of competitive ball sport (Giulianotti 1999). The development of football in England was the most significant not only because of England's international presence but also the high degree to which the game was developed.

Before national rules were established in England, football games served to unite and define towns and regions. Factory and community clubs battled neighbouring teams, creating a feel of solidarity among the constituents and good-hearted competition with the neighbours. In these days (around the 18th century), the rules were established pre-match between involved parties and there was no central governing body. Common to these variations was the goal: to get the ball to a specific place, generally by any means necessary (Wilson 2008). The means used were barbaric by today's standards, resulting in severe injuries or even death. It was, of course, a step or two apart from actual battle and for practicality's sake, the game continued to develop into a more tame and organized affair.

The game was eventually brought into the universities and achieved "sport" status, at which point universities started establishing rules (Wilson 2008). Some universities continued to allow handling the ball, others did not. In 1814, Harrovians from Harrow were the first to play with 11 on each side and minimal handling. They took their version of the game to Cambridge and another similar set of rules was created there in 1848 (Murray 1994). Schools, universities and clubs still had their own rules so in 1863, representatives from regions with slightly different rules gathered to create one national set (Association 2010). This was the start of the English Football Association (The FA) and allowed for consistent national play. In 1863, the laws of "Association Football" were codified, marking the start of modern-day, hands-free football.

The word "soccer" is said to be an evolution from "Association Football", once abbreviated *assoc.* In keeping with the modern vernacular of the country that first established the Laws the Game, the author will use *football* to refer to the game and the ball.

Toward the end of the 19th century, several modifications were made to the initial laws of the game. The Internal Football Association Board (IFAB) was created in 1886 essentially to care for the game, assuring that any changes were in the best interests of the players and fans. Initial modifications included corner kicks, penalty shots, and regulations involving officials and referees. More recently, the IFAB declared automatic goal-sensing technology to be not in the best interest of the sport.

Current FIFA Secretary General Jerome Valcke describes the present-day IFAB as the "…guardian of the Laws of the Game: that's its power." (TheFA.com 2010). FIFA, the Fédération Internationale de Football Association was established at the turn of the 20th century in France. FIFA joined IFAB in 1913 and the two are currently jointly responsible for maintaining or changing rules as necessary. The declaration against goal line technology has since been reversed and there are several approved companies with a variety of solutions falling into two groups – high speed video, or ball-borne circuitry and goal-mounted sensors (Cairos_Technologies 2013).

Football has since become the most popular sport in the world with an estimated 265 million people playing (FIFA 2006). Only 113,000 of those are professional players but the audiences drawn to the FIFA World Cup, the pinnacle of professional competition, are greater than audiences for any other sporting event. In high schools and colleges in the United States of America, there are nearly 800,000 registered players, a figure that has doubled in the last 20 years (FIFA 2006). The involvement provides the market for a large industry. In the USA alone, 4.6 million footballs were sold ($79.5m) (NSGA 2012). Though the majority are inexpensive balls for a 'kick-about' in a park, major sports brands around the world often consider their elite-level football to be a flagship product, an expression of brand identity and quality. It is one of the most engineered and researched pieces of consumer sports equipment, fusing practical testing and development with research on the underlying principles at play.

1.2 Football Development and Requirements

Since its official creation as a single game at the end of the 19th century, the game, the rules, and the ball have co-evolved to form what we know today. To gain perspective, consider the extremes: in 1863, the ball was neither remarkably round nor consistent in any manner, making long passes or far-out goal shots quite a gamble. When wet, the ball would be too heavy to kick far anyway and in addition, the offside law essentially forbid forward attacking passes. Early cork-filled spheroids (Cox et al. 2002) and inflated animal bladders (Wesson 2002) limited kicking power and accuracy because of inertia in the former and frailty in the latter case. Charles Goodyear's vulcanisation of rubber in the middle of the 19th century enabled the creation of a football that was more uniform, spherical, and durable. The uniformity removed some of the chance of an odd bounce and shifted the emphasis further toward player skill and increased durability allowed for more powerful kicks. Though the ball itself could be more consistent, this advancement did little for the consistency of the game. In 2010, the ball was remarkably round and designed specifically for aerodynamic stability on long shots. Water retention was not an issue and the offside law was significantly more relaxed.

Though both 1863 and 2010 matches fit under the same *Laws of the Game,* the actual play, strategy, and flow are completely different.

1.2.1 Football Regulations

In 1863, *The Laws of the Game* were created to establish a universal game for the purpose of fair competition between regions. Recognising the importance of a consistent ball, Law 2 (FIFA 2009) was created specifically to deal with the ball and its management. Law 2 consists of only five lines relating to the intrinsic properties of the ball: it must be a sphere of leather or "other suitable material" and it must be within established ranges for circumference, weight, and internal pressure. Despite these regulations, footballs still varied significantly.

As mentioned at the start of this section, the increased weight of leather outer panels in the presence of moisture can have drastic effects on the play of the ball but there were also safety concerns. English footballer Jeff Astle (1942-2002), for example, was known for his powerful headers with leather footballs and after he retired from active duty, it was determined that the frequent and hard impacts had damaged his brain beyond repair (Harris 2004).

Later advances in materials and construction have significantly reduced such moisture problems but there was still a need to improve match ball quality. The 133 years following the creation of *the Laws* saw modifications in many areas but Law 2 remained completely unchanged until 1996. In an annual meeting, the IFAB approved a FIFA-proposed amendment to Law 2 (FIFA 1996). "Decision 4", as it is called, requires that official matches be played with a ball that is both sanctioned by FIFA *and* meets Law 2's requirements.

There are two levels of official FIFA qualification: *FIFA Inspected* and the more prestigious *FIFA Approve* (Figure 1). The *FIFA Inspected* standards mirror those provided in the *Laws of the Game* but include additional criteria covering the ball's deviation from an ideal sphere, water absorbency, internal pressure retention, and rebound. The *FIFA Approved* balls must meet tighter tolerances on the previous criteria and pass a shape and size retention test, which involves inspecting the dimensions after two-thousand impacts.

Figure 1: FIFA Qualification Seals

The need for a limit on water retention has already been made apparent but air pressure retention is also an important factor that could potentially influence a match. The pressure of a football contributes greatly to the overall performance (Udeshi 2010) so ensuring consistent pressurisation is a logical and necessary step toward consistent play.

The rebound test was added to address dynamic properties of the ball. From a two-meter drop onto a steel (rigid) plate, *FIFA Approved* balls must bounce back between 135 and 155cm (*FIFA Inspected* 125-155cm) at 5°C and 20°C . In the world of science (and this report), a ball's bouncing characteristic is called the coefficient of restitution (COR) and is expressed as a ratio of inbound and outbound ball velocities.

1.2.2 Football Loading Conditions

A football experiences thousands of impacts in a single match and is expected to have a lifetime of many years. A very fast kick produces a ball speed of around 30m/s and the deformation around the boot can be as much as 30% of the ball diameter (Shinkai et al. 2009). In addition to these high-deformation events, a football can also be characterised by its response to slow impacts with low deformation. The light impacts that merely indent the outer foam are crucial for predictable control and are arguably just as important as the high-speed power shots. Unlike many pieces of sports equipment, the football is used year-round in a very wide variety of environmental conditions and must have a fairly consistent response to the same loading scenarios.

1.2.3 Current Constructions, Materials, and Manufacturing Methods

The modern football is a composite thin-walled pressurised shell. Each manufacturer has different constructions and manufacturing procedures but the vast majority of footballs can be broken down into four main layers or components, each with a specific purpose. From the inside outward: bladder, fabric, foam, and skin.

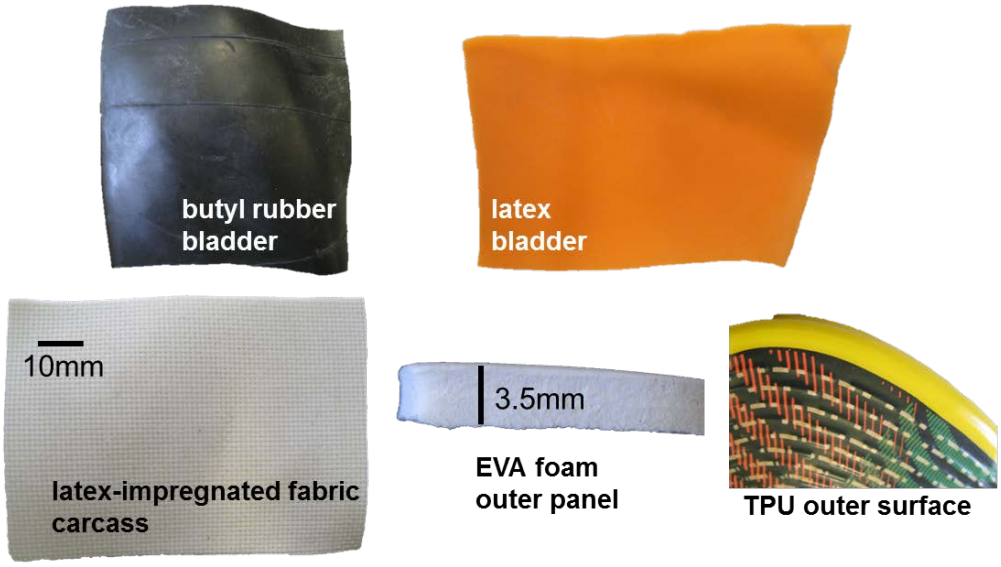

Figure 2: Typical Football Materials (butyl, latex, fabric, EVA foam, TPU outer skin)

The bladder is typically made of a hyperelastic polymer such as butyl rubber, latex, or TPU. It is responsible for retaining pressure and it contributes relatively little to the overall stiffness of the ball. The valve is frequently but not necessarily made of the same material but created as a separate component and bonded in with adhesive. Some bladders are moulded with additional material opposite the valve to balance the mass of the bladder. The fabric layer provides the structure and stiffness of the ball. Typically woven orthogonally from blends of natural and synthetic fibres, this layer is both very strong and very anisotropic. The foam layer is one or more layers of EVA, PU or other polymer foams. This layer deforms locally and is responsible for the touch characteristics of the ball and has a great influence on the surface-to-surface interactions with the boot and pitch. The outermost layer, the “skin”, aids in water repellence and also holds the graphics.

In one manifestation or another, these four layers have been present in footballs since synthetic materials entered mainstream use in football in the 1980s. Currently, there are two main ways of building the football with these layers. The most common method (“stitched”) involves first preparing flat sheets of fabric, foam, and skin layers. Panels are stamped out and stitched together by hand or with a machine. The footballs are stitched inside-out, the bladder is attached, the ball is flipped inside-in, and the remaining three or four seams are stitched by hand.

Figure 3: Left -Machine Stitched, Right - Thermally Bonded

The second method, called thermal bonding, is protected by patent (Shishido et al. 2004) and only utilised by one brand. The four basic layers are the same, but they are not bonded prior to assembly. First the complete "carcass" is created by stitching together individual flat fabric panels with the same methods used for the entire ball assembly in the "stitched" method. Independent of the carcass, the foam and skin layers are then combined in a second sub-assembly and finally the carcass and outer panels are bonded in a heated, pressurised spherical cavity. This construction offers designers more freedom because the inner and outer layers can be made with different panel shapes. While useful for aesthetic reasons, freedom in outer panel shape also gives a blank canvas for aerodynamic design while allowing for structural optimisation of inner components.

Figure 4: Thermally Bonded Construction

This basic bladder-carcass-outer panel design has several forms. In addition to the stitched carcass used in the 2010 FIFA World Cup, there is also a stitch-free carcass manufacturing method that uses overlapping layers of fabric on the bladder similar to papier-mâché techniques. A third type of carcass, called a filament wound carcass or filament wound bladder, is a butyl bladder covered evenly by a large number of random windings of a single yarn. This type of carcass is used on some inexpensive footballs and other inflatable sports balls like basketballs. The stitch-free, overlapping

panel carcass, called the “patch carcass” was used in the 2011 adidas Speedcell and 2012 adidas Tango12 (right, Figure 5). It was based loosely on a cube, with six identical ‘faces’ each comprised of three pieces of fabric or ‘panels’. The centre piece of fabric was shaped differently to the outer two for each face but they all overlapped to provide between one (the darker regions in the figure) and three layers of coverage around the butyl bladder. The stitched carcass and patch carcass were studied in this work. The patch carcass was particularly useful because of the flexibility in panel size and positioning allowed by the manufacturing process.

Figure 5: Stitched Carcass (left), Overlapping Panel Carcass (right)

1.2.4 Recent developments

The introduction of synthetic materials to the football in the 1980s marked a substantial departure from the previous centuries of the game and recent years have seen advancements in football technology aimed at small, fine improvements. The 2008 adidas Europass was based on the 2006 adidas Teamgeist with for modifications made to the surface textures to improve boot-ball grip in the. The 2010 adidas Jabulani was advertised as the roundest football ever and the first to be made with 3D-moulded outer panels. Nike’s Total 90 Tracer in 2010 had research-driven graphics to aid perception of the ball in motion (Nike 2010). When releasing new footballs, manufacturers sometimes claim material enhancements aimed at improving feel and controllability as well as ‘power’. Studies on which these claims (material, shape, graphic perception) are based are generally not published and difficult to replicate but at the very least, these claims suggest a direction in which development is progressing. As more information is collected on the game and the football, more materials developed, and new manufacturing methods conceived, there becomes a need to keep the ball performing well at the ever-increasing standards of the elite level.

1.3 Research Aims and Objectives

The purpose of this thesis and the work that supports it was to determine how football materials and construction may contribute to non-uniform behaviour during and after impact, how individual materials contribute to the overall performance of the ball, and how construction can influence the acoustic properties of a football. This involved creating and developing methods for assessing

dynamic consistency of the football and using those methods to determine the reasons for inconsistency and ways of mitigating the problem. In addition to these goals, the work aimed to create novel concepts and prototypes that benefited from and validated the new theories behind football rebound inconsistencies. It was the intention that the methods used to study the football as well as the resulting theories on impact behaviour would be applicable for footballs and perhaps other pressurised membranes well into the future. Prototypes and concepts used for validation may also find practical use immediately or inspire designs further down the road.

2 Literature Review

The purpose of this chapter is to prepare the reader for the following chapters with an overview of relevant topics and highlight recent published work pertinent to the topics at hand. It is assumed that the reader is technically savvy but background information about specific topics will serve to refresh the memory as well as establish a common vocabulary for the work. Though football is a relatively new topic for the scientific community, there exists a sizeable body of published work approaching the game from different angles that was used to inform and support this research.

Although manufacturers rarely release their testing or research in scientific publications, there is an academic presence in the topic. In addition to work investigating the ball alone, there is also a focus on injury prevention and biomechanics with the intention of improving technique. The biomechanics studies generally place emphasis on tracking the motion of the body and assume the properties of a football are consistent. The ball-specific studies are more focused on understanding phenomena and the physics of the situation rather than translating results to practical information for training or manufacture. It is these studies that were useful in preparing to undertake the research at present.

2.1 Football Impact Behaviour

The impact behaviour of a flexible thin-walled pressurised sphere is dramatically different to that of a stiff thin-walled sphere (e.g. table tennis ball) or a solid sphere (e.g. ball bearing). Stiff thin-walled spheres derive their global response from a combination of the bending (and consequently snap-through stiffness) of the material and geometry and the gas pressure increase due to volumetric change (Hubbard & Stronge 2001). Elastic solid sphere contact mechanics is described by Hertzian contact forces and is remarkably different from large deformation hollow body contact, focusing on stresses inside the solid bodies behind the outer surface (Sondergaard et al. 1990).

The first known work taking a theoretical approach to football impacts considers the material of the ball to have negligible flexural stiffness (Johnson et al. 1973). The calculations also assume an inelastic material, focusing only on the deformation of the ball and the resulting volume and pressure change as the sole energy storage and return mechanism. By determining the changing contact area and volume, the overall force from pressure was calculated and that dynamic force, when applied to the changing mass in motion (the part of the ball not touching the impact surface), gave accelerations that outlined the whole scenario. To emphasize the importance of the volume and pressure change, the authors also ran the calculations with a constant pressure. Close agreement between theory and physical experiments for contact time suggest that the assumptions of negligible bending stiffness and inextensible materials were valid.

The concepts of these early calculations have been taken further to explore oblique (angled) impacts on a flat plate (Stronge & Ashcroft 2007). Momentum and potential imbalances were calculated as a flux when moving ball material contacted the impact surface and stopped. The work considered the finite deformations present as the material transitioned from moving to stationary at the contact surface but these inclusions did not have an overwhelming influence on the result when compared to the earlier calculations with assumed rigidity. All theoretical work known to the author assumes uniform stiffness (whether rigid or deformable). Imbalances in momentum flux (Stronge & Ashcroft 2007) may be amplified in the presence of anisotropic materials.

Whether oblique, normal, or foot/boot impacts, the changing internal pressure is critical in understanding the rebound characteristics but the pressure itself can be seen as dependent on the global ball stiffness. When a ball is pressurised, the material is under balanced biaxial tension (Abeyaratne & Horgan 1984). As it becomes deformed, the areas of high stress appear in more of a 'hoop' configuration, following a circular equator parallel to the impact plane. The hoop stress/strain allows the material to pull on itself, resulting in a primarily tensile mode of material deformation. Due to the construction of a football, the hoop forces pass through many individual panels around the circumference of a deformed ball and this band of stress has noteworthy implications for the deformation characteristics (Price et al. 2006).

When impacts are carried out in a lab or simulated, there are several standard measurements taken to characterise the ball's behaviour. Coefficient of restitution, contact time, force, and deformation are used in the dialogue about ball performance. Changes in a football's construction and materials can be observed in the changes to these main measurements.

2.1.1 Coefficient of Restitution

The coefficient of restitution represents the amount of energy stored and released by the ball. The actual COR is representative of the complete interaction including all bodies but impact surfaces are generally chosen to be hard and heavy enough to allow the properties of the ball to dominate the results. Recalling that the kinetic energy of an object is $KE = \frac{1}{2}mv^2$, a simple ratio of post- to pre-impact velocities gives the percentage energy loss. The same calculation can be performed with potential energy, but with the square root of the variables $\sqrt{\frac{h_2}{h_1}}$ (Daish 1972). The potential energy method is often chosen for experimental ease and because it aligns with the dynamic test prescribed by FIFA. A ratio of one indicates zero energy loss and is impossible. Through drop test rebound height requirements, FIFA specifies a coefficient of restitution of 0.82-0.88 for FIFA Approved status (FIFA 2010b).

The coefficient of restitution is the energy in an impact, using one number to describe the complex interaction between objects as well as their individual behaviours. Falcon (Falcon et al., 1998) broke it down into three modes of energy dissipation: plastic deformation, vibration, and dissipation through viscoelastic effects. Although the coefficient of restitution is a complex phenomenon, it can be simplified greatly for theoretical and practical purposes. Cross (Cross 2000) considered tennis balls theoretically and experimentally by considering an impact in terms of spring constants and energy loss. Based on collected data showing an increase in COR with increase in deformation, Cross reasoned that material stiffness plays an important role in the energy loss of an impact. Homes and Bell (Holmes and Bell, 1985) came to related conclusions by finding that increased pressure (and global ball stiffness) led to higher COR as well. Though there may be correlations with material stiffness or pressure, the complex materials and construction of the modern football make it unlikely that a simple linear relationship describes all scenarios accurately.

Aguiar and Laudares (Aguiar & Laudares 2002) have developed a method for determining COR using the sound of the collision. With a known drop height and the time between impacts, not only the COR, but also the acceleration due to gravity could be determined. This method, however, assumes a consistent, speed-independent COR which is not always the case for footballs (Price et al. 2005).

Daish (Daish 1972) performed a variety of experimental testing on footballs, golf balls, and snooker balls. One interesting result also observed in the research of Price (Price et al. 2005) was that COR decreased with increased impact velocity. It is important to note that the finding for footballs relating COR and impact speed was opposite between tennis balls and footballs. This is not necessary contradictory, as tennis balls derive more of their rebound properties from the shell stiffness than footballs. In a drop-test study, it was found that a lower inflation pressure produces a lower rebound height (Holmes & Bell 1985). These two examples further support the idea that deformation and material stiffness are quite important. In the same study, Holmes and Bell also concluded that the internal pressure's influence on drop test rebound was less than that of material and construction.

2.1.2 Contact Time and Contact Force

Once the ball first touches the surface, it starts slowing to a stop. Immediately after the stop, the ball accelerates away from the plate until it no longer touches and a constant velocity is maintained (unless influenced by another force like air or gravity). Contact time is the length of the interaction or period of influence and the contact force is the response of the impact surface. For an impact with determined initial and final velocities (and COR), a shorter contact time will require a higher acceleration ($a = \frac{\Delta v}{t}$) (Johnson & Sherwin 1996). A higher acceleration requires a higher force

(*f=ma*) so the contact time and force required are tied together (Arakawa et al. 2009; Johnson et al. 1973).

The contact force of an impact can be calculated using Newton's equations of motion and the masses and velocities of all involved objects. As this is only kinematics, everything is based off motion so energy losses need not be considered. However, force plate readings from high impacts must not be blindly accepted. It important for the natural frequency of the force plate and (and rigid mounting system) to be significantly greater than that of the impact. If the force plate/mounting system is agitated at its natural frequency, the ensuing vibrations can make the readings unreliable (Walker et al. 2010).

There are three main ways of measuring contact time: force plate, high-speed camera, and electrical circuit (J. R. Roberts et al. 2001). With a sufficiently quick sample rate, a contact time can be easily observed on the force-time curve of a force plate. Using a high-speed camera and knowledge of the time between frames and the number of frames between initial contact and final contact, the contact time can be calculated. Both of these methods have the advantage of providing additional data as well. High speed imaging can also provide pre- and post-contact velocities and the force plate will give a force profile for the event. Any sort of image processing, however, requires some sort of edge interpretation. Whether digitisation is automated or manual, discrepancy in pixel selection introduces error into the measurements. Inherent distortion and aberrations in single-lens imaging systems (Jacobson et al. 1988) can also provide misleading information, particularly with respect to velocity at the edges of the frame. A third method specific to contact times involves applying a conductive substance to both plate and ball to create a circuit with the impact interaction acting as the switch (J. R. Roberts et al. 2001). All are means to the same end and together cover most impact scenarios when used appropriately.

The duration of a football impact against a rigid plate is around 6-10ms (Lees & Nolan 1998; Nunome et al. 2002; Price et al. 2005; Wesson 2002). With golf balls, where the contact times can be around 0.5ms (Arakawa et al. 2009), golfers comment on the interaction and how the ball comes off the club (J R Roberts et al. 2005). Roberts saw little correlation between perception and actual contact time in experiments with elite golfers. In a later study, (J R Roberts et al. 2005) determined the sound of the impact to have the largest influence on a golfer's perception of an impact. In addition, Daish (Daish 1972) explains that the time it takes the shockwave from impact to travel through the shaft to the hands is actually longer than the impact itself. By the time a golfer feels the impact, it is already over.

A football equivalent to Roberts' (J.R. Roberts et al. 2005; J. Roberts et al. 2001) research does not yet exist so it is difficult to say whether a player can use a longer or shorter contact time to his or her advantage. Players certainly make claims about the ball leaving the foot fast (Cech & adidas 2009) so it is worth considering contact time as a potential metric of interest.

2.1.3 Deformation

A given surface area can contain the most volume if that surface area exists as a sphere. Just as everything in nature tends toward the lowest possible energy state, an enclosed, internally pressurised volume will tend toward a spherical shape. Soap bubbles illustrate this principle well. If a spheroid cavity is pressed between two plates, the volume decreases, increasing the internal pressure (Cengel & Boles 1989) which pushes outward on the un-restrained sections of the sphere. The expansion of the sphere is opposed by the stiffness of its surface and each region depends on adjoining regions. The result, for an isotropic hollow sphere is a continuous band of strain parallel to, and directly between the two plates. This band of strain is appropriately referred to as hoop strain. For isotropic materials of uniform thickness, the maximum hoop strain will be at the inner surface of the cavity (Abeyaratne & Horgan 1984). Batra (Batra 2008) provides an analytical solution for the hoop stress in a thin-walled sphere

$$\sigma = p_{in}\frac{R}{2t}$$

where σ is the hoop stress, p_{in} is the internal pressure, R is the radius of the sphere and t is the thickness of the wall. In addition to the stresses and strains of a deformation, the shape of a deformation can be useful in characterising balls.

Hubbard and Stronge (Hubbard & Stronge 2001) observed the deformation characteristics of a table tennis ball. They used a glass plate as the impact surface in order to closely observe the interaction from a different perspective. At higher speeds (and larger deformations), the centre of the contact area would actually pop back, into the ball, creating an open ring, rather than a circular contact surface. Unlike footballs, table tennis balls derive most of their stiffness from the material, with only a small contribution from internal pressure. A similar effect, however, can be predicted for normal football impacts. Finite element analysis (Price et al. 2005) shows decreased stress and strain at the centre of impact at full deformation.

Zouari (Zouari et al. 2008) performed simple tensile tests on orthogonally woven fabric cut in strips along directions in 15° increments from the orthogonal. Strips oriented at 0° and 90° (in line with the fibre direction) were found to be the stiffest and the 45° strips the most compliant. Price (Price

et al. 2005) used a finite element analysis model to draw connections between carcass material orientation, COR, and deformation characteristics. Past studies have created a framework for understanding the active mechanisms in a deformation-reformation impact scenario. Observations from past studies have created general conclusions but more detailed descriptions of impact phenomena require an active investigation in which the subject is modified and tested, thereby isolating the effect of individual parameters.

2.2 Materials

The 1986 adidas Azteca was the first non-leather official FIFA World Cup football. It was not, however, the first time synthetic polymer materials had been used on a football. The previous World Cup ball, the 1982 adidas Tango España, used a polymer sealant on the seams between leather panels to improve water resistance (Cooper 2011). Though synthetic materials and treatments had been in play for some time, the departure from leather panels marked a dramatic change in football engineering. In addition to a wider range in mechanical properties, synthetic materials offered the potential for greater consistency and precision in the manufacturing process. The extra flexibility in material property selection ushered in an era of football engineering; after the adidas Azteca, elite-level footballs were released to the public with mention of their technical innovations and enhancements.

2.2.1 Material Properties of Interest

Thermosetting polymers are made of long twisted chains of molecules (mers). As the material is strained, the chains untwist and straighten (Anderson et al. 1985). Relatively speaking, this rearrangement requires little force but once the recently-straightened chains are subjected to the tensile loading, the stiffness increases. This transition is progressive – not all molecules are in the same configuration at once – and the result is a non-linear behaviour from the material.

The cross-linked molecule chains in polymers can also help describe the thermal dependency of the materials. High temperatures and the associated thermal agitation resists the structured bonding of crystalline structures but as the temperature drops, more bonds between molecules form and the material becomes stiffer and harder (Anderson et al. 1985). This transition is marked with the glass transition temperature, the temperature in the spectrum between fluid and glass-like properties. There are many materials for which the glass transition temperature lies well outside the typical temperature range for humans (e.g. glass – cannot be touched when in the molten state) but there are some materials for consumer (like the EVA found sometimes in footballs and running shoes) that transition around 0°C (Liu & Tsiang 2003). Another aspect of foam relevant when considering testing and characterisation is the skin. The mould surface of EVA, PU and other foams can form a skin, the

thickness of which is dependent on the temperature gradient. This skin of un-foamed material can have different properties for hardness, energy absorption, density and stiffness (Michaeli et al. 2009). The difference in properties can be great enough so selecting the thickness of the skin is an integral part of the engineering process for foam components (Gupta & Khakhar 1990).

Viscoelastic properties are closely related to the thermal dependencies of a material. Viscoelasticity is a combination of viscous and elastic responses and the former aspect is especially susceptible to thermal effects (Anderson et al. 1985). A completely elastic material subjected to cyclical loading will have an *immediate* displacement response to the input force and the response of a completely viscous material will be 90° out of phase (Callister 2000). In reality, no material is completely elastic or completely viscous but the long molecular chain structure of polymers makes the viscoelastic behaviour more noticeable (Serban et al. 2012). Practically speaking, this means materials loaded at high strain rates will respond stiffer than at slow strain rates (Price et al. 2008). Viscoelasticity can be measured by observing the phase difference in input and output force and displacement peaks at different loading frequencies. It is often represented mathematically with springs and dashpots, which include a time component (Johannknecht 1999).

Anisotropy is the characteristic of some sort of directional dependence and variation in material properties. In footballs, fabric is a critical contributor to the overall characteristics and a large source of anisotropy (Price et al. 2006; Zouari et al. 2008; Hearle 1967). The fabric used in many footballs uses a simple orthogonal under-over-under-over weave with perpendicular warp and weft. When pulling in the direction of the warp or weft, the full tensile strength of the yarns provides a very stiff response but when pulling at an angle to the yarns (45°, for example), only the friction between yarns resists the strain (Lomov et al. 2006). The fabric used in footballs is often coated or impregnated with a latex-based polymer. This can serve as a bonding agent to improve adhesion with inner or outer panels and it also aids handling in the in the manufacturing process. The pliable polymer matrix gips the yarns, making them less able to slide over each other, and also blocks the space yarns would deform into, creating a physical compressive barrier to deformation. This phenomena increases the 45° stiffness over that of untreated fabric but have little effect in the stiffer warp and weft directions. The inclusion of a polymer matrix into woven materials has the ability to alter the base weave beyond a simple homogenous increase in stiffness so fabrics must be tested with their polymeric infusion, paying special attention to shear properties (Wei & Xingwen 2009).

2.2.2 Material Characterisation for FEA

For computational efficiency in virtual simulations, the complex behaviour of materials is often characterised with simpler equations (Serban et al. 2012). Modern finite element (FE) analysis is capable of combining test data from various modes of deformation to create a build up an accurate approximation of material behaviour (Abaqus 2010). Simulia's Abaqus (Abaqus 6.12, Simulia, Dessault Systèmes, Vélizy-Villacoublay Cedex, France) was the code used for this body of work but other FE codes work with the same principles. Hyperelasticity is typically characterised with strain energy potentials (or strain energy density functions), methods of relating stress and strain using theory of stored elastic energy (Johannknecht 1999). Using a strain energy potential to define hyperelastic behaviour avoids the slow option of using a lookup table to find corresponding stresses and strains and it is capable of including more than one mode of deformation (ie. more than just linear tension). There are a variety of strain energy functions, each with strengths and weakness in terms of available raw data inputs, accuracy of approximation, and computational time so they must be chosen deliberately.

Ogden (Ogden 1972)and Van der Waals forms of the strain energy potential are suitable if there is data from several different material tests (Abaqus 2012). Arruda-Boyce (Arruda & Boyce 1993), Yeoh (Yeoh 1993), and other reduced-order polynomial functions work well with less test data. If only one type of material test is available, the Marlow function will fit the test data exactly, almost like a lookup table (Abaqus 2012).

2.2.3 Material Testing for FEA

In many engineering applications, data can be taken from a library of common, well-understood and -tested materials. The materials used in footballs are not typically seen in engineering applications and there are enough varieties to make a standardised database unrealistic so the test data must come directly from samples. Of all the ways to deform and measure a material, uniaxial tension is frequently the most useful and the nature of (hoop) strains in footballs makes it particularly relevant. The test involves a long specimen clamped at both ends and strained quasi-statically, keeping track of strain and load (Abaqus 2012). Tensile tests can be used for simple quasi-static measurements as well as dynamic tests and anisotropic studies.

Equi-biaxial extension is another useful test for characterising hyperelastic materials (Johannknecht 1999). This test uniformly deforms a sheet of material in all in-plane directions. It offers the same mode of deformation as simple compression, in which a vertical force deforms a material radially, but it works well on thin materials. Though not influenced by friction like a traditional compression

test, the equi-biaxial test has practical challenges of its own, namely the implementation of a large test rig in a standard load frame.

2.2.3.1 Tensile Testing

Tensile testing is one of the simpler material tests but there are still many distinctions and decisions to make about the exact methodology. The ideal test allows for collection of corresponding stress and strain values without influence from geometry or clamping forces. Stress has two representations. Nominal stress is often preferred because it considers the force per un-loaded cross sectional area, which is straightforward to measure. Alternatively, true stress considers the force per loaded (deformed) cross sectional area and can be practically challenging to measure (Pytel & Kiusalaas 2003). Common practice is to use material sample geometry (colloquially called a 'dog bone' or 'barbell') that flares outward at the clamp surfaces to ensure that the location of the greatest stress is known to be at the centre of the test specimen (ASTM International 2003; ASTM International 2008; ISO 2012). Material testing standards were devised to establish a common classification system for efficient communication of material properties. The testing methods do not necessarily represent the best way to create models for finite element analysis but the general concept behind the "dogbone" or "barbell" geometry with flared clamp regions is sound and broadly applicable.

The first loading cycle of a rubber or elastomer can cause a reduction in stiffness, called the Mullins effect (Mullins & Tobin 1947). In test data, the first loading cycle will be stiffer than subsequent cycles at or below the maximum strain of the first cycle. This is due to an unfolding and partial straightening of molecular chains. There is also a directionality, or anisotropy to the effect as well (Diani et al. 2006). The effects are not negligible (Gentot et al. 2004) and must be considered when designing any type of test for polymers. The effect is usually modelled with damage laws (Gentot et al. 2004) but it can also be removed from consideration by using material properties taken after the stress softening has occurred (Luo 2014).

2.2.3.2 Viscoelastic Testing

Time-dependent, viscoelastic properties of materials can be interrogated in a variety of ways falling into two categories: long term and short term. Stress- or strain-relaxation tests are long term tests that involve placing a constant strain or stress on a specimen and monitoring the other value. If strain is held constant, for example, the stress required to maintain that strain will decrease over time (relaxation) (Callister 2000). The close relationship between viscoelasticity and temperature means repetitions of these relaxation tests at different temperatures can essentially be overlapped to provide a big picture of the material's thermal and temporal dependence. Long-term and short-

term testing can also be overlapped to build a more complete picture of a material (Johnson et al. 1995).

Short-term testing uses high-frequency excitation of a specimen to determine viscoelastic properties. Dynamic mechanical analysis is a technique (and machine type) that performs typical mechanical testing (tensile, compressive, shear) at high frequencies up to 1kHz (Mettler Toledo 2005). The machine measures the small difference in time between strain and stress peaks at different frequencies and temperatures and produces calculated data for storage and loss moduli and a damping coefficient (tanδ, the ratio of loss to storage and the phase difference between input strain and output stress). Hyperelastic materials, with different stiffness at various strains, can be difficult to test with a DMA because the strain magnitudes are typically very small. The high frequencies require small samples and small displacements so the strain can be on the order of 2%. In order to get dynamic data at greater strain magnitudes, DMA methods can be employed in larger dynamic machines at lower frequencies 1-10Hz as well (Serban et al. 2012). A challenge and potential limitation with this type of testing is clamping the sample properly. Rubbers and other compliant samples can experience slippage when measured at high frequencies and displacements (Shim et al. 2004).

2.2.3.3 Fabric Testing

Fabric modelling happens at several scales. At the micro scale, work has been done to look at the stresses and strains through the cross sections of individual yarns as they bend and slide over other yarns. The twisting, bending, sliding, and deformation have been investigated as residual effects of the weaving process as well as the dynamics of fabric deformation (Hearle et al. 2001). Individual yarns in 'unit cells', small repeating sections of a weave, have been simulated (Lin et al. 2009) based on the properties of individual yarns and their interaction with each other. TexGen is an open-source software designed to model technical fabrics of different weaves at the yarn level (TexGen 2013). Modelling at the yarn scale is computationally expensive when large pieces of fabric are involved so ways of testing and characterising overall fabric behaviour have also been implemented (McCartney et al. 2005). These methods of larger-scale modelling are more useful for football work.

Engineering standards for fabric tensile testing recommend long rectangular strips of specific dimensions but any specimen type and methodology agreed upon by those involved in the communication of material properties is also deemed acceptable (British Standards 1999). With the large variation in fabric properties and applications, it makes sense to consider each scenario individually rather than rely on a standard. The greatest challenge with fabric is characterising the anisotropy and there are several ways anisotropic materials can be represented in Abaqus.

The linear elastic model (elastic lamina) allows users to specify tensile stiffness in warp and weft directions, Poisson's ratio, and shear moduli for transverse behaviour (Simulia 2012). This method has been used successfully to model fabric in footballs with a simple lab test procedure and reverse engineering (Price et al. 2006). Strips of fabric with yarns from 0° to 90° in 15° increments were tested in tension. Warp and weft Young's' Moduli came from 0° and 90° tests, and the shear moduli were adjusted until single-element tensile tests at different yarn orientations matched the test data. The elastic lamina model is intended for modelling anisotropy but it assumes that warp and weft will always be 90° apart (Simulia 2012), an assumption that may be more relevant for stiffer materials or lower strains. The linearity of the model also makes it less appealing, given the hyperelastic nature of the materials used.

Abaqus has a built in phenomenological woven fabric model that simulates the effect of individual yarns, allowing the relative warp-weft angle to change, without modelling individual yarns (Abaqus 2012). This extra functionality, combined with the ability to account for hyperelastic tensile behaviour makes the fabric model attractive for football modelling. For inputs, the model takes stress-strain curves for warp and weft directions and a shear test called the 'picture frame' test (Abaqus 2012). The picture frame (Lomov et al. 2006; Johannknecht 1999) holds fabric samples at the edges of a square frame with hinged corners. Opposite corners are fastened to a load frame and the square is stretched to a diamond shape. The geometry and setup creates a scenario in which the only deformation is in the form of yarns sliding across each other – individual yarn length does not change. By removing any influence of yarn stiffness, the shear properties are isolated and this data is used to build up the phenomenological fabric model (Abaqus 2012).

2.3 Football Simulation

Ball-focused structural and aerodynamic simulations have allowed researchers and engineers to delve deeper into the science behind football to study aspects of the sport that are otherwise difficult to observe. Simulation has also been used to study injury in the sport (Asai et al. 2004; Schneider & Zernicke 1988) but the models used in such analyses were not designed to shed light on the ball itself.

2.3.1 Aerodynamics

Computational fluid dynamics (CFD) is used in aerospace and automotive industries to optimise vehicular aerodynamics and its use in sport is growing. Swimming body position and technique have been studied with CFD (Marinho et al. 2011; Minetti et al. 2009). Professional cycling has benefited from CFD investigations in drafting (Blocken et al. 2013), body position (Defraeye et al. 2010), and frame geometry (though manufacturers keep details of studies out of the public domain). CFD

works well for flow interacting with large bodies but the small textures and seams of a football present a challenge. Sub-millimetre surface features and textures have a large influence on the aerodynamic boundary layer of the football and creating an analysis to include the tiny surface vortices and larger-scale flow patterns is computationally challenging (Cotton & Jones 2007). Aerodynamic simulation relies on empirical data and mathematical flight models that incorporate changing ball spin (Passmore et al. 2008), drag and velocity. The models help predict behaviour and flight paths on the pitch for different ball configurations and atmospheric conditions (Tuplin et al. 2012; Carre et al. 2005). As codes improve and computation costs drop, CFD may see more applications in football simulation. It is not merely a question of power, however. With a mesh fine enough to capture the detail of seams and texture and large enough to enclose the entire flow around the ball, there may be too many elements. Computational cost will decrease but each additional element will require more calculations and it is possible that the accumulation of the small errors in such a simulation becomes noticeable. Some of the error may be predicted and removed (Ferziger & Peric 1996) but lab-based testing remains the prominent method used with footballs. For now, the existing empirically driven mathematical models may serve to provide boundary conditions for structural simulations.

2.3.2 Structural Simulation

Finite element analysis has been used in golf (Tanaka et al. 2012), tennis (Goodwill et al. 2005), baseball (Burbank & Smith 2012), football and other ball sports to understand the influence of structural properties on deformation and rebound characteristics. Compared to other traditional fields, the use of advanced simulation techniques is relatively new in sports. Researchers have made use of available software and validated with bespoke methods focused on the purpose of the model. There are trends, but no industry standards or best-practice methodologies to follow.

Early football finite element analysis was used to study basic deformation shapes of a 2D cross section (Hubbard & Stronge 2001) but since then complete ball models have been developed to study carcass anisotropy and viscoelasticity (Price et al. 2006; Price et al. 2008). The ball model used in Price's work was made of shell elements and defined with a composite material section to include all the layers of a ball. The sphere was pressurised with a specified influx of fluid into a defined cavity before the impact. This fluid flux and other uniform pressure methods assume a single pressure throughout the entire cavity. The model used a linear elastic fabric definition (elastic lamina) and a reverse-engineered damping coefficient to achieve the proper energy characteristics for the impact. Even with these simplifications, the simulation accurately predicted deformation shapes during impacts against a flat plate at different angles, as verified with physical lab tests. Properly characterising the energy properties of materials has also been a challenge for the rigid

foam used in baseballs and soft balls – reverse engineering the damping coefficients was more reliable and representative than isolated material tests (Burbank & Smith 2012). The work of D. Price and colleagues demonstrated that simulations can be used to predict an aspect of dynamic football behaviour but there was no study into the mechanisms that relate specific deformation shapes and the arrangement of anisotropic elements within the ball. Furthermore, the potential connections between fabric anisotropy, ball uniformity, impact deformation, and rebound consistency have not yet been investigated.

Though common and effective in football modelling (Price et al. 2006; Rezaei et al. 2011) and passenger safety airbag simulation (Lee & Youn 2006), the uniform pressure method is an approximation of the dynamic spatial variance within the cavity. There are no published studies that simulate the football cavity with a spatially-defined, volume-dependent fluid, rather than a uniform volume-dependent surface pressure. Airbag simulation, especially for out-of-position impacts (when the occupant hits the airbag before inflation is complete), has employed the use of a coupled Eulerian-Lagrangian (CEL) method, simulating the fluid-surface interaction as a multi-physics problem (Marklund & Nilsson 2002; Simulia 2011a). This method uses separate domains traditional Lagrangian structural elements and Eulerian fluid elements that are allowed to interact where specified. Eulerian elements, unlike structural elements express deformation and motion not as nodal displacements, but as volume-fractions for individual elements and pressures at nodes (Abaqus 2012). The fluid 'flows' through the grid of elements so the method is good at handling large motions/deformations (NAFEMS 1992). Another method of simulating fluid, called smoothed particle hydrodynamics (SPH) was first described in an astronomical context (Gingold & Monaghn 1977). This is a completely Lagrangian method that discretises a fluid with many points but without elements or a mesh (Abaqus 2012).

There are two types of structural simulation differing mainly in behind-the-scenes calculations. A standard (implicit) analysis breaks a load or displacement into a series of discrete increments and iterates, finding complete solutions to each increment sequentially with a stiffness-based technique. Explicit analyses take a more dynamic approach, constantly incrementing forward in time while solving for the current state of stress and strain in all elements. The two methods use computational resource differently and have different contact algorithms, element types and other capabilities (Abaqus 2010). Dynamic motions and wave propagation (present in football impacts) are better calculated with an explicit analysis (Simulia 2011a; Abaqus 2010).

2.3.3 D.O.E.

In some cases for fields in which simulation is a new tool, developing the model itself can be a challenging process of discovery and innovation. Football simulation is not unexplored territory, but among other aspects, new modelling techniques (eg. new fabric modelling methods) and new capabilities (eg. acoustics) required significant experimental phases before use as tools. Though there was model development, the focus in this work was on the results and what they say about football behaviour rather than the simulations and models themselves. A model can be created with specific inputs for materials and geometry with the intention of getting specific types of outputs but modern computational methods can replicate this process automatically and intelligently to either achieve a goal, or explore the effect of parameters throughout their design space. Optimisation studies achieve a goal by iterating with new input parameters based on the results of the previous simulation. Design of Experiment (DOE) studies map out design spaces by creating a matrix of possible input combinations and correlating those with the results from the body of simulations. Both of these types of studies are often thought of as multi-dimensional matrices, where each axis represents an input parameter and range of possible values and each point, defined by X,Y,Z…N coordinates represents a simulation with a specific combination of input parameter values.

Design of Experiments may be traced back to the work of S. Fisher (Fisher 1971) in devising methods of setting up and organising experiments to minimise error. In the most basic definition it encompasses almost any set of experiments, but DOE has come to refer to a more structured approach in both selecting the input parameters and the subsequent statistical analysis of results. Leveraging computational power, a series of combinations of different parameter values can be created and analysed efficiently on a scale that would have been too large to manage by hand.

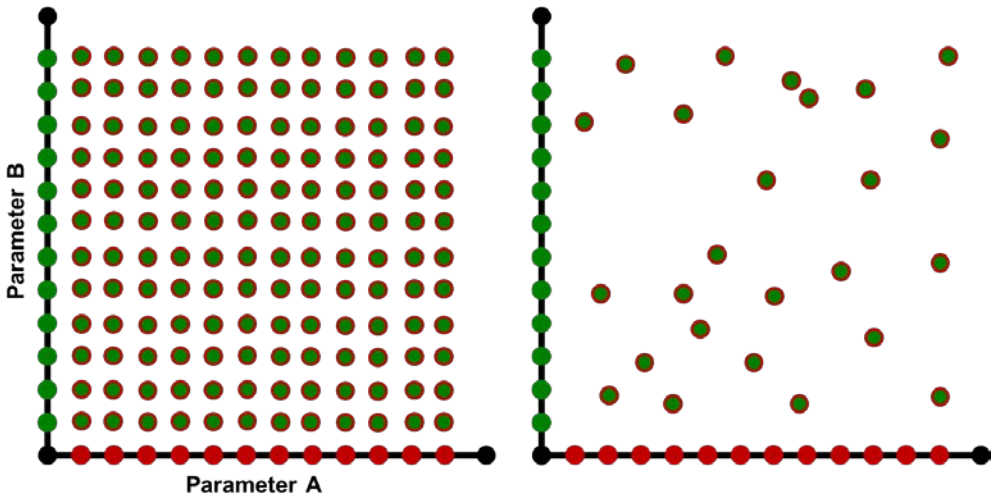

Figure 6: Design of Experiment, left: full matrix, right: optimised test procedure

When exploring variable spaces by hand, the traditional way would be to define limits for parameters, discretise the range evenly to give a series of values for each parameter, and create one test scenario for each possible combination of parameter values. This is a very complete way of creating a series of experiments, but it is also very computationally expensive, especially with a large number of input parameters (left, Figure 6). Using modern DOE algorithms, the discretised design spaces for independent parameters can be combined in such a way as to minimise the number of individual test scenarios while still able to quantify the relationships between inputs and outputs.

An optimisation also runs simulations constructed with combinations of different values for input parameters, but the values are chosen automatically by an algorithm that uses knowledge of previous design attempts. The investigator must carefully specify objectives, constraints that must be maintained, and a possible range for all the input parameters that may be modified. The optimisation algorithm that choses each subsequent point must also be selected to best suit the design space and goals. There is large variety available, and both the creation and implementation of optimisation algorithms are themselves complex tasks. One of the simpler styles of algorithm uses a gradient based approach in which the effect of changing inputs is expressed as a 'direction' with respect to the objective (Bartholomew 2012). Knowing which direction the result will follow with a given change in input parameters helps the algorithm pick the next point. The dependence of this algorithm on the local characteristics (or the relationship of inputs and outputs in a smaller region of the design space) makes it susceptible to getting 'stuck' in local optima. An analogy is focusing only on climbing the hill to reach the highest elevation without noticing there is a taller hill somewhere else. Other algorithms take inspiration from genetic or evolutionary patterns, with 'parents' dispersing to random 'offspring' and there are also techniques that mimic foraging behaviour of hive animals (Simulia 2011b).

Multi-objective optimisations require extra input on the relative importance of each objective. In the case of multiple objectives, the result will create a Pareto front, which, with two dimensions (two objectives), looks like a line representing the optimal solution. For example, the line may represent combinations of weight and cost, both of which should be minimised. There are many possibilities for which the lowest cost at a specific weight or the lowest weight at a specific cost are mathematically equivalent, but the user must decide whether cost or weight is the more important output (and by how much).

2.4 Ball Impact Acoustics

There are three mechanisms of sound generation: turbulent fluids, vibrating surfaces, and rapid pressure changes (Davies 2010). The three physical processes are essentially beginnings of pressure

differential that propagate. When a fast-moving fluid interacts with a slow-moving fluid, the resulting turbulence (a term for localised regions of changing pressure) can set up sound waves. With a vibrating surface (e.g. a bell), the fluid is pushed and pulled cyclically, also creating a pressure/sound wave. Any rapid pressure change, for example the sudden local heating in a thermal explosion, can create a sound wave (Davies 2010).

Pressure waves travel through air at the speed of sound until they reach a solid medium that reflects, absorbs and transmits the sound. A reflected wave can return in the same direction and interact with the original wave to create a different shape. If the volume is enclosed and has a length equal to whole multiples of half wavelengths, a 'standing wave' will be created (Fahy & Walker 1998). In simpler terms, this is a wave folded back on itself at the reflection surface in such a way that the nodes of the wave are stationary (standing, not travelling).

When investigating the sound of a football impact, the latter two are the most likely mechanisms of sound production. The ball's deformation, reformation and short period of subsequent oscillations may have a somewhat 'bell-like' influence on the surrounding air. There is also a sudden pressure rise and fall when the air is squeezed out from between two impacting bodies immediately prior to contact and rushes back immediately after. The click from billiard balls is not from a bell-like structural vibration, but from this sudden removal and replacement of air between the two balls (Lyon 2000).

Microphones or sound meters measure the pressure waves and record time-domain pressure data but human perception is not so linear. Though related to intensity, loudness is only a perception and it does not have a linear relationship with measurable quantities (Mather 2009). Though the textbook auditory spectrum is between 20 and 20,000 Hz, the complex arrangement of inner hairs, membranes and cavities create a neural output inconsistently proportional to the input. Generally speaking (variation with age and exposure to sounds), humans are most sensitive to frequencies around 3kHz and less sensitive at the extremes (Lawrence 1989).

Most of the acoustic work in sport has related to golf equipment. The sound of a driver is often considered a mark of quality and a clean shot and there have also been correlations drawn between acoustics and a perception of quality (J R Roberts et al. 2005). In golf, impact duration is short enough to make it impossible to use any perception, acoustic or otherwise to adjust or 'shape' the swing (J.R. Roberts et al. 2005) but the sound of impacts is very useful in other sports. Table tennis players will stop to mask the sound of their shots, depriving opponents from information on the spin and power of the oncoming shot (Wade 2012). The bounce sound and ring of a basketball may help

players keep track of the ball when their focus is elsewhere. The influence of 'good' or 'bad' acoustics may be difficult to quantify, but people are more comfortable using a product that sounds as expected, making it easier to trust other, non-acoustic properties (Lyon 2000).

Acoustics of basketballs has been studied from a theoretical perspective, looking at the initial 'thump' and following 'ring' sound. The thump is a monopole-type deformation that falls somewhere between the aforementioned vibrating surface and sudden pressure change. The sudden shape and volume change creates a big, low-frequency sound (Katz 2010). The following ring was believed to rely not on the large-scale deformation or small surface vibrations, but on the oscillating internal pressure waves. The internal resonant frequencies and standing wave mode shapes have been explored mathematically – boundary conditions of the spherical shape, zero particle velocity at the surface and finite pressure at the centre allowed for the theoretical calculations of resonant frequencies. Lab data for a basketball impacts correlated well with the calculated resonant frequencies, though small deviations from sphericity may have masked some of the predicted frequency peaks. For a basketball, the frequency peaks of greatest amplitude were around 2700Hz and 4500Hz, with many smaller peaks from 1000 to 6500Hz (Russell 2010). Graphical representations of mode shapes were also calculated, and the number of nodes and antinodes was seen to increase with increasing resonant frequency but there was no lab-based validation or spatially discretised calculation to support the investigation into mode shape.

Though not specifically aimed at acoustics, a modal analysis approach has been taken to improve the understanding of football structural behaviour (Ronkainen & Harland 2007). Laser Doppler vibrometry revealed resonant frequencies for thermally bonded and machine-stitched footballs between 150Hz and 1359Hz with commonalities at 150Hz, 334Hz, 950Hz, 981Hz, and 1000Hz. At low frequencies, the mode shapes existed independent of outer panel configuration and the lobes of the higher frequency (>500Hz) mode shapes were at the centres of the outer panels (32-panel construction).

2.5 Summary

The literature review revealed a number of useful published studies in football, sports in general, simulation, acoustics, and material characterisation. It has been demonstrated that simulation can be a useful tool for investigating the behaviour of sports equipment, including the characterisation of materials in a dynamic environment. In football specifically, links have been drawn between materials and deformation, but a detailed study of material anisotropy, ball uniformity, and resulting rebound consistency has not been undertaken. The mechanism through which fabric anisotropy influences ball rebound has not been investigated and there are now improved simulation tools

better able to represent anisotropic fabric behaviour, as well as experiment with different pressurisation scenarios.

Acoustic work with basketballs has theorised the presence of internal resonant modes and validated from one angle with physical lab frequency data but no such studies have been identified with footballs or any other sports balls. This leaves the open the question of construction and material influence on acoustic properties.

3 Materials Characterisation for Footballs

3.1 Intentions

Materials testing methodology should be developed deliberately with general context and specific end-usage in mind. The variety in test protocol used in different industries and applications gives a myriad of possibilities but ultimately, the correct test setup is the one which allows for the best numerical representation of the material in the specific calculations in question. In the case of football science and engineering, one must look to both the ball and the game to help select proper materials test procedures.

Studying the game can provide information on loading scenarios like strain rate and strain magnitude. Environmental conditions, especially temperature, must be considered as well. The ball shape and size, as discussed earlier, can indicate probable prominent modes of material deformation. Together, the materials and loading scenarios make proper characterisation an unusual challenge. There were several distinct areas where two or more potentially 'correct' methods gave different results. The best method was then chosen at the discretion of the author, keeping in mind the end use and practical matters of testing ease and repeatability.

This chapter covers the influence of specimen size and shape on hyperelastic and anisotropic measurement as well as attempts to capture representative strain rate and strain magnitude in dynamic material testing. In addition to the data included in simulations, in some cases this material testing directly informed theories on football behaviour. Results from a variety of tests are presented and the implications of the advantages and disadvantages of each are discussed.

3.2 Basic Test Protocol

The majority of the data used to generate material models for finite element analysis came from tensile data. This was deemed appropriate because of the tensile hoop strains expected during deformation. Tensile testing was carried out on an Instron 5567 (Instron, Norwood, Mass., USA), a screw-based load frame, using a 100N load cell for latex, butyl, EVA, and TPU and a 1000N load cell for fabric. Material was clamped either with pneumatically-actuated or vice-type grips and stretched quasi-statically at no more than 60mm/min (typical strain-rate 2mm/mm/s). Strips of material were cut to be 20mm wide with 70-110mm between the clamps. Latex and TPU test specimens were created with a dog bone stamp with 6mm wide gauge length regions and EVA foam used a smaller, 4mm wide dog bone stamp (Figure 7 to accommodate available sample material sizes. Figure 8 shows examples of the material specimen used in the testing. For size reference, the small squares in the background have 10mm edges.

Figure 7: Dogbone specimen sample stamp (cutting edge) - 80mm long, 25x4mm gauge length

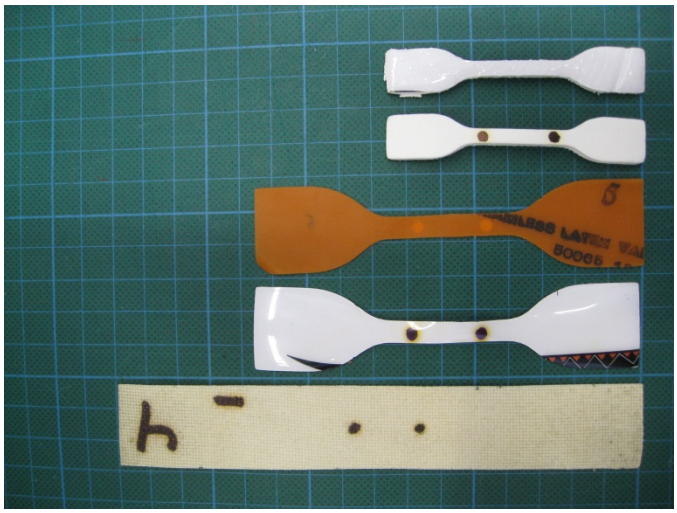

Figure 8: Material specimen examples, from top to bottom: EVA+TPU skin, EVA, latex, TPU skin, carcass fabric

Materials, especially TPU, EVA, and carcass fabric, exhibited the Mullins effect. This effect can be modelled with damage algorithms or phenomenologically but it was decided to remove the effect from the data in the material testing process. In manufacturing and assembly, materials undergo deformations and most football impacts happen after the 5-10 loadings typically required (Cantournet et al. 2009) to reach a consistent stiffness so it is more appropriate to consider the material after any stress softening. A simple pull to the elastic limit exhibited the stiffest behaviour and following extensions evoked a more compliant response. Using the data from the last of a series of extensions avoided any initial stiffness, but there was the chance that the higher strain altered the behaviour at lower strains. To condition the materials and remove the Mullins effect, the materials were loaded for 5 cycles to one strain level before incrementing to the next strain level (1% increments for the bladder, 0.5% increments for carcass fabric, TPU, and EVA). The stress at the fifth cycle at each strain level and that set of stress/strain values were used to build up a 'Mullins adjusted' curve. The strain increments for butyl, latex, TPU, and EVA were 1% and the increments

used for the carcass were at 0.5% strain. In building up the strain amount slowly over a series of cycles, the effect of high strain on the material behaviour at low strain could be accounted for.

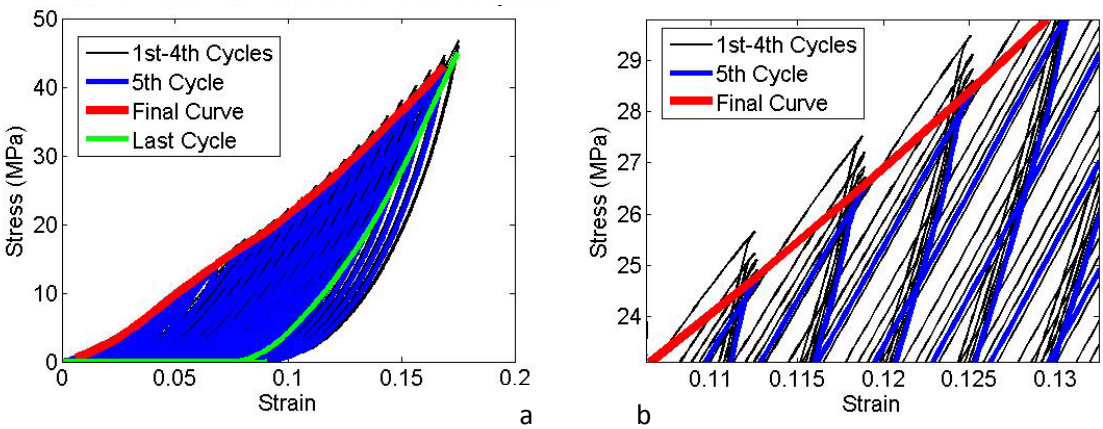

Figure 9: Carcass Fabric 90° Yarn Orientation Mullins Effect

Figure 9 is an example of the data collected and what was extracted from it. The 'Final Curve' was created by connecting the peaks of the fifth cycle at each strain increment and the green 'Last Cycle' represents the last loading cycle at the final strain increment. The Mullins effect can be seen clearly in Figure 9 b with stress peaks at the strain increments that started high and decreased after the five cycles. The difference, however, was relatively small compared to the overall magnitude (approximately 3% of the strain amount at 12% strain, not 3% strain at 12% strain). A long single pull on the material would be the equivalent of connecting the peaks of the first cycle at each strain increment.

The 'Last Cycle' in the figure shows a considerable amount of plastic deformation and damage that can be seen throughout the strain range. In these tests, physical damage (e.g. splitting yarns, tears) was not observed so there may have been bond separation within the polymer and a re-organisation of fibres and yarns. Fibres may have unwound, lengthening the yarns to make the fabric longer and respond stiffer. This potential change in the fabric should be considered damage because it is not reversible, but it does not necessarily represent a limit in the material testing. During assembly, the fabric is stretched to have a spherical shape and heated, and these processes may influence the propensity to damage seen in material tests of pre-processed material.

The greatest drop in stiffness due to the Mullins effect was after the first cycle. The latex, EVA, TPUEVA (TPU and EVA bonded together), and TPU exhibited decreased stiffness between the first and second loading of 0.7%, 1.2%, 2.3% and 2.6% respectively at 10% strain. The softening effect grew slowly with more cycles but it was never a dramatic departure from an equivalent single pull test. Incremented cyclic loading generated the most information possible from a tension test by

avoiding the effects of high strain cyclic loading on the stiffness of the material at low strains. The test captured the effective single pull load curve, the Mullins effect, as well as the slow onset of plastic deformation. Given the observed differences, a single-pull test was not thrown out as inaccurate, and cyclical loading to a high strain magnitude was observed to have a large conditioning effect at low strains.

The 'Final Curve' in the graphs was used as the primary source of data for comparing materials and creating material models for simulations. Figure 10 shows a region defined by the extremes seen in the testing and the average of the five individual material samples (based on the 'Final Curve'). For each material, the range in stiffness due either to testing protocol or material inconsistency was on the same order of magnitude as the difference between data from a first pull and the Mullins-adjusted ('5th curve') data.

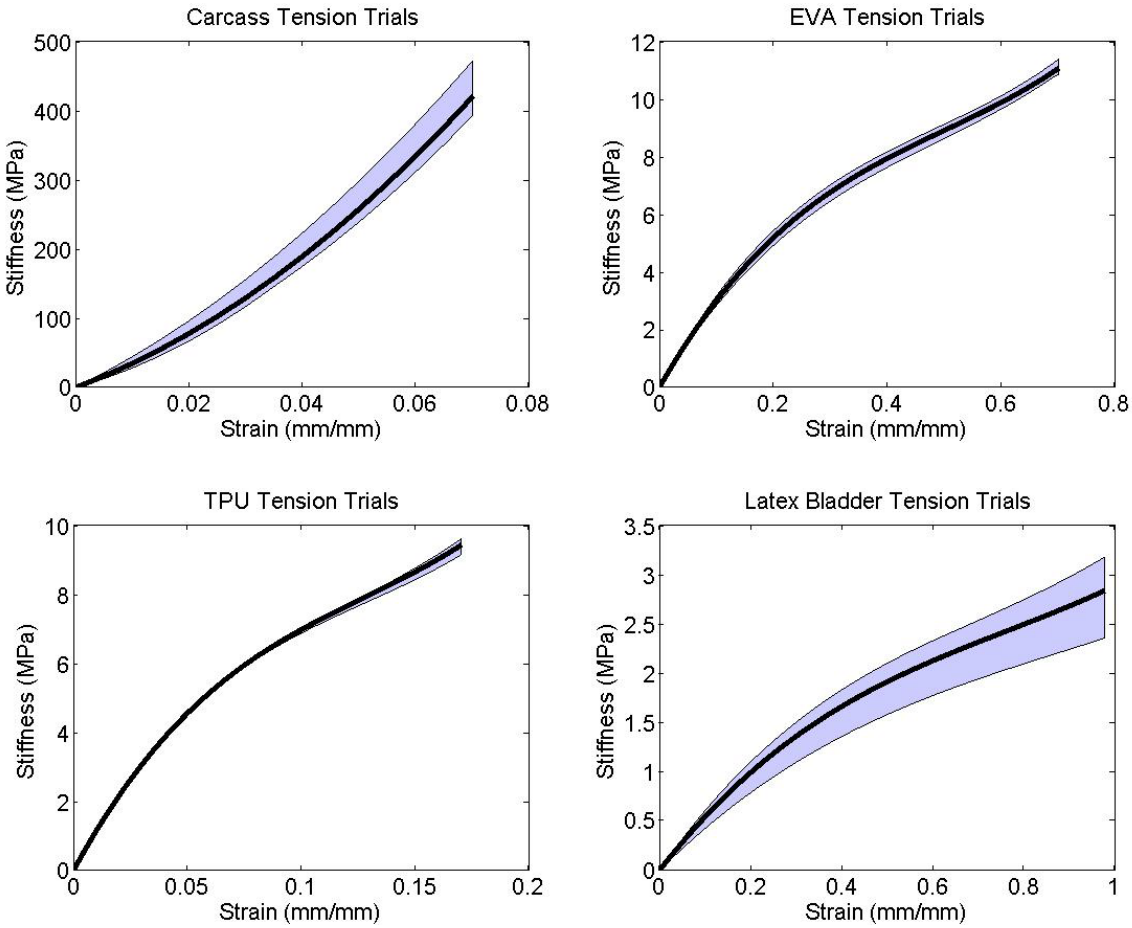

Figure 10: Material Tension Repeatability, carcass tested at a 90° orientation, shaded area represents minimum and maximum values seen

3.3 Variations in Test Protocol

3.3.1 Representative Strain Rate vs. Representative Strain Magnitude

During an impact, a football spends less than 10ms deforming and reforming while in contact with the ground. The ball reaches total deformation and up to 25% strain in only 5ms. Such short times and high strain magnitudes equate to very fast strain rates which are problematic when trying to develop material tests representative of expected loading scenarios. Machines capable of high strain magnitudes and high strain rates are difficult to create because of the energy required to move clamps great distances quickly. For this work, a DMA machine (Mettler Toldeo International, Columbus Ohio), capable of high frequencies (on the order of 100Hz) and low strain magnitudes (< 2% strain on 5x25mm samples) was available. With opposite attributes of higher strain magnitude (7%) and low strain rate (<10Hz), an electromagnetic dynamic load frame (Instron ElectroPuls E3000, Instron, Norwood Massachusetts) was also used in this comparative study.

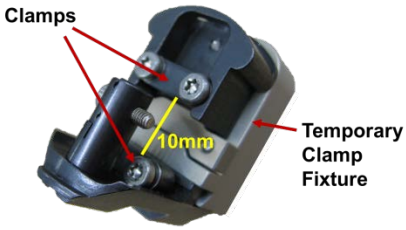

Figure 11: DMA Tension Clamps

Figure 12: ElectroPuls, lightweight clamps, base-mounted load cell

Tanδ (tangent of delta), the ratio between loss and storage moduli, is a measure of strain-rate dependency and viscoelastic effects and it is representative of the information that is used in FE

material models. The DMA output tanδ and other relevant parameters (elastic modulus, storage and loss moduli) at a range of loading rates (specified by frequency) automatically. Due to the small specimen size and material compliance, consistent clamping was challenging. Tension tests were chosen because it was the primary mode of deformation expected in the football. The 5x25mm samples were clamped by plates held with screws that were tightened with a torque nut driver but as the material was compressed between clamps, the portion between the clamps lengthened slightly. Light tension on the sample while tightening the clamps reduced the bowing effect but determining the pre-test strain then became a challenge. Figure 13 shows two tanδ curves of the same sample tested back-to-back and the tanδ values are relatively close to each other between 150 and 250Hz, the section of data likely to be used most in the simulations.

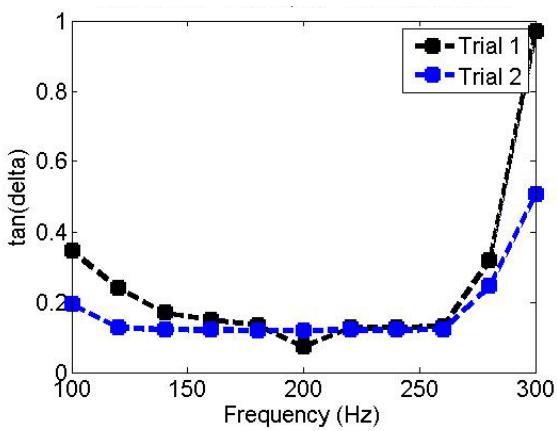

Figure 13: DMA Back-to-back Comparison, Carcass Fabric, 90° Yarn Orientation

The Electropuls is not normally used for this type of analysis so a more deliberate approach based on dynamic mechanical analysis methods was developed. By mounting a small, 250N load cell on the base plate and using light-weight clamps, the electromagnetically actuated piston could move +/- 2mm about the preloaded displacement at up to 10Hz. With this small displacement, the TPU, EVA, latex, and butyl materials were too compliant to provide a resistive force within the recommended range of the load cell so fabric at a 90° yarn orientation was chosen for the tests. Tensile strips (20mm x 50mm gauge length) were chosen over dog bones because of the ease in strain calculation and the maximum strain seen was 7%. Driving with displacement, the machine oscillated the specimens to the maximum strain magnitude at 10, 8, 6, 4, 2, and 1Hz sequentially. Fifteen cycles were completed at each frequency to let the automatic control loop adjust electromagnetic power to hit the desired strain. The desired strain was set based on the physical limits of the machine, set by the power of the machine and the weight of the moving components in the load string. The phase difference between force and displacement peaks in the time domain for the last cycle at each frequency was calculated using a bespoke program written for Matlab (Mathworks 2014, Mass. USA)

(see Figure 14). The phase difference, δ, could then be used to calculate storage (M') and loss (M") moduli with stress (σ_0) and strain (ε_0):

$$M' = \frac{\sigma_0}{\epsilon_0} \times \cos\delta$$

$$M'' = \frac{\sigma_0}{\epsilon_0} \times \sin\delta$$

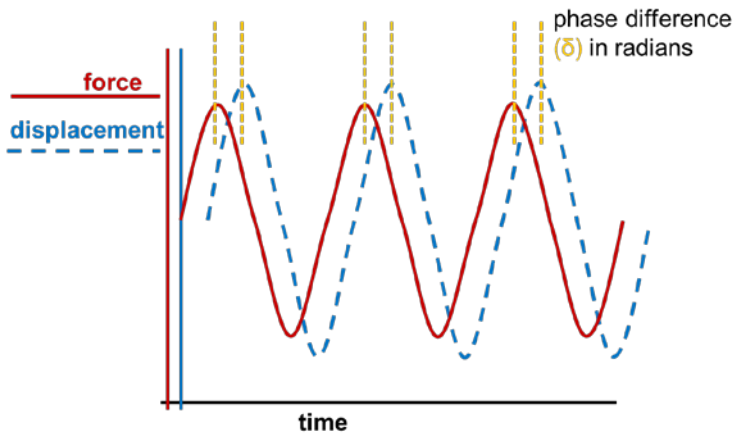

Figure 14: Dynamic Data Processing Example Diagram, time difference (phase) between force and displacement sine waves

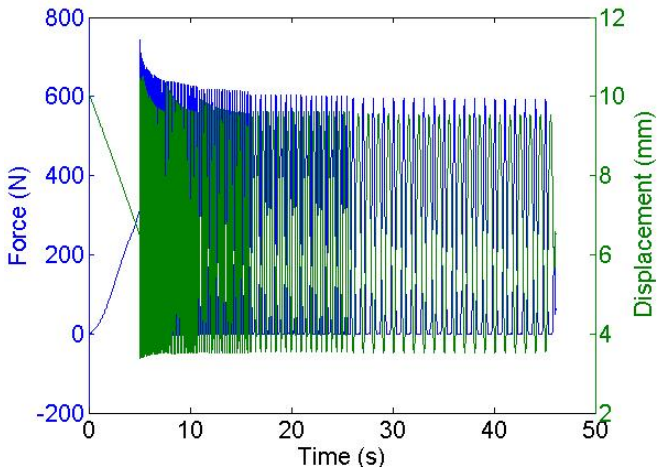

Figure 15: Time Domain Force and Displacement from ElectroPuls (fabric test example)

Figure 15 shows the force/time and displacement/time data extracted from the Electropuls software. Greater frequencies were run first to minimise creep or conditioning that may happen at very slow frequencies. The DMA tests were run in a similar frequency range to provide an even comparison but the maximum strain was around 1% (DMA was force driven, low strains). Five Electropuls and DMA tests were run and representative trials of each are presented in Figure 16.

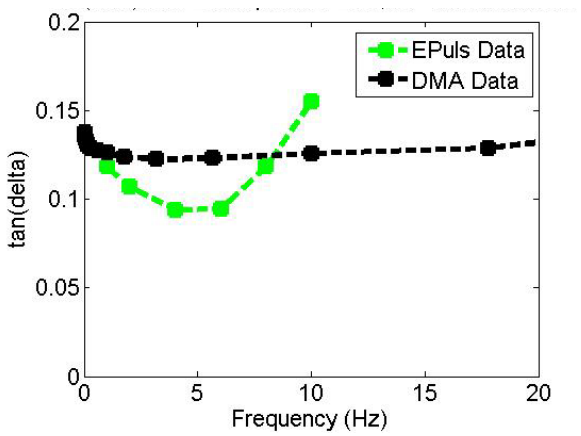

Figure 16: Tan(delta) from Electropuls and DMA at low frequencies, Carcass Fabric 90° Yarn Orientation

The general shape of both curves – high-low-high – was as expected based on what was seen in the literature (Price et al. 2008). A high tanδ represents more energy loss and low frequencies will start to exhibit effects of creep and stress relaxation. At higher frequencies, a high tanδ could also be the result of viscous behaviour as the fast loading pulls at and breaks polymer bonds, losing stored strain energy. It was not clear whether the Electropuls test data or DMA test data was most representative or suitable as the basis for a material model; both were in the same range as previous DMA work on similar materials (Price et al. 2008). As discussed earlier, the best judgement of a material characterisation method is whether it contributes to a model that accurately represents reality. In scenarios where the model will be used to compare the effect of various materials or material properties on the overall behaviour of the football, repeatability and consistency of the test method is most important for characterisation. It may be more important to know if two materials are within 5% of each other than if the measured value of one material is within 5% of its actual stiffness. Both absolute and relative comparisons have value in simulation. For this reason, the Electropuls was chosen as the primary method of energy storage/loss related data collection and included in the model as a Prony series which was extrapolated to 100 Hz as necessary in the simulation. The variability seen when clamping materials for the DMA decreased confidence in the ability of the machine to give both absolute results and consistent representation of multiple materials for comparative studies.

3.3.2 Fabric Characterisation

3.3.2.1 Dog Bone vs. Strip Specimens

If stress and strain are measured properly, dog bone and strip tensile tests should provide the same result for isotropic materials within the elastic range. For the anisotropic fabric, the situation was a little different because of the scale of the anisotropy and the two materials involved. The synthetic polymer matrix and yarns, with dramatically different properties allow for a fair amount of variability

in measured tensile stiffness. Dog bones and strip specimen were tested to explore the sensitivity of the material to specimen configuration in a variety of yarn orientations. The differences are useful to keep in mind when considering temperature testing and simulation results and they may allow for more level comparisons with previous work by other researchers.

The dog bone shape used standard punch die that produced a gauge length of 25mm and width of 3.8mm before widening out to about 12mm at the clamps, similar to a type V sample in the ASTM standard D638 (ASTM International 2003). The strips had 70mm between the clamps and were cut with a sharp blade to 22mm wide, taking advantage of the entire available clamping surface. In these tests, strain was measured with a video extensometer, an optical device that precisely measures strain between two drawn-on marks 20mm apart. Specimens were cut with yarns in line with the tensile pull (0°) and at 15°, 30°, and 45° strains to at least 6% (longer for the strips than dog bones).

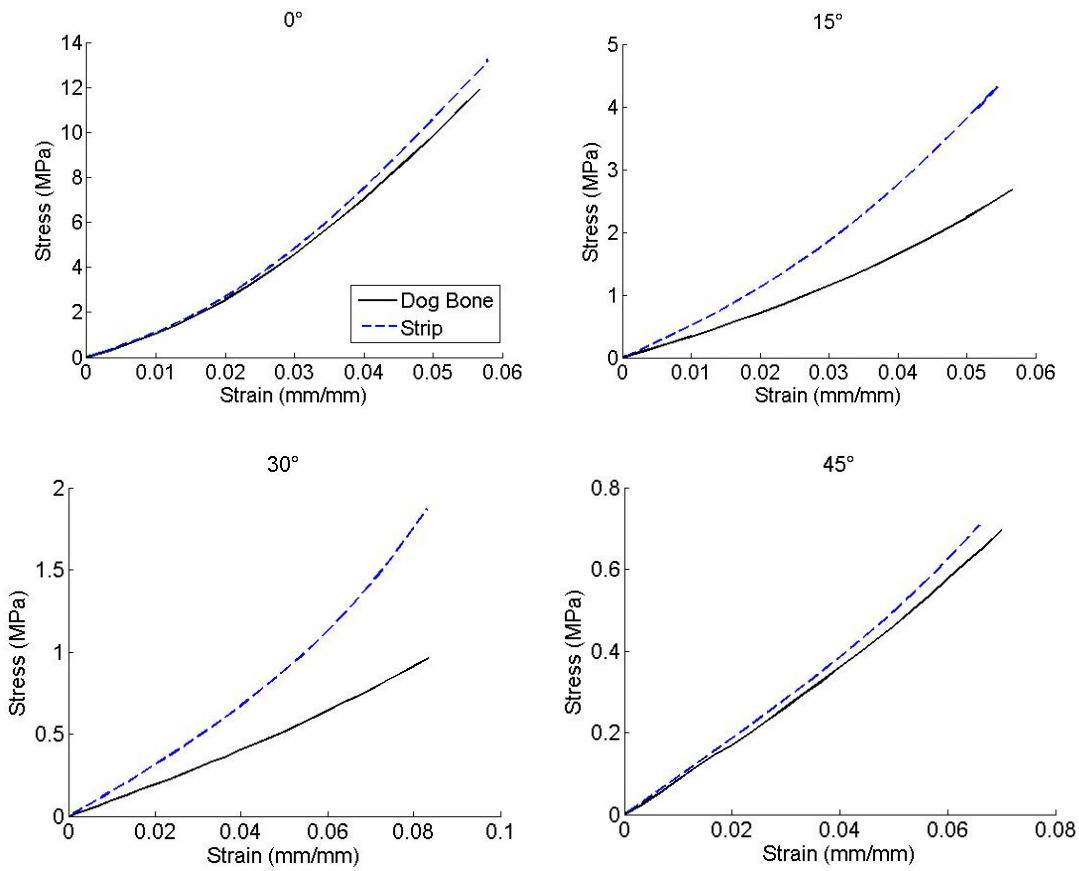

Figure 17: Dog Bone vs. Strip Fabric Tension

The graphs in Figure 17 (note: with different y axis scales) show the stiffness for each yarn orientation when measured with the two different specimen geometries. The results at 90° were nearly identical but the gap in stiffness widened at 15° and 30° before closing to nearly identical

again at 45°. This indicated a relationship between anisotropy measurements and specimen geometry that could produce misleading results if using the data without fully understanding the testing. Inspecting the yarns in the specimens helped explain the discrepancy in tensile stiffness.

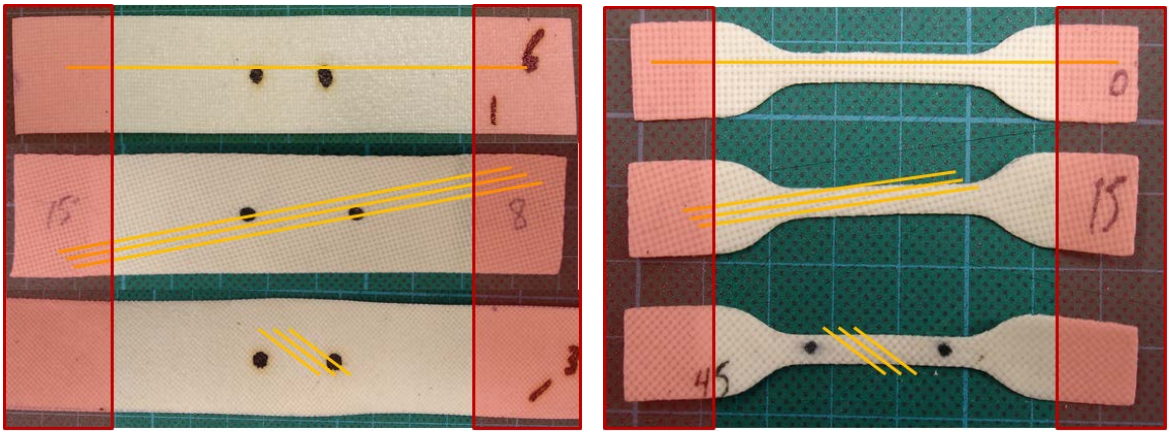

a b

Figure 18: a) Fabric Strip Specimens, b) Fabric Dog Bone Specimens, yellow lines represent the yarn direction, red boxes represent the area held in clamps

At a 0° orientation, yarns in each specimen span the clamps depicted with red boxes in Figure 18). Pulling directly in line with yarns and pulling the yarns directly elicited the stiffest response from the material independent of specimen width. At a 15° angle, yarns in the strip still extend from clamp to clamp but the angle combined with the dog bone shape prevents any single yarns from covering the entire distance. The result for the dog bone was a much more compliant response, as the dependency on the latex matrix and yarn interaction became more important relative to the tensile stiffness of the yarns. At a 45° angle, neither the strip nor dog bone samples had continuous yarns between clamps so they once again produced similar stiffness results. Orthogonally woven fabric was expected to be stiff at 0° and compliant when stretched at 45° to the warp and weft but exactly where the intermediate angles lie between the two extremes was difficult to decide.

In earlier work (as discussed in the literature review), anisotropic models have been built up from individual tests at range of yarn orientations (elastic lamina). Though the 0° and 45° orientations seemed relatively independent of sample geometry, the anisotropic models may have not captured the gradual transition from stiff to compliant orientations. These anisotropic properties could be better tested with longer samples (greater length-to-width ratio) but for practical reasons, specimen length was limited. For this reason, and the inability of the model to capture the obvious non-linearity at any angle, the elastic lamina model was set aside in favour of the *fabric modelling methods within Abaqus/Explicit and new material characterisation tests. The * notation (ie *fabric) is frequently used in finite element analysis code to denote a keyword used to call a specific function into use.

3.3.2.2 Picture-Frame Fabric Anisotropy Test

A picture frame material test apparatus was constructed in-house to carry out testing for the *fabric material model in Abaqus. The apparatus (Figure 19) was built of steel with smooth rotating plastic bushings at the hinges. The square section (marked in Figure 19) was 70mm and the frame had 110mm between clamping surfaces. Fabric was clamped in on four sides between semi-cylindrical 3D-printed inserts resting in semi-cylindrical cut outs on the steel clamp face. The inserts had a bump and groove that served to secure the fabric in place and they were interchangeable to accommodate various material thicknesses.

Figure 19: Picture Frame Shear Apparatus

The picture frame apparatus fit in a screw-type load frame (Instron 5569) and was extended quasi-statically by 40mm (at 50mm/min) to give a maximum of about 20% strain. The force-displacement data from the machine was converted to stress and strain (represented by shear angle) with the following equations (Harrison et al. 2004):

$$\theta = \frac{\pi}{2} - 2\sec\left(\frac{1}{\sqrt{2}} + \frac{d_{xhead}}{2l_{frame}}\right)$$

$$\sigma = \frac{f_{tensile}}{\left(2l_{fabric}t_{fabric}\sin\left(\frac{\pi}{2} - \theta\right)\right)}$$

θ = shear angle

σ= shear stress

d_{xhead}= crosshead displacement

l_{frame} = length of one side of frame (hinge to hinge)

$f_{tensile}$= tensile force (from load cell)

l_{fabric} = length of inner fabric square edge

t_{fabric}= fabric thickness

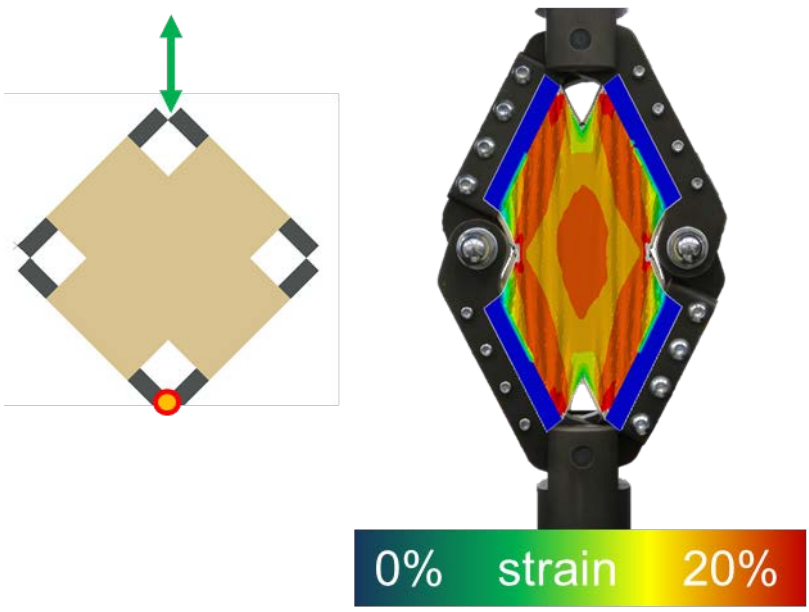

Figure 20: Picture Frame Shear Simulation

These data, combined with tensile test data in the 0° and 90° (warp and weft) directions, create a nonlinear fabric model in Abaqus using the *fabric keyword. To test the computer's approximation of material behaviour, the picture frame test was replicated in a finite element simulation with the same type of 2D shell elements intended for use in the complete football model (1mm target element edge length). On qualitative observation, the simulation matched the slight out-of-plane waves seen at full extension in the physical lab tests. Comparing force-displacement data, the *fabric model used in the simulation shows very good agreement with the lab test (see Figure 21).

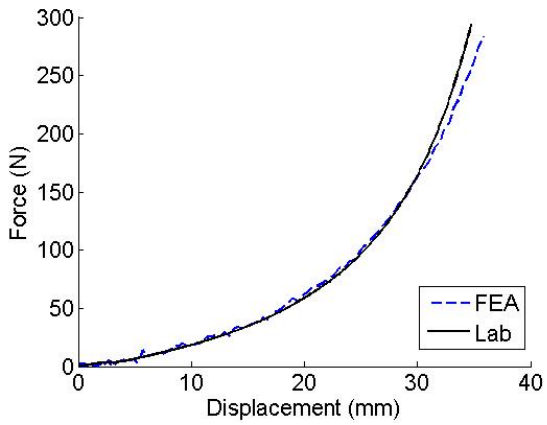

Figure 21: Picture Frame Shear, FEA vs. Lab Test

Considering the documented influence of anisotropy on football deformation behaviour, accurately measuring and modelling the fabric was important for capturing one of the defining aspects of an impact.

3.3.2.3 Tensile Test Simulation and Validation

As an initial comparison of the fabric measurement and modelling differences between "*elastic" and tensile-only data and "*fabric" with the inclusion of the picture frame test, tensile tests were simulated. Boundary conditions (prescribed displacements and/or loads, forces, pressures) were designed to replicate those used in physical lab testing and the two material properties were applied with 0°, 30°, and 45° yarn orientations.

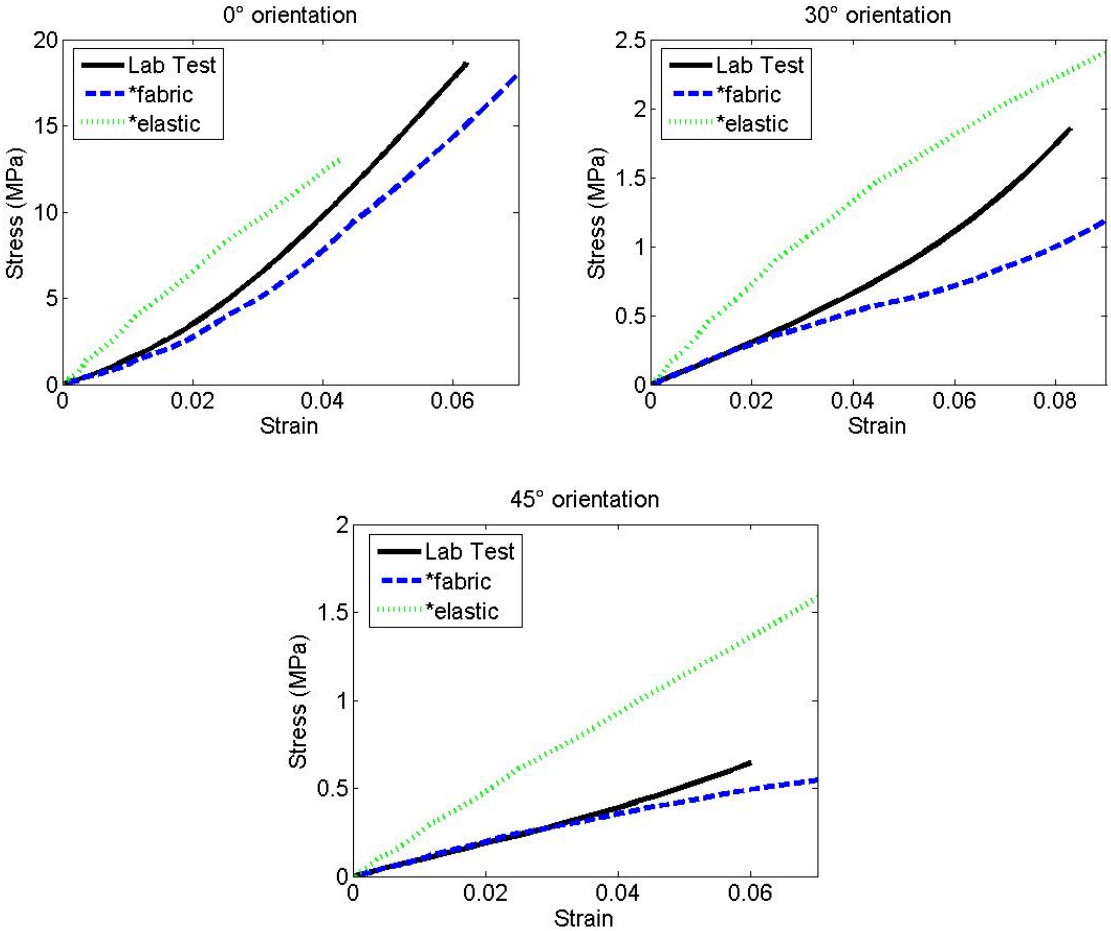

Figure 22: Tension strip-only linear (*elastic) and tension with shear (*fabric) simulations vs. lab data

Due to the non-linearity of the *elastic model, the stiffness was likely only correct at one strain magnitude. Figure 22 shows similar stiffness between *elastic and lab data at roughly 2% strain in the 0° orientation but at greater and lower strains, the trends in the simulation were not representative. The disparity was also large at 30° and 45° yarn orientations, which may also have been due to poor linear approximations of non-linear data but the yarn configuration and specimen size/shape discussed in the previous section likely influenced the result as well. The *elastic differed from the lab test in that it would have a given stiffness for a yarn orientation that is completely independent of specimen size or shape. The *fabric model followed lab test data more closely and captured the general trend better than the *elastic model.

3.3.3 Materials Before and After Processing

Predictive modelling can be a valuable tool, allowing engineers to virtually test prototypes before a complete product is made. This involves building the model from the ground up, starting with the geometry and properties of individual material constituent components. In this work, raw, pre-processed materials were available for testing but the manufacturing procedures have the potential to make predictive modelling a challenge. When building a football, each material undergoes

multiple forming and bonding processes that may influence stiffness, compressibility, and energy properties.

The thermo-plastic polyurethane (TPU) outer skin used on some footballs begins as a flat sheet but the graphics add a measured 0.05mm and the sheet is vacuum formed under elevated temperature to add “aero-grooves” (a brand specific term), small bumps for texture, and the spherical contour. This process causes changes (detailed later) in thickness and weakening from potential deformation outside the elastic range. The EVA foam is not produced then moulded like the TPU but rather created in the desired shape first as either flat sheets (as in adidas Tango12 2012) or spherically moulded panels (like adidas Jabulani 2010). Test samples of EVA, however, were available as a thick sheet (1x10x10cm). The ‘skin’ of the foam, where the surface of the part meets the mould, has different properties than the open cell material at the centre of a block (not dissimilar to crust and bread) (Michaeli et al. 2009). Different foam thickness and ratios of foam skin to internal foam will likely exhibit different stiffness. Figure 23 shows images of foam with and without skin – effectively the outer surface, and a cross section view. The inner section has a much more open structure and can be expected to behave more compliantly.

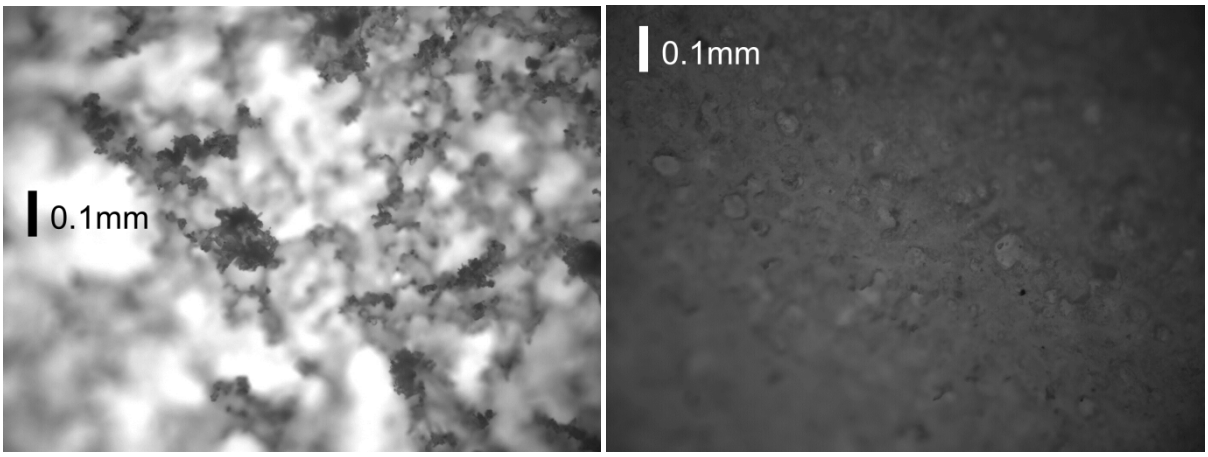

Figure 23: EVA foam, inner - blade-cut surface (left) and outer moulded surface (right)

The carcass fabric and latex polymer matrix are subjected to temperatures of 130°C in the forming process, potentially altering material properties of the polymer and consequently removing residual stresses in the yarns and their positioning. Fabric before and after assembly as well as other materials from a 2010 adidas Jabulani were tested in various stages of assembly.

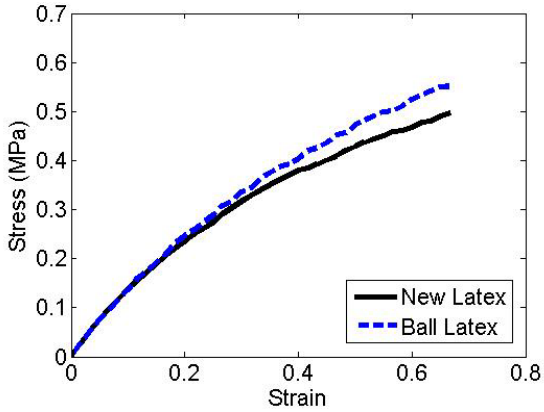

Figure 24: Pre- vs. Post-Assembly Latex

The latex material shown in Figure 24 was tested as a 6mm wide dog bone stamped from a bladder before ('New Latex') and after assembly ('Ball Latex') and had the smallest change of the materials tested. The bladder in a football is not expected to strain more than 20%, where the difference starts to become more noticeable.

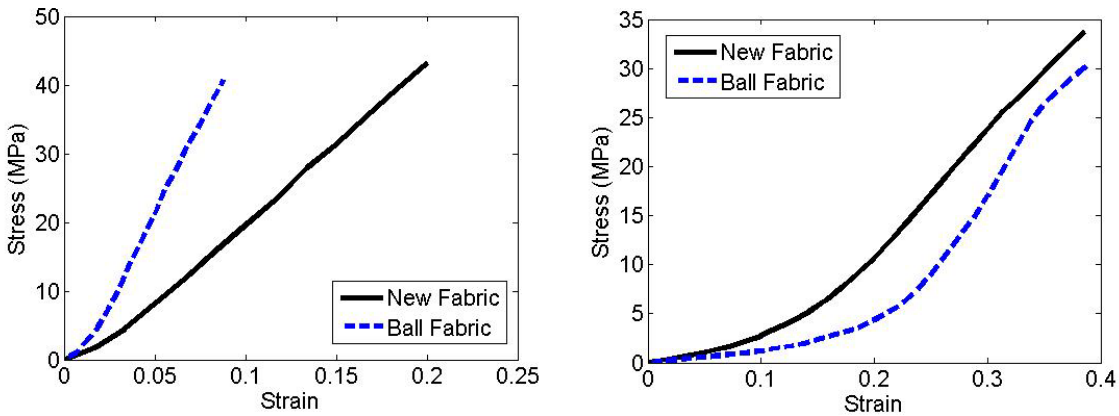

Figure 25: Pre- vs. Post-Assembly Fabric, 90° (left) and 45° (right) yarn orientation

The carcass fabric exhibited a significant change in the assembly process. Figure 25 shows the material tested at two yarn orientations with opposite results. When pulling in line with the yarns in the 90° sample, the material taken from the ball was more than twice as stiff (440MPa vs. 210MPa based on linear approximations). This difference may be accounted for by considering the strain required to make the football spherical during both production and match play. The 12 flat pentagons used to create the stitched carcass for the Jabulani (from which materials were extracted) must strain a predictable amount to have a spherical profile. Dimensionless calculations showed that the arch between the two most distant corners of the pentagon is 7.3% longer on a sphere than as a flat shape (see calculations in Appendix 9.1) and the spherical-contoured pentagon as 2.5% more surface area than the flat shape. These values were supported with a simple finite element

model simulating the inflation of a flat-panelled dodecahedron with isotropic materials. In this basic model, the panels were modelled with 2D shell elements with target element edge length of 4mm, 1mm thickness and arbitrary material properties. The internal pressure was increased, forcing the dodecahedron into a sphere, the shape of lowest strain energy, and the resulting strains (shown in Figure 26) corresponded with the geometrically predicted strains.

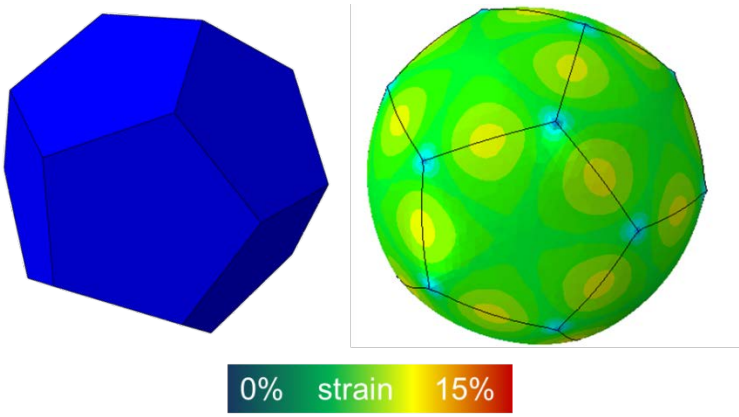

Figure 26: Flat-panel dodecahedron (left), after inflation (right)

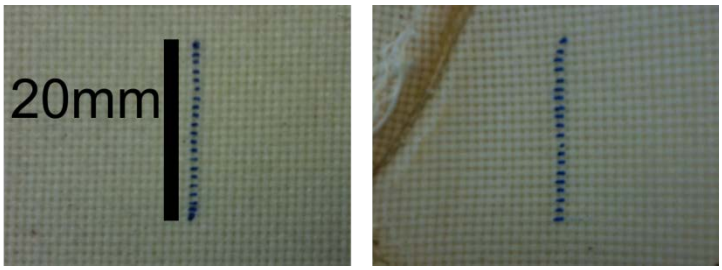

Figure 27: Carcass fabric before assembly (left), and cut from an assembled ball (right)

Knowing the fabric must strain to assume a spherical profile, samples were cut out of a ball and examined in a relaxed state to determine whether the strain remained. When comparing the yarns in the fabric before and after assembly (Figure 27), the spacing went from approximately 20 yarns per millimetre to 21 yarns per millimetre, a 5% increase in spacing (strain). Though there was no strain energy stored in the strained fabric, the assembly processes removed any initial slack in loosely-spun yarns providing a much stiffer response.

The 45° yarn orientation had the opposite result presumably because the yarn stiffness played a smaller role. Heat from the forming process may have damaged the polymer matrix and strains could have weakened the bond with the yarns, allowing for more slippage and a more compliant response. At higher strains, the slope of the stress-strain curve for post-assembly fabric approached

that of pre-assembly fabric. This may be attributed to the yarn direction approaching alignment with the clamp axis at higher strains, allowing for a greater influence of yarn tensile properties.

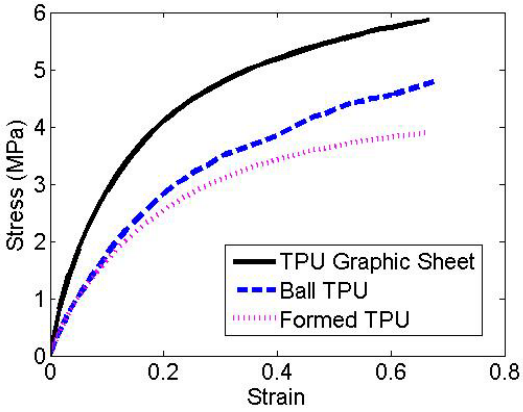

Figure 28: TPU Skin - graphics, forming, post-assembly

The TPU material was available in several states. Before any forming or bonding, the TPU sheets were normally clear but the graphics added 0.3mm. The vacuum-formed TPU sheets did not have the graphics, but had a spherical profile including the bumps and grooves and the TPU taken from the ball was cut from panels and the EVA foam was removed by hand (NOTE: The foam could not be removed from a complete ball in pieces large enough to test – it came away in chunks). Vacuum formed parts with the graphics before assembly were not available. The results of tensile testing in Figure 28 suggest that the process of applying graphics strengthens the material and the vacuum forming weakens it. TPU stiffness as low in comparison with the carcass fabric; materials must be considered together in the appropriate context when trying to determine the effect of small changes on the end result.

3.3.4 Testing Composite Sections

In an attempt to include the bonding effects between materials in addition to other artefacts of assembly, materials in sub-assemblies were tested as well: TPU bonded with EVA before final assembly with the carcass, and fabric bonded with TPU and EVA cut from a ball. The anisotropy was modelled with the linear elastic model based on 90° and 45° material tests. To gauge stiffness differences, the material configurations were put in virtual ball simulations of inflation to observe the materials in situ. Only pre-assembly latex was used because of the small differences seen with post-assembly latex. The football models (discussed in detail in Chapter 4) were inflated to 90 kPa and the resulting post-inflation pre-impact volume was taken as an indication of relative stiffness. Table 1 gives an indication as to the effect of the state of tested materials on the end result. The stiffest ball configuration (that with the lowest volume), included the fabric taken from the ball. The general progression was an increase in compliance as more pre-assembly materials were included.

Scenarios 2 and 3 were within less than a per cent of each other and cannot be compared but Scenarios 4 and 5 suggested that the bonded EVA and TPU, despite the weakness introduced by vacuum forming, was stiffer than the two materials tested and represented independently.

Table 1: Testing Composite Sections

	Tested Material Configuration	**Simulated Volume (mm^3)**
1	latex + (fabric from ball) + (EVA + TPU)	5420
2	latex + (fabric from ball) + EVA + (TPU from ball)	5530
3	latex + (fabric from ball) + (EVA + TPU before final assembly)	5540
4	latex + (new fabric) + (EVA + TPU before final assembly)	5690
5	latex + (new fabric) + EVA + (TPU, graphic, before forming)	5740

The 5.4% difference in volume between pre-assembly materials (Scenario 5) and post-assembly materials (Scenario 1) was measured to be 4.1mm over a 220mm diameter and must be considered when creating and using predictive models. Identical footballs after a season or a typical service life exposed to thousands of impacts and environmental changes were not available for destruction and testing. Regulations are in place to ensure that FIFA Approved footballs maintain the same size and shape after 2000 sequential 20m/s impacts and the polymers are assumed to change little throughout the life of the ball. It is possible that post-season materials are as different from post-assembly materials as post-assembly were to pre-assembly. The work at present does not investigate the durability of the football.

For virtual experiments in which the overall behaviour of the football is important, these composite material section tests may serve as a time-efficient way of gathering information for the models. The effects of processing during assembly were tangible so there is a good case for using materials in various stages of processing. The work of this document was more concerned with the individual contributions of the different components and materials. Though the model created from pre-assembly material data may have differed slightly from the properties of a physical production ball, the flexibility and opportunity for manipulation provided by individual material models was judged to be worth the small cost in accuracy. When interpreting results of simulations created with pre- or post-assembly material models, the nature of the input data must also be taken into consideration.

3.4 Temperature-Dependency

There was potential for a glass-transition to fall within the wide range of possible match-day temperatures so a study into the effects of temperature on football materials was conducted. Even without the official glass-transition, it was expected that the materials would stiffen with decreasing temperature. An understanding of possible stiffness changes for the ball materials provides a starting point for establishing reasonable upper and lower bounds when exploring the effects of material property changes in general. The test was conducted with tensile dog bones for the polymers (EVA – 3.5mm, TPU – 6.5mm, latex – 6.5mm) and strips for fabric (~22mm wide, but individually measured). After the results of the incremented strain tests used to explore the Mullins effect, the decision was made to evaluate the materials based on data from the first extension. The difference between the Mullins adjusted curve and the first pull was judged to be worth avoiding the risk in plastic deformation. A digitally controlled temperature chamber (Instron 3119 series), heated with electric elements and cooled with liquid nitrogen, was used to condition and test the specimens. Specimens were left in the chamber for at least ten minutes and their temperature was verified with a laser thermometer (Minitemp FS, Raytek (Fluke), Santa Cruz, California, USA) before testing. Tensile extension was at 2mm/s and the materials were strained well within their elastic limits. For the room-temperature tests, strain was measured with a video extensometer using a 20mm gauge length. Due to practical difficulties, the video extensometer could not be used with the climate chamber; flecks of frost distracted the optical system. Rather than base strain for the chilled trials directly on clamp displacement, a linear relationship between displacement and strain from video extensometer was drawn for each material and specimen size. Of the dog bone specimens tested, the R^2 values for the linear fit relating displacement and strain for the latex, TPU, and EVA and TPUEVA were 0.9995, 0.9719, 0.9964, and 0.9877 respectively.

Qualitatively, the EVA foam, TPU, and polymer-infused carcass fabric samples felt noticeably stiffer to the touch at colder temperatures and the latex appeared slightly more translucent. The medial stress-strain curves of the five specimens tested for each scenario are presented in Figure 29.

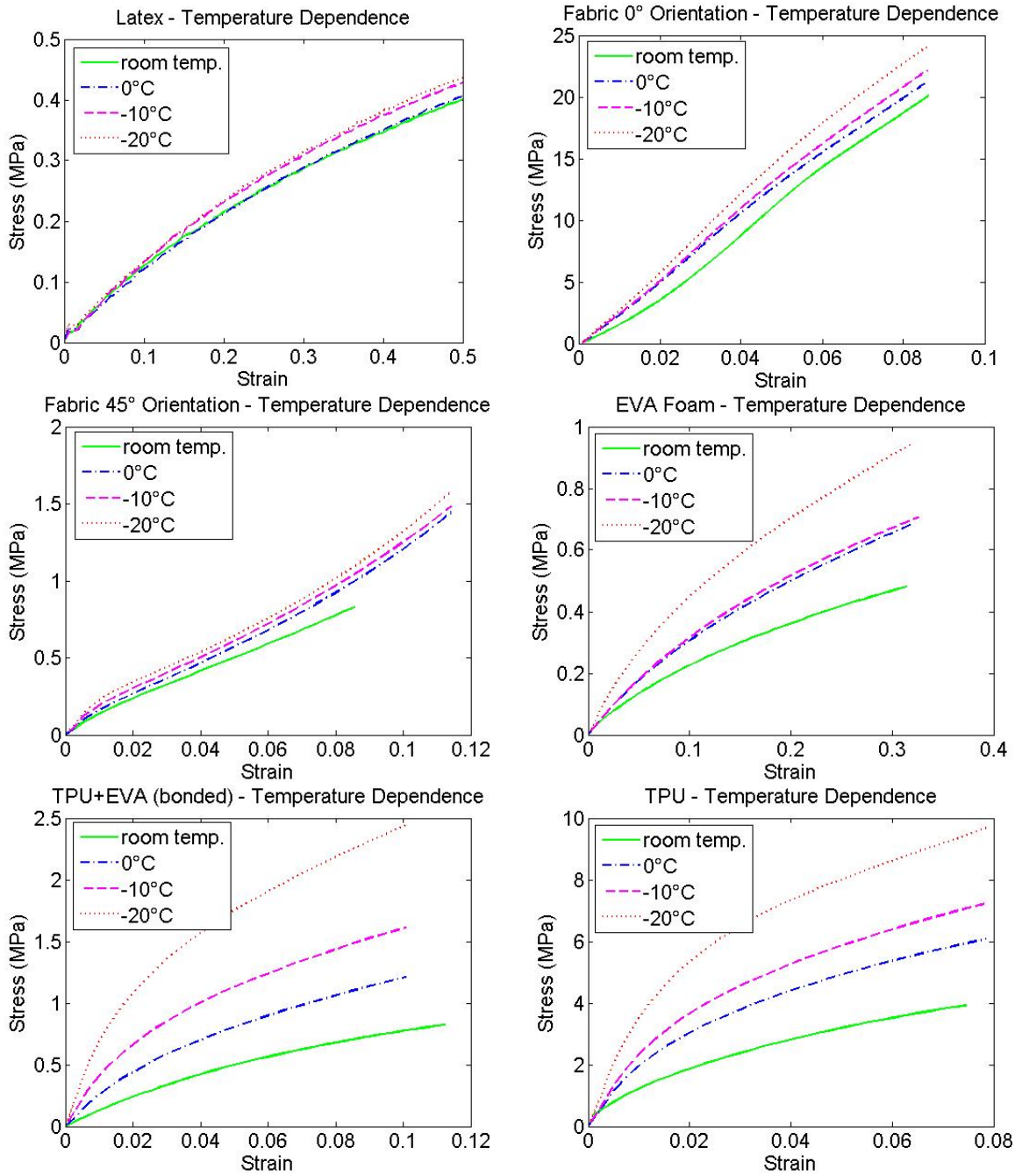

Figure 29: Temperature Dependency

The stiffness of the latex and carcass fabric (which includes a latex-based polymer matrix) showed considerably less temperature dependence than the TPU and EVA outer panel materials. The small, yet clear difference between 0°C and -10°C indicated an abrupt change that was likely due to nonlinearity in the temperature-stiffness relationship rather than crossing the transition threshold to glass-like behaviour. The two fabric samples did not seem to follow any trends, perhaps because the majority of the stiffness was due to the relatively temperature-independent yarns.

The TPU, EVA, and the bonded combination exhibited great thermal dependence. Comparing the materials at -10°C and room temperature, both at 10% strain, EVA showed a 59% increase in stress, TPU was 84% stiffer, and the bonded combination was 92% stiffer. Considering the stiffness change in the context of the entire ball, it may seem small – a fraction of the carcass fabric stiffness. Though these changes in EVA and TPU may not significantly alter the global behaviour of the ball as a pressure-volume relationship or large-scale deformation deviation, greater stiffness in the outer panels may be readily perceived in local, smaller deformations such as slow kicks or handling.

3.5 Summary

This chapter has explored variations in material testing techniques for the purpose of creating a finite element model. Studies included dogbone vs. strip tension testing, methods of accounting for the Mullins effect, two methods of capturing time-dependent data, temperature dependence of materials, two methods of testing for and representing anisotropic behaviour of fabric composites, and the influence of manufacturing processes on the constituent materials.

The sample geometry shape was seen to have an influence on testing fabrics with different yarn orientations but an in-plane shear testing method and characterisation algorithm (*fabric) allowed for adequate anisotropic characterisation. The relative compliance of subsequent loading cycles known as the Mullins effect was seen in the football material tension tests. Cyclic loading at incrementally increasing strain intervals prevented high-strain repetitions from influencing the materials' behaviour at low strains.

DMA testing was used in a frequency sweep to capture time-dependent data of the football materials but challenges with clamping consistency and the low, non-representative strain magnitude favoured a test protocol developed to use an electromagnetic dynamic load frame. The new protocol collected the same data but at strain magnitudes representative of what was expected in the football and much lower strain rates. The data were used in a Prony series for viscoelastic characterisation.

Testing with a climate chamber indicated that the most thermally-dependent materials were the polymers, specifically the TPU outer skin and EVA foam. This data could be integrated into the simulation but it was also useful on its own, indicating potential changes that may happen in varying climates.

Tests of materials and components in various stages of assembly/consolidation indicated that the effects of processing and assembly were not negligible. For example, the carcass fabric cut from the ball was stiffer than the fabric before processing. This was an important finding because it exposed

the limits of material testing for FEA development. Though the individual material data may not combine to make the most accurate assembled ball, the flexibility afforded by testing and modelling individual materials was deemed worthwhile for relative comparisons and investigative purposes.

4 Finite Element Analysis Models

4.1 Intentions

Models were created individually to help efficiently address specific aspects of the football research. Laboratory experiments with a variety of football constructions and different materials was not possible for reasons of cost, time and availability but simulation provided a unique opportunity to rapidly predict the behaviour of different football configurations, helping to establish likely trends in the physical world. Finite element analysis is a trade-off between computational resources and detail – it is costly to have high levels of detail about every aspect of a large simulation – so models are often created to provide detailed results only in the area of interest. For the football simulations, there was not one model created to represent all aspects of the ball perfectly but a collection of models designed with specific purposes (output) in mind. Models were created to closely study phenomena related to carcass anisotropy and these were different from the models modified specifically to run very quickly in automated optimisation and design-of-experiment algorithms. Models were also created to investigate local aspects like contact pressure and small-scale deformation and yet another set of models was created to look only at the global effects of material changes.

Due to the variety of ways the models could be constructed, it was important to keep the details of the particular modelling methods used in mind when considering the results. This chapter covers the development of the football models as well as the boundary conditions, outputs, and ways of implementing the model beyond single isolated impacts.

4.2 Basic Model

Due to availability both in standard, off-the-shelf configurations and custom variations thereon, the 2010 adidas Jabulani and 2011 adidas Speedcell served as the basis for virtual models. The two represent a significant difference in carcass construction. The Jabulani used a 12 panel stitched carcass and the Speedcell used a bonded patch carcass but both the dodecahedron and patch carcasses were bonded to composite foam outer panels.

The basic model was built in Abaqus/Explicit with reduced-integration 2D shell elements meshed on a 3D sphere with partition lines drawn to replicate important features of the carcass. Two-dimensional elements are appropriate when the overall dimension is around ten times (NAFEMS 1992) greater than the thickness and they can dramatically reduce computational time (Abaqus 2012). Accurate modelling with three-dimensional elements requires two or three elements through the thickness; one element will not perform adequately in bending. Shell elements have

proven adequate in similar applications (airbags (Marklund & Nilsson 2002; Sinz & Hermann 2008; Marklund & Nilsson 2003), football (Price et al. 2006; Rezaei et al. 2011)). The elements were assigned composite sections with the bladder, carcass, and/or outer panels as required. A fluid-containing cavity was defined using the inner surface of the elements and the surface pressure was tied to a special degree of freedom (the 8th, after translational, rotational and temperature) of a reference node inside the sphere. By placing a boundary condition on this degree of freedom, the ball could be uniformly pressurised with a simple specification at one node (airbag simulation example (Hirth et al. 2007)). The model's pressure response was governed by equations representing the thermodynamic properties of air but at any given time, the internal pressure was identical at every point on the inner surface. For the uniform pressure model, air was specified as follows:

- Molecular Weight: 0.0289
- Molar Heat Capacity c_p: a=28.11, b=1.976e-3, c=4.802e-6, d=-1.966e-9, e=0.0 J/MOL
    - Where $c_p = a + b(\theta - \theta^z) + c(\theta - \theta^z)^2 + d(\theta - \theta^z)^3 + \frac{e}{(\theta - \theta^z)^2}$
        - θ=temperature in Kelvin, (Abaqus 2012)
- Universal Gas Constant: 8.314 J/(mol*K)
- Absolute Zero: 0K

Three methods of implementing the uniform pressure method, each with different strengths, were identified and compared. The first was simply assigning a specific pressure to the volume through the cavity's reference point. The second involved specifying a timed mass flow-rate of air and the third put a defined gradual increase in pressure over 0.04 seconds. The first method, because of its simplicity and the short (instant) time of pressurisation, had the potential to be computationally efficient but any advantages at the beginning were lost while waiting for the dynamic system to reach static equilibrium. The initial inflation was too fast, creating a situation not unlike a small explosion in which the inner surface of the ball was exposed instantly to high pressures. The result was an oscillating ball that required analysis time before the vibrations were dampened.

Controlling the mass flow rate in the second inflation method was judged to be the most representative of physically inflating a ball with a pump. Attempting to mirror reality in the simulation required a significantly longer time period in the analysis step and consequently more computational time. As in the physical world, the amount of air required to reach the desired pressure depended on the stiffness of the ball so reaching the correct pressure required adding an amount of air, then checking the pressure and adding or removing iteratively. This was simple

enough to do once or twice but the inflation parameters would need to be calibrated for each football with different (stiffness) properties.

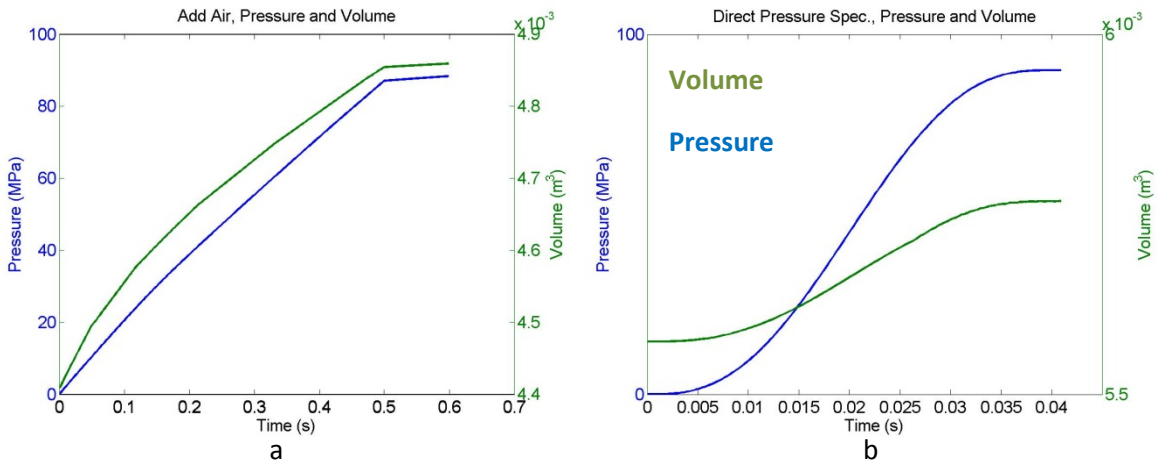

Figure 30: a) Adding Air vs. b) Direct Pressure Specification, pressure and volume curves show a faster yet smoother inflation

In specifying the pressure directly Figure 30 (right), the third method stepped a bit further away from a physically realistic scenario but the method met the end goal and the path to get there was relatively quick and efficient. The method was a compromise between the other two – direct pressure specification, but with a gradual increases – and it retained some of the positive characteristics of each.

Instant pressurisation as in the first inflation may be most appropriate for balls or cavities with very high energy damping characteristics but it was not efficient for the types of footballs in question. The second method's strengths lay in similarity to physical inflation. The method may be useful in situations where the mass of air inside is of greater importance, like investigating the effects of altitude or other external pressure change on internal pressurisation. For most simulations, however, the third method was judged to be the most flexible and computationally efficient.

4.2.1 Mesh Refinement

Mesh refinement and mesh density refer to the number of elements used to represent a structure. With a small amount of large elements, the results are not typically as reliable but as the element size decreases, the results are more accurate (Becker 2004). The appropriate number of elements depends heavily on geometry, boundary conditions, load scenario and desired results (NAFEMS 1992) so it is necessary to select an appropriate mesh density before progressing too far with an analysis. When starting with new projects, geometries or loading scenarios, the element size is decreased (increasing mesh density) in increments for a series of otherwise identical simulations and characteristic outputs are compared. As the mesh density increases, the size of the element will

have a smaller effect and the output will converge asymptotically at the theoretically most accurate solution. This 'converged mesh' is defined as one in which more elements are not worth the extra computational cost (NAFEMS 1992).

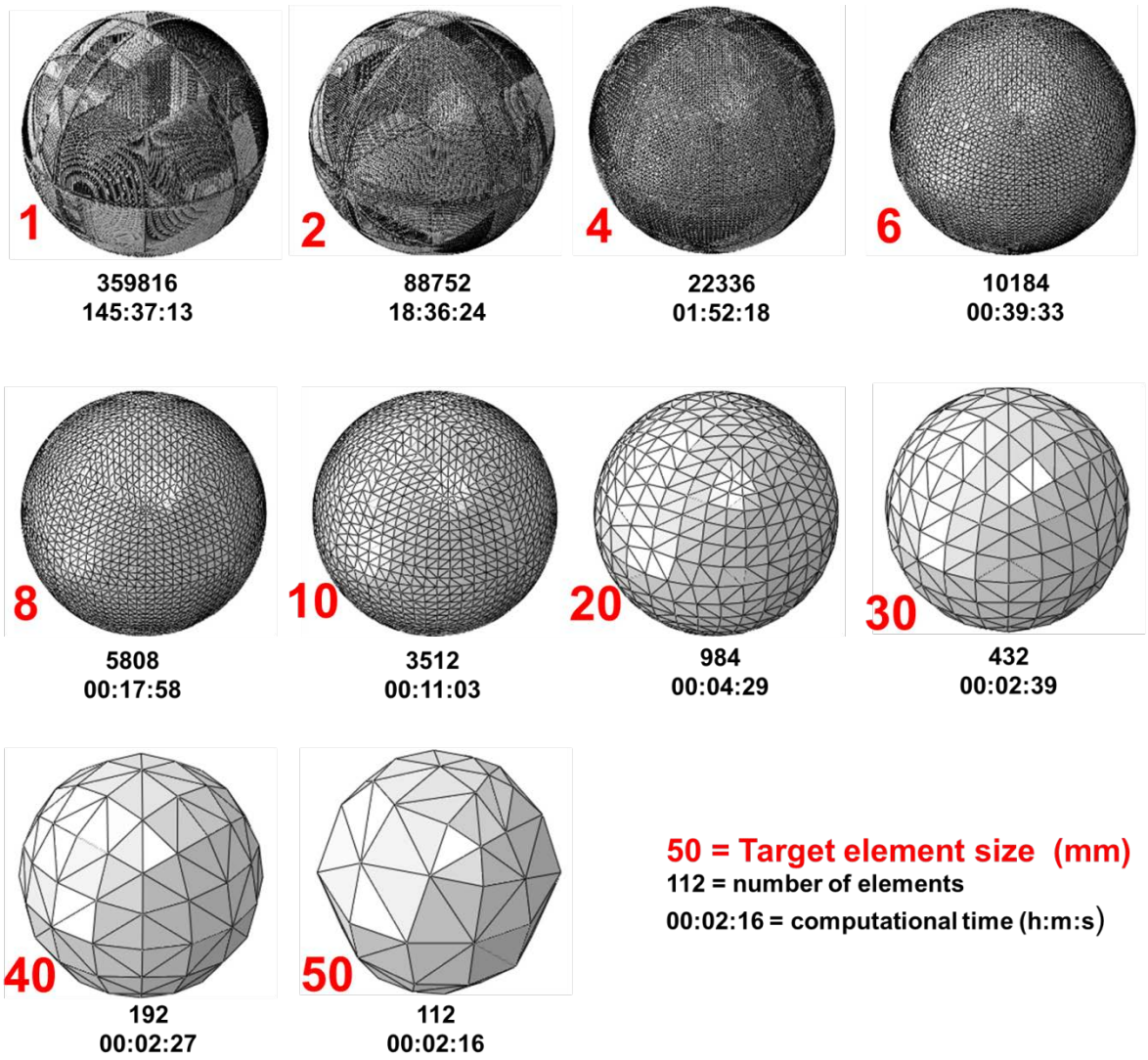

Figure 31: Mesh Refinement Study – range in mesh densities and their respective computational requirements

In this study, a mesh convergence test was performed with target element sizes from 50mm to 1mm, monitoring perpendicular deformation (Figure 32), impact plate reaction force, and volume change. Three-node triangle shell elements identical to those used in the complete model were given isotropic material properties with football-like thickness and isotropic stiffness. Figure 31 shows the meshes used, listed by target element size in millimetres. Table 2 shows the cost of a very fine mesh.

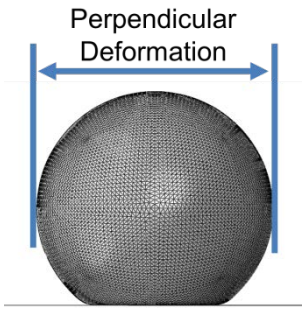

Figure 32: Description of Perpendicular Deformation

Table 2: Mesh Density and Computational Time

Mesh Target Edge Length (mm)	Number of Elements	CPU Time h:m:s
1	359816	147:37:13
2	88752	18:36:24
4	22336	01:52:18
6	10184	00:39:33
8	5808	00:17:58
10	3512	00:11:03
20	984	00:04:29
30	432	00:02:39
40	192	00:02:27
50	112	00:02:16

Figure 33 shows the deformation and volume change outputs with the different target element sizes. Though the main purpose of a mesh refinement study is to study how stress and strain can be influenced by the number of elements used, in this case, the geometry is also related closely with the number of elements. The dramatic difference above and below 10mm elements may be due to the poor spherical approximation of larger elements. Especially in the volume comparison, though the figure shows a change relative to the starting volume, an angular impact surface, rather than the more spherical shape of finer meshes, may alter the deformation characteristics beyond the overall stress-strain relationship. Considering the effect of the mesh on the results as well as the computational time required, the 4mm element size was chosen as the target and this served as a guideline for all football meshes.

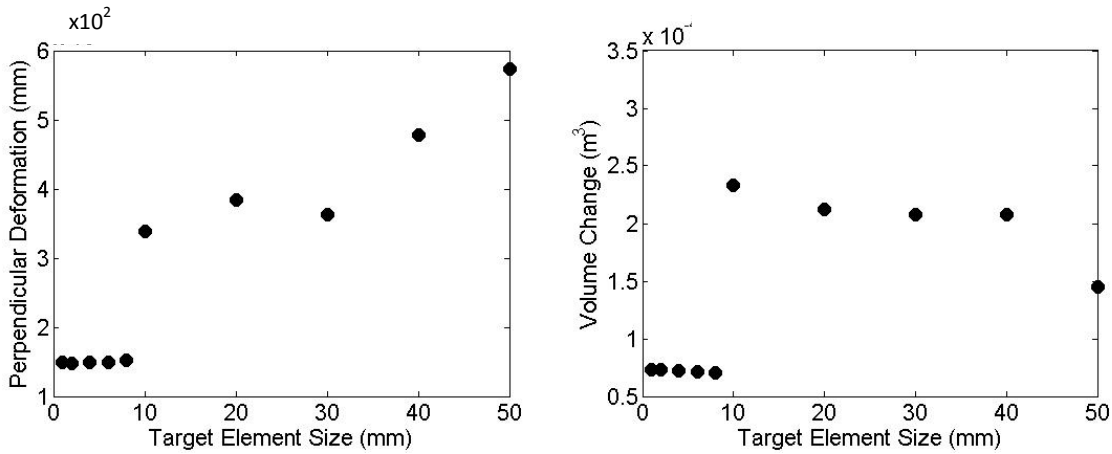

Figure 33: Mesh refinement study comparison – pressurisation and deformation at impact

4.3 Desired Outputs

When configured properly, a finite element analysis can provide a wide range of useful types of results. The complete models could be viewed from all angles before, during and after impact and this flexibility in observation helped create a more complete qualitative understanding of dynamic events. Strain and stress were plotted using a colour scale on the deformed geometry to highlight regions of interest and vectors gave more information pertaining to the direction of forces in the football panels. Studying small, subtle motions qualitatively was useful when looking at one or two impacts in isolation but quantitative measures were required for comparison purposes in simple studies as well as automated optimisations.

Inline deformation was defined as the change in diameter between the point of impact and the point directly opposite. Perpendicular deformation was defined as the change in diameter in directions perpendicular to inline deformation. For example, if inline deformation were along the Y axis, perpendicular deformation would be the average of diameter changes in the X and Z directions. Contact pressure between impacting surfaces was recorded, as was the total reaction force throughout time. Contact time was taken from the reaction force data and had a resolution equal to the equivalent 'sampling frequency', or simulation analysis "frame rate" of 0.5ms (unless otherwise specified). The XYZ coordinates of the centre of mass of the ball could be retrieved easily and these were used to keep track of post-impact motion. Incoming and outgoing speed were monitored as an indication of energy storage/release properties. Calculating the post-impact velocity vector was useful for quantifying the anisotropic behaviour of the ball. Though most simulations only had no more than 0.1s of post-impact simulation, the positions of the ball much later (penalty kick distance, for example) were extrapolated to give the anisotropic deviations more real-world context. The rebound deviation 2m after impact was taken as the standard in simulations (Figure 34).

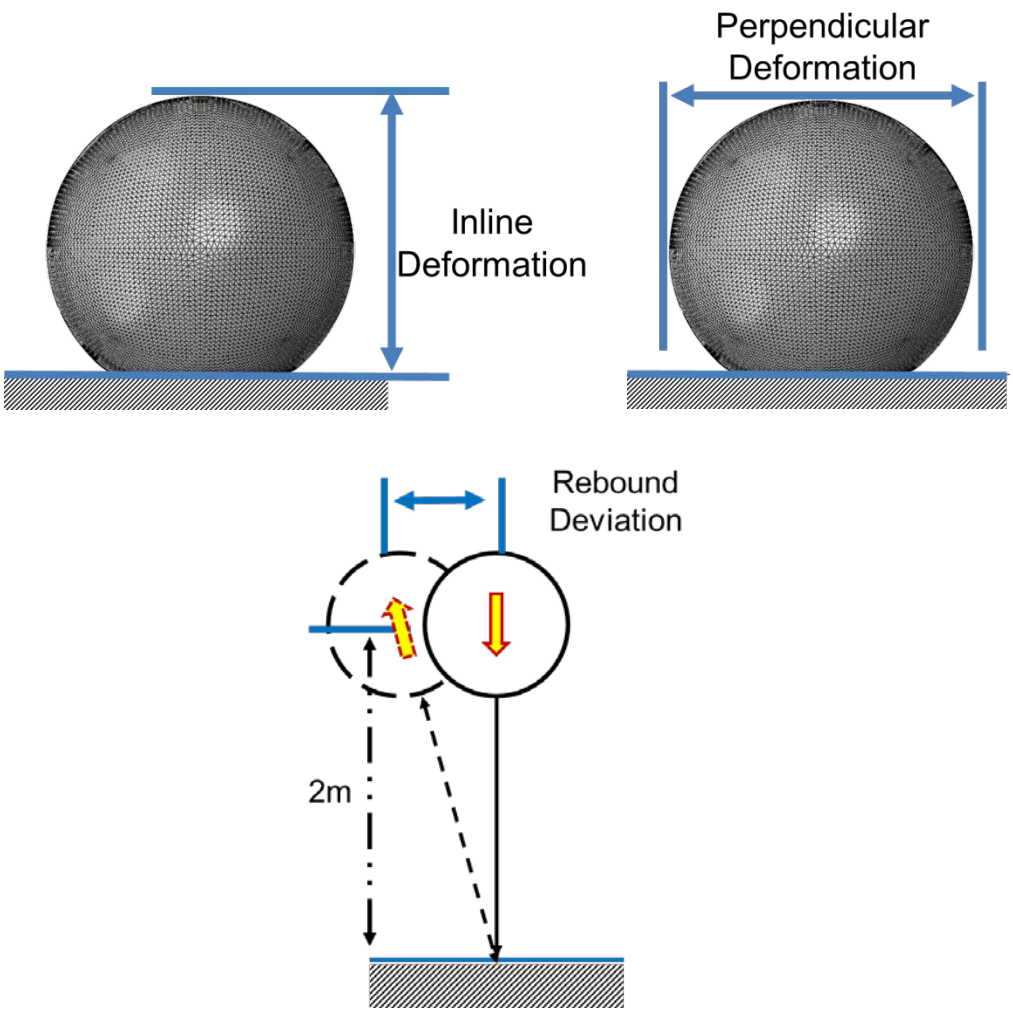

Figure 34: Inline deformation and perpendicular deformation midway through the contact time, and rebound deviation, expressed as the horizontal motion 2m away from the impact plate after the rebound

Internal pressure and cavity volume extremes during impact were used as a measure of stiffness for different impact orientations of the same football. Pressure and volume were also recorded throughout the pressurisation phase and the average ratio between the two was used as an indication of global stiffness differences between footballs of a similar construction. In some special analyses, the internal pressure throughout the volume was collected for advanced quasi-static fluid dynamics with applications in both structural and acoustic studies.

4.4 Surface Deformation Modelling

Shell elements are appropriate for modelling the global, large-scale behaviour of a football but smaller deformations may require a different approach. At the very least, a new mesh refinement study must be conducted to assess the model's representation of local, small-scale deformation. In- and out-of-plane compression (normal to the surface) can be simulated with shell elements but solid continuum elements are better suited for those small-scale surface-only loading scenarios. In the

interest of computational efficiency, only the region of interest was meshed with tetrahedral solid elements and the remainder of the ball was only shell elements. This was done by splitting the ball (based on the 2010 adidas Jabulani) up into three parts or components: a shell for the complete carcass/bladder, a shell for seven outer panels, and a single component represented with solid elements for the remaining panel. The carcass and outer panel shells were tied together and the solid panel was tied directly to the carcass. The seven outer panels' mesh only had 25,000 elements but due to the element size required to get four elements through the 3.5mm thickness of the foam panel, the single solid panel had about 430,000 elements. Each element was slightly smaller than the 1mm element tested in the mesh refinement study. Figure 35 shows the panel alone and its configuration on the ball (Note: ball shell elements are shown without thickness visualisation. The shell elements' thickness brings the shell surface flush with the solid element surface.).

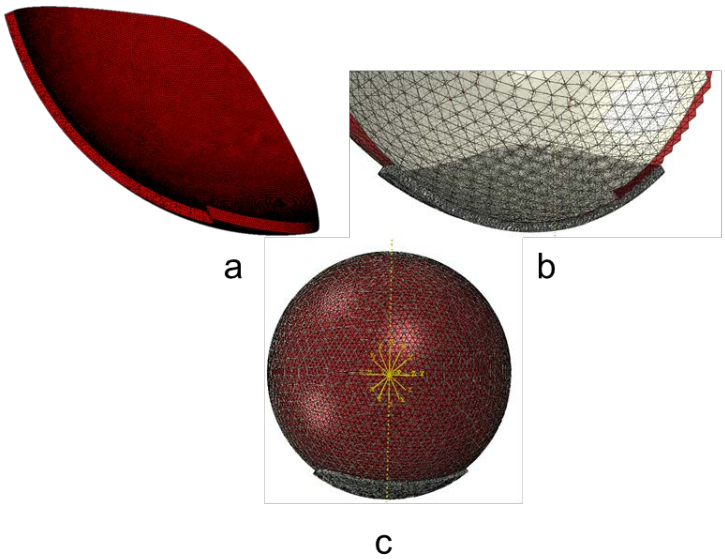

Figure 35: a) Solid Element Panel, b) cross-section of the 3D panel tied to the sphere, c) the 3D panel on the lower side of the complete ball

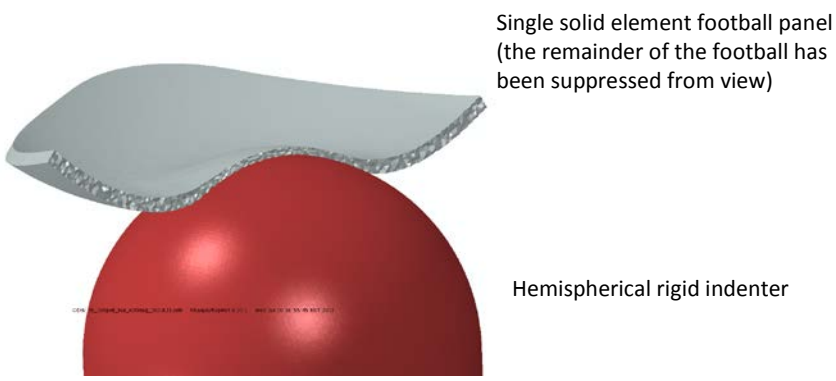

Figure 36: Solid Element Panel (deformation cross section)

Figure 35 shows a partial cross-section of a panel constructed with 3D elements (a), tied with a cross-section of the complete ball (b) and the entire assembly (c) (note: shell thickness is not visible). An example output of the simulation can be seen in Figure 36 – the compression of foam material at the centre of impact. The simulation was a simple straight impact with a 90mm diameter hemisphere at 2m/s.

4.5 Simulating Spatial Variation of Internal Pressure

The uniform pressure method works well for models intended to simulate the large-scale deformation behaviour of the football. This may be considered a phenomenological approach, as it less concerned with the detailed mechanisms by which the end result is achieved. Such characterisations and ways of presenting results are acceptable when used within their limits but a more detailed investigation would be required to validate the uniform pressure approximation and deepen the understanding of the role of air within the ball. Measuring the air pressure at multiple locations inside a football during an impact is practically difficult in a lab but finite element analysis is well suited to this type of analysis.

The coupled Eulerian-Lagrangian (CEL) method was chosen over smoothed particle hydrodynamics (SPH) because the ratio of material (fluid) to void (potential space in which the material can exist) is relatively high. Furthermore SPH fluid cannot be split into individual domains for computation so the method does not take advantage of parallel processing. Though computational cost between SPH and CEL methods may be similar, in theory, CEL simulations in this application can run quicker.

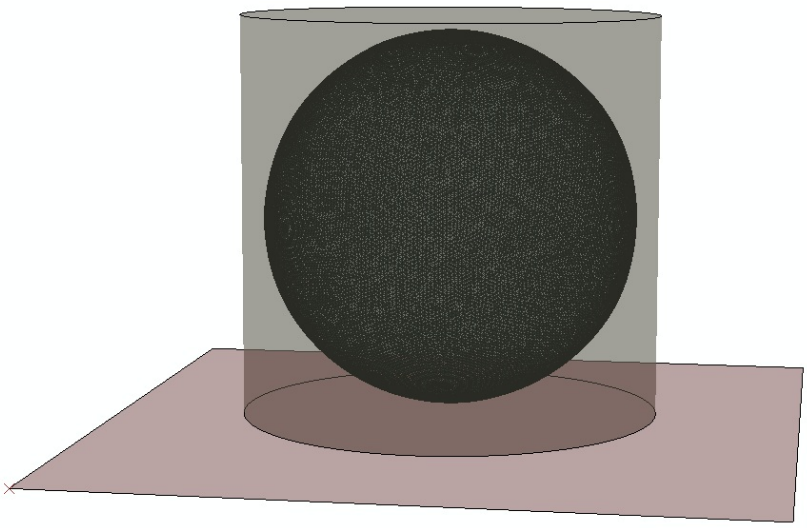

Figure 37: Eulerian Domain (translucent cylinder) surrounding the Lagrangian elements of the football

To keep the number of elements low, the Eulerian domain (Figure 37) was a cylinder with at least one full element between the edge and the surface of the ball. The cylinder was chosen over a tight-fitting sphere due to ease of meshing, resultant quality of elements, and the ability to follow the ball during deformation without significant mesh distortion. The target element size was 4mm, creating 206,000 Eulerian elements, 114,000 of which were within the sphere. The mesh was allowed to move and morph, following the surface of the ball and these changes did not artificially 'strain' the fluid. In first simulation attempts, the pressurisation was carried out by first 'inflating' the football structure alone with a uniform internal surface pressure of 100kPa, then importing that strained geometry into the CEL model, which contained pre-pressurised Eulerian fluid elements. Pressurised fluid outside the ball flowed easily out of the elements, giving an external gauge (and absolute) pressure of 0kPa. After initial trial and error of finding the proper pre-strained state and corresponding pre-pressurised elements, the method was found to work well, resulting in a pressurised football in static equilibrium ready for an impact. In the course of working with the model, a new method was devised that required only one simulation without any pre-straining or pre-pressurisation. Fluid elements inside the ball were isolated and pressurised gradually before impact in much the same way as the uniform pressure method described earlier. This newer method eliminated some setup hassle and unnecessary computational time. In these simulations, the outer foam panels were omitted as they were not the focus of the model.

Computational time was found to be dependent on the duration of simulated time in the analysis. The longest CEL analyses took 544 CPU hours for 0.5s of inflation and 0.1s of impact/post-impact coverage. A shorter analysis with 0.01s of impact/post-impact analysis took 167 CPU hours. For comparison, a similar job with the uniform pressure fluid surface cavity definition and uniform pressure method took approximately 9 CPU hours. A CEL results file was around 20 gigabytes (as much as 40gb depending on the information requested) and the file for a comparable impact using the uniform pressure method was on the order of 1gb. The CEL result was able to provide pressure at every node within the cavity at any pre-specified sample rate, in addition to the usual structural stress and strain of the football structure.

Figure 38 shows the typical output from a simulation of a flat plate impact with the CEL method. In response to the simulated impact with the plate, the pressure wave started at the impact surface, propagated upward and dissipated. Both the plotted image and the individual elemental data used to create it suggest discontinuous pressure in the form of local lows and highs at the inner surface of the ball. This anomaly could be explained with the way in which the Eulerian fluid domain was discretised. The elements that crossed the boundary of the ball were part pressurised and part

atmospheric so the average calculated was significantly less than the pressure of elements completely within the football's shell. The pressure for these boundary elements was likely to be heavily influenced by the amount of the element on the inside at any one time and though the Eulerian mesh was set to deform and translate as necessary to follow the surface, the inside-outside volume ratio of the boundary elements could not be guaranteed. Fortunately, this modelling phenomenon affected only those individual elements volumetrically averaged over a boundary so the inner elements were believed to be an accurate prediction of the pressure. Unlike the CEL method, the uniform pressure method could not provide different pressure data throughout the cavity; the uniform pressure method assumed a single pressure throughout.

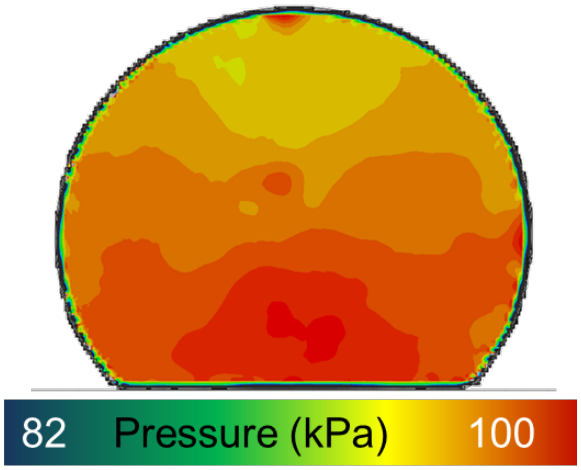

Figure 38: CEL Model - Internal Pressure

As one step in evaluating the model, pressures at two opposite points 2cm from the walls were extracted from a simulation of a flat plate impact and plotted together. The large hump in the curves of Figure 39 shows the increase in pressure as the volume decreased during impact. The phase difference (taken at the linear portion of the leading edges of the curves) is the time it took the pressure (wave) to travel from one point to the other. For the flat plate impact test, the time difference was 0.5ms. With the speed of sound at 343m/s, covering the approximate 0.18m between those measurement points would have taken 0.524ms. The pressure wave should have travelled at the speed of sound and the 0.024ms discrepancy between the simulation and calculated theory might be accounted for in the continuing motion of the far side measurement point. Though the two points started out 0.18m apart, when the ball was fully deformed mid-impact, they were approximately 0.16m from each other so the distance the wave travelled decreased as time goes on. Accounting for this distance closes the small gap between measured and calculated wave propagation rates. The magnitude difference (1.34kPa) between the maximum pressure at near and far sides was attributed to dispersion of the wave during its travel from the near to the far side

measurement point. This simple connection with the speed of sound and the football's dimension suggests that the Eulerian method of modelling fluid accurately represents wave propagation.

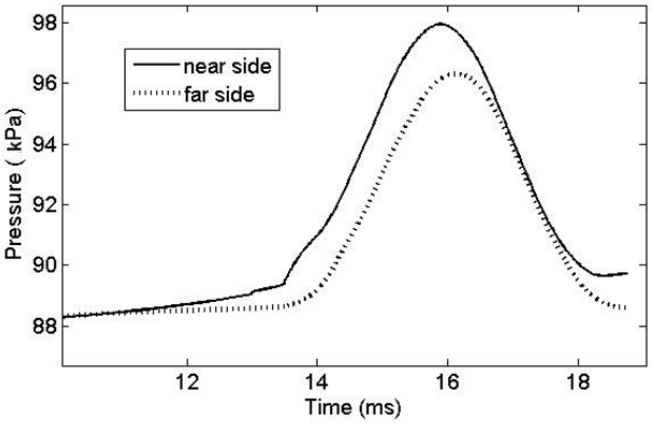

Figure 39: Tracking the internal pressure wave at two points on opposite sides of a ball pressurised with the CEL method

With confidence that the CEL method represented the fluid well, a small series of analyses were run to benchmark the method against the uniform pressure method in terms of the football's structural response. In these tests, only the carcass/bladder assembly was simulated to keep the model simple and the focus on the pressurisation method. A flat plate impact and a simulated robot kick using a 'bullet' shaped end-effector were used as the test scenarios. The bullet, chosen as a simple means of approximating the level of deformation seen with a boot kick, was a 90mm diameter hemisphere moving in an 880mm radius arc. The dimensions for the simulation were taken from a physical kicking robot used in work presented in this thesis. The bullet impact showed similar trends in pressure but with greater duration and magnitude than the flat plate impact.

Figure 40 shows the pressure taken from a point at the centre of the ball. With a smaller indenter, the pressure at maximum deformation was expected to be greater than with a flat plate impact or larger indenter and the simulations reinforced this expectation. The size of the flat plate constrained the deformation of the ball to be mostly in the stiff hoop strain direction relatively early on in the time period of contact (indicated with white arrows in Figure 41. Note: the indenter appears to be off centre because it follows a 90 cm arc and the ball tended to roll off downward, in the case of this image. The 90 cm arc and indenter dimensions were chosen to replicate an available kicking robot to allow for physical comparisons if necessary). Conversely, the bullet was able to penetrate the ball in a way that the plate could not and the result was a greater volume change and consequently higher pressure.

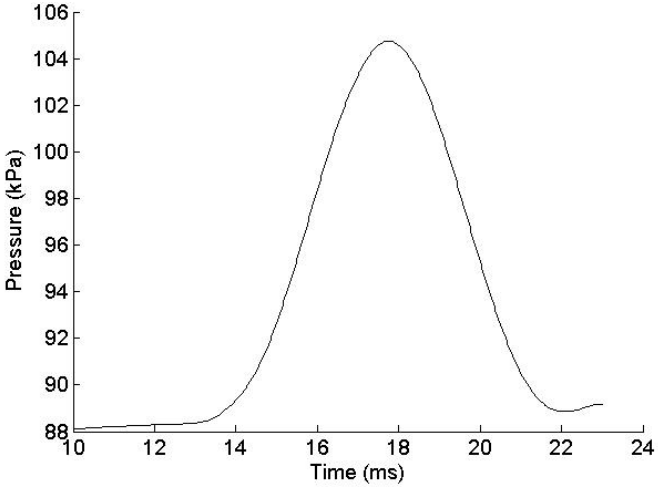

Figure 40: Simulated bullet impact pressure response at the central node of a CEL method impact

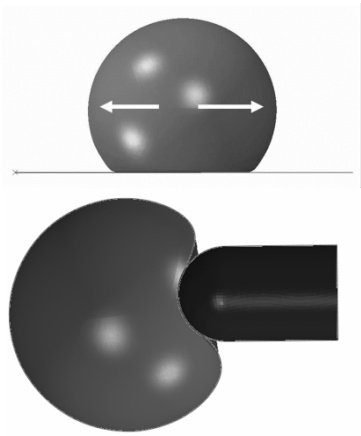

Figure 41: Flat plate vs. bullet deformation in impact simulations

The uniform pressure method exhibited lower maximum pressures than the equivalent CEL models in both impacts (Table 3). The maximum pressure value of the CEL model was likely greater than that of the uniform pressure method (UPM) version of the same impact because of the difference in averaging of the measurement. As seen in the pressure contour plots for the CEL model, the pressure was predicted to be greatest closer to the point of impact and disperse as the wave propagated throughout the ball so the local peak values were likely to be greater than the peak value averaging over the entire volume. There were also slight differences in the material definition for air, necessitated by the computational requirements available for each method. Though the two sets of parameters described the same fluid, any rounding or computational differences may have contributed slightly to the response.

Table 3: Maximum simulated internal pressure (kPa) at full deformation

	Flat Plate	Bullet
CEL	97.95	104.8
UPM	92.5	95.7

The quantified deformations supported the results seen in the pressure trends. Table 4 shows that the bullet penetrated much further into the ball than the flat plate. With the uniform pressure method, for example, the flat plate brought the sphere's volume to 96.5% of its original, compared to 94.3% for the bullet. The data in Table 4 confirms that the flat plate impact deformed more in the hoop strain/stress direction, eliciting a stiffer response. For comparison, inline deformation simulated and measured by D. Price was between 50-70 mm, and perpendicular deformation was between 4.5-6 mm (Price et al. 2006) but the earlier work was carried out with a football of a different construction.

Table 4: Maximum simulated deformation (in line with motion) (mm)

	Flat Plate	Bullet
CEL	33.1	56.7
UPM	31.6	56.0

Table 5: Maximum simulated deformation (perpendicular to direction of motion) (mm)

	Flat Plate	Bullet
CEL	8.3	6.2
UPM	7.6	6.8

The deformation measurements for CEL and uniform pressure methods differed on average by 5.4% for the bullet and 6.9% for the flat plate, and their relative relationship was on the same order of magnitude as that of the maximum pressure difference. The measured contact times in this study (Table 6) were much lower than the 7-10ms for a complete ball. Generally speaking, stiff objects deform less and have shorter contact times during impact. Foam outer panels, though they do add stiffness to the already quite stiff fabric sphere, contribute extra mass and compressive compliance that serve to increase the duration of contact. Such physical testing is rare but (Price et al. 2006)

carried out experiments with foam-less football carcasses similar to those modelled in this study and saw contact times between 5-6ms at 20m/s on a flat plate.

Table 6: Simulated contact time for different pressurisation methods and impact scenarios (ms)

	Flat Plate	Bullet
CEL	5.25	8.601
UPM	5.299	8.469

From the inside, the two pressurisation methods looked very different but from the outside, the structural responses were nearly identical. Though this result was generally expected when two modelling approaches are applied to the same problem, one of the reasons for performing the study was to determine whether the approximations made in one modelling approach made it less representative of reality. Upon close inspection of the CEL model, there were no small structural responses to the local pressure changes. During the impact, the approximately 10% increase in internal pressure was found to translate to a small difference in force on the walls likely to be negligible to the relatively massive and rigid structure over the short time that it was applied. The CEL method did not seem to provide additional insight above the UPM model into the structural response of the ball in terms of deformation but it had the potential to provide enormous amounts of information about the dynamics of the internal pressurised air, which may help explain structural behaviour during the impact.

The CEL method and the investigation in to spatial variance of pressure did not bring to light any previously unseen or un-simulated structural phenomena, but a better description of how the internal air behaves may help inform theories on the impact behaviour.

4.6 Parametric Model Creation

Part of the value of a finite element model of a football is its flexibility and the opportunity it provides to quickly change definitions of materials, dimensions and boundary conditions. A model can be a more useful tool if it can be easily reconfigured to meet the needs of many scenarios. Changes made in the graphical user interface of a FE program are naturally much faster than setting up new lab tests or constructing new footballs but the process can be expedited further by making values of interest parametric. By changing fixed values to variable parameters, a model and/or simulation could be quickly modified.

The finite element models used in parametric groups of simulation were based on the standard model but configured to make modifications as simple as possible. Material models were entered in

such a way as to preserve the material test data from which their strain energy potential coefficients were derived. The individual layers of the composite shells could be easily manipulated to be thicker or thinner. Temperature could be changed. Impact velocity and ball orientation with respect to the impact plate were reduced to simple, adjustable values as well. In some cases, multiple rigid surfaces were placed in the model and selected by parameters to change the type of impact. The communication between the processor and pre-processor happened via an input text file and this file was modified to turn all of the aforementioned variables into parameters that could be referenced by name. This created a type of model that could be easily and swiftly manipulated by code rather than a human user.

Adding these points of flexibility provided a significant time savings over manual modifications to the models. Consequently, a greater number of simulations could be run. This was useful, for example, when impacting a football at a range of angles or orientations, and the parametric capability became essential when running hundreds of jobs using automated optimisation software.

4.7 Boundary Conditions

When establishing boundary conditions for evaluating the performance of the assembly or component in question, the goal is to replicate realistic usage and keep track of meaningful results. Compared to those of many engineered objects, the boundary conditions and loading scenarios of a football are difficult to measure and reproduce. The biomechanical differences between players and the vast array of different kick types and intentions combine to create an enormous number of possible impact scenarios too large to serve as a list of lab tests. In selecting boundary conditions for this work, the goal was not to mirror actual impact scenarios in terms of boot shape, motion path and speed, but to isolate the important aspects of that event and reproduce them simply and consistently. The non-linear (hyperelastic) rate-dependent materials of the football place an emphasis on loading rate and strain level which are both indicators of the severity of an impact. These measures were kept in mind when considering the boundary conditions for simulations and lab tests.

Even if the precise dynamic kicking boot shape cannot be re-constructed, proper boundary conditions on a simulation will create the same amounts of strain and deformation as seen on the pitch and approximate the amount of impact energy present. With representative levels of strain and deformation, the hyperelastic and viscoelastic behaviour of the materials could be explored in situ and serve as a backdrop for other studies.

As an impacter, a flat plate was chosen in part for its ubiquity and repeatability and also implementation in the FIFA standardisation process (FIFA 2010b). Additionally, a 90cm diameter hemisphere was used as an alternate loading scenario aimed creating a deformation scenario more similar to boot-ball contact. The dimensions were chosen to replicate an available implement for physical testing, and because of existing data with a similar implement (Neilson 2003). The tangential contact relationship between impacter and ball was described with a simple coefficient of friction set to 0.8. This high value was chosen to prevent slipping between surfaces during contact. Though an amount of slippage likely happens in typical use, the actual effect must vary with environmental conditions and the characteristics of the specific impacter. Such surface interactions have been explored in the past (Cotton & Jones 2007) but in the interest of keeping the present studies manageable and focused on impact, deformation and rebound, the zero-slip scenario seen in the lab was used and replicated in the simulations.

To prescribe motions to the ball and implement, a study was conducted to explore the possibility of calculating and inferring loading scenarios from real match data in the form of notational analysis. Using time-stamped XY coordinates of players during ball-related events on the pitch throughout the game, the ball's average velocity was calculated and assumptions allowed for an approximate initial velocity. The study included data for 16 European matches provided by Prozone Sports (Leeds, UK) and also yielded information about the frequency of different types, speeds, and distances of kicks throughout the match. More information can be found in Appendix 9.2. To limit testing to a realistic and manageable set, a single impact velocity of 20m/s was chosen to represent a high-powered kick.

4.8 Validation

When possible, it is useful to validate computational simulations using well-known physically tested scenario to ensure that the material models, geometries, and boundary conditions come together without incident. Simple comparisons between simulation and lab work can build confidence in the model when simulating things that are practically difficult to do in reality. The 3D element-based model designed to explore small local deformation was practically difficult to validate. The thickness change and compressibility of the foam in the ball could not be measured experimentally so pressure measurement was considered as a potential differentiator. Of the pressure measurement systems available, none had the spatial resolution or capture rate high enough to adequately measure the short contact time.

The coupled Eulerian-Lagrangian model was structurally similar enough to the model created with the uniform pressure model to not require special validation methods for the structure. Measuring

internal pressure at various spaces within a physical ball (for model validation) was not possible and considered one of the unique benefits of that type of simulation. The air and pressure waves in the simulation followed basic speed-of-sound rules and this was enough to validate and give confidence in the fluid modelling for pressure wave representation.

General football model structure and dynamic behaviour has traditionally been validated with several parameters characterising the ball response during and after a flat plate impact. Coefficient of restitution can be used to confirm the viscoelastic properties of the ball. Carcass deformation in millimetres can be used to validate material stiffness as well as some anisotropic effects. The anisotropic effects can also be quantified in terms of deviation from a perfectly vertical rebound during a drop test or high-speed flat plate impact.

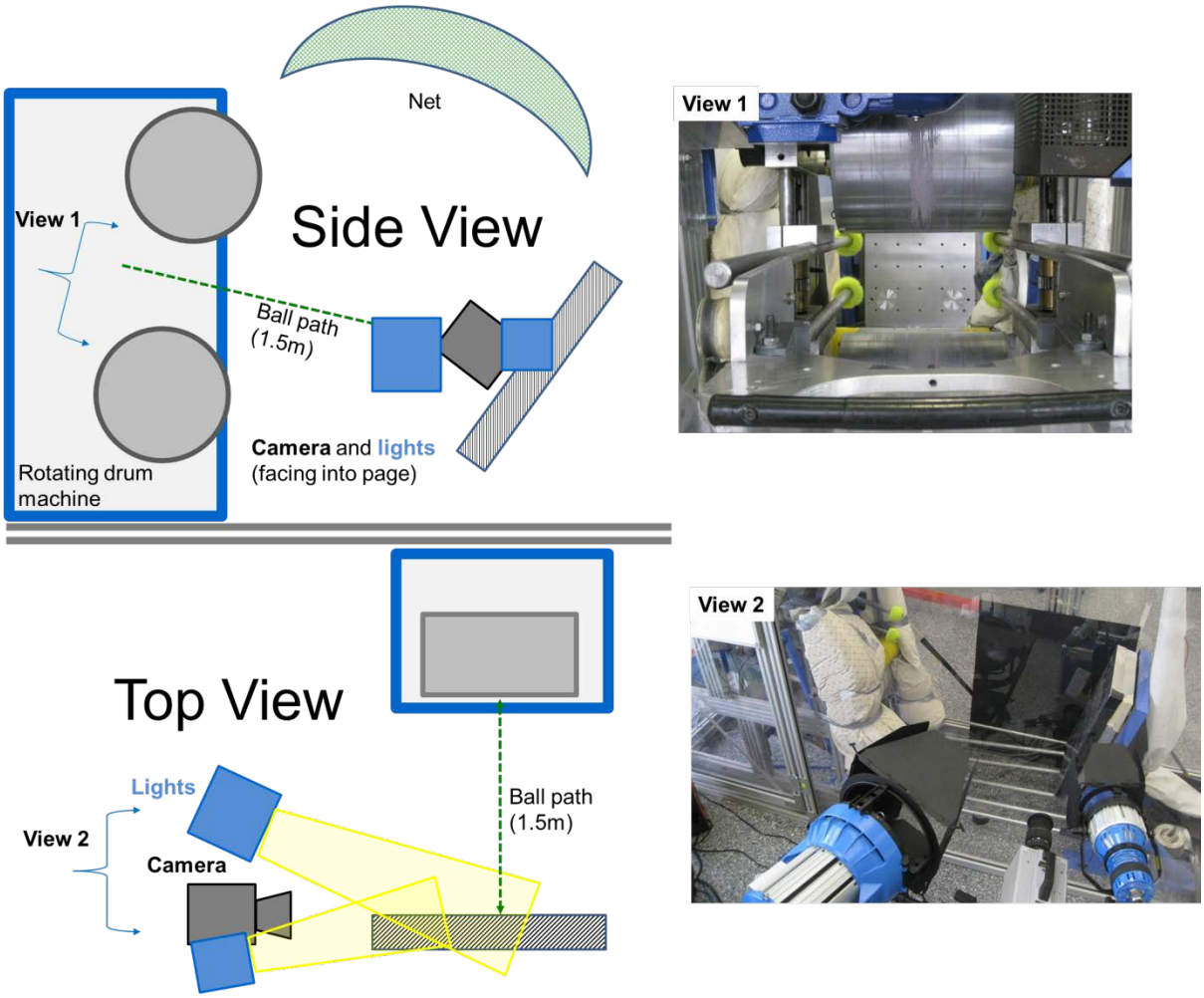

Figure 42: Counter-Rotating Drum Impact Machine

Standard validation procedure suggests performing many identical lab impacts and replicating the different types of test in a simulation to compare the results. Re-creating lab boundary conditions is a fairly straightforward task in FEA but it was challenging to carry out repeatable lab testing. One

test machine used for impacts in this study used two counter-rotating 40cm diameter drums with a 20cm gap (Figure 42). Each football was fed into and squeezed through the gap, projecting the ball toward a rigid steel plate positioned 1.5m away. Minor, uncontrollable differences in relative drum revolution speed imparted small and inconsistent spin and subtle differences in friction also influenced the resulting velocity. The spin, though it may not have had enough rotational energy to influence the rebound direction, made it difficult to accurately and consistently impact a specific section of the ball.

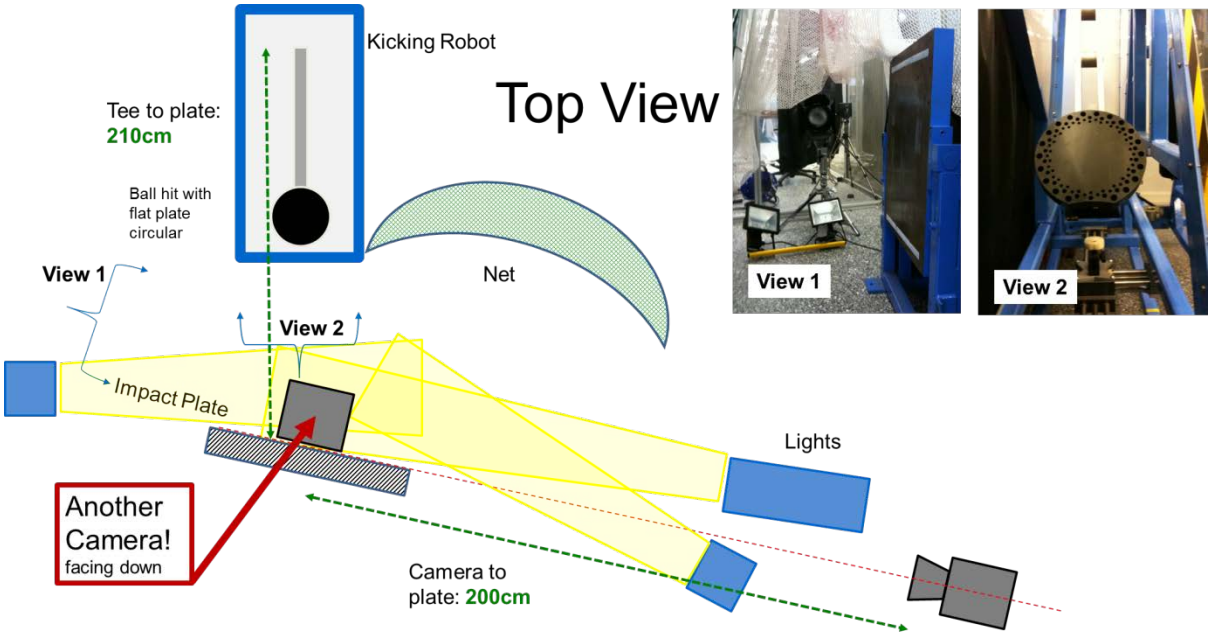

Figure 43: Kicking Robot Setup

A second machine designed to simulate a kick was also used in some impact testing. Chosen because it avoided the drum-related errors of the previous method, the robot kick still had its own peculiarities. The robot, an 88mm rigid rotating arm mounted to an electric motor suspended in a steel frame, was fitted with a flat rigid nylon plate. The natural arc of the 'leg' induced a top-spin on the ball and the anisotropic effects under investigation also influenced to small degree the ball's spin in its short 2.1m flight. The same rigid steel plate from the rotating-drum apparatus was used and positioned at a small angle (15°) to keep the balls from bouncing back into the path of the machine. This kicking robot setup also allowed for the placement of two cameras, capturing top and side views of impact (Figure 43). Despite several improvements in consistency and usability over the rotating drum apparatus, it was still very difficult to get accurate and repeatable impacts. This may simply have been the nature of this type of testing – the inconsistency that was intended to be measured interfered with the consistency of the measurement method. With this in mind, most of

the model validation was done by closely examining individual physical impacts and their bespoke virtual counterparts rather than by considering an average of many impacts and specimens.

4.9 Summary

A basic football model was developed using shell elements with a composite thickness comprising the individual material layers. The basic model was pressurised with the uniform pressure method (UPM), given its realistic air representative advantages over a simple distributed pressure. In addition to the uniform pressure method, a method of describing the dynamic and spatially varying internal pressure was also developed, using a coupled Eulerian-Lagrangian (CEL) simulation approach. Both of these inflation methods, coupled with the unique way of characterising the individual materials yielded similar deformation values to previous work seen in the literature. Though it involved a more accurate way of modelling the internal fluid, the CEL simulation did not provide results that differed greatly from the more computationally inexpensive UPM. Additional football models were created to allow for a study of local, small-scale deformation, and allow for optimised simulation run-time and flexibility through parameterised material and impact conditions.

Simulation validation procedures were established using a high-speed impact initiated by a rotating implement ("kicking robot") and high speed video capture. Though this concept of validation has been implemented in the past, inconsistencies in the ball made it practically unrealistic to gather repeatable data.

5 Impact Behaviour

5.1 Intentions

The contact time the athlete has with a football when kicking is likely to be less than 10 ms (Shinkai et al. 2007). Just as in other sports with short-duration impacts (J. Roberts et al. 2001), the athlete does not have enough time to both perceive and send new muscle instructions in a reaction to the ball deformation. Without an extra layer of control, it is important that the football behaves consistently and as expected when it is struck at any point on the surface. A perfect thin-walled sphere will respond consistently when struck at any position on the surface, but the materials and construction of a football are known to influence the impact and deformation shape. The purpose of the study into the impact behaviour of footballs was to understand mechanisms responsible for measurable characteristics with the intention of applying the knowledge to create new designs and impact scenarios.

5.2 Validation

Virtual simulations were used extensively when investigating football impact dynamics. To test the capability of the FE models created for this work to accurately simulate a real scenario, a series of impacts was carried out in the lab. In addition to comparisons with the model for validation purposes, these impacts were also useful in outlining trends of rebound and impact orientation with respect to the carcass. A series of impact simulations was carried out to locate potential regions, which, when struck, were likely to produce particularly unusual or varied deformation behaviour. Differences were seen starting at the centre of a panel or face, and progressing in one direction in 15° increments. In the patch carcass used in the adidas Speedcell, the face is one of the six groups of three panels. Figure 44 shows two different directions of rotation at 15° increments and the associated impact positions with respect to the carcass. The circles represent the locations of first contact (normal to the surface) during the impact.

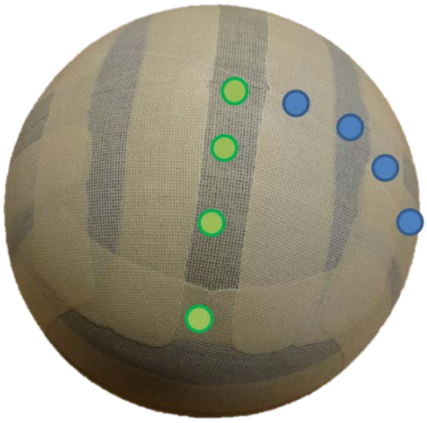

Figure 44: Example of impact positions on a patch carcass

5.2.1 High-Speed Impact Validation Lab Methods

Due to the nature of the adidas Speedcell footballs used in the experiments, the angular position of the carcass within the football was unknown and partially independent from the outer panels. The location of the valve helped define two axes of the carcass position and X-ray imaging was used to establish the third Figure 45.

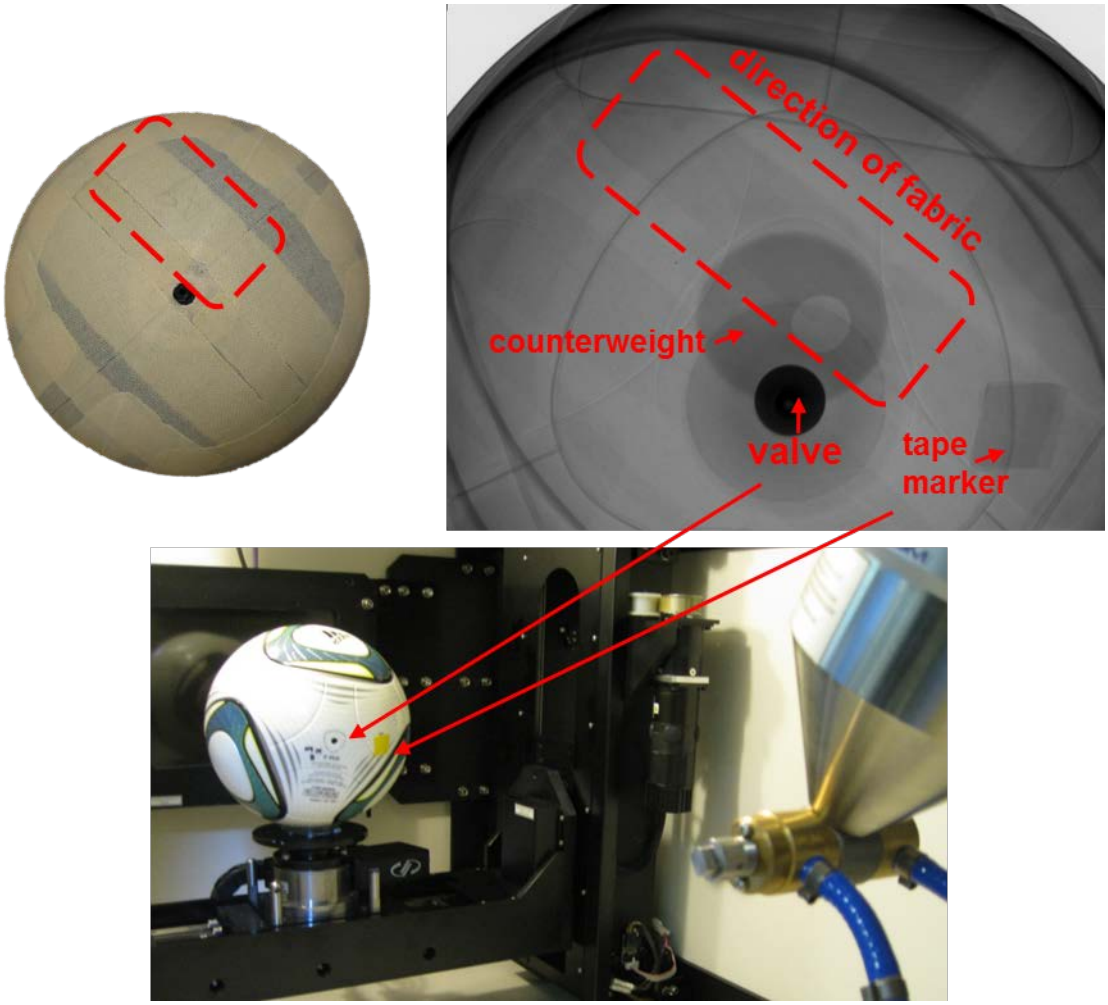

Figure 45: X-Ray Imaging to Determine Carcass Orientation

As described earlier, the kicking robot (kicking with a flat nylon pad) and a flat rigid steel impact surface were used in the testing. Footballs were positioned in the machine with the intention of creating a specific impact orientation. This was done iteratively and typically involved a slight rotation to account for spin imparted by the arc of the swinging pad. The two high-speed cameras were synchronised to record manually from the same trigger and they recorded greyscale and white 1024x1024 pixel images at 5000 frames per second (1/5000 second shutter speed) for about 1 second. Videos were cropped to only include the frames immediately before the ball was visible through the frame immediately after the ball left the field of view. Despite careful positioning of the footballs, it was often the case that the ball did not impact the plate with the desired orientation. All videos were classified and organised based on the actual impact orientation as identified by high-speed video and the markings on the balls, rather than the original or intended orientation.

5.2.2 High-Speed Video Processing Methods

A program was written in Matlab (2013,Mathworks, Natick, MA. USA) to automatically process the videos. Each frame (represented as a large matrix of pixel values) was compared to a reference frame just before the ball entered the field of view. If the difference in pixel intensity was greater than a pre-defined threshold, the pixel was considered to be "1". Otherwise, the pixel received the new value "0". The result was a binary representation of where the ball was. In simpler terms, this method subtracted the background from a frame with the background and the ball to leave only the football. From this stage, the centre of the ball was defined as the average XY coordinates of all the pixels which held a "1" value and the diameters (in parallel and perpendicular directions) were determined by counting the "1" values starting at the centre point and working outward. The maximum deformation was defined to be at the time at which a specific diameter in the direction of the plate reached its lowest value and this also served as the midpoint in contact time during the impact (Figure 46 a). Pixels were related to millimetres using a unique conversion factor for each ball based on the relationship between average diameter (in pixels) before and after impact and the actual diameter based on a physical circumference measurement in millimetres. Figure 46 shows in red and blue the binary result of the image subtraction for a frame at full deformation ('impact') as well as before and after impact. The green circle represents the centre of the ball. Figure 47 is an example frame of the video before processing. It is the pre-processed equivalent of the left-most image in the previous figure.

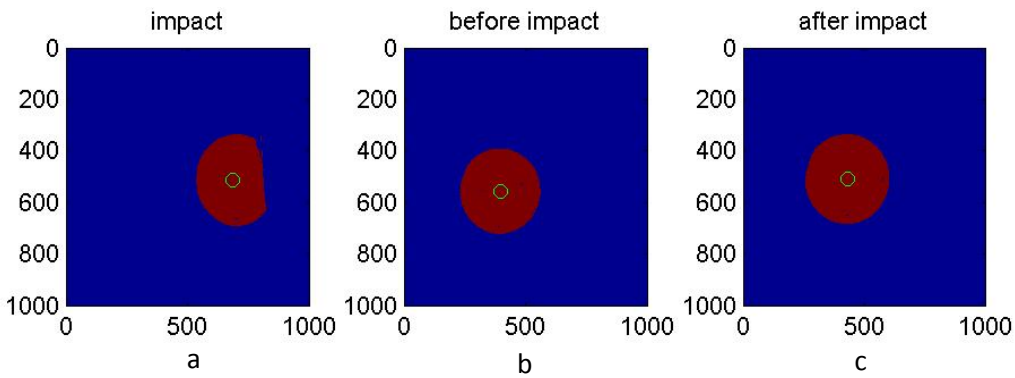

Figure 46: Images from the automated video processing of high speed impact testing

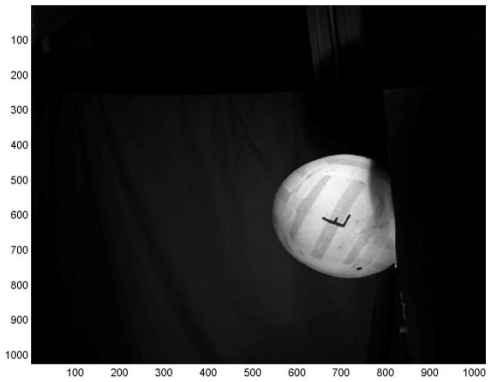

Figure 47: Greyscale image – an example input for the automated processing program

5.2.3 High-Speed Impact Validation Challenges

The high-speed impact validation method was designed deliberately to limit the number of variables under investigation, focusing only on the carcass impact orientation. Though precautions were taken in the impact, video capture and processing aspects of the testing, there was still enough variability in the test to overshadow potential ball and ball orientation-related trends. The challenge, as with the dual rotating drum mechanism, was sending the ball toward a plate consistently without spin. Though the robot kicking did not have the same inherent spinning in the system as the rotating drum system, the in-homogeneity in the ball did induce enough spin to influence the output. Some orientations of the ball would result in a slight spin after the kick as it approached the impact plate. In these cases, the very in-homogeneity of the ball made it difficult to analyse the effects thereof in a controlled impact.

These challenges were not anticipated and required a re-considering of testing protocol. Though high speed impacts were desirable for their proximity to in-game loading scenarios, the potential for improved experimental control with a slower impact led to the consideration of a simple 2m drop test.

5.2.4 Drop Test Validation Methods

The challenges of high-speed impact validation were not anticipated and required a re-considering of testing protocol. Though high speed impacts were desirable for their representation of in-game loading scenarios, the potential for improved experimental control with a slower impact led to the consideration of a simple 2 m drop test. The main purpose of validation studies was to determine whether the FE models could accurately represent the trends seen in physical testing and a slower impact still fulfilled that need. With a drop test, the ball could be sent toward the plate without any dependence on orientation or anisotropy as seen in the high speed impact validation attempt. With

slower speeds, and lower deformations, differences in carcass orientation were expected to be smaller so only the individual carcass (without foam panels) was used in this study.

The drop test rig used a vacuum pump to de-pressurise a tube with a horizontal circular opening 4cm in diameter. The pressure differential held the ball against the circular opening until a manually-actuated valve restored atmospheric pressure to release the ball. A high speed camera recording at 2000 Hz was placed 2.1 m away from the drop path at 0.9m above the impact plate. The footage was digitised manually using Image-Pro Analyzer 7.0 (MediaCybernetics, Rockville, Maryland) to track the centre of the carcass as well as three points drawn on the ball before testing to help identify angle. Based on preliminary simulations, rebound deviation was expected to be primarily in one plane (the equator), so that plane was kept parallel to the imaging plane to provide the best chance at viewing the rebound deviation. An imbalance had the potential to influence the type of deviation caused by anisotropy and though the valve had a counter-balance, it was always kept pointing toward the camera to keep any influence out of the primary plane of expected rebound deviation and measurement. The ball was dropped at 60 impact orientations around the circumference with approximately even spacing. The inbound angle was measured afterwards and used to reference the impact in subsequent analysis steps.

The range of impacts around the circumference gave a better picture of the entire ball than one or two specific impacts so it was considered a reasonable way to assess the relationship between simulation and lab tests. The circumferential path along which the impacts were oriented could be split into identical (or mirror image) 90° sections based on yarn and panel orientation. A 0° and 180° orientation were simply equivalent. Similarly, 15° and 105° impact orientations both represented a 15° offset from the centre of one of the six faces of the ball but they were mirror images according to panel orientation. Data from impact orientations greater than 90° was translated to sub-90° equivalent angles for ease of viewing.

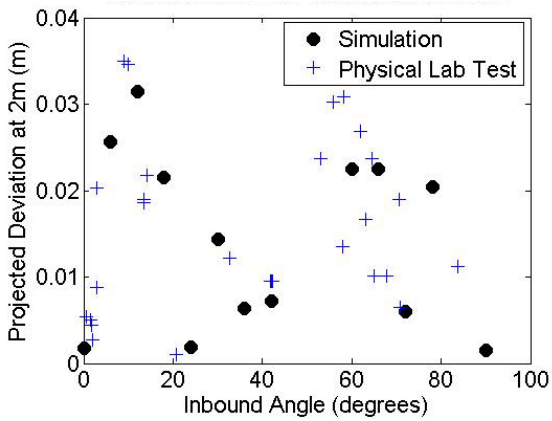

Figure 48: Simulated deviation at 2m vs. carcass orientation

Figure 48 shows the deviation (defined in Figure 34) in rebound trajectory from a completely normal trajectory but with different ball orientation (angles). Simulated rebound deviation was due only to anisotropic effects of the carcass fabric and the resulting inhomogeneity of the ball (see Figure 34 for diagram of rebound deviation). In the graph, deviation represents a magnitude only and not a direction; different inbound angles produced different rebound *directions* as well as magnitudes. For each simulated angle, the closest lab-tested angle produced a similar rebound deviation. The greatest deviations were seen around 15° and 70°, and the lower deviations around 0°, 45° and 90°. Both simulation and lab work reflect the trend, including the rather abrupt difference between 0° and 15°. Due to the aforementioned challenges in creating consistent impact conditions, especially impact orientation angle, multiple trials for each orientation angle could not be reliably carried out so there are no error bars for the lab data.

Another metric for comparison, in-plane rotation was measured by tracking two points on the ball and comparing their relative motion. Figure 49 presents the information as degrees rotated after impact for the physical drop tests and their simulated counterparts. At a 0° impact orientation, the carcass was observed and measured to rotate very little. The same was true of orientations around 45° and 90° and beyond 45°, the rotation direction reversed. These trends were common between lab tests and simulations, with slight differences in magnitude that may be attributed to differences in friction.

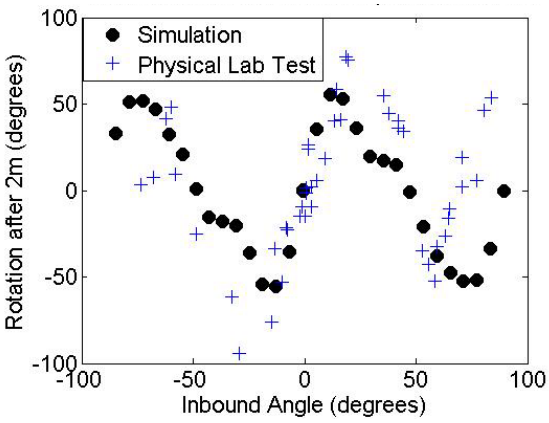

Figure 49: Simulated post-rebound rotation at 2m vs. carcass impact orientation

5.2.5 Deformation at 0° and 45° Impact Orientations

To assess the model's ability to accurately represent deformations during impact, two high speed impacts were selected from the robot kicking dataset mentioned earlier. High speeds were chosen to accentuate the deformation expected in the balls. In focusing on a limited number of impact

orientations, individual attention was given to each scenario, rather than working with an average of many impacts. The practical difficulty in precisely repeating impacts may have made an average of many impacts misrepresentative of a single impact orientation. Carcass orientations of 0° and 45° were chosen because they exhibited significantly different behaviour and the impact speeds were 18 m/s and 18.8 m/s, respectively.

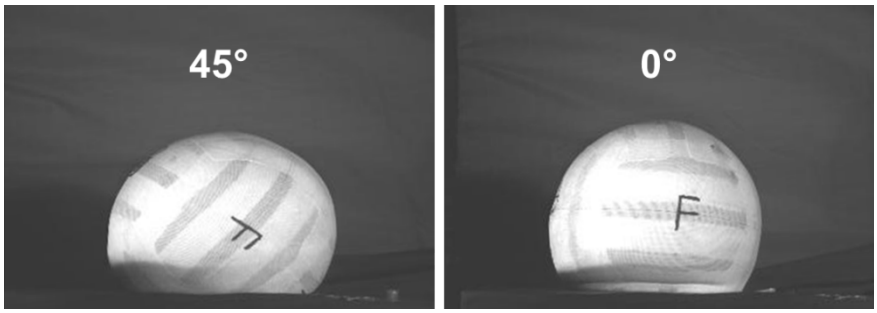

Figure 50: High speed video frames at full deformation for two different carcass orientations exhibiting different deformation characteristics

Table 7: Simulated deformation comparisons of two metrics for different carcass impact orientations

	Inline Deformation (m)	**Perpendicular Deformation (m)**
45° - Lab Test	-0.044	0.024
45° - Simulation	-0.049	0.026
0° - Lab Test	-0.036	0.007
0° - Simulation	-0.038	0.011

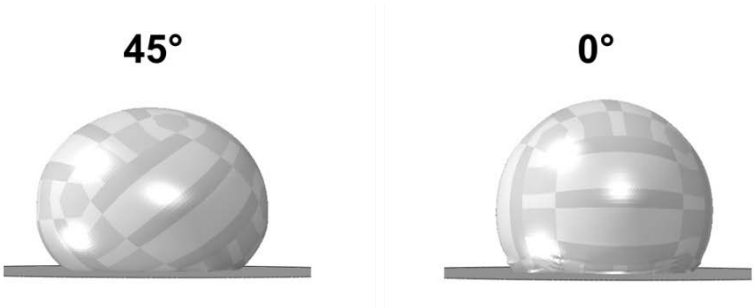

Figure 51: Simulation of high speed carcass deformation at two carcass impact orientations exhibiting different deformation characteristics

Table 7 shows inline and perpendicular deformation for the two impact orientations in simulation and physical lab testing. Values for the lab tests were taken from automated digitisation and

processing and the simulation results came from nodal displacements. Though not identical, results followed the trend to suggest that the model represented anisotropic behaviour and overall stiffness enough to capture trends. The small wrinkle parallel and close to the plate of the 0° impact in Figure 50 was also captured by the model (Figure 51).

It is worth noting that the perpendicular deformation taken from the simulation was determined with one diameter measurement in the plane of the image, as was done with the lab testing. In the simulation, the other diameter perpendicular to the one measured (in to and out of the page) was less in the 45° impact. Looking from the top, as in Figure 52, the ball appeared ovoid, with a longer and shorter diameter. In the 0° impact simulation, there was a slightly lobed shape, with four protrusions corresponding to the 'faces' of the cube-based geometry. Though this could not be observed in the physical testing for practical reasons relating to the availability and placement of high speed cameras, there was no evidence to suggest the physical scenario differed from the simulation in this respect.

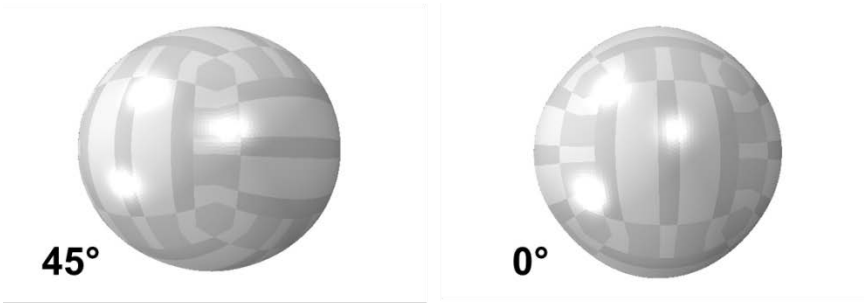

Figure 52: Impact Deformation, Top View of Two Carcass Orientations

5.3 Patch Carcass Deformation and Rebound Deviation

An asymmetrical rebound from a normal impact on a flat surface can receive a component of force parallel to the plate only from friction during the impact. Friction can come only from relative motion, so the football must have had some rotation induced by its structural properties. Alternatively, the angled departure from a normal impact could be considered to be the result of a misalignment between the footballs' centre of mass and the normal reaction force. Either way, the ball experienced a shift or rotation perpendicular to the normal direction that must be attributed to the structural properties. The deformation study highlighted a potential mechanism of the shift in the relative compliance and stiffness of different carcass orientations. The more compliant 45° orientation offered less resistance to deformation than the 0° orientation and that difference, as well as the gradient between the two extremes, created the structural imbalance that resulted in asymmetric deformation and rebound deviation.

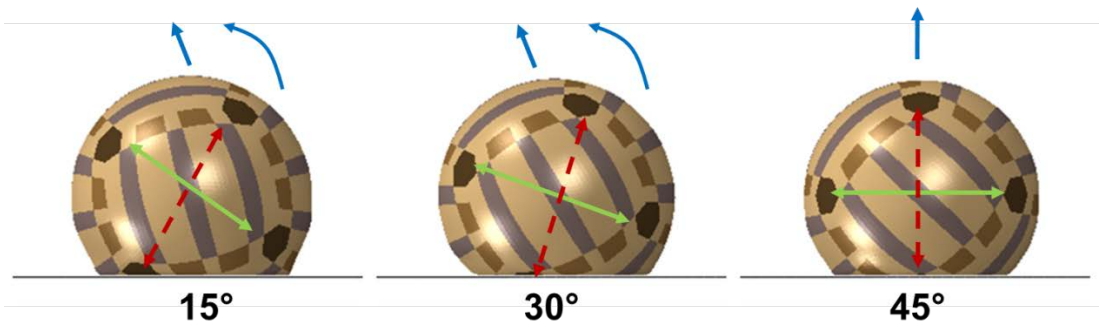

Figure 53: Compliant panel directions (green and red arrows) corresponding to the directions of decreasing dimension (red arrows) and increasing dimension (green arows) and the resulting motion (blue arrows)

Simulating the rebound deviations seen in the drop tests at higher speeds helped identify potential reasons for the deviation. The blue arrows above each football in

Figure 53: Figure 53 indicates the general rebound direction and rotation after impact. The solid green arrows indicate the positive direction of the most compliant deformation direction as seen in the high speed impacts and the dashed red arrows show the direction of 'negative' deformation, or a decrease in distance between opposite points on the sphere. In an isotropic football, the strain in a football during deformation could be expected to happen mostly in the hoop direction, parallel to the plate at the largest diameter. With inhomogeneity and compliant and stiff directions, however, the strain may follow the path of least resistance. Figure 54 shows strain vectors in a 45° impact following the hoop direction. The colours and lengths of the lines represent the magnitude of strain (red and long is high, blue and short is low). The orientation of the lines represents the direction of the average strain for the element. The 15° carcass orientation impact in Figure 55, by contrast, shows strain vectors splitting the difference between the hoop direction and the most compliant panel direction (which was at a 45° angle to the square face of the football). In finding the easiest path for deformation, the football was predicted to deform unevenly, effectively bulging locally down on one side of the contact area to create a horizontal shift and rotation. With reference to Figure 53, if the football were to bulge in the direction of the green line, the 15° and 30° carcass orientations would experience a shift to the left opposing the bulge. In 0° and 45° impacts, the inhomogeneous deformation was balanced evenly without a bias in either direction.

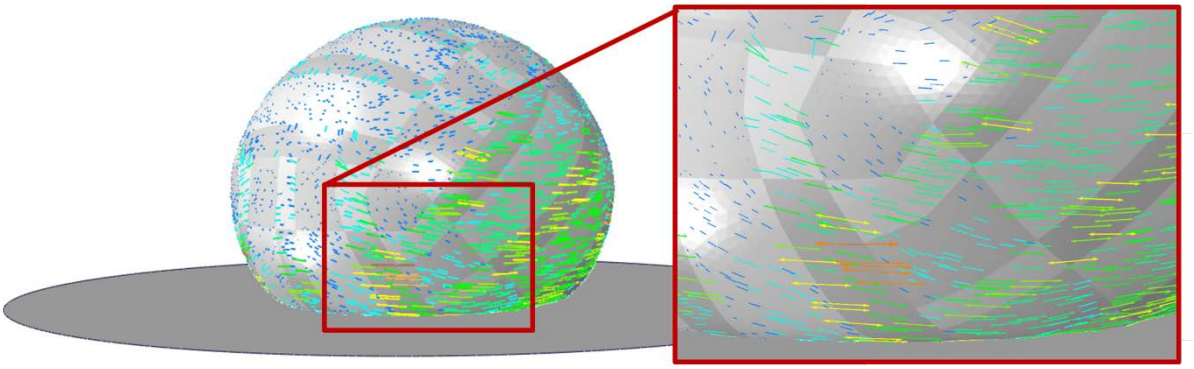

Figure 54: Strain Vectors, 45deg Carcass Orientation

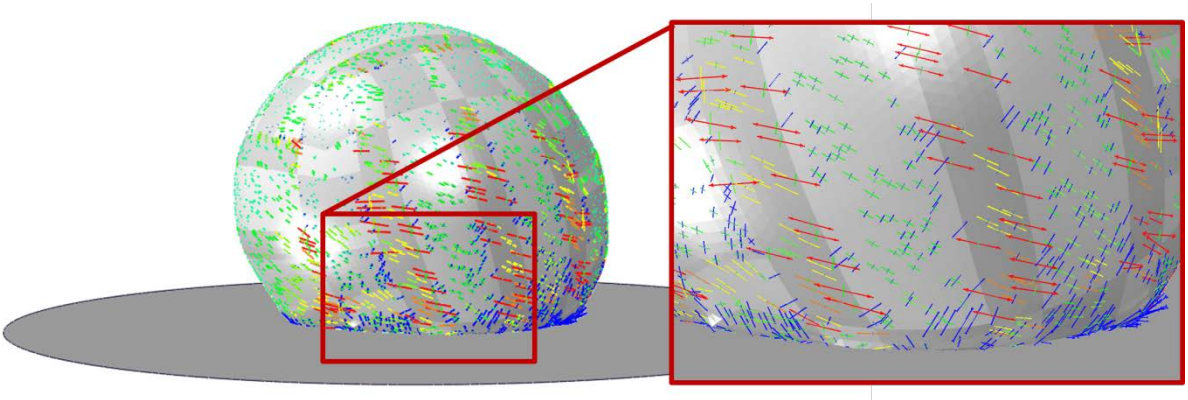

Figure 55: Strain Vectors, 15deg Carcass Orientation

Differences in the amount of strain at different carcass orientations with respect to anisotropic fabric regions can also be visualised with a contour plot of strain magnitude. Figure 56 shows a large difference in strain magnitude when the hoop direction is 45° offset from the yarn direction. The 15° carcass orientation in the figure also illustrates the shift, accompanied by a parallelogram-type collapse or deformation of the front face of the football.

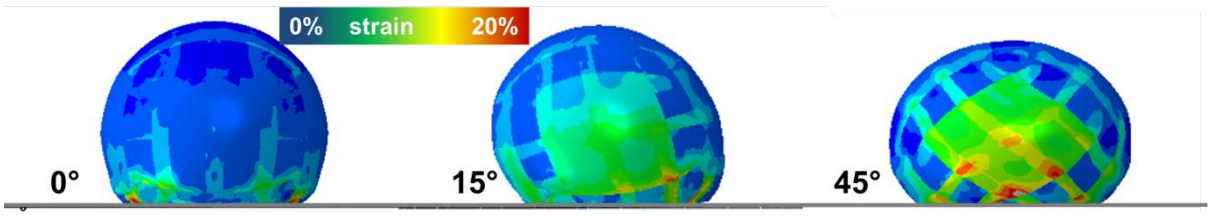

Figure 56: Strain magnitudes for different carcass impact orientations

With low deviation at 0° and 45° and high rebound deviation between these extreme angles (see Figure 48), it might seem logical that the impact orientation angle with the greatest rebound deviation would lie directly between 0° and 45° impact orientations but there are likely factors relating to the dynamic nature of the event that account for the offset. The rebound deviation was

believed to be a result of an imbalance in forces caused by asymmetric deformation. The imbalanced induced a spin which was resisted by horizontal friction forces to provide horizontal motion. The greatest induced rotation was likely dependent on the direction of the unbalanced deformation bulge with respect to the plate and the stiffness of the impact. It is likely that the 15° carcass orientation simply has the synergistic combination of inhomogeneous deformation and stiffness that cause the maximum amount of rotation.

These examples only used one type of carcass but the general principles are likely applicable to any consideration of anisotropy in football deformation. The size symmetry of the eighteen individual pieces of fabric on this particular carcass design resulted in six large regions corresponding to the faces of a cube. Despite the number of pieces of fabric, the layout and orientation of each produced six identical regions, each with a specific and orthogonal yarn direction. When considered alongside the orthogonally woven fabric, the result for the entire carcass was six identical faces, each with a stiff tensile direction and a compliant tensile direction. With large regions of consistent anisotropy, there were significantly different responses depending on whether hoop strains pulled in line, or at an angle to the yarn direction.

5.4 Impact Size vs. Anisotropic Element Size

Non-uniform behaviour in response to a load is dependent, to a certain extent, on scale. To an insect, a surface that a human perceives as smooth and flat may appear rough and irregular. To a human, the Earth may seem hard and rocky in some places and smooth and compliant in others but to a large colliding asteroid, it may appear fluid. These extreme examples illustrate the possibility that the size of deformation, not just the anisotropic region size or construction of carcass, is important in determining the overall behaviour.

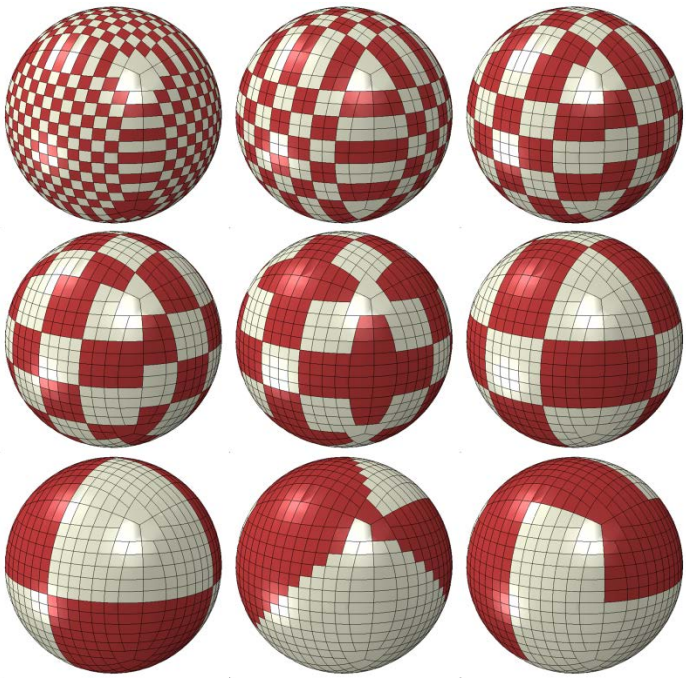

Figure 57: Anisotropic region variations, white and red regions have yarn orientations offset by 45° from each other

A study was conducted to determine the relationship between anisotropic element size, deformation size, and resulting deviation. The football was a carcass-only model created using methods described in Chapter 4. Nine different anisotropic configurations were created, using six identical square-like spherical-contoured faces discretised to create a chess board-like arrangement of separate anisotropic regions (shown in red and white in Figure 57). Adjacent regions had yarn orientations alternating between 0° and 45°. For reference, a completely isotropic model using the same materials and mesh was also included. The football model was collided at 20m/s with four different impactors (Figure 59) at eleven different orientations. The orientations, depicted as impact locations in Figure 58, were selected to represent locations around the entire ball. Blue lines represent planes of symmetry (plane parallel to sheet bisecting the ball is not shown). Symmetry was exploited to reduce the number of necessary impact orientations. With ten football configurations, four impactors, and eleven impact positions, 440 simulations were run.

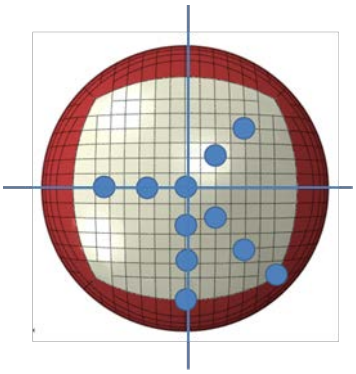

Figure 58: Impact positions and orientations used in the anisotropy study

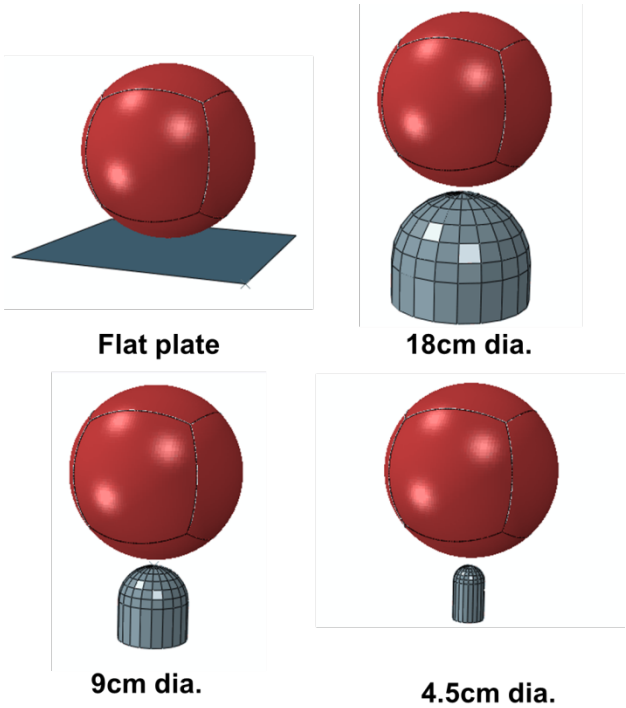

Figure 59: Different impactors sizes and shapes for the anisotropy/impactor study

Maximum deformation, and XY position (after 2m rebound in the Z direction) were recorded for comparison. Table 8 shows the deviation seen in each impact as well as the deformation, represented as a change from the inflated state. Figure 61 shows cross sections of the football at full deformation. The flat plate caused more of a 'flattening', with deformation largely in the hoop directions, as seen in the X and Z deformation results, while the small bullet had a greater 'poke' into the ball, resulting in greater deformation in the Y direction. The minimum cavity volume during impact can be considered to be an indication of deformation magnitude and the results suggested an increase in deformation with smaller impactors. It was easier (from a pressure and force perspective) to make an indentation in a ball by bending the material, than it was to flatten the ball

and experience the pressure resisted by the strong hoop stress. With an effective spring constant greater for a flattening-type deformation than a poking deformation, in order to store the energy of an impact, the travel, or *x* in $PE = \frac{1}{2}kx^2$, must be greater for the smaller impactor. In addition, a smaller volume equated to the higher pressures needed to push against the smaller surface area of a small impactor to generate forces necessary to accelerate the football (in positive and negative directions).

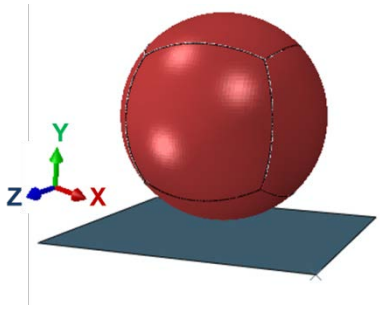

Figure 60: Impact coordinate system XYZ

Table 8: Comparison of impactor based on resulting ball deformations in simulations

Impact Type	Average of XZ Deviation (m)	Standard Deviation of XZ Deviation (m)	Inline (Y) Deformation (m)	Perpendicular (X) Deformation (m)	Perpendicular (Z) Deformation (m)	Minimum Volume at Impact (m^3)
Flat Plate	**0.0349**	**0.0188**	**-0.0452**	**0.00785**	**0.00828**	**0.005168**
18 cm dia. Bullet	0.0116	0.00643	-0.0595	0.00468	0.00478	0.005067
9 cm dia. Bullet	0.0235	0.0123	-0.0661	0.00414	0.00418	0.005069
4.5 cm dia. Bullet	0.0248	0.0146	-0.0718	0.00381	0.00388	0.005082

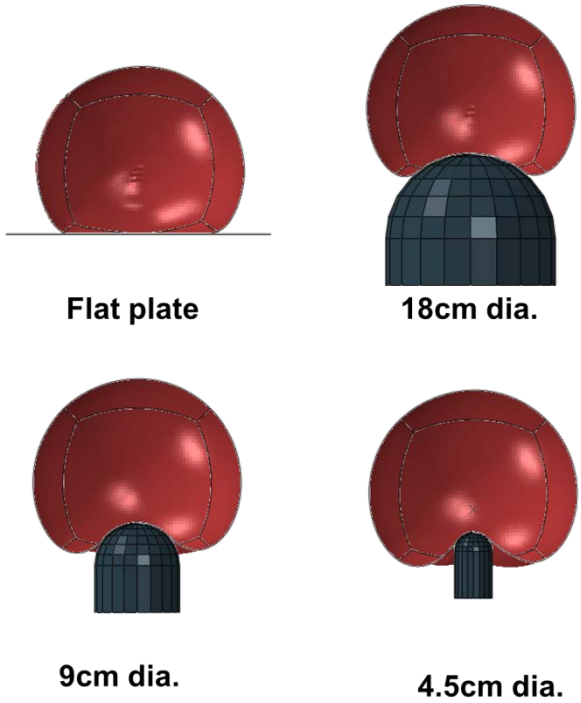

Figure 61: Anisotropy Size Study - Impact Cross Sections

For analysis, the surface area of the anisotropic region was used as the measurement of the scale of the anisotropy. In Figure 62, no clear trends emerged from the data. The flat plate impacts resulted in a greater rebound deviation on average but the next closest impactor, the 18cm dia. bullet did not follow that trend.

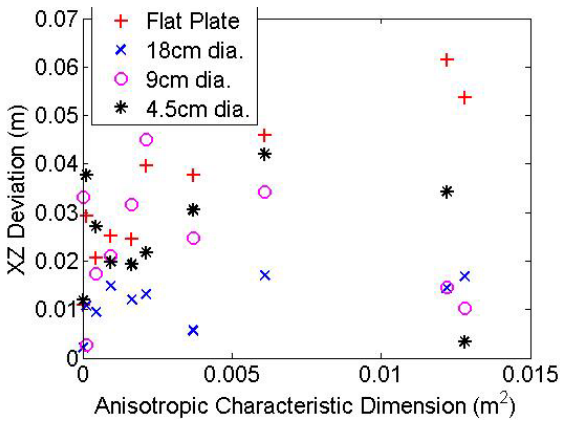

Figure 62: XZ deviation and anisotropic region size (detailed in Figure 58)

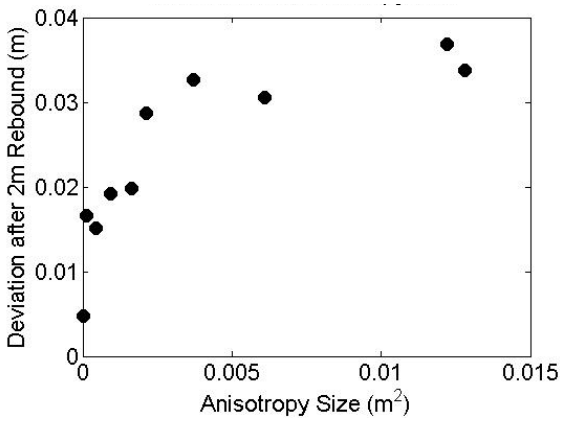

Figure 63: Deviation and Anisotropy Size

Figure 63 combines all impactors and carcass impact orientations to highlight only the influence of anisotropic region size on the rebound deviation. Each point on the chart represents the average of 44 values and the slight upward trend in the graph had a R^2 value of 0.633. The trend following anisotropic region size was stronger than the rather ambiguous relationship between impactor size and deviation shown in Figure 64. An understanding of the effect of anisotropic region size has the potential to act as a design criteria when developing new carcass constructions.

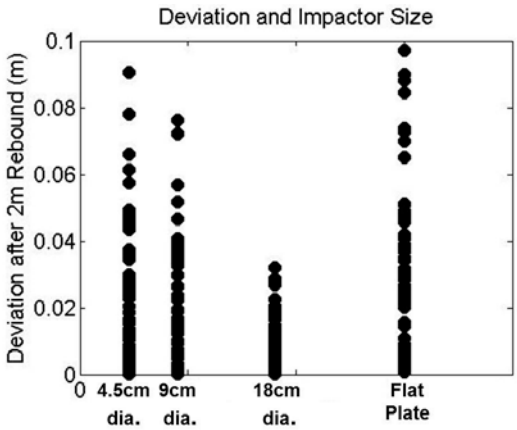

Figure 64: Impactor Size and Rebound Deviation

In the tests, there was a correlation between anisotropic region size and deviation from a straight rebound but no correlation between impactor size and deviation. The first result was expected and the second was not. With more (smaller) anisotropic regions, it was expected that there would be greater chance for all the anisotropic effects to balance out around the ball. It is possible that large anisotropic regions still maintain a stiffness-compliance balance around the ball and this may have decreased the presented average for footballs with large anisotropic regions. The results of this study de-emphasised the importance of the impactor size, suggesting that the directional rebound

behaviour of a football is more dependent on the global properties of the ball, rather than the local region of immediate deformation.

From the chart (and the numbers in Table 8) the flat plate was predicted to cause greatest rebound deviations, if only by a small margin. Whether an accentuation of effects seen on the pitch or a more true representation of an impact than a hemispherical indentor, the flat plate proved to be a good test of anisotropic behaviour in the football and it was used in subsequent studies. Knowing that the flat plate did not produce dramatically different impact deviation results to smaller indentors provided confidence that the impact simulations may also be representative of kicks with a boot.

5.5 Outer Panel Local Deformation

A brief series of simulations was conducted to explore the utility of the model designed with one 3D foam panel. The intention was to quantify or differentiate between different 'touch' characteristics with an emphasis on the athlete interaction rather than deformation or motion of the football. Touch characteristics were considered to be properties of the ball influencing the feel to the touch with fingers, and also performance in light 'touches' with the boot in which outer panel foam compression plays a greater role. At the time of writing, there are no regulations that govern the *feel* of the ball either in abstract ideas or quantifiable measurements but it is anecdotally one of the qualities elite athletes mention in interviews about footballs. The simulation used the model described earlier – a dodecahedron carcass with one 3D foam panel and the rest of the panels represented with shell. With different balls and different manufacturers using a variety of constructions and materials, outer panel stiffness is likely to vary considerably. In this study, the difference in outer panel stiffness was created with temperature variation, using material data from the thermal-dependency trials in Chapter 3. For the impact scenario, a rigid head form was chosen. From the match data analysed, there was an average of 64 headers for each half of a match and it is an event for which contact and local deformation were believed to be of considerable importance. A 1m/s impact was used to represent an impact where carcass deformation was minimal, focusing only on the foam, and a faster 10m/s impact speed was implemented to give a more game-specific impact scenario. The match data indicated that the average post-header ball speed was around 8.5m/s (see Appendix 9.2).

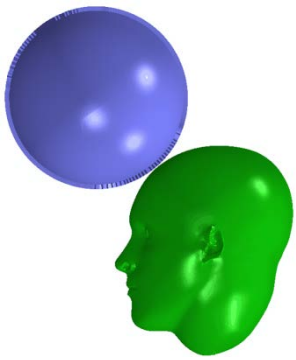

Figure 65: Header Setup Cross Section

Figure 65 shows the simulation setup and Figure 66 shows impacts at 20°C and -20°C, chosen due the availability of material data at those temperatures. In general, the colder temperature had a smaller contact area and higher peak contact forces. This was expected of the stiffer material. In the faster impact (Figure 67), the contact forces are also higher for the colder ball.

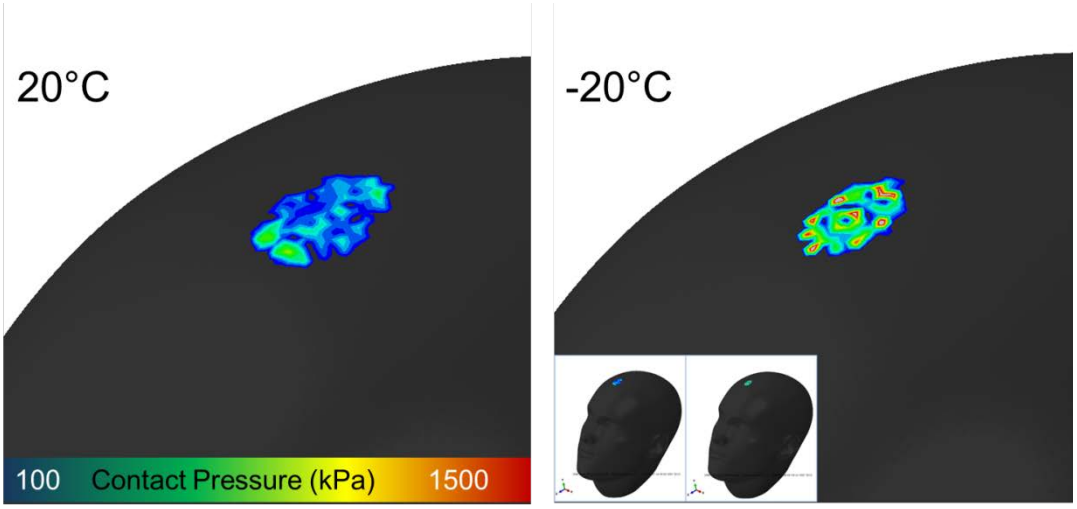

Figure 66: Contact pressure on the forehead form at from a 1m/s ball impact

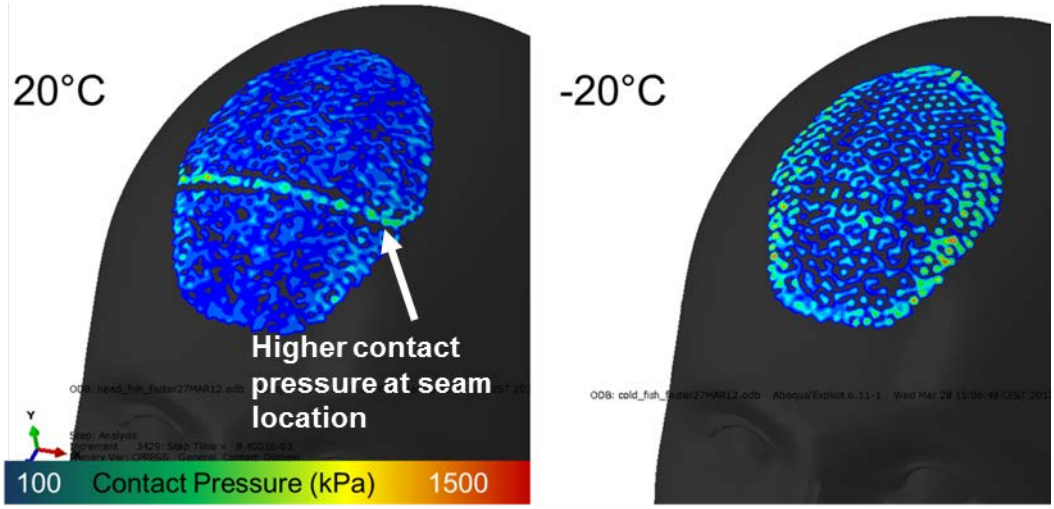

Figure 67: Contact pressure on the head from a ball impact at 10m/s

A phenomenon worth noting in the 10m/s impact (Figure 67) was the presence of the seam in the contact pressure. The light green line (indicating higher contact pressure) seen in the middle of the 20°C impact was due to the greater stiffness of the carcass seam behind the foam panel. In the colder -20°C impact, however, the contact pressure on the head form was more evenly distributed, and slightly greater overall. This was the first indication that carcass geometry may be perceived in a tactile sense. There have been studies in neuroscience and biology circles to characterise tactile perception from the electrochemical creation of the signal to the processing side. Each region of skin is different and sufficiently detailed information about forehead sensitivity to short-duration pressures was not found. One source aimed at understanding human limits for the purpose of robotic replication indicates that finger sensitivity may be as fine as 0.2g/mm^2 (200Pa) (Dargahi & Najarian 2004) so the magnitude of the pressure difference caused by the seam may be well within the scope of human perception.

This brief study suggested that thermal differences (or different materials altogether) may change the contact pressure during impact an appreciable amount. The effect of temperature on individual sports equipment materials and their performance in situ has been studied and taken into consideration (Smith & Duris 2009; FIFA 2013; Wiart et al. 2011), but this evidence of a secondary or second order relationship in which the change in one material may influence the role of another points in a new direction. The concept of second order dependencies was explored further and is presented in section 6.4. Pressure measurements were not validated however, so the simulations can only suggest possible trends. In addition to mechanical validation of contact pressures, a better understanding of athlete perception was necessary to really understand what, if anything, in a

contact pressure measurement is important. These validations were outside the scope of the current work so contact pressure was excluded from further studies.

5.6 Patch Carcass Case Studies

Informed by observations of patch carcass deformation behaviour, carcass modifications and entirely new panel shapes with novel arrangements were created to mitigate the local inhomogeneous effects resulting from fabric anisotropy on the global performance of the ball. In addition to design criteria based on performance, the context of the prototypes was considered. As a commercial product, the carcass had to use raw materials efficiently and be easily produced. These case studies only experimented with the manufacturing process used for the patch carcass ('overlapping panel carcass' described earlier). This process had the necessary flexibility to try different panel arrangements with the same materials, an ideal scenario from a modelling perspective. Furthermore, facilities were available to create working physical prototypes as well. From a manufacturing perspective, the goal was to keep production time low by limiting the number of pieces of fabric to be placed. The case studies and prototypes were created to explore and illustrate theory so manufacturing concerns were secondary.

One modification to the patch carcass was explored (designated patch carcass modification or PCMOD) and three completely novel carcass panel arrangements (designated Picasso, Triakis, and Tucasa) were developed and simulated. The PCMOD and Triakis carcasses were physically created for testing as well.

5.6.1 Modified Patch Carcass

The modified patch carcass, or PCMOD, was conceived as a simple adjustment to correct one of the greatest observed irregularities of the patch carcass. The strong anisotropic behaviour of each of the large six faces of the standard patch carcass was identified as a potential cause of unusual deviations from a straight rebound. The 3-panel face was very stiff when strained in directions orthogonal to the edges of the cube face and considerably more compliant when strained in corner-to-corner directions. To even out these irregularities, the PCMOD employed a similar construction, but with the centre panel of each face rotated by 45°. This rotation aligned the stiff warp/weft directions of the centre panel with the previously weakest orientation of the face and the more compliant direction of the centre panel with the stiffest orientations of the face. Figure 68 shows the standard and modified patch carcasses and the yarn orientations for an area in the centre of a face.

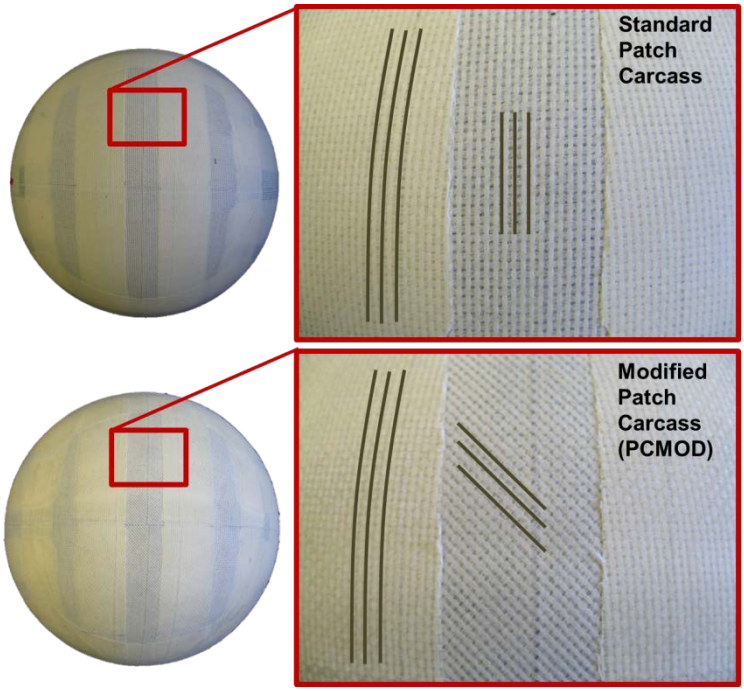

Figure 68: Standard (top) and Modified (bottom) Patch Carcass

Before the physical model shown above was produced, the PCMOD was simulated to determine the effect of rotating the centre panel of each face. The model used in the analyses was the carcass only, including only fabric and butyl layers to accentuate carcass anisotropy rather than outer panel properties and it shared the same basic geometry and material properties as used in the validation process described earlier. The rotated panel was specified with an additional material orientation specification for specific elements in the corresponding regions.

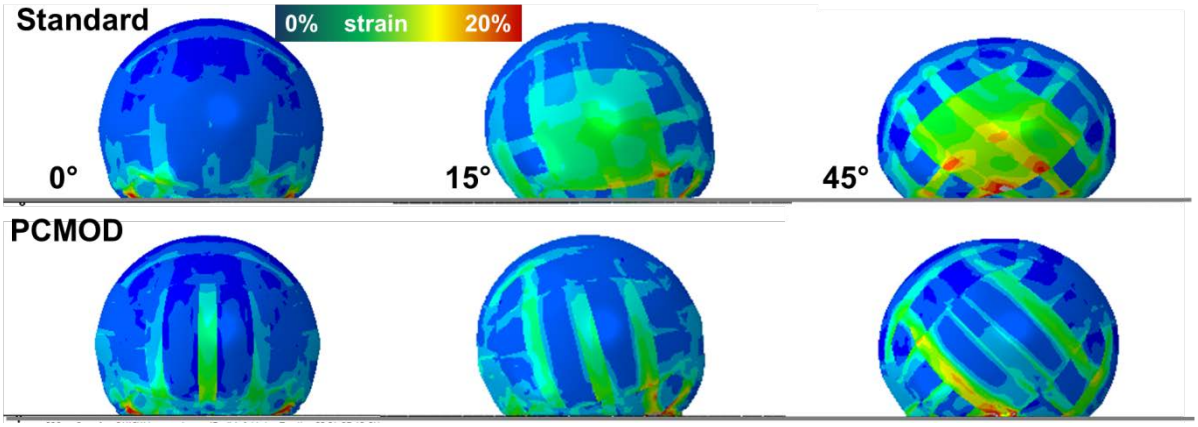

Figure 69: PCMOD Strain Comparison

Figure 69 shows a significant decrease in the overall amount of strain in 15° and 45° orientations between the standard and modified patch carcasses. In the 15° orientation impact, the reduction in strain correlated with a smaller horizontal shift that was quantified by looking at the rebound angle.

The rotated centre panel meant there was a section of each face with only one layer set at a 45° offset to the rest of the fabric layers. This, by design, made the face more compliant, but the centre section did strain more than other regions, as seen in the green bar in the lower left image of the figure.

To quantify the change, rebound deviation was measured for both the standard patch carcass and PCMOD in a variety of impact orientations. Rebound angle was projected to Z=2m away from the impact plate to give an XY position as the measure of deviation. The FE models were parameterised, allowing for relatively easy manipulation of carcass impact orientation and the ability to create a large number of simulations for good coverage and representation of the football's impact behaviour in general. Figure 70 shows the eighteen impact locations used. This system was also used in other prototype simulation evaluation in later sections of this document.

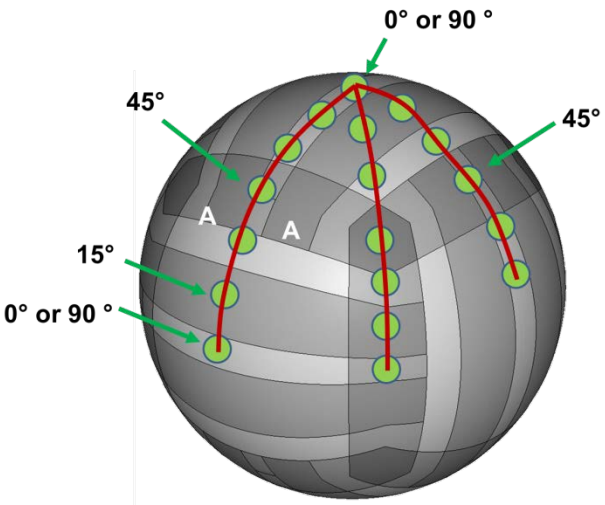

Figure 70: Standard Carcass vs. PCMOD, Impact Locations

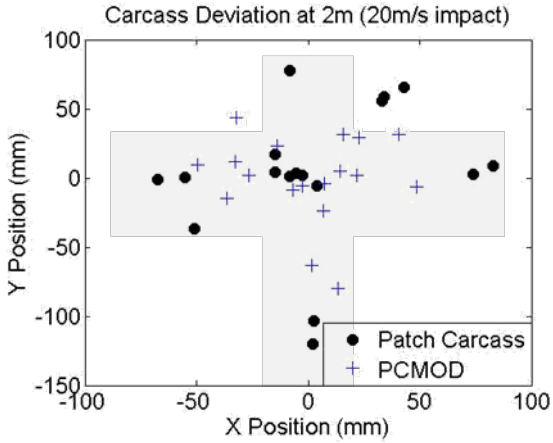

Figure 71: Carcass Deviation at 2m (20m/s Impact)

Figure 71 shows a tighter cluster of points for the PCMOD than the standard patch carcass. On average, the deviation from a completely vertical rebound was 35mm for the PCMOD and 54mm for the standard patch carcass. There is somewhat of a cross-type pattern in the point dispersion of the plot and this can be attributed to the cross-like pattern used to select the impact positions. The 0° and 45° positions had little deviation with points toward the centre of the plot and the deviation was focused along the X or Y axis for the other points because each of the points along the outer two arcs in Figure 70 had a symmetry (regions A and A in the figure are mirror images about the arc of impact positions between the two points referenced as 0° or 90°.

Disrupting the large inhomogeneous regions of the standard patch carcass with the rotated centre panel produced a more even strain distribution at full deformation and less of a horizontal shift and rebound deviation in simulations. Physical copies of the PCMOD were created to compare against the physical standard patch carcasses as well as the simulations as another way to check validity of the models. As mentioned earlier, greater strain was observed in the centre section of the 45° offset centre panel during full deformation. This compliance was also seen in the physical manifestations of the carcass using digital image correlation (DIC) software called GOM Aramis. By tracking individual points in a hand-drawn random assortment of small spots, the software calculated strain between still images or frames in a video. Strain was tracked while the carcasses were inflated from an atmospheric internal pressure to the recommended 13.5psi to produce the images seen in Figure 72. Strain in the centre panel of the PCMOD was approximately twice as high as in the standard patch carcass and this in-plane deformation translated to a 3D shape change as well.

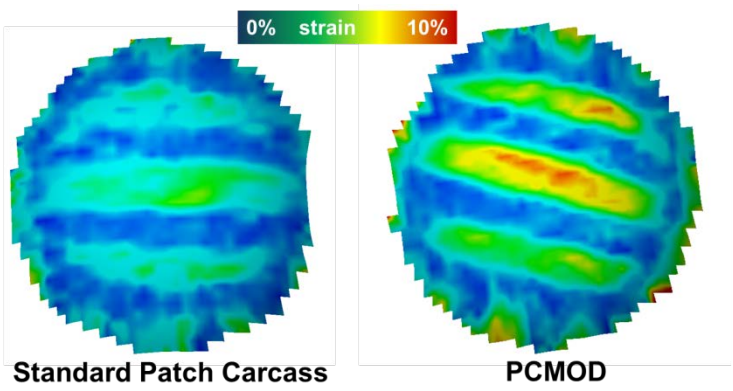

Figure 72: Strain in carcass due to inflation, DIC.

An optical 3D scanning system called Phase Vision was used to create clouds of about 110,000 points representing the surfaces of the standard patch carcass and PCMOD. The system observed the ball from a variety of angles and used image processing algorithms to determine the shape based on the distortion of a series of special patterns projected onto the surface. The manufacturer stated 50µm accuracy of surface geometry (PhaseVision 2011). After removing the protruding rubber valve stem, a centre point was calculated as the average XYZ position of all surface points. Radii between each point on the surface and the centre point were calculated and are presented as a coloured point cloud in Figure 73. Red represents a bulge. In the figure, the edges of panels are faint but a horizontal region of greater radius can be seen on the PCMOD following the compliant single-layer centre section. The differences in sphericity represented in the colour plots were also noticeable to the eye; the PCMOD bulged slightly at the centre of each face on the cube-based construction.

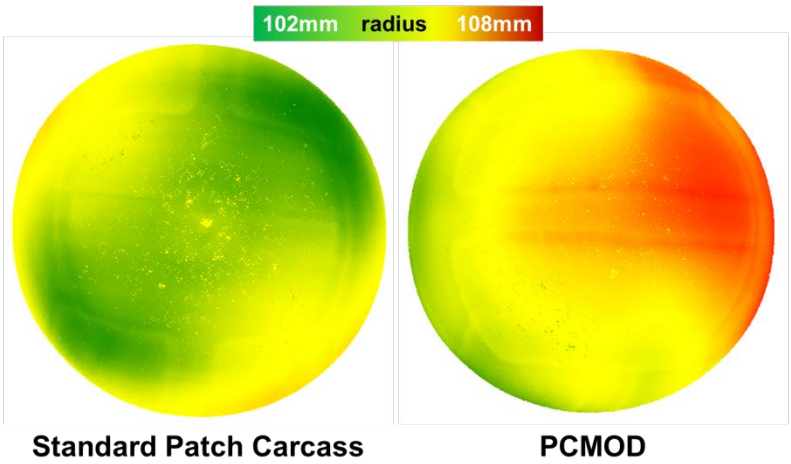

Figure 73: 3D Scan, Radius on colour scale

For the standard patch carcass, the average radius was 104.6mm and the standard deviation was 0.8mm. For the PCMOD, the average radius was 104.9mm and the standard deviation was 1.2mm

(see Figure 74). From the standard deviation and uneven distribution of radius points in the historgram for the PCMOD, it seemed the modified carcass panel arrangement had reduced the sphericity of the ball, potentially by weakening the centre section of each face.

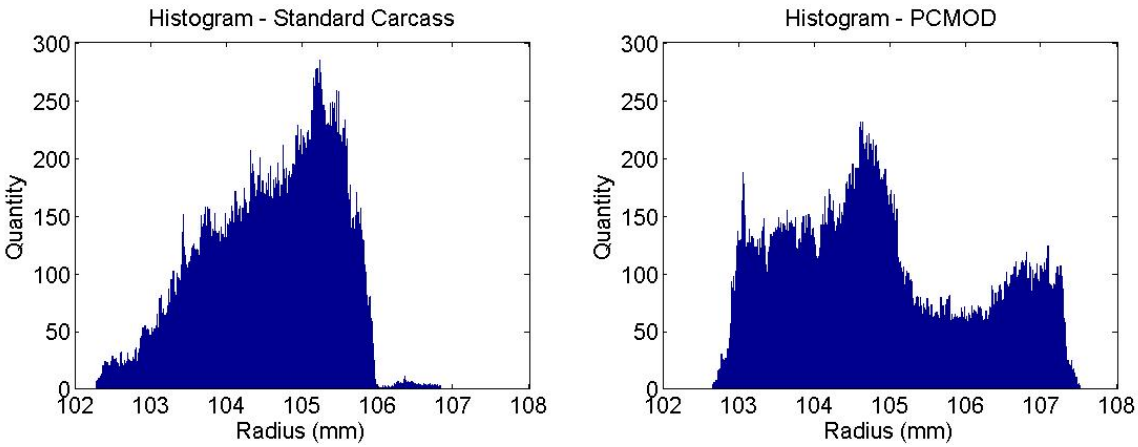

Figure 74: Standard Patch Carcass and PCMOD Scanned Radii

Though the modification on the patch carcass broke up the large region of anisotropy to allow for a more even distribution of strain during impact, the decrease in sphericity rendered the PCMOD configuration a step backward in creating a more uniform football carcass. The PCMOD study did illustrate the importance of balancing anisotropic effects as well as potential imbalances in stiffness from isolated single layers of fabric. This information proved useful in creating new carcass designs.

5.6.2 Novel Carcass Concepts

The patch carcass and PCMOD experiments demonstrated the importance of minimising the size of regions dominated by one material orientation as well as the need to have consistent stiffness through consistent fabric layering. A novel method of arranging panels on the surface of a sphere was developed to cover all regions of the ball with the same number of layers and to have those layers positioned in such a way as to minimise the effects of their anisotropy. The new designs were based on the Platonic and Archimedean solids and their duals because their projections onto the surface of a sphere discretise it relatively evenly. For simplicity's sake, the new designs were first conceptualised (and will henceforth be discussed as) flat-faced polyhedral. It was only after a 'solution' was found that it was projected onto a sphere for simulation or other visualisation purposes.

All polyhedrons can be 'unfolded' to be viewed as a 2D 'net', or a series of interconnected polygons. The concept for the novel design involved breaking the nets further into 'partial nets' consisting of polygon faces to overlap. Each partial net represents a piece of fabric cut from a sheet, and the entire group of identical partial nets for one ball can be assembled in a specific series of overlapping

polygons to completely cover the ball. It can be thought of as a geometric puzzle and a 'solution' is declared when a partial net and corresponding arrangement were found that covered each face of the polyhedron the same number of times, and each edge between polygons the same number of times. In its most basic sense, a solution was constrained by the number, or more specifically, the ratio of edges and faces on a polyhedron. Euler's relationship $E = V + F + 2$, where E represents edges, V represents vertexes, and F represents faces, holds true for the convex polyhedrons chosen as potential base structures and it was helpful in identifying potential solutions.

A cube has six faces and twelve edges so the partial net must have a complimentary face-to-edge ratio, where 'edge' is an internal or shared edge between two polygon faces. For a cube, there are many solutions and the first is a partial net made of two square faces joined along one edge. With one internal edge and two faces, twelve partial nets will ensure that each edge is covered once. The twenty-four faces (2 faces per partial net, 12 partial nets) distribute evenly to provide four layers of coverage on each face. This simple solution of two polygons and one internal edge is applicable for any uniform regular polyhedron because they all have a number of faces evenly divisible by two. Selecting potential partial nets that meet the criteria for edges and faces is relatively straightforward and with those criteria alone, there are a very large number of solutions. Just as any whole number can be a factor of some bigger number, many partial nets can be solutions if enough are used. A 'base solution' is one in which the minimum number of partial nets to satisfy the ratios does indeed constitute a valid solution. A 'multiple-solution' is one in which more than the base number of partial nets to satisfy the ratios is necessary to constitute a valid solution.

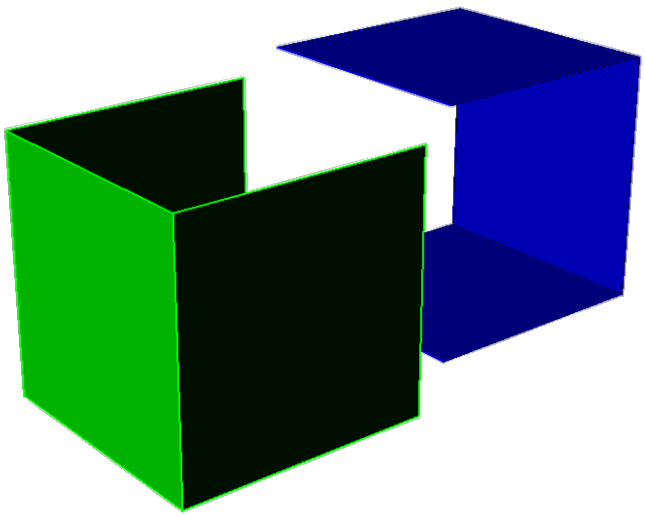

Figure 75: Two partial nets for a cube, exploded view

Looking further, a 3-square partial net with two squares on opposite edges of a centre square gives three faces and two edges. Based on these numbers, six partial nets should be a solution that

provides triple coverage of each face and 1 layer at each edge. The six partial nets are positioned so the centre face of each partial net lies on each of the cube faces and partial nets on opposite faces of the cube are oriented at 90° with respect to each other as shown in the exploded view in Figure 75.

There is a second possible configuration for a three-panel partial net – one in which the panels are joined to form an "L" or right angle shape. Though the ratio of edges and faces remains the same, the specific arrangement makes it impossible to position six partial nets evenly around the cube. A multiple-solution, however, is still possible. With twelve partial nets, and the centre squares of two partial nets spaced 90° apart (looking like a "+") on each face of the cube, each face would get 6 layers and each edge would be covered twice.

Multiple solutions, though valid mathematically and geometrically, sometimes lose relevance when considering the football context. Ease of manufacture decreases with more components and six layers of fabric, for example, would likely make a football far too stiff so attention was focused on the more desirable base solutions.

To identify potential solutions, partial nets and the quantities that satisfied the face/element ratio were identified for all Platonic solids. Next each potential was considered individually, trying to manually position each partial net to determine whether it is possible to do so to evenly cover the entire polyhedron. As in the cube example mentioned earlier, some partial nets worked and some did not. In attempt to determine which partial nets did and did not work geometrically, record was kept of all attempts for all partial nets and polyhedral including all the edges, faces, internal edges, partial net configurations, partial net quantities, and resulting edge and face coverage. These values were compared to identify potential trends manually and with the help of automated DOE software (Simulia Isight) designed to find correlations in data. Unfortunately, there was no correlation found between any of the 'inputs' of polyhedron and partial net characteristics and the 'output' of likeliness of the partial net fitting geometrically to provide even coverage. This meant each partial net that met the edge/face requirement had to be explored in a trial-and-error method to determine whether it did geometrically allow for even coverage.

For Platonic solids, fifteen partial nets were identified (1 tetrahedron, 3 cube, 2 octahedron, 1 dodecahedron, 2 icosahedron) and from those, nine were identified as able to provide even coverage based on the ratios of edges and face *and* the geometry (excluding multiple-solutions).

Table 9: Partial net solutions for Platonic solids

Polyhedron	Edges	Faces	Polygons per Partial Net	Internal Edges per Partial Net	# Partial Nets	Face Coverage	Edge Coverage
Tetrahedron	6	4	2	1	6	3	1
Cube	6	12	2	1	12	4	1
Cube	6	12	3	2	6	3	1
Cube	6	12	4	4	3	2	1
Octahedron	8	12	2	1	12	3	1
Octahedron	8	12	4	3	4	2	1
Dodecahedron	12	30	2	1	30	5	1
Icosahedron	20	30	2	1	30	3	1
Icosahedron	20	30	4	3	10	2	1

Archimedean solids, those composed of more than one type of regular uniform polygon (ie. squares *and* triangles), presented an additional challenge. With different types of faces and edges (eg. triangle-triangle and triangle-square), satisfying the requirements of an entire polyhedron with partial nets became more complicated. Table 10 shows the basic edge and face calculations. The lower half of the table describes the configuration of each polyhedron and the upper half deals with the edge and face ratios for the variety of shapes. The difficulty in maintaining edge and face ratios with multiple shapes can be seen in the column 'min faces/panel keeping edges/panel ratios'. The minimum number of faces per panel (i.e. partial net) climbed dramatically as the complexity of the polyhedron increased. Beyond the truncated cuboctahedron, partial nets had too many faces to consider for practical reasons. It is not known whether these complicated partial nets can even be positioned in such a way as to provide even coverage. The mental visualisation and paper model methods used to determine whether simpler partial nets could fit the simpler polyhedral were not capable of handling the more complex geometries.

The group of Platonic solids also contains the duals for the Platonic solids but Archimedean duals are an entirely different group of shapes called Catalan solids. Catalan solids are made of identical non-regular polygons. The dual to the truncated cube (Archimedean solid) is the triakis octahedron (Catalan solid), so-called because each face of the octahedron is split into three triangles. The triakis octahedron served as a starting point for one of the carcass concepts and the icosahedron (Platonic solid) was the base geometry for two others. In addition to the three concepts created in this study,

there are many more possibilities in the Catalan solids, and perhaps in concave Kepler-Poinsot polyhedrons or stellations of other convex polyhedrons.

Table 10: Archimedian Solids, Partial Net Solutions

polyhedron	edge types	type 1 edges	type 2 edges	type 3 edge	min faces/panel (based on panel ratio)	min edges/panel (based on edge ratio)	min faces/panel (considering edges)	min faces/panel keeping edges/panel ratios	edges per panel	number of panels required (total faces)/(faces per panel)
truncated tetrahedron	2	6	12	0	2	3	4	4	3	6
cuboctahedron	1	24	0	0	7	1	7	7	6	4
truncated cube	2	12	24	0	7	3	7	7	6	6
truncated octahedron	2	12	24	0	7	3	7	7	6	6
rhombicuboctahedron	2	24	24	0	13	2	13	13	12	4
truncated cuboctahedron	3	24	24	24	13	3	13	13	12	6
snub cube	2	24	36	0	19	5	19	19	18	3.33
icosidodecahedron	1	60	0	0	8	1	8	8	7	8.57
truncated dodecahedron	2	30	60	0	8	3	8	40	39	2.31
truncated icosahedron	2	30	60	0	8	3	8	40	39	2.31
rhombicosidodecahedron	2	60	60	0	31	2	31	31	30	4
truncated icosidodecahedron	3	60	60	60	31	3	31	31	30	6
snub dodecahedron	2	60	90	0	23	5	23	46	45	3.33

polyhedron	faces	edges	nodes	triangles	squares	pentagons	hexagons	octagons	decagons
truncated tetrahedron	8	18	12	4	0	0	4	0	0
cuboctahedron	14	24	12	8	6	0	0	0	0
truncated cube	14	36	24	8	0	0	0	6	0
truncated octahedron	14	36	24	0	6	0	8	0	0
rhombicuboctahedron	26	48	24	8	18	0	0	0	0
truncated cuboctahedron	26	72	48	0	12	0	8	6	0
snub cube	38	60	24	32	6	0	0	0	0
icosidodecahedron	32	60	30	20	0	12	0	0	0
truncated dodecahedron	32	90	60	20	0	0	0	0	12
truncated icosahedron	32	90	60	0	0	12	20	0	0
rhombicosidodecahedron	62	120	60	20	30	12	0	0	0
truncated icosidodecahedron	62	180	120	0	30	0	20	0	12
snub dodecahedron	92	150	60	80	0	12	0	0	0

5.6.3 Picasso

From Table 9, the most appealing option was the icosahedron in the final row. The name "Picasso" was used as a combination of "Patch carcass ICoSAhedron", and because early coloured renderings of the model were reminiscent of cubism. This concept had two layers of even coverage from ten partial nets. Though the octahedron had fewer partial nets, the faces of the icosahedron were smaller, decreasing the size of individual anisotropic regions as well as the overall partial net size. In addition, through informal trials, it was discovered that wrapping a large piece of carcass fabric (latex-impregnated) around the sphere was difficult to do without wrinkles. The polymer infused into the fabric limited the ability of the fabric yarns to shift to accommodate the spherical contour. The partial nets for the Picasso carcass consisted of four triangles connected point-to-base to line up as in Figure 76 (note: four triangles are connect and make up one piece of fabric, the figure shows each partial net split into individual triangles to emphasise the origins for the resulting panel shape). Though all ten partial nets were identical, five were placed 'backwards'.

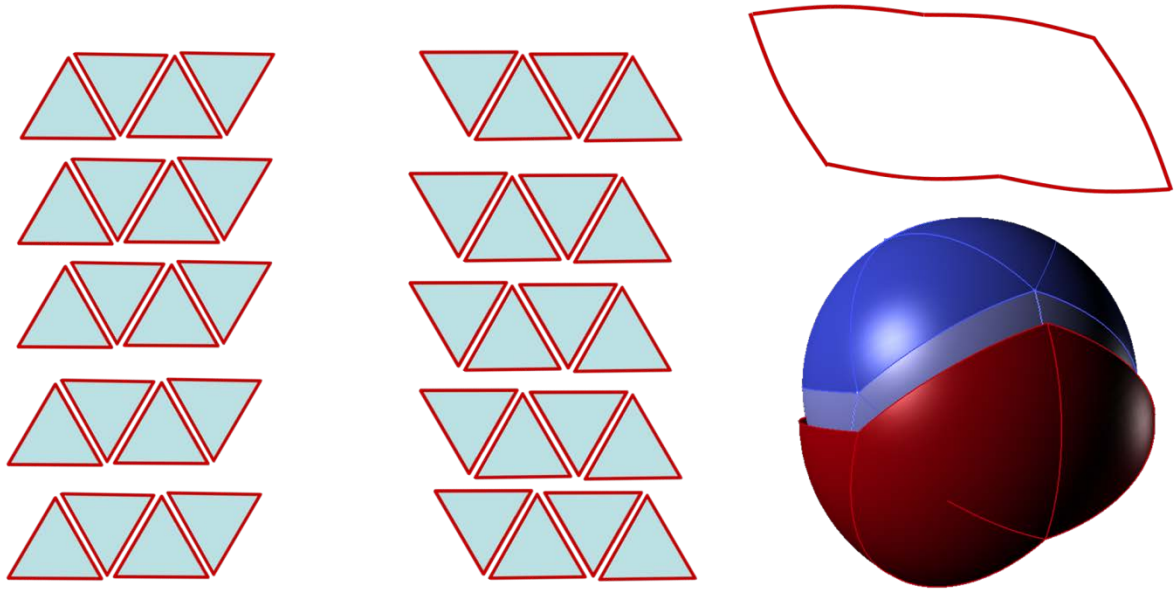

Figure 76: Picasso Partial Net Shapes

In addition to proper alignment between the ten partial nets and the triangles of the icosahedron, each piece required specific placement. Of the concepts created, the Picasso had the most elaborate or elegant placement of partial nets. There was a very precise method of panel placement; the panels could not simply be positioned at random to get a result of even coverage.

Figure 77 shows the assembly process using a 3D printed polymer model. Reading from left to right, top to bottom, the panels were put on sequentially in a series of overlaps. Note: some images in the figure show only a rotation of the previous image, and are intended only to provide a better view of the next panel placement.

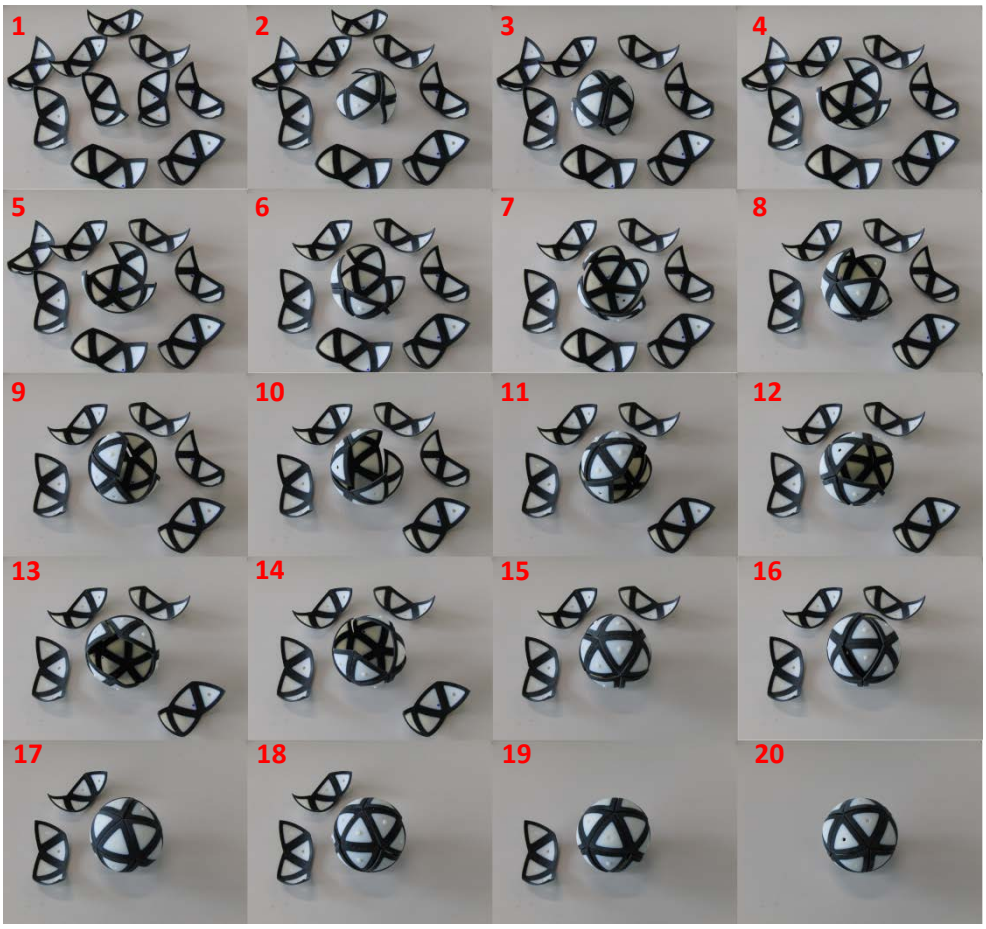

Figure 77: Picasso assembly process, right to left, top to bottom

With orthogonally woven orthotropic fabric, the two layers on each triangle were offset by 60°, meaning that each of the twenty triangles of the icosahedron had yarns at 0°, 60°, 90°, 150°, 180°, 240°, 270°, and 330°. On the left, Figure 78 shows two partial nets with layers (green and red) along the length overlapping to create the intersection seen in the diagram at the right of the figure.

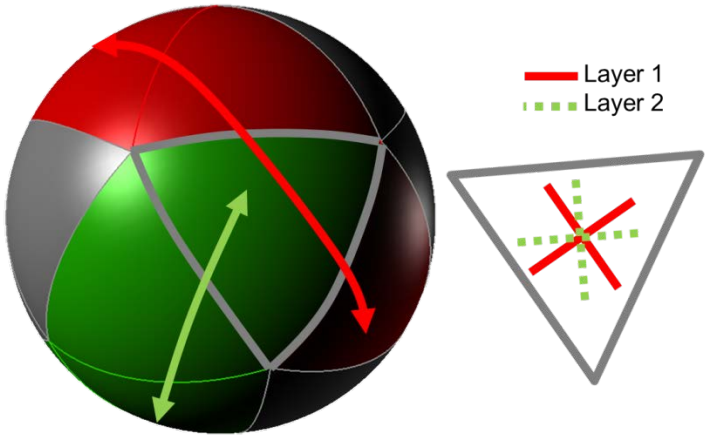

Figure 78: Picasso Panel and Yarn Orientations

5.6.4 Tucasa

The Tucasa concept was also based on the 20-triangle icosahedron but involved a far simpler arrangement of panels. The name "Tucasa" was a combination of "two" (for the number of panels), and "-casa" from iCOSAhedron. Each partial net consisted of two triangles and thirty partial nets were required for complete coverage (one partial net for each edge). The panels were arranged evenly by first placing six panels opposite to each other (similar to faces of a cube) and maintaining this placement pattern working around the ball for the remaining four sets of six. The result was triple coverage of every triangle and one layer covering each edge. As in the Picasso, each triangle had an identical combination of yarn directions from all three layers, but the result was even more uniform, with yarn directions spaced every 30°.

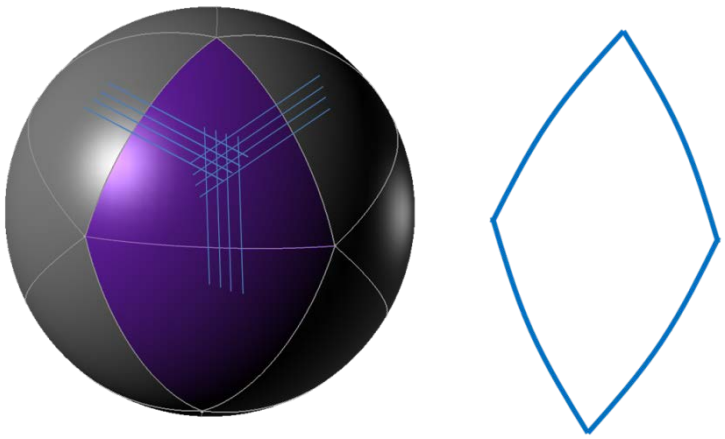

Figure 79: Tucasa Panel and Yarn Orientations

5.6.5 Triakis

The Triakis concept was based on the triakis octahedron, an octahedron with each face split into three wide-based isosceles triangles. The partial net for this geometry used four triangles, connected in a backwards "S" shape as seen in Figure 80. The result was two layers covering each triangle and one layer over each edge. The two layers' yarn orientations were offset by 30°, similar to the Picasso concept. Physical Triakis concepts were produced as complete carcass-bladder assemblies and full balls in the production facilities and with materials used to produce the 2012 adidas Tango12. The handful of carcasses made all had small (<3mm) overlaps at the edges, providing double coverage at the edges and a very thin strip of triple coverage at the edge of a triangle.

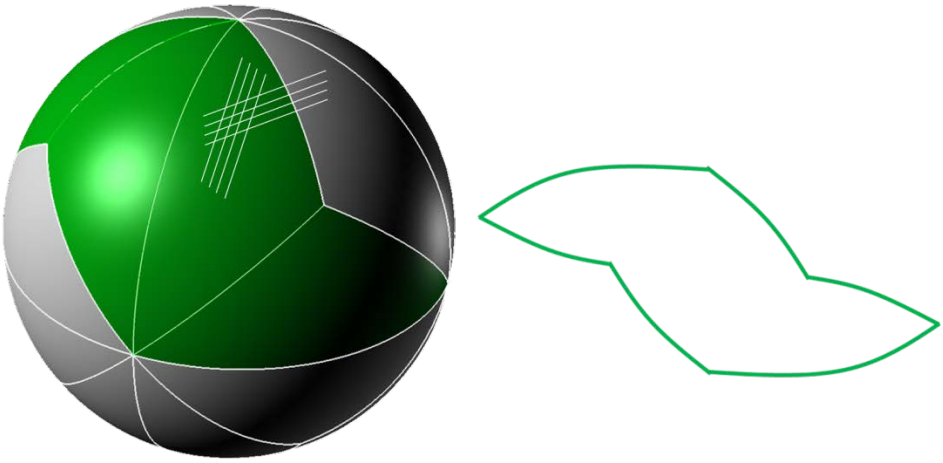

Figure 80: Triakis Partial Net Shape

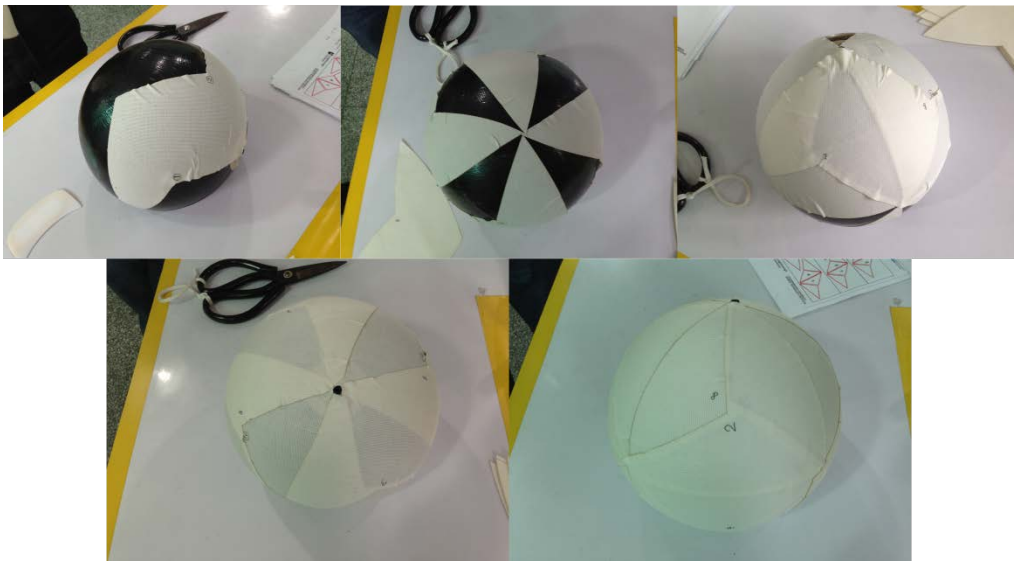

Figure 81: Triakis manufacturing procedure

5.7 Partial Net Carcass Prototype Comparisons

The patch carcass, Picasso, Triakis, and Tucasa were subjected to a series of simulated impacts following the series of orientations described earlier in Figure 70 with the same 20m/s impact speed and deviation output. An inspection of the surface strain patterns suggested that the attention to yarn orientation and layers of coverage in the partial net carcass prototypes had an effect in equalising the strain distribution on the carcass. Figure 82 shows abrupt high strains where the fabric coverage changed from one to two or three layers, especially close to the impact surface. Triakis and Picasso had similar strain magnitudes and the regions of different yarn orientation were made evident by the strain patterns but not as dramatically as in the standard patch carcass. Qualitatively, the strain appeared to have a more even distribution. The contrast between the standard patch carcass and the concepts was even more visible when comparing the strain during an impact with a 45° orientation (seen in Figure 83). The Tucasa concept was much stiffer, presumably because of the three layers of fabric. This was shown in the relatively low strain magnitudes in the contour plot as well as the perpendicular and inline deformation measurements.

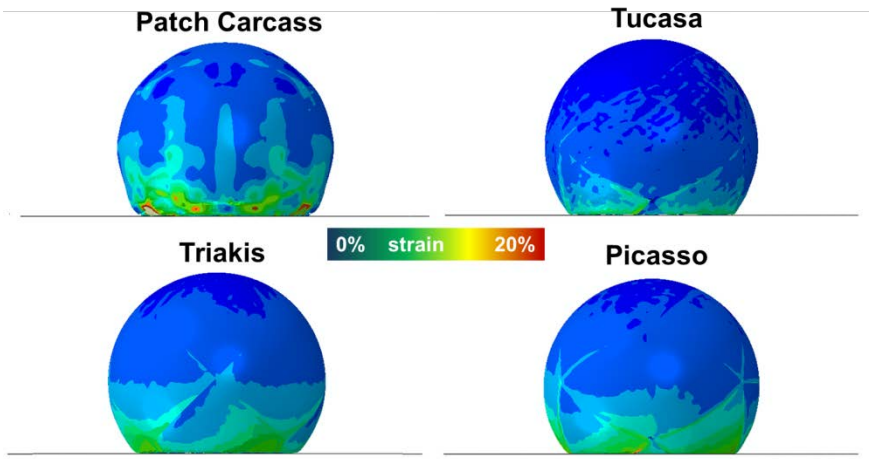

Figure 82: Partial net carcass concept strains (0deg orientation)

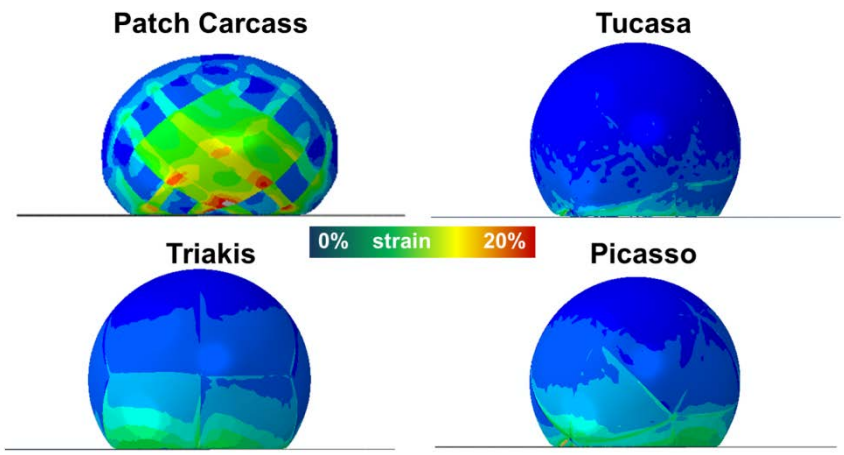

Figure 83: Partial net carcass concept strains (45deg orientation)

Table 11: Carcass Concept Deformation and Strain (20m/s, 0deg orientation imapct)

	Inline Deformation (m)	Perpendicular Deformation (m)	Max. Strain (%)
Patch Carcass	-0.038	0.011	31.4
Picasso	-0.037	0.006	16.0
Tucasa	-0.035	0.002	15.9
Triakis	-0.041	0.003	10.8

Even strain distributions were found to translate to a more uniform bounce. The average rebound deviations for the Picasso, Tucasa, and Triakis concepts were 23mm, 5.4mm, and 6.5mm respectively, which represented a significant improvement in carcass consistency over the standard patch carcass with an average rebound deviation of 54mm. The two plots in Figure 84 show the same information on different scales. The partial net concept carcasses did not exhibit the same cross-like point spread as the standard patch carcass because the faces or anisotropic regions were smaller and not aligned with an orthogonal grid.

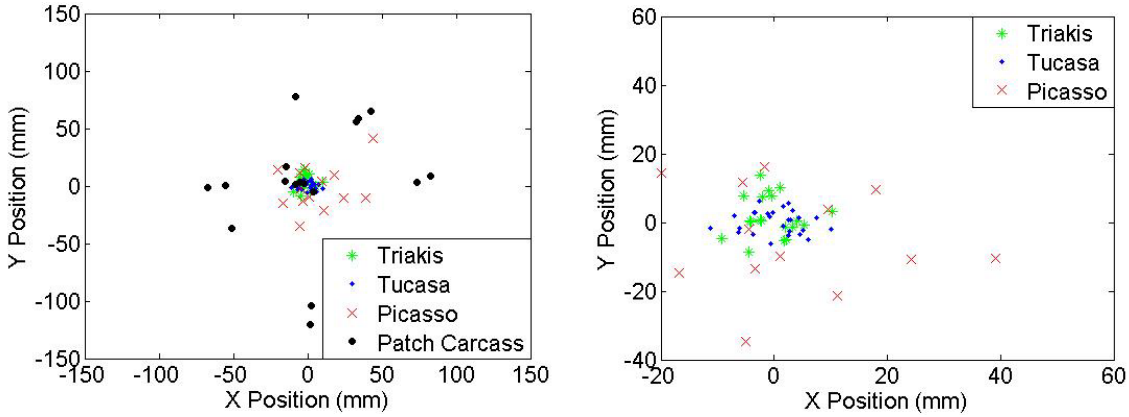

Figure 84: Carcass concept rebound deviation simulation from normal Impact at 2m

Comparing pressure and volume (Figure 85) for the four football carcasses gave an additional indication of global stiffness. The Tucasa, with three layers of fabric, was stiffest, followed by the two two-layer configurations. The relative compliance of the standard patch carcass emphasised the amount of compliance that is introduced with only small sections of one layer of fabric. Earlier material tests identified a stiffening of carcass fabric throughout the assembly process so this overall stiffness should be considered along with rebound consistency when evaluating overall performance.

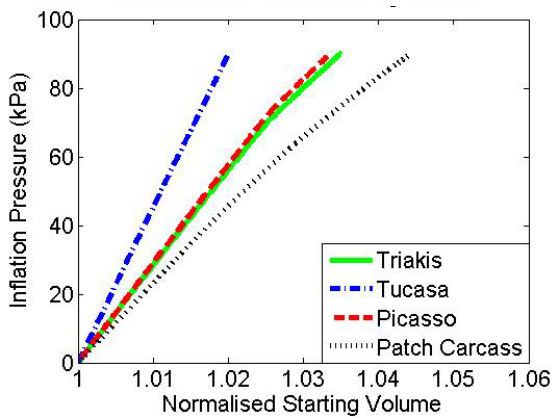

Figure 85: Simulated prototype stiffness comparison, pressure vs. volume

In another measure of stiffness, the physical Triakis was compared against the standard patch carcass with quasi-static compression of 5cm between a flat plate and a 10cm diameter cylinder. Five orientations (Figure 86) were chosen for each carcass to include a wide variety of overlaps, layers, and intersections and three of each carcass were tested. The standard patch carcass had a average maximum reaction force of 1438N and the average for the Triakis was 6% greater at 1525N. The standard deviation for the measurements on the patch carcass was 228N and the spread of the data for the Triakis was much tighter with a standard deviation of 21N.

Figure 86: Carcass Compression Orientations

5.8 Summary

The same trends connecting the patch carcass material and panel configuration with rebound deviation after a flat plate impact were identified in both physical lab drop tests and simulations. The deviation from a vertical rebound was attributed to a non-uniform asymmetrical deformation dependent on the locations of anisotropic regions on the carcass. The asymmetrical deformation induced a rotation which sent the ball off at an angle.

The effect of indenter on the rebound deviation was studied with a matrix of simulations, revealing that the size and shape did not have as great an effect on rebound deviation as the size of the inhomogeneous regions on the ball. With evidence to suggest that larger regions of inhomogeneity on a ball contribute to inconsistent rebound behaviour, a series of prototype football carcasses were developed to decrease rebound deviation while using current materials and manufacturing processes. The three prototype carcasses were based on a novel system of overlapping series of connected polygons orientated on the faces of specific polyhedra and simulations suggested that all would out-perform current carcasses in rebound consistency tests.

6 Design of Experiments and Optimisation

6.1 Intentions

Design of experiments (DOE) and optimisation studies were carried out to expand the utility of a single football model and explore trends in construction and performance characteristics. The sets of simulations used earlier to investigate carcass geometry and evaluate carcass concepts could be considered simple DOEs and optimisations but the work presented in this chapter focused on automated methods and case studies. Though the purposes of the two types of studies are very different, they operate along similar principles, leveraging computational power to develop a more comprehensive view of a physical scenario. They each had their benefits and could be used individually or together to investigate different aspects of football impact behaviour.

The primary use of DOEs was in experimenting with the effect of one or more inputs on the variety of measured responses used in previous studies. The influence of one material or component on the global performance of the ball was expected to be nonlinear, and also dependent on the other materials and components, making the problem a multi-dimensional web of interconnected parameters and a good candidate for DOE exploration.

With the premise of automatically progressing toward a tangible goal, an optimisation takes the exploratory concept of a DOE and a mapped design space further into implementation. The merits of this type of study in research-based work are mixed. Using algorithms and automated data management and analysis techniques, many simulations with different parameters can be created and used to find the answer to a specific question if configured properly. A simple answer is often useful but in research applications, if misused, automated optimisation can become a “black box” which produces an answer from inputs while obscuring the solving mechanisms. In this work, the optimisation was used as an investigative tool, in part to check hypotheses that had been created from a more in-depth look at the football impact system.

Some characteristics of a football may shift with match- and tournament-specific requirements or changes in consumer preference. Size, weight, energy return, materials, global stiffness, and thermal dependence, among other properties, could conceivably be manipulated sometime in the future to follow changes in the game or players. Rebound consistency, however, was assumed to one characteristic which should always be maximised so it was used as a goal in these optimisation studies.

6.2 Simple Yarn Orientation Study

As a first step into automated optimisation, a simple study was devised to test dependency of deformation on yarn orientation. A carcass-only football was modelled with coarse mesh (target element size 4mm) to minimise computational time. Rather than the typical nonlinear fabric model used in studies mentioned earlier, a simpler anisotropic linear elastic model based on fabric strip tension testing was used. A projected icosahedron divided the mesh into twenty triangles and two sections of three triangles on opposite sides of the sphere were designated as regions of variable fabric orientation while the rest of the football remained isotropic. Red areas in Figure 87 were specified to be isotropic. White areas were assigned a variable yarn orientation. From a 20m/s impact, perpendicular deformation as measured and taken as a characteristic output likely to be influenced by the yarn angle. Earlier experiments with the standard patch carcass showed a strong relationship and the goal was to automatically determine the yarn orientation that created the stiffest response. The expected result was a 0° yarn orientation, or yarns running parallel to the impact surface and in line with the hoop strains around the equator of the football.

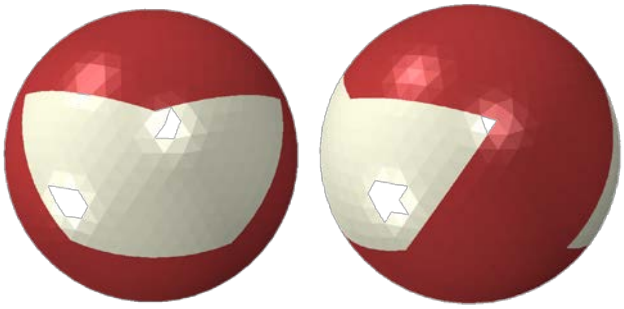

Figure 87: Yarn orientation study, anisotropic vs. isotropic regions

Simulia Isight (product of 3DS Dessault Systèms, Paris, 2014) was used to run the design of experiments. This program was chosen for its compatibility with the FE solver (Simuila Abaqus) and available DOE and optimisation pre- and post-processing algorithms. A “Pointer” algorithm was chosen because it incorporated genetic, downhill simplex, NLPQL, and a linear solver. The variety of solving types made the process more flexible and it was recommended by the software provider for its ability to work in a variety of design space configurations. Though not necessarily the quickest computationally, the human time saved by selecting a general algorithm over iteratively configuring a special algorithm made it worthwhile. Eighty simulations were conducted, each with a different yarn angle chosen automatically.

The strain contour plots (with overlaid approximate yarn orientations) showed a trend similar to what was seen with the standard patch carcass. Strain was greater when the fabric was oriented at

its weakest 45° orientation in line with the hoop strains. The optimisation was set to start with a 45° angle and progress toward the lowest average of maximum deformation of two perpendicular diameter measurements parallel to the impact surface between nodes at the middle of the ball. The simulated maximum average diameter occurred at full deformation and for the 45° angle, it was 0.218m. At the end of the optimisation study, the stiffest result was found to predict an average diameter of 0.2093m at a yarn orientation of 3°. The expected 0° orientation produced an average diameter of 0.2094m. Diameter could only be measured between nodes and a slight offset from a measurement parallel to the plate may have influenced the optimisation. The 0° iteration was attempted immediately after the 3° optimisation, indicating that the algorithms had identified the trend of lower yarn angles and stiffer responses. The optimum solution was reached after only eight iterations but subsequent simulations continued to explore the rest of the design space to ensure that the first result wasn't only a local optimum. In this relatively simple example, the design space was continuous and nonlinear as shown in Figure 89 (note, the straight line is a best fit line, included only to emphasise the nonlinearity of the response). The nonlinearity of the response was particularly interesting given the results of carcass material testing. The material tests (discussed earlier) performed on strips with different yarn orientations suggested the greatest change in tensile stiffness between 0° and 15° but the gradient for the global football change was steepest around 20°.

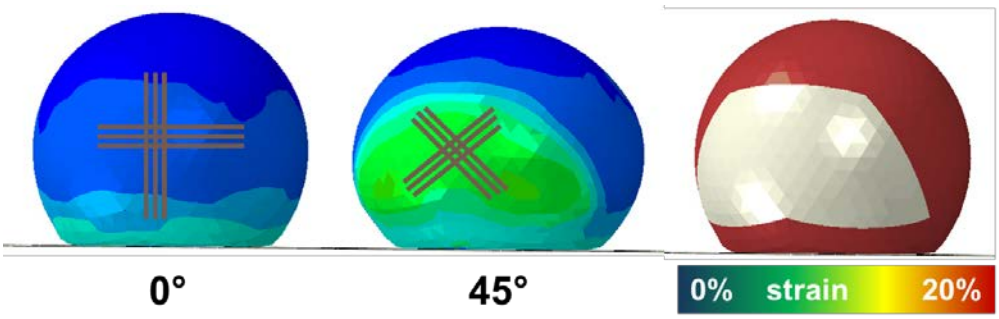

Figure 88: Yarn orientation optimisation, strain plot

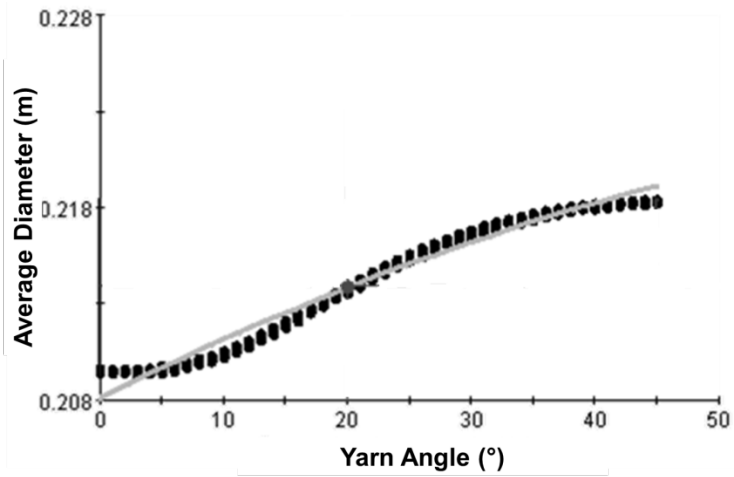

Figure 89: Yarn angle and average deformation perpendicular to the direction of motion

Two possible causes were identified to explain the difference between the logical result given the known material properties and simulated global ball behaviour. Either the simple multi-orientation fabric strip testing and accompanying linear elastic anisotropic material model did not accurately represent the material, or the football shape and mode of deformation introduced a type of geometric nonlinearity. The difference seen in the material testing between strip and dog bone tensile tests with fabrics at different orientations highlighted the potential inadequacy of that style of testing; with differences between the two specimen geometries, the behaviour of yet another shape of material (in situ, for example) would be unknown. To investigate further, an identical optimisation was run using the picture-frame anisotropy test and the *fabric material model. The 45° yarn orientation produced a perpendicular deformation of 0.219m, the 3° orientation gave a deformation of 0.208m and the 0° deformation gave 0.2088m. These values indicated a slightly more compliant material model then the linear elastic formulation but the general trend for the football response was the same (Figure 91). The persistence of nonlinearity in deformation with different yarn orientations despite multiple material models was a good indication that geometric nonlinearity was present. Material properties cannot be assumed to translate evenly to football deformation characteristics.

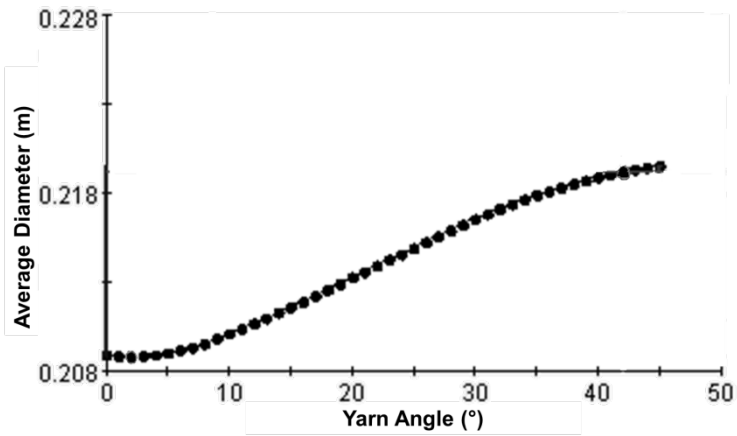

Figure 90: Yarn angle and deformation (*fabric model)

6.3 DOE: Relative Panel Contribution

The effect of fabric yarn orientation of panels in the great circle hoop direction was first noticed in the standard patch carcass and explored further with the optimisation but the studies did not explain its influence on other regions of the ball. Building from the simple yarn optimisation study, a DOE was created to better understand the contribution of regions above and below the great circle parallel to the plate. The model used in the optimisation study was modified to have additional anisotropic panels with variable orientation. Two single triangles of the icosahedron mesh pattern were given anisotropic properties and a fabric orientation as well. The new blue regions, in addition to the white regions, had variable fabric panel orientations. The DOE was configured to give a variety of yarn angles to the white and blue regions independently (all white panels had 1 yarn angle, each blue panel had a yarn angle). There were many ways to combine the multiplier parameters. A simple (but multi-dimensional) grid of points could specify all possible combinations of parameter values, or combinations could be specified individually (manually). For computational efficiency and uniform coverage of the design space, an automatic system of combination generation was implemented. One such system, a Latin Hypercube, divides the design space for each parameter uniformly and creates random combinations to cover the entire design space. In this work an Optimal Latin Hypercube structure was chosen. The Optimal Latin Hypercube followed the same basic principal of combing discretised continuous variables as a standard Latin Hypercube, but the combinations were optimised to provide the best coverage of the design space with the lowest number of individual combinations. The result was a computationally efficient way to cover the design space that could be easily interpreted and analysed by post-processing algorithms. This study used five hundred design points.

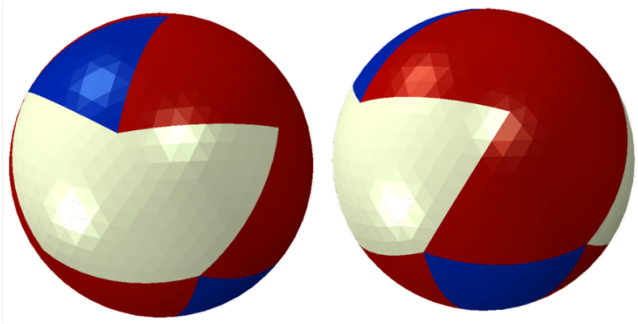

Figure 91: Yarn orientation DOE, white and blue panels were assigned an anisotropic property definition, red was isotropic

Strong trends relating the centre panels of the football (with respect to impact orientation) to deformation suggested that other regions of the ball may not be as effective in controlling impact behaviour. Rather than inspect the table of numerical results generated by the simulations, 'approximations' were created to extrapolate and expand the utility of the data as well as make it more comprehensible. The automatic process involved viewing the DOE as a system with inputs and outputs and creating a function that approximated their relationship. A radial basis function (RBF) was used to create the approximation functions (Simulia 2011b). The RBF is based on principles derived from biological neural networks' abilities to draw connections. The functions relating variables made it easier to identify trends between inputs and outputs but they also provided the capability to see 2nd order dependencies, or the influence of input A on the relationship between input B and output C. Leveraging the power of algorithms helped to present themes that came from the large number of simulations. In this simple case with only three inputs of yarn angle from 0° to 45° and one output (perpendicular deformation), the results could be summarised in three trend plots (Figure 92). The two on the right show the effect of the blue panel yarn angle on the average maximum diameter measurement – the same measurement in the optimisation in the previous section. The flat line means that as the yarn angle changes, the average maximum diameter stayed relatively consistent. The white panel yarn angle shown in the left plot, however, shows a dramatic change, similar to the plot seen for the optimisation. With only a couple input parameters and one output of interest, the data could also be viewed as a 3D plot (Figure 93).

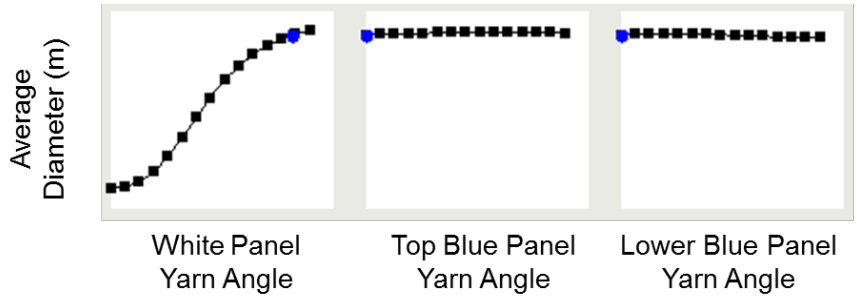

Figure 92: Yarn angle DOE trends

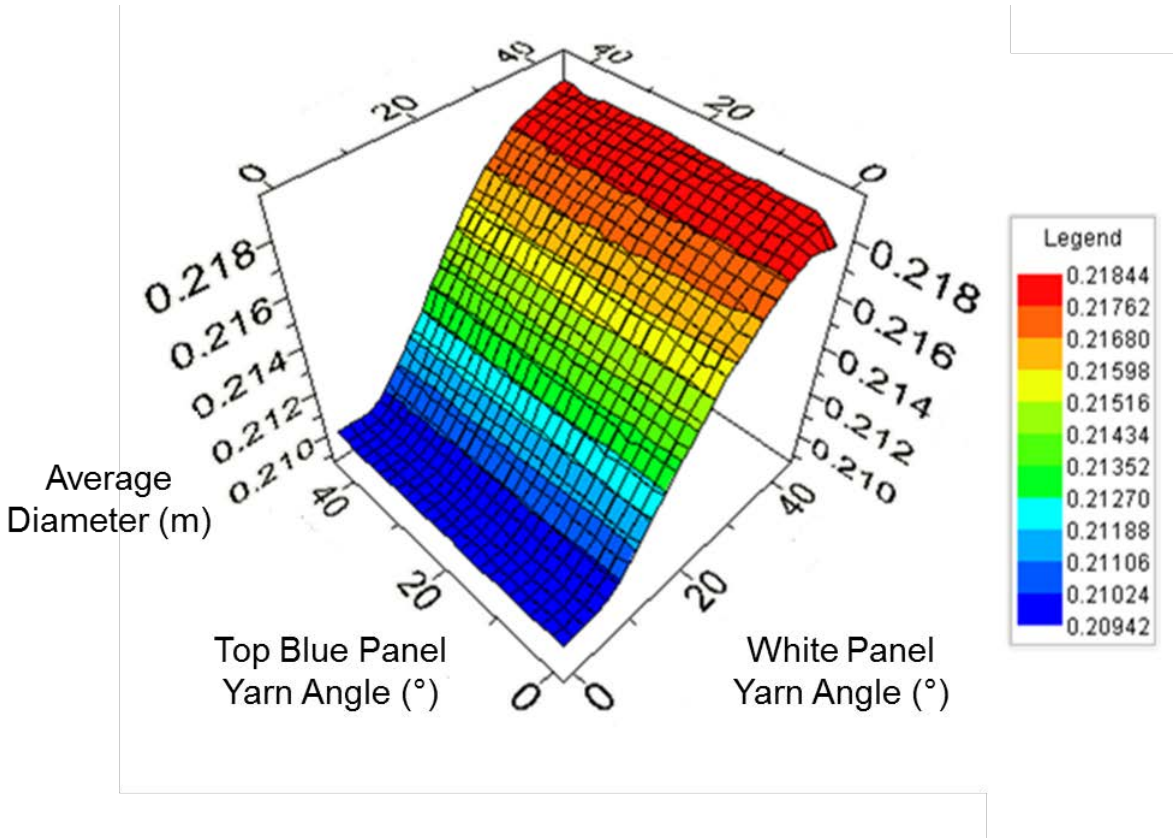

Figure 93: Yarn Angles and Average Diameter

The difference could also be expressed quantitatively as gradients based on a regression analysis. The bars in the graph (Figure 94) representing the blue panels show that, on average between 0° and 45°, a change in yarn orientation has about 1/5th the effect on perpendicular deformation as the yarn orientation of the white panels. The effect on an output parameter can be presented as local or global gradients. The gradient of an approximation function varies in all but simple linear relationships. A local effects gradient shows the effect of a change in each input parameter if the model starts at a specific design point. A global effects gradient averages the effect across the possible range of each input parameter. In this particular example, due to the relatively simple relationships, the local and global effects plots showed the same trends.

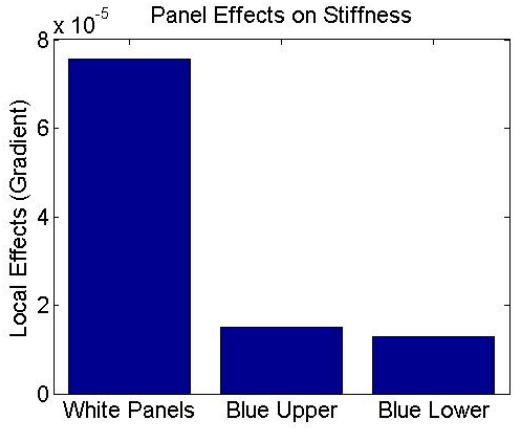

Figure 94: Panel Effects on Global Stiffness

The conclusions from this DOE and the earlier optimisation may have been reached with intuition or an educated guess but numerical validation was a useful exercise. In addition to confirming theories on anisotropy and deformation, the studies laid the groundwork for understanding more complicated constructions.

6.4 DOE: Relative Component Contribution

In being a part of the system, each material must add something to the overall performance of the football but in the past, the individual contributions have been lost in the combination. Isolating the effect of each material on measureable characteristics during an impact had potential to provide a unique insight into the relationship between materials, construction and football performance. By systematically altering material properties, a DOE study was able to separate and assign relevance to the components of a football in a normal flat plate impact.

The same basic construction as earlier optimisation models was used (Section 6.2), with shell elements and composite sections, but the mesh density was reduced (4mm target size) and mass scaling was increased to decrease analysis time. Due to the individual availability of materials from each of the layers – outer skin, foam panel, carcass, stitched regions between carcass panels, bladder – the specific ball was based on the 2010 adidas Jabulani. Unlike other, multi-orientation studies performed earlier, the DOE incorporated only one impact orientation. The dodecahedron carcass was not known to exhibit the dramatic differences in response seen with the standard patch carcass. Using a single impact orientation de-emphasised the role of anisotropy in the ball and allowed for a more direct focus on the other material properties.

The materials had specific properties and thermal dependencies discovered earlier. For the purpose of the DOE, the materials were taken as a starting point, on the reasonable assumption that

footballs will have similar components and materials with similar properties. From this baseline, the DOE modified the material properties to explore a range of possibilities.

Tensile material behaviour was characterised with curves prescribed by nine stress-strain data points. For the polymeric materials, polynomials for the strain energy potential Yeoh (3rd order reduced polynomial) were calculated before the analysis and the data points were used to describe tensile and shear stiffness for fabric materials. These nine stiffness data points were manipulated using a linear multiplier on the stiffness (multiplier of 1 made no change, a multiplier of 2 doubled the stiffness). Each material had an individual multiplier, which was allowed to be between 0.25 and 6. Impact speed was also set to vary between 2 and 30m/s. The DOE selected combinations of multiplier values to use in the simulations with an optimal Latin hypercube distribution as used earlier. Four hundred simulations were run.

The following information was extracted from each individual simulation: perpendicular deformation (X and Z), inline deformation (Y), contact time, maximum reaction force, rebound speed, maximum cavity pressure, minimum cavity volume, and XYZ coordinates of the centre of mass (used to calculate COR and deviation). Results were stored in a database with the input parameters as well. The range in input values produced a broad spectrum of outputs within the limits outlined in Table 12.

Table 12: DOE – Ranges of outputs

Output	Minimum	Maximum
Coefficient of Restitution (COR)	0.06	0.84
Contact Time (ms)	0.0016	0.0099
Perpendicular Deformation (m)	0.0003	0.016
Deviation from Vertical Rebound (m)	0	0.015
Maximum Reaction Force (N)	203.3	10280
Pressure vs. Volume Stiffness (Pa/m^3)	53815	$5.8x10^8$
Inline Deformation (m)	-0.007	0.173

As in the yarn orientation study, an automatic approximation was created to identify potential 1st and 2nd order trends. As a test of the approximation, ten values for each output generated with approximation's functions were compared with output values taken from the series of simulations. The RMS errors for each output are presented in Table 13 in which an error of zero means the approximation functions produce the same result as a simulation. The values represent the root

mean square difference between the FEA simulated value and the algorithm used to generate an approximation of the output. The RMS values are normalised by the output variable range to allow for comparison of error between different outputs approximations. In the table, the error for contact time is clearly too large, indicating that the algorithms did not generate an acceptable approximation of the relationship between contact time and material properties.

Table 13: RMS Error for materials approximation

Output	**RMS Error**
Coefficient of Restitution (COR)	0.024
Contact Time (s)	0.114
Perpendicular Deformation (mm)	0.051
Deviation from Vertical Rebound (mm)	0.053
Maximum Reaction Force (N)	0.090
Pressure vs. Volume Stiffness (Pa/m^3)	0.057
Inline Deformation (mm)	0.016

The dataset resulting from the large DOE can be interpreted by selecting two inputs and visualising their influence on one output with simple charts. Figure 95 shows relationship between carcass fabric tension and perpendicular deformation (expressed as a maximum diameter at impact) at two different impact speeds. The relatively flat line at low impact speed indicates that the stiffness of the carcass has a relatively small effect for slow speeds but at high speeds, the gradient is much larger, showing that a stiffer carcass results in smaller deformations.

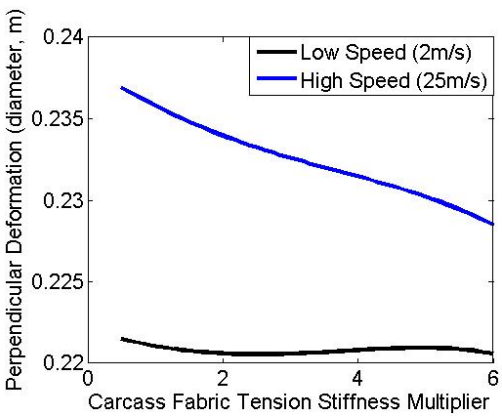

Figure 95: Effect of carcass stiffness on perpendicular deformation at low (2m/s) and high (25m/s) flat plate impact speeds

Viewing the same data from a different perspective, Figure 96 shows the relationship between impact speed and perpendicular deformation for three carcass stiffness scenarios. The black line represents the standard carcass material, the blue line has the yarns 5x stiffer, and the red line shows the data with stiffer yarns, as well as a 5x increase in shear stiffness. This graph shows that stiffer carcass fabric has a shallower speed-deformation gradient, and that the yarn tensile stiffness has a greater effect than the shear stiffness in the relationship between deformation and impact speed.

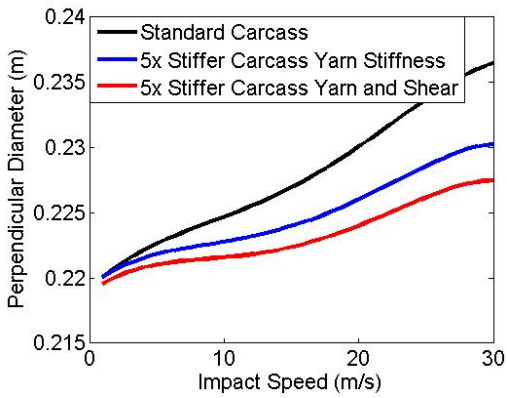

Figure 96: Effect of impact speed and carcass properties on perpendicular deformation

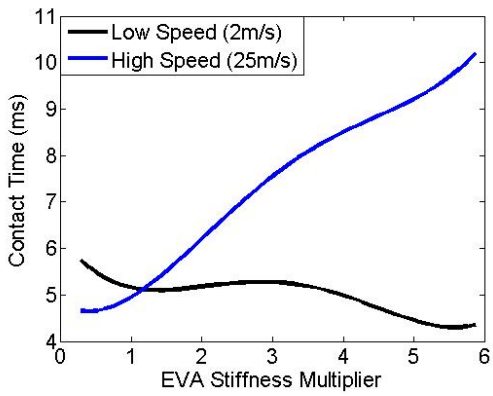

Figure 97: Effect of EVA stiffness on contact time at low (2m/s) and high (25m/s) flat plate impact speeds

EVA had a greater effect on contact time at high impact speeds than at low impact speeds. Like the trends shown in Figure 95, Figure 97 shows a greater gradient between the input and output at higher speeds than at lower speeds. The humps or slight curves in the trend lines can likely be attributed to the material and geometric nonlinearities in the analysis. In general, the influence of changes in material stiffness was greater at greater impact speeds than at lower impact speeds. At greater impacts speeds, deformation was greater and the materials were consequently working in a higher strain region. The football materials tested and used in these simulations behaved

nonlinearly – increasing stiffness at greater strains – and this material behaviour may be responsible for some of the trends identified in the DOE.

Figure 98 removes the effect of speed by including all impact speeds in the algorithm to show the effect of bladder stiffness on maximum impact force at high and low EVA stiffness. When the foam was stiffest, the effect of the bladder was not as great as when the EVA foam was more compliant. Intuitively, this makes sense; if all the materials on the ball except the bladder were extraordinarily compliant, the properties of the bladder, which is usually the most compliant component, would play a larger role in determining the outputs.

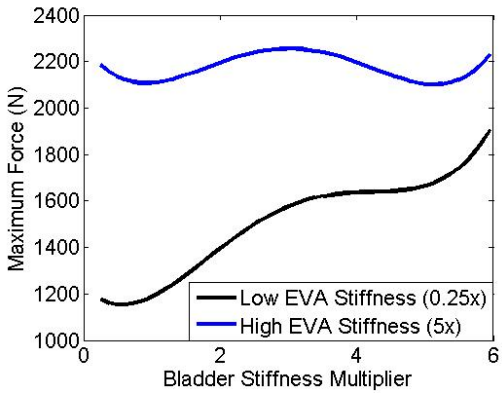

Figure 98: Effect of bladder material stiffness on maximum impact force at high and low EVA stiffness

The ability to generate 2nd order relationships like this was one of the benefits of using DOE methods; the results were too complicated and unexpected to reach with a traditional simulation workflow and a deliberate investigation.

6.5 DOE: Fabric Yarn Offset Angle

A DOE was created to help better understand the effects of additional layers, specifically the yarn orientation. In the study, each triangle of an icosahedron was given an arbitrary yarn orientation and assigned to one variable angle value between 0° and 45°. The 2nd fabric layer for each triangle was assigned to one angle offset between 0° and 45°. This simple setup was controlled by only two input parameters to limit the number of necessary iterations, but it still allowed for an indication of the overall influence of the 2nd layer yarn offset over the range of possible 1st layer yarn orientations. Figure 99 shows the general trend generated with an automatic approximation made with the results from 100 simulations. The actual rebound deviation magnitude depended on the orientation of the first layer so it is presented as a trend rather than absolute values. A 45° yarn offset meant the stiffest orientation of the two-ply section occurred every 45° and this improved consistency was evident in the lower rebound deviation values.

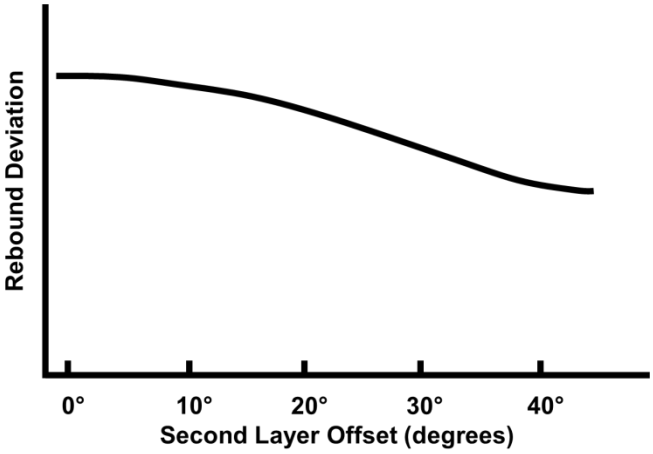

Figure 99: Second layer yarn orientation and deviation

This result revealed another benefit of the Archimedean solid-based novel patch carcass concepts; the 30° yarn orientation offset introduced by the triangular shapes of the uniform polyhedrons and the orthogonally woven was close to the ideal offset. The trend seen in the DOE supported the patch carcass concepts but also suggested that there is room for improvement. A patch carcass design which necessitates a 45° offset between two layers of fabric may be a further improvement over the current most consistent carcass concepts. In addition to the offset angle, the geometry of the panels must also be considered. Despite both having 30° yarn offsets between their layers, the Picasso and Triakis produced significantly different results for rebound deviation. An explanation for the difference may be the anisotropic region size. The Picasso had 20 triangles with different yarn orientations and the Triakis had 24 triangles so the size of adjacent regions with different properties was smaller, creating a more uniform distribution of anisotropy. The Tucasa, though it was also divided into 20 triangles, had three layers fabric so it cannot be compared in this way.

6.6 Summary

Using the finite element models optimised for parametric alteration and short computational times, a series of DOE and optimisation studies were performed to support ideas about the relationship between fabric anisotropy and rebound deviation. One study showed that panels along the equator of the ball have a greater effect on deformation than those at the poles. Another study confirmed that aligning the yarns in the direction of the hoop strains and stresses creates the stiffest response with the lowest amount of deformation.

In addition to yarn orientation-based studies, a DOE was constructed to highlight the effect of individual materials (or components) on the deformation, contact time, COR, and reaction force during a flat plate impact. At high impact speeds, the effects of carcass stiffness had a greater effect on deformation than at lower impact speeds. Also at high impact speeds, the effect of EVA stiffness

was greater on contact time than at low impact speeds. When the EVA foam was stiffer, the bladder stiffness had less of an effect on the maximum impact force than when the EVA foam was more compliant. These and other relationships were extracted from automated approximations fit to 400 simulations.

7 Acoustics

7.1 Intentions

Throughout experiments with footballs and while handling other inflatable sports balls, qualitative differences in sound were noticed. In particular, older machine-stitched footballs had a short dull sound and the new patch carcass and patch carcass concepts had a longer ringing sound. With the different constructions, material and sounds in mind, football acoustics was approached as potential for additional insight into structural behaviour – a way of ascertaining structural information by means of a different measurement method.

Though not yet well understood or studied in football, the effects of acoustic perception in other sports have been well documented. There is no evidence that football brands, manufacturers, or researchers have taken deliberate steps to modify the acoustic properties of a football, but sound engineering may emerge, following examples set by tennis and golf, as a way to enhance performance and product differentiation in the future. The purpose of the acoustic studies in this chapter was not to comment on positives or negatives with regard to performance, but to approach the topic simply as another measurable component of an impact. A goal was to understand the mechanisms responsible for producing different sound and to determine what could be changed to alter the acoustic response while still maintaining other structural characteristics.

The research consisted of lab studies and simulations. The lab testing was carried out over several sessions but can be broken into two main groups based on balls tested. First, a wide variety of pressurised sports balls was tested to explore and categorise the spectrum of acoustic response. The different sizes, materials, constructions and masses were intended to provide information beyond the typical football sound to provide context and perspective. The second set of testing was on a group of footballs created specifically for the acoustic study to standardise some parameters and highlight certain aspects of the ball. Simulation work accompanied the lab testing as a way to visualise and explain observed phenomena. The model used in the studies was based on the coupled Eulerian-Lagrangian simulation originally created to look at the structural effects of dynamic location-sensitive internal pressure.

7.2 Physical Acoustic Testing

7.2.1 Methods

Lab testing was carried out to quantify the difference in impact sounds from a variety of different sports balls. To minimise the amount of noise, sound was collected in an anechoic chamber. The inner chamber had concrete walls 230mm thick and was suspended on vibration isolation mounts

inside a brick outer chamber. Glass-fibre acoustic dampening pillows lined the walls, ceiling and floor with a cable mesh and removable metal grates to suspend researchers and equipment. The room was certified to absorb anything over 100Hz. Each impact was repeated five times and recorded with a sound meter sampling at 20480Hz.

Given the different masses and general physical characteristics of the balls tested, it would have been practically difficult to introduce the same amount of energy in each impact. With differing impact severity, the magnitude or amplitude of the sound waves could not be compared between balls so the focus of the study was placed on the frequency differences between balls and the relative amplitudes of frequencies present in individual balls. The impact methods used were created to be reasonably repeatable but there was no attempt at ensuring equal impact severity. A variety of impacts were used to explore different possible interactions with the ball.

The *bar strike* method involved holding then releasing the ball immediately before striking it upward by hand 0.5-2m with a nylon bar (outer diameter 36mm). This method of striking left the impact severity to the discretion of the person performing the test. Though it did little for consistency, balls could be hit harder if necessary to place the sound within the range of the sound meter. Furthermore the small indenter caused a greater deformation into the ball – something that is difficult to do with a flat plate or boot shape within the confines of an anechoic chamber. The bar was held on an antinode to decrease the chances of it contributing to the ringing sound.

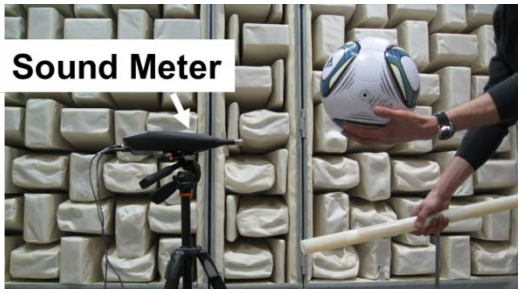

Figure 100: Bar Strike Method

The two metre drop test has been a standard in structural evaluation and it was re-created for acoustic measurements for the same reasons of repeatability and standardisation. Due to the nature of the chamber, a rigid plate could not be mounted to the floor so a 40kg block of steel with a smooth machined surface was placed on a block of compliant foam 10cm thick resting on the tensioned cable suspension 'floor'. The steel block was unconstrained on the foam. Microphones were placed 5cm and 1m above the impact surface, approximately 20cm from the centre line of the drop.

The small pendulum test was intended to consistently simulate a low-deformation scenario akin to handling the ball with the hands, as if the athlete were getting a first impression. The pendulum was a golf ball suspended by two strings to give it a 25cm arm. The ball specimen was suspended with rubber bands and the pendulum was dropped through 90° to strike at the equator.

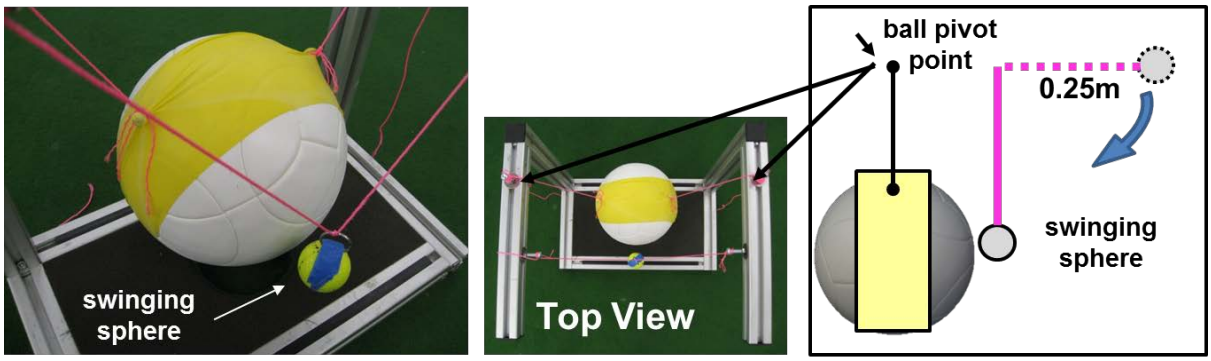

Figure 101: Small Pendulum Test

The bar strike, drop test, and pendulum tests were reviewed in depth but a series of tests were also performed to capture sound from low-deformation impacts. A finger-flick, open handed slap, and one-handed catch were recorded for all balls as well. Amplitude aside, all of the excitation methods produced very similar trends in frequency response. Spectrograms for the heaviest (most ring-prone) football are available in Appendix section 9.6. These extra tests de-emphasised the role of the excitation method on the frequency response; knowing the frequency response would be the same, focus could be directed towards tests with higher amplitudes and more repeatable excitation methods.

7.2.2 Bar Strike Testing

The first set of testing used the bar strike method and a wide variety of inflatable sports balls: traditional stitched football, thermally bonded football (patch and stitched dodecahedron carcasses), cheap replica football, basketball, volleyball, tennis ball, American football, football bladders, and football carcass/bladder sub-assemblies (dodecahedron stitched and standard patch carcass). The complete balls met the highest standard specified by their respective governing bodies and were inflated to pressures within the acceptable range (FIFA 2013; FIBA 2010; FIVB 2009). In the first set of testing, the goal was to populate the otherwise empty space with acoustic information about inflatable ball impacts as a way to create references against which to compare football sounds.

Table 14: Characteristics of balls used in acoustic testing

Ball	Pressure (psi)	Mass (kg)	Circumference (cm)
Footballs	13.0	~0.420-0.445	68.5-69.5
American Football	13.0	0.397-0.425	53.3-54 (small direction)
Football Carcasses	13.0	~0.2	~68.5-69.5
Latex Bladder	0.7	~0.1	~68.5-69.5
Butyl Bladder	1.0	~0.1	~68.5-69.5
Volleyball	4.0	0.260-0.280	65-67
Basketball	8.0	0.624	74.93-75.88

Fast Fourier Transforms (FFTs) were used to break the time-pressure signal into constituent components and highlight the dominant frequencies. In general, FFTs work well for consistent or repeating sounds from steady vibrations like engines, but short duration events can be difficult because of different types of sound present. In a ball impact, the duration of the fading sound and the changes that happen throughout are of interest so spectrogram plots were also used. The spectrogram was created from FFTs over short (500 samples at 20480Hz) sequential overlapping time windows and shows the amplitude or power of sound (colour scale, db/Hz) at different frequencies (X axis) throughout time (Y axis). The FFT plot was created using the entire 0.1s of collected information. In both FFT and spectrogram plots, the basketball had a very distinctive frequency response and it serves well to illustrate the types of information found useful in the study. Figure 102 shows vertical bars of high intensity sound in the spectrogram correlating with the frequency peaks in the FFT. The FFT shows louder sound around 400Hz, 950Hz, 1600Hz, 2100Hz, 2600Hz, 3200Hz, 3400Hz, 3600Hz, 4200Hz, 4700Hz, 5200Hz, and more frequencies up the spectrum and the spectrogram indicates durations of the sounds at different frequencies. A basketball impact in the literature showed a very similar collection of frequency peaks - 963Hz, 1565Hz, 2111Hz, 2129Hz, 2664Hz, 2780Hz, 3154Hz, … 3619Hz, …. 4213Hz, and others between (Russell 2010). There are some very close connections to the theoretical work, and it's possible that the other resonant frequencies that the mathematics predicted were also present in the test data but with amplitudes overshadowed by the more powerful resonances. The high-amplitude sound just above 0Hz may be in part due to the thump of the ball as it hit the plate or any low frequency noise not absorbed by the anechoic chamber. Qualitatively, the basketball had a long distinctive high-pitch ring after impact, which, when compared to a tennis ball sound, had significantly more content in the frequency spectrum.

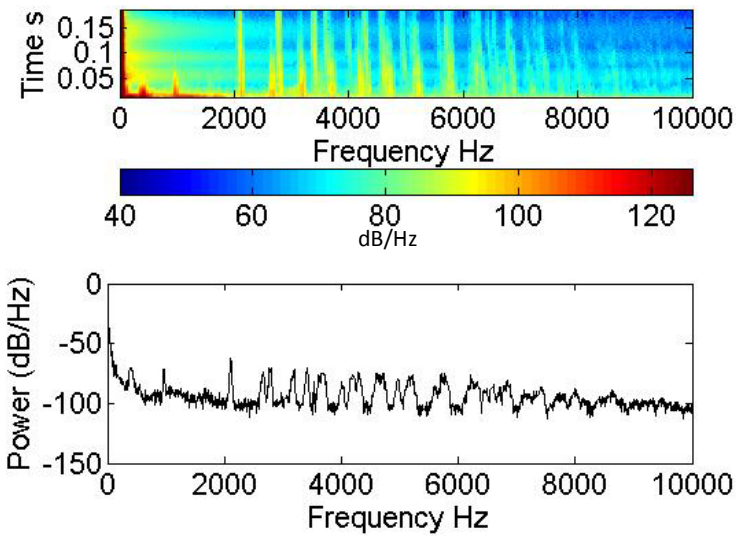

Figure 102: Basketball – bar strike, FFT and spectrogram

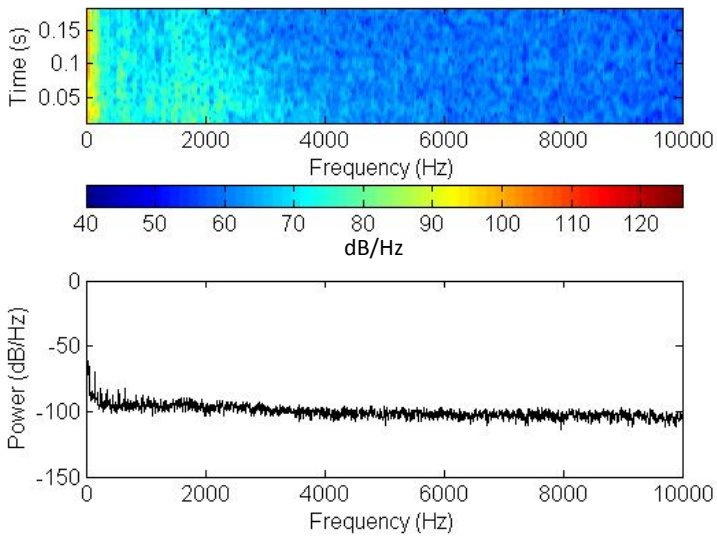

Figure 103: Tennis ball - bar strike, FFT and spectrogram

In contrast to the basketball, the sound captured from the tennis ball did not have distinctive frequency peaks visible in the FFT or vertical bars of high amplitude in the spectrogram. The higher amplitudes shown in yellow in the spectrogram did not have the continuity and duration seen in the basketball. Qualitatively, the ball had a very short, dull sound without anything resembling the post-impact ringing of the basketball. The tennis ball and basketball represented opposite extremes of the range of balls tested. The volleyball had a series of long duration frequency peaks between 2.5kHz and 6.5kHz. The American football had notable frequency peaks at 1.4kHz, 2.3kHz and 2.8kHz with little above 4kHz. The cheap replica football had a short ring with a lot of distinct

content at frequencies between 1kHz and 6kHz. The FFTs and spectrograms for these balls are in the Appendix in section 9.6.

The latex and butyl bladders, both significantly more compliant than the complete balls and carcass sub-assemblies, had what may be best described as a 'warbling' sound – a low frequency, low pitch oscillation. Figure 104 shows a high amplitude noise around 500Hz in addition to peaks spaced throughout the higher frequency regions. The latex bladder had a similar frequency profile (see Appendix section 9.1).

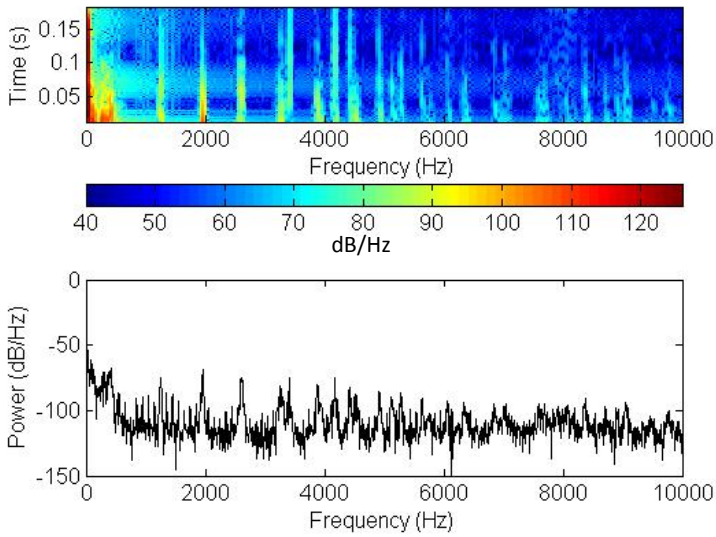

Figure 104: Butyl Bladder Sound

Despite similar structural properties (as certified by FIFA), there was a fair amount of acoustic variation in the footballs tested. The machine stitched football (Umbro, 2010) had a spectrogram and FFT more similar to the tennis ball than the basketball. There was a short peak at 1kHz but very little content elsewhere in the frequency spectrum. To the ear, the sound was a solid thud with no noticeable post-impact ringing.

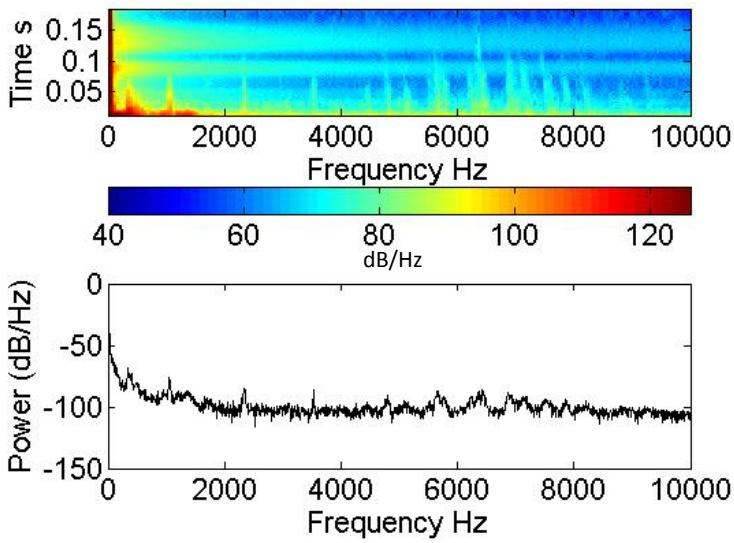

Figure 105: Machine Stitched Football, FFT and Spectrogram

In addition to the peak at 1kHz seen in the machine-stitched ball, bonded footballs with the standard patch carcass and dodecahedron carcass had more content higher in the frequency band with an emphasis around 3kHz (Figure 106, Figure 107). Like the basketball, the spaced-out distribution of long duration frequency peaks was indicative of a post-impact ring; to the ear, both thermally bonded football constructions (dodecahedron and patch carcasses) had an audible ringing sound. With confirmation that the acoustic trends could be seen in measurements and examples defining a wide range of pressurised sports ball sounds, testing continued with the more consistent 2m drop test. As seen in the bar strike tests, the measurable outputs of interest were the frequency peaks' absolute locations within the frequency spectrum and the relative duration and amplitude of individual peaks with respect to the rest of the rest of the signal.

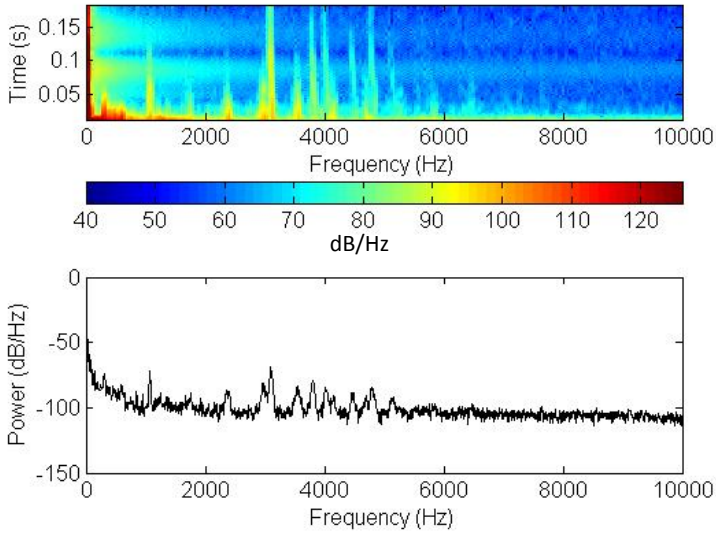

Figure 106: Thermally Bonded, Patch Carcass - Bar Strike

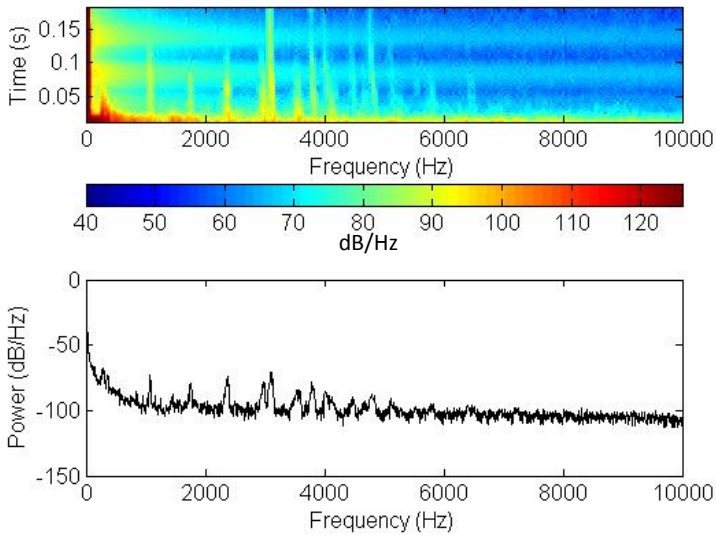

Figure 107: Thermally Bonded, Dodecahedron Carcass - Bar Strike

7.2.3 Two-Metre Drop Testing

Taking advantage of the modular construction of thermally bonded footballs, carcass sub-assemblies and complete balls were tested to investigate the influence of outer panels on impact sound. The plot in Figure 108 compares the stitched dodecahedron carcass and complete ball (each line represents the average of five impacts with one carcass or ball, dodecahedron equivalent is Appendix section 9.1). From the plots, it may be understood that the addition of outer panels can remove energy at some frequencies. The basic frequency response of the ball seemed dependent on the carcass and the outer panels only removed content.

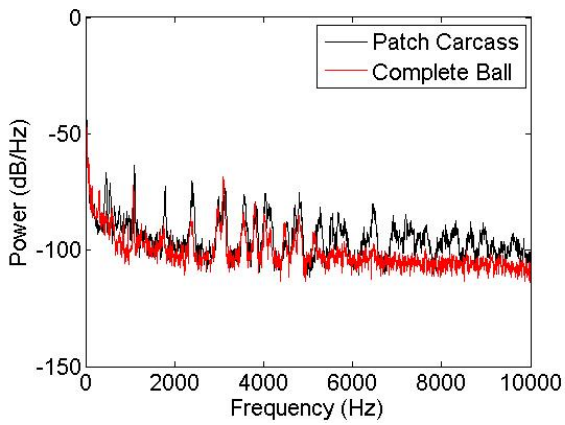

Figure 108: Complete Ball vs. Carcass - Bar Strike

A comparison was made between the frequency peak locations from basketball and football impacts. The averaged result of five impacts for one example of each ball is shown in the three spectrograms in Figure 109. The basketball's acoustic frequency response consisted of more frequency peaks higher in the spectrum and the greater amplitude for longer durations suggested that it was louder as well. Though the 2m drop test is more consistent, the precise loudness was still not considered to be an accurate measurement. The difference in amplitudes may support an anecdotal case for a louder ring from the basketball. This may be due in part to the difference in mass (624g vs. 440g) between the basketball and football and resulting disparity in impact energy, or there may be other unidentified factors. The location of the frequency peaks, however provided for a useful, quantifiable comparison. Black arrows in Figure 108 show a pattern that repeats all three balls. Arrows marked **a** (short-long neighbours) and **b** (low amplitude peak between two greater peaks) show two common features of the sequence. Looking at only the common sequence, the basketball's frequencies were shifted nonlinearly down between 280Hz and 440Hz from the sequence in the patch carcass ball. Each element in the dodecahedron carcass was shifted only 40Hz higher than the patch carcass. The similarity between the thermally bonded patch carcass (complete) ball and the dodecahedron carcass despite different construction differences (and stiffness and mass), when contrasted with lower frequencies in the basketball, suggested that construction was not responsible for the specific frequencies present in the post-impact ring. In addition to construction, mass and stiffness, the basketball differed in diameter – 24cm to the football's 22cm (based on the middle range of acceptable circumferences (FIFA 2010b; FIBA 2010)).

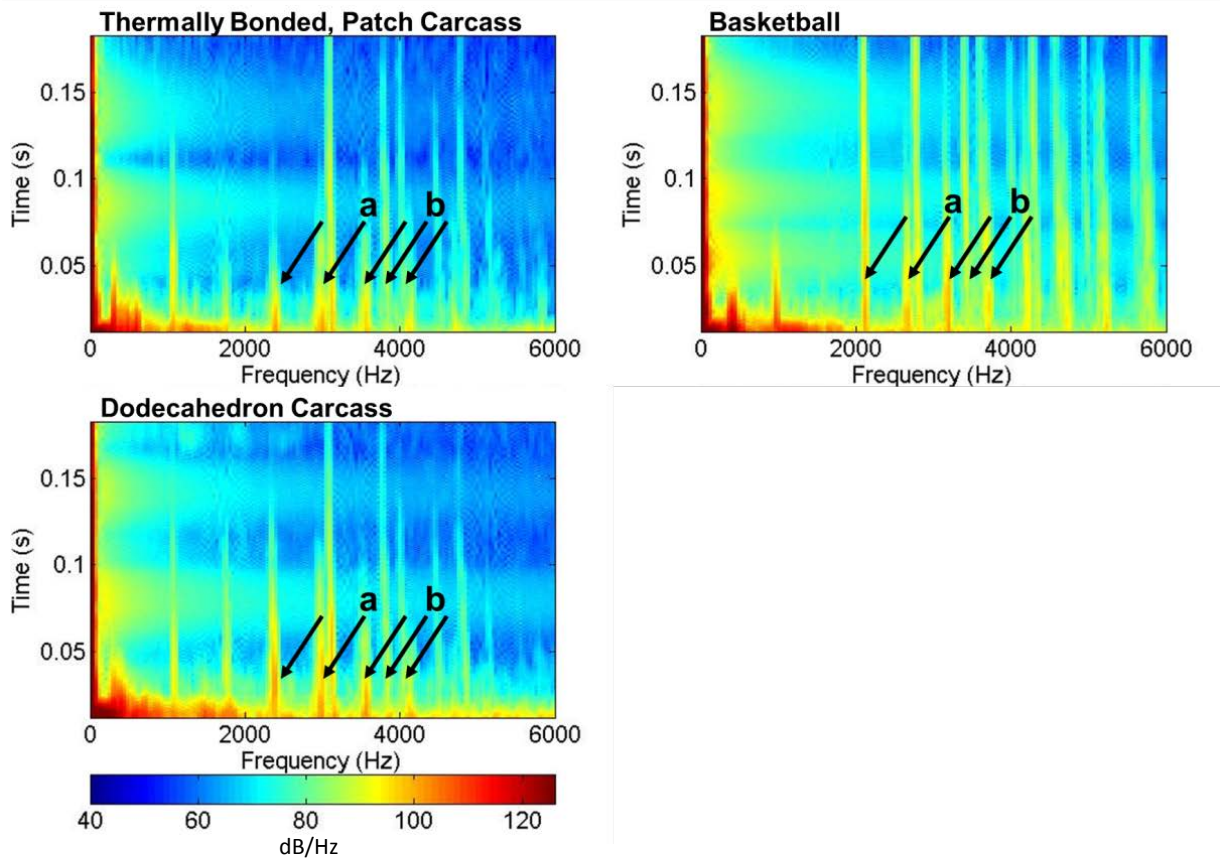

Figure 109: Basketball and footall post-impact rings

To control for diameter and construction when considering the impact of mass on the post-impact ring, bespoke footballs were created using the same manufacturing facilities as standard footballs but with different materials for the outer panels and the patch carcass construction. Basketballs have an approximate surface density of 3.47kg/m^2, notably higher than the 2.8kg/m^2 of a football. By creating outer panels with a PU compound rather than the EVA used in previously tested footballs, two densities could be achieved, producing footballs with different masses and otherwise identical construction. Three low density and three high density footballs were created with average masses of 429g and 559g respectively (surface densities of 2.82kg/m^2 and 3.68kg/m^2). The averaged result of five impacts per football weight (fifteen impacts for each mass) is presented in Figure 110. The same general frequency profile was present in both footballs, but the heavier football had greater amplitudes initially and at the end of the duration of the recording. Initially, it was thought that the difference in amplitude may have been due not necessarily to the effect of additional mass on the acoustic properties of the ball, but the greater impact severity that came with a slightly heavier ball. The aforementioned pendulum test, however, which guaranteed a consistent impact severity, also showed a louder and slower decaying sound. Sound decay is discussed later and shown in Figure 118.

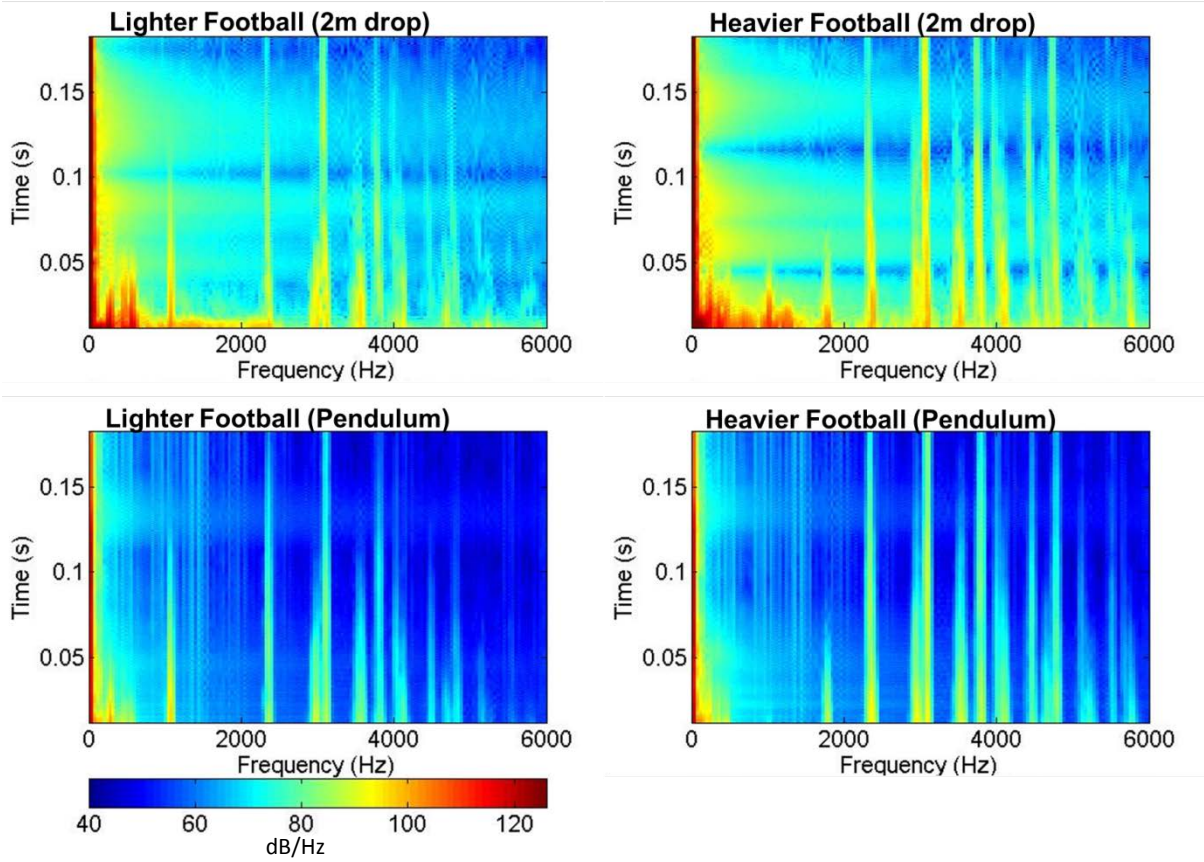

Figure 110: Heavy and light footballs compared in a 2m drop and with the pendulum test

Disregarding the effect of outer panels, there was also a relationship observed between the frequency decay and the construction of the carcass. Spectrograms in Figure 111 were created from the average of five impacts each for the patch carcass, dodecahedron carcass, and manually-stitched football. The patch carcass produced the greatest amplitudes, especially above 4kHz and the manually stitched football was remarkably different. Graphs of the decay of the sound can be seen in Figure 118. This trend was readily apparent to the ear; unlike the other two, the manually stitched football did not have an audible post-impact ring.

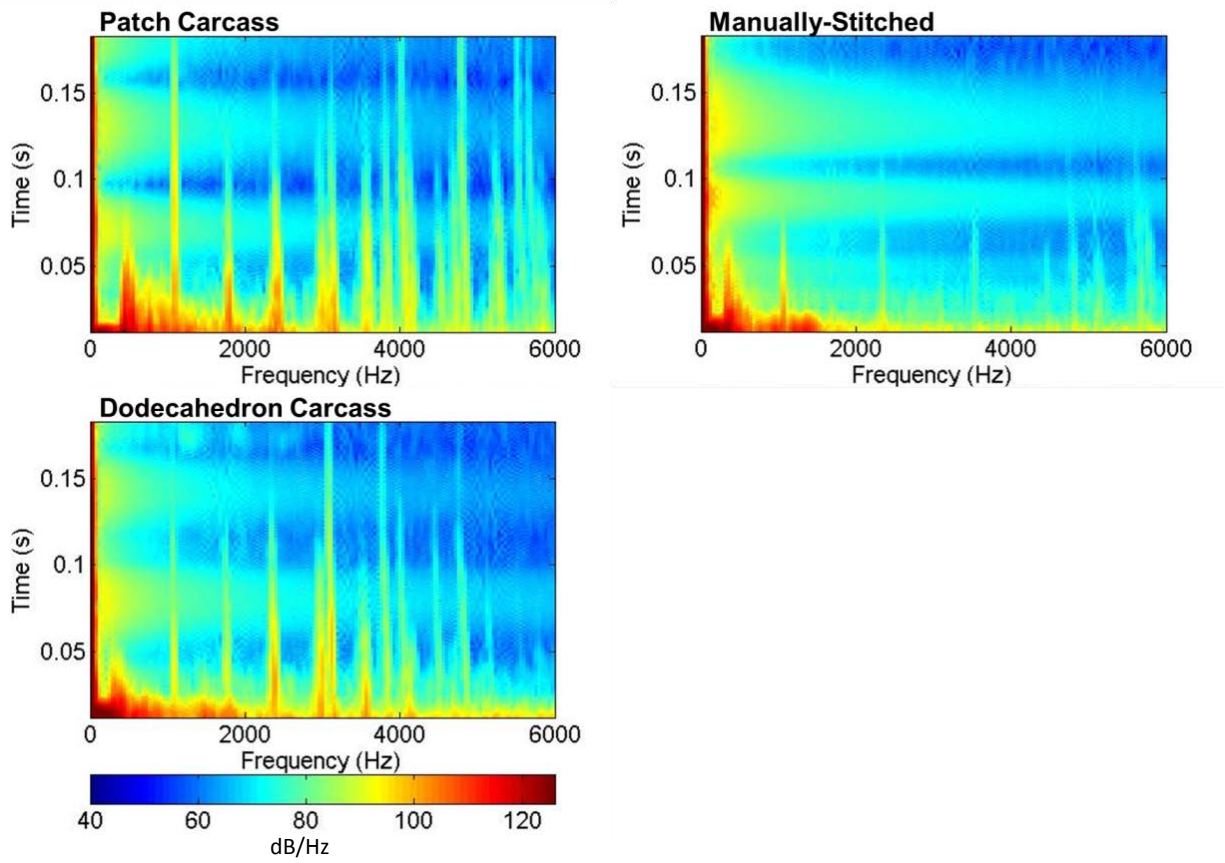

Figure 111: Carcass and manually stitched ball acoustic comparison

Upon inspecting the construction of the footballs, it was hypothesised that a rougher internal surface contributed to the decay of the post-impact ring. The traditional stitched ball (based on a truncated icosahedron but with twelve panels made of pairs of pentagons and hexagons) had 78 seams, each of which created a ridge approximately 45mm long, 5mm wide and 3mm tall on the inside of the ball. With the latex bladder pressed against the inner surface, the abrupt seam geometry may have been smoothed out but the inner ridges on the surface would have still had a noticeable presence. The dodecahedron carcass had 30 stitched edges approximately 70mm long with a similar cross section to the traditionally stitched ball. The patch carcass construction did not have any seams on the inner surface. There were small ribs following two perpendicular great circles that were formed when the bladder was vulcanised. These ribs were about 4mm wide and 2mm tall, much smaller than a stitched seam. Finally, at the other end of the scale in terms of internal roughness-smoothness, the basketball had ribs similar to the patch carcass but smaller, and a light texture from the wound filament. The relationship between inner surface and ring duration was one topic of investigation in the next set of testing.

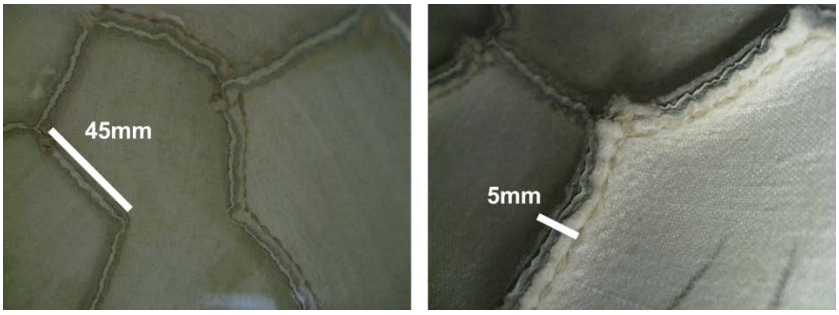

Figure 112: Stitched Ball Inner Seam Ridges

Figure 113: Dodecahedron Carcass Seams

a b

Figure 114: Patch Carcass (a), Basketball (b) Inner Surface

7.3 Acoustic Response Modification

The lab-based testing suggested relationships between frequency and diameter, and ring duration and internal surface disruption. The frequency of dominant mode shapes were dependent on ball diameter and the sound decayed slower if the ball was heaver and with a smoother inner surface. Of these two variable characteristics of football sound, only modifications to the duration of the ring were possible within the ball regulations; diameter, and consequently ring frequency, is controlled in the laws of the game. To better understand the effect of the inner surface on the ring duration and explore the realms of possibility, a second set of bespoke footballs was constructed with modifications to the inner surface.

The leaf and cylinder foam components were added to assess the potential relationship between inner surface and post-impact ring. Adding additional seams or ridges would have been practically difficult and may have influenced the weight or global ball stiffness. Foam was chosen to disrupt the inner surface with minimal influence on other aspects of the football. The footballs had a butyl bladder and patch carcass and the outer panels were the same as those used on the 2012 adidas Tango12. Three with each foam configuration were manufactured in a standard commercial production facility. Figure 115 shows the two different foam configurations. The leaf foam image shoes a butyl bladder sliced open to reveal the approximately 150x100x5mm ovoid foam insert bonded to the inner surface. The cylinder foam image shows a cut open ball with the 20 individual cylinders (20x10mm) bonded to a TPU bladder. The balls used for testing all had butyl bladders.

Figure 115: Acoustic management foam in two varities

In addition to the professionally-produced footballs, a dodecahedron carcass was modified to have additional seam-like features at the centre of each panel. Two 5x50mm strips of carcass fabric were stitched on top of each other to disrupt the centre of each pentagon Figure 116). The strips were attached with only two stitches to minimise any influence on global stiffness. Modifications to the interior of the carcass meant cutting two machine-stitched seams and re-stitching by hand so consistency and stiffness may have been compromised. Throughout testing, the seam did not appear to widen and the ball maintained pressure and shape. Only one such football was available for testing.

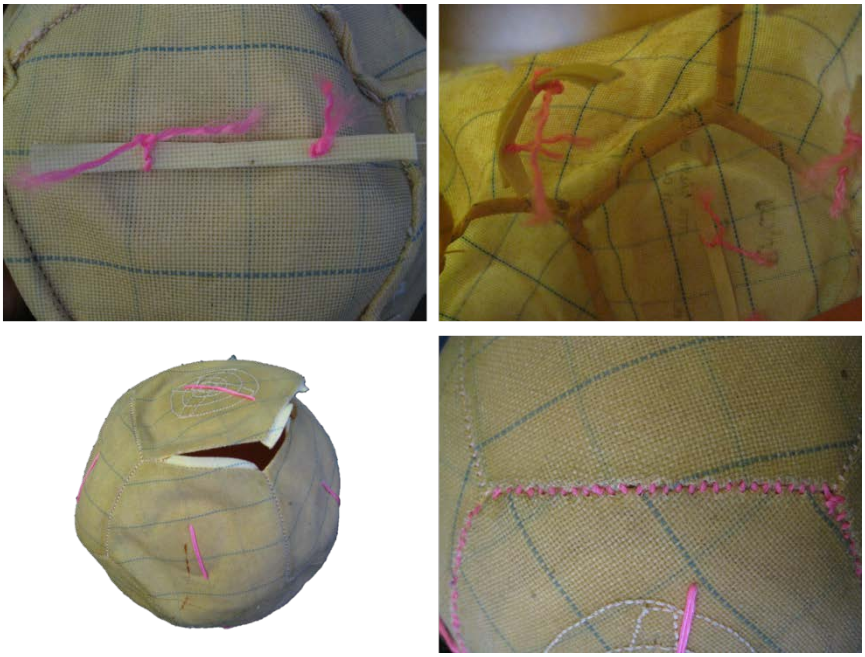

Figure 116: Modified dodecahedron carcass, individual strips of carcass fabric were stitched in to act as additional seams

The acoustic management footballs and the modified carcass were subjected to the same 2m drop test procedure used in earlier tests and the results are presented as averages of fifteen impacts (5 per ball, 3 balls for each foam configuration - Figure 117). The reference 'Standard Football' was made at the same time and identical to the others but with the omission of internal foam components. Though slightly different from the other footballs tested, the standard football still had the characteristic frequency peak around 3kHz, and the specimens with internal foam showed almost no distinct lasting content around 3kHz.

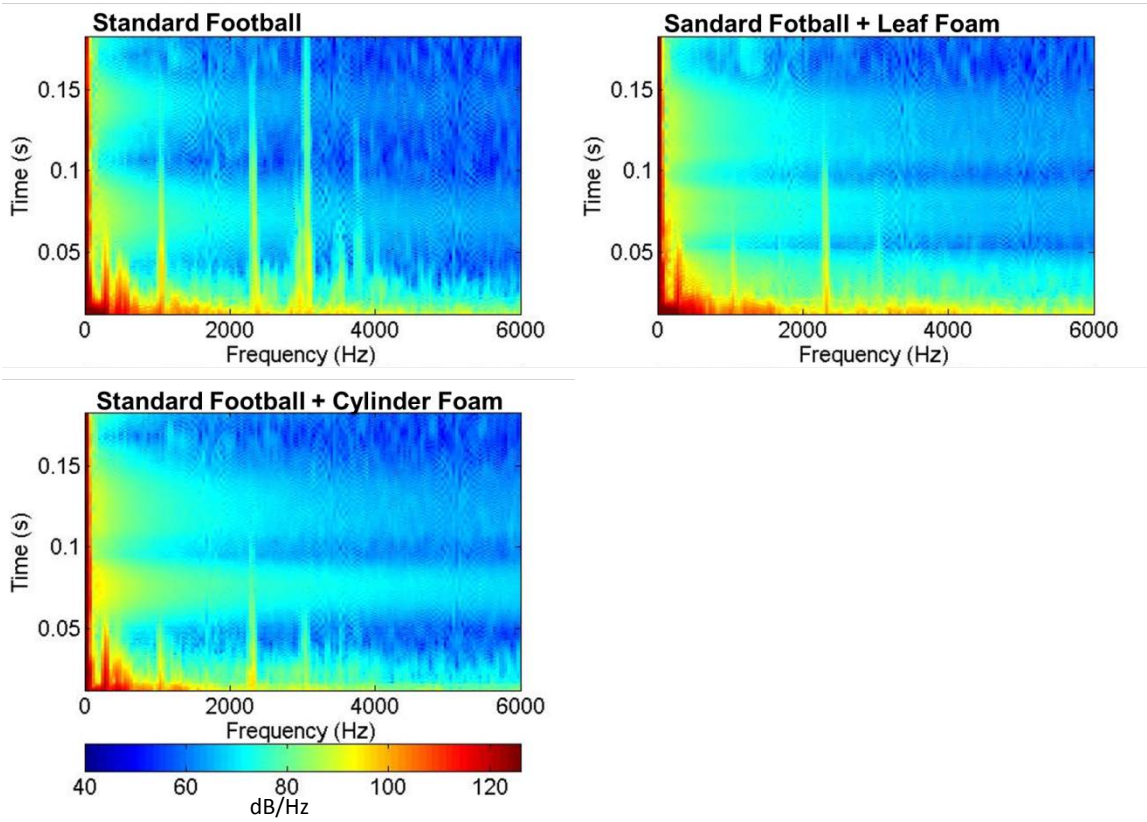

Figure 117: Comparison of post-impact ring from footballs with acoustic management foam

Plotting the amplitude shown the colour scale against time highlights the differences in decay rate between the balls. Figure 118 shows the decay for a fixed-width band encompassing the dominant frequency for each ball. For the footballs, this band was between 2840Hz and 3160Hz. For the basketball, the band was slightly lower, between 2600Hz and 2840Hz. The results can be roughly split into three groups. The basketball and heavy PU football had the shallowest slopes (slowest amplitude decay) but were followed closely by the standard footballs and the patch and dodecahedron carcasses. The third group consisted with the quickest amplitude decay consisted of the modified dodecahedron carcass, the patch carcass footballs with acoustic management foam and the machine-stitched football. Classifying the three groups based on similar properties, the first group was heavier with a smooth inner surface, the 2nd group was a standard weight with a smooth surface, and the third group was a standard weight with a disrupted surface.

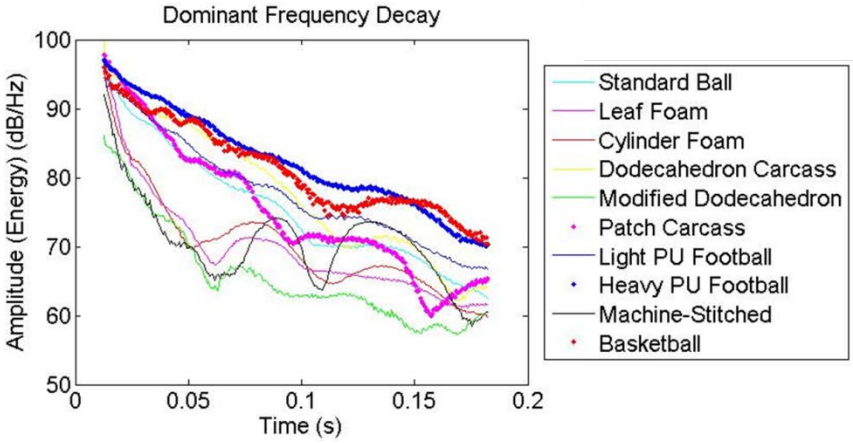

Figure 118: Decay of the dominant frequencies of post-impact rings in a variety of pressurised balls

The trends in the graph are most clear up to 0.07s before starting to oscillate. This phenomenon is also apparent in the spectrogram; in addition to the narrow vertical bars representing content in small frequency bands, there were horizontal regions indicating broad frequency, short duration pulses. The pulses had an emphasis in low frequency sound and happened in nearly all impacts, including those simulated virtually. Comparing the pendulum and 2m drop tests suggests that the magnitude of the pulses was related to the severity of the impact but correlations with football properties were not observed. From the decay plot, it seemed like the pulse intensity may be correlated with a lack of post-impact ring but this was not verified. The two metre drop tests were recorded with the microphone at two positions and the effect was present for each, suggesting that it was not caused by wind from the moving ball or other motion-related effects.

7.4 Acoustic Simulation

As in other simulation applications, computationally modelling the acoustics allowed for precise and independent control over all parameters. In this study, finite element simulations were used to further explore the phenomena identified in the first set of lab testing. In lab testing, stiffness, size and weight were related to construction so the end result could not be attributed to single attributes but the simulation allowed for greater flexibility in ball properties. By independently adjusting size, stiffness, and construction, the changes in post-impact ring duration and frequency content could be associated more closely with specific characteristics of the balls. A better understanding of the acoustic response had the potential to transform football sound into an engineered characteristic.

7.4.1 Acoustic Model Setup

There are a variety of methods for simulating the acoustic response of an excited structure. Some, including the boundary element method, focus on a surface or only a point, calculating the acoustic response perceived in a localised region. Though computationally expensive, the method chosen for

the simulations used in this study was able to provide acoustic information throughout the volume of the football as time-domain pressure. For computational reasons, the outer (ambient) pressure was not included in the simulation except as a reference for the internal (gauge) pressure.

The acoustic model was based on the coupled Eulerian-Lagrangian simulation used earlier to investigate any potential influence of spatially-variable internal pressure on local deformations throughout impact. The model included pressure data for each element of the Eulerian domain and this information, when extracted at sufficiently short time intervals, was processed like the time-domain pressure information collected by the sound meter in the anechoic chamber. The cavity had approximately 110,000 elements, each capable of exporting a representative pressure for their individual volumes, but in comparisons against physical tests, data from one central point was used to represent the sound of impact. This discrepancy between measurement locations in the simulation and lab was expected to have an influence on the result, most notably in amplitude or loudness. In the model, pressure was sampled at 100kHz for 0.01s following a 20m/s impact with a flat plate.

Several football configurations were used in the simulation study to investigate the effect of size and density/weight on dominant frequencies and the post-impact ring duration. In addition to the standard football, there was one at 80% normal size, one with 63% greater foam density, one with 3.4x stiffer carcass fabric and a football with added ridges to simulate the collection of internal seams on a 32-panel stitched football. The foam density was increased to make the kilogram/surface area ratio similar to that of a basketball. The stiffness increase was chosen to be great enough to have a structural difference as observed in the earlier DOE study. Inner rib dimensions of 4x4mm were patterned after the seams and followed the lines of a dodecahedron with an additional line through the centre of each pentagon. The ribs were modelled with the properties of butyl bladder material because it had to be stiff enough to not collapse under pressurisation and as compliant as possible as to not influence the ball's global stiffness.

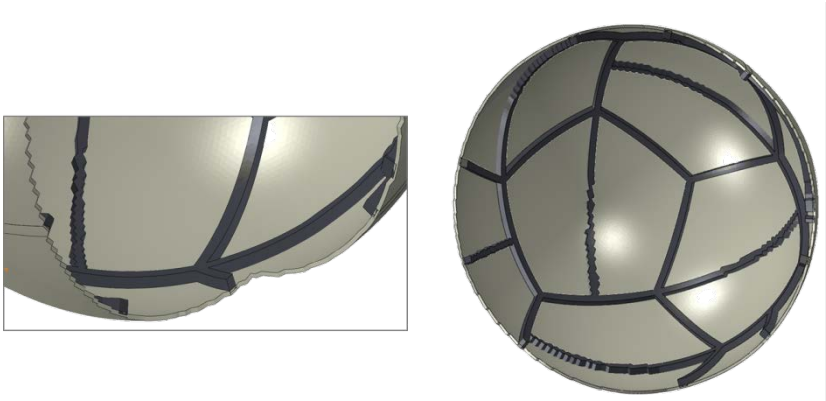

Figure 119: Acoustic Simulation - ribbed interior

7.4.2 Acoustic Simulation Results

The simulated acoustic information was processed with the same methods used to understand the lab test results. Viewing the entire duration of pressure/time data revealed a large hump as the pressure increased and decrease during impact but this rise and fall was relatively slow with respect to the frequencies of interest and should not have influenced the acoustic response. The FFT and spectrogram plots were generated as before but the spectrograms were created with a Hamming window size of 1024, overlapping 1000 points and split into 1024 frequency ranges for the FFT. This may have influenced the magnitude of energy present at the various frequencies.

Figure 120 shows a direct comparison of an experimental flat plate impact with a complete ball (complete ball, patch carcass) from anechoic chamber data and a simulation. In the figure, the time scale of the lab test was shortened to align with that of the simulation. Computational limits kept the simulation duration much shorter than the time of data collection in the lab. Sample rates for simulation and lab work were selected independently to give enough information throughout the capture duration. For comparative purposes, this presented a challenge. The magnitude of the signal on the colour scale could not be directly compared between simulation and lab tests because of the duration of the data collected, and sample rate and windowing methods. Furthermore the difference in sound measurement location between virtual and lab scenarios could not be accounted for. Working within these limitations, the simulation did capture some of the trends seen in the anechoic chamber data concerning frequency and duration of the post-impact ring. The dominant frequency peak (in terms of magnitude and duration) was slightly above 3kHz, with additional content at 4kHz and above. In addition to the vertical bar trends seen in the spectrograms, there was also a horizontal broad-frequency pulse seen in both spectrograms. Looking at a longer duration for the lab data, scaling based on signal decay rather than absolute values, Figure 121

highlights the 3kHz trend seen in the simulation, as well as some of the decaying content higher in the frequency band.

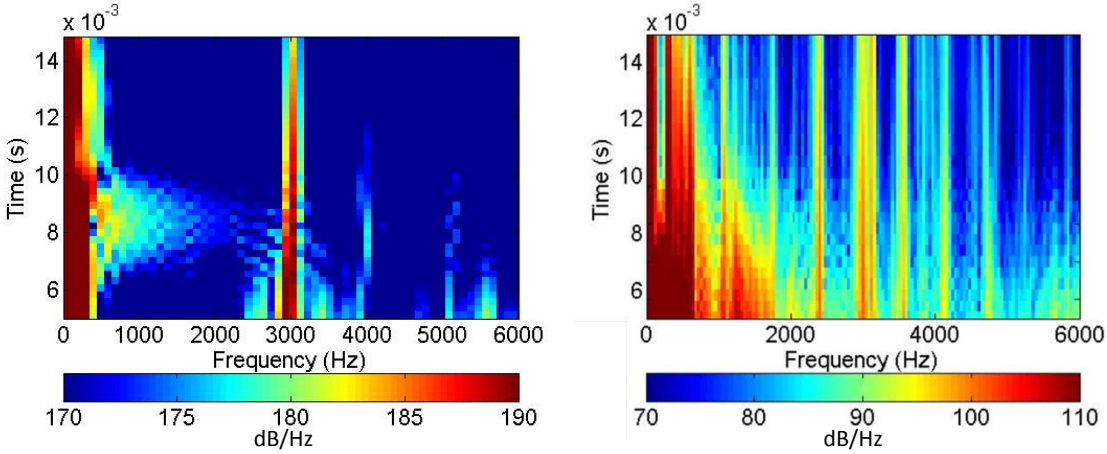

Figure 120: Simulation (left) vs. Lab Test, complete standard ball

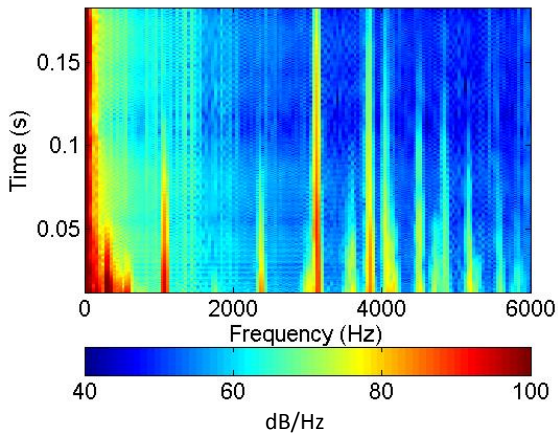

Figure 121: Standard ball spectrogram with longer time scale, experimental data

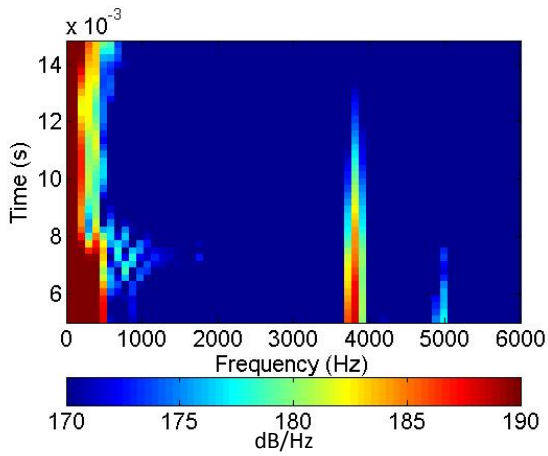

Figure 122: Simulation, 80% standard size football

The 80%-sized football had a frequency peak at 3.9kHz (shown in Figure 122), slightly higher than the standard football's 3.1kHz. This result provided further evidence to support the suggestion of a relationship between ball diameter and dominant frequency. To the ear, the difference in the post-impact ring pitch between basketball and football could be heard. Though the simulations produced sound-like data with reasonable frequencies, the resulting audio files (converted from time-domain data to .wav files) were unintelligible and could not be compared. This may have been due to the low frequency data coming from larger, slower pressure oscillations. Furthermore, the sound from the lab tests was a composite of everything in the frequency spectrum; missing parts, as the simulation did, likely had an undesirable effect on the quality of the sound.

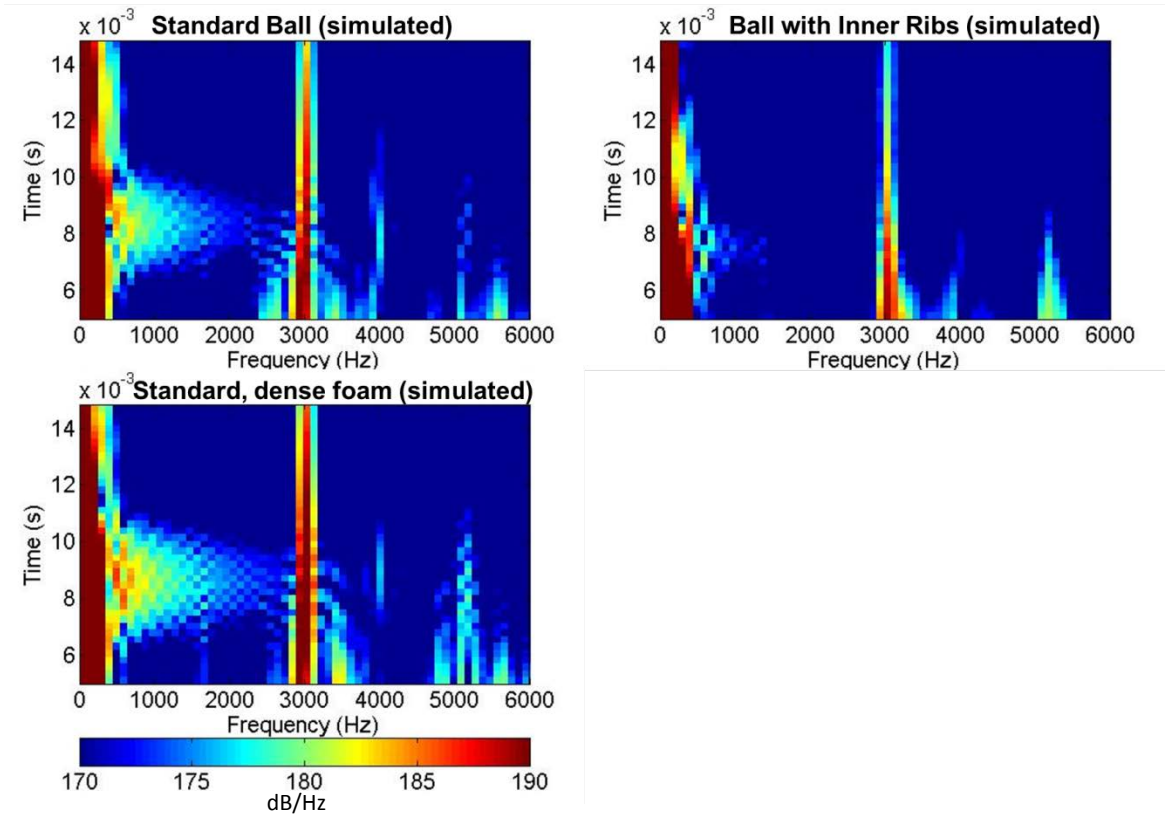

Figure 123: Differences in ring duration from simulations

As in the spectrograms of lab-based data, decay was observed in the amplitudes of dominant frequency peaks of the simulated sound. This was interpreted as an indication of the post-impact ring decay and duration. Compared to the standard ball simulation, the 3kHz sound from the football with artificially weighted outer panels decayed slower, and the sound in the ball modified with internal ribs decayed faster (Figure 123. The sound, in the 3027Hz section, decayed from 187-182 for the standard ball, 189-177 for the ball with ribs, and 187-185 for the ball with dense panels. As absolutes, these values had tenuous relation to reality but as relative indicators, they followed the trends seen in the lab testing. Similar to the lab testing sound decay plot, Figure 124 shows the

energy decay in a frequency window around the dominant frequency (between 2830Hz and 3125Hz in this case). The initial increase may be due to a transformation of energy from other modes to the 3kHz resonant frequency.

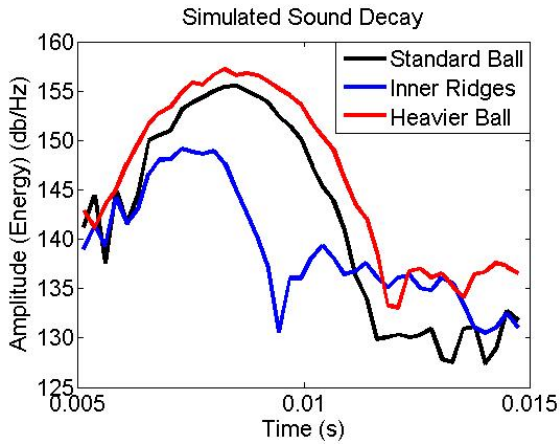

Figure 124: Simulated sound decay

In another scenario only possible with virtual simulation, a pressurised football was excited with a small 'explosion' of pressure at the centre. This experiment removed all structural deformation caused by an impact or other external excitation method used in the lab as a way to control for variation in impact type and focus on the acoustic dynamics alone. Instantly increasing the pressure of one element at the centre of the pressurised ball (from 90kPa to 200kPa) sent a shockwave through the volume. The spectrogram from the centre element shown in Figure 125 reports the similar trend of a dominant frequency around 3kHz, reinforcing the independence of impact type and frequency response. The lack of the horizontal pulses seen in impact-based simulations and the lab data suggests that the phenomenon is related to a structural dynamic but the exact mechanism remains unknown.

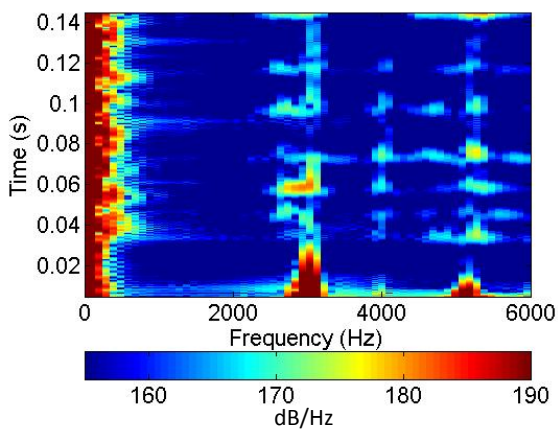

Figure 125: Inner Explosion Simulation

7.5 Internal Acoustic Pressure

The literature suggested that structural vibrations of the football take place at relatively low frequencies; the 1000kHz frequency peak seen in many of the spectrograms may be attributed to the structural modes identified with laser Doppler vibrometry (Ronkainen & Harland 2007). Throughout lab tests and simulations, it was the air inside the cavity that seemed more important in determining the characteristics of the dominant frequencies. From the coupled Eulerinan-Lagrangian fluid modelling earlier, it was known that the pressure wave initiated at the impact surface and propagated upward. Simplifying the scenario to two-dimensional wave propagation, the approximate 0.215m diameter of a football could be traversed by a 343m/s air pressure wave in about 0.6ms. In this scenario, the pressure wave could cover the diameter twice (from one side to the other and back) about 3190 times in one second, which aligns closely with the dominant frequencies seen in post-impact ring FFTs. This indicates a type of standing wave or echo that exists most prominently at the frequency with a wavelength that corresponds to the inner radius of the ball but there is also content elsewhere in the frequency band with different mode shapes. In the simplified linear case across a diameter, the mode shape in the air pressure can be imagined but with the complexity of the 3D spherical cavity, the actual mode shape of the dominant frequency and higher frequencies can be difficult to conceptualise. Measuring the dynamic pressure at different spaces inside the football in a physical lab setting is challenging but the coupled Eulerian-Lagrangian simulation method had the capability to provide information about pressure within the football cavity throughout the duration of the simulation.

The post-processing software was able to present 3D colour plots to show internal pressure for the flat plate impact but it could not filter the data. A script was written to extract the pressure information from the simulation results file and create a text file for each element (114,000 elements). The element pressure data was associated with a spatial location based on the centre point of the eight nodes that made up each element. With the pressure vs. time data and location, the data could be filtered with band-pass filters and the 3D colour plot could be reconstructed in a separate program. Data filtering and processing was handled between Matlab and MS Excel and the information was plotted as a coloured point cloud with the Grasshopper plugin for Rhino 4.0. With this processing system in place, the pressure wave and node location could be plotted at different frequencies. Viewing the instantaneous pressure throughout the volume over the duration, though possible, was a lot of information to conceptualise at once so the RMS values were used to condense the changing time domain pressure data into a static presentation of the nodes or antinodes within the cavity. The following plots show RMS value on a colour scale but points were filtered to display only the high or low RMS values. This was necessary to highlight mode shapes; despite the colour

scale, trends could not be seen because the sheer number of points obscured the regions of interest. The greatest and lowest 5% of the RMS values were discarded due to artificially large and small fluctuations in the elements at the outer surface of the ball. Figure 126 shows the cross-section of the RMS values for pressure passed through a 3-3.1kHz band-pass filter encompassing the dominant frequency observed in the ball (note: The nature of the grid of points in the cloud makes it difficult to view straight on – points overlap. The point cloud is shown at a slight isometric angle). The outer green 'shell' represents a low RMS where the pressure did not change outside the ball (discarded for the remainder of the images). The large values in the middle indicate a node, as do the red regions along the surface. The right-most region of the image is the side of the ball that made first contact with the plate, and the origin of the pressure wave.

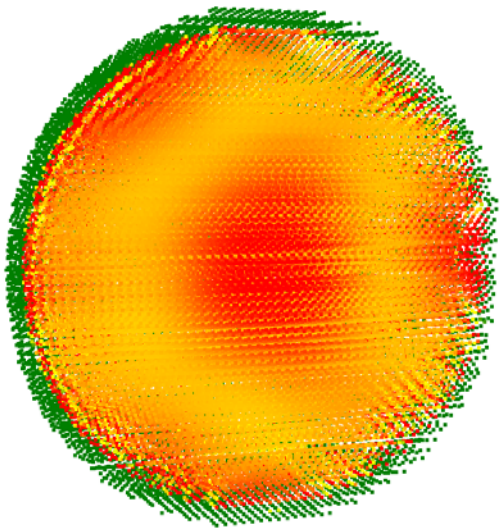

Figure 126: Filtered Sound Pressure RMS 3-3.1kHz, Cross Section

Keeping a similar perspective on the same data but viewing only the points in the volume in the top 24% of RMS values and re-adjusting the colour scale, interesting mode shapes can be seen. Figure 127 shows a lobed anti-node in the centre. The left image is at the same orientation as Figure 126 and the right image is rotated 45° about an axis in plane and parallel to the long side of the sheet. These mode shapes did not correlate with carcass or outer panel shape or quantity in the virtual model.

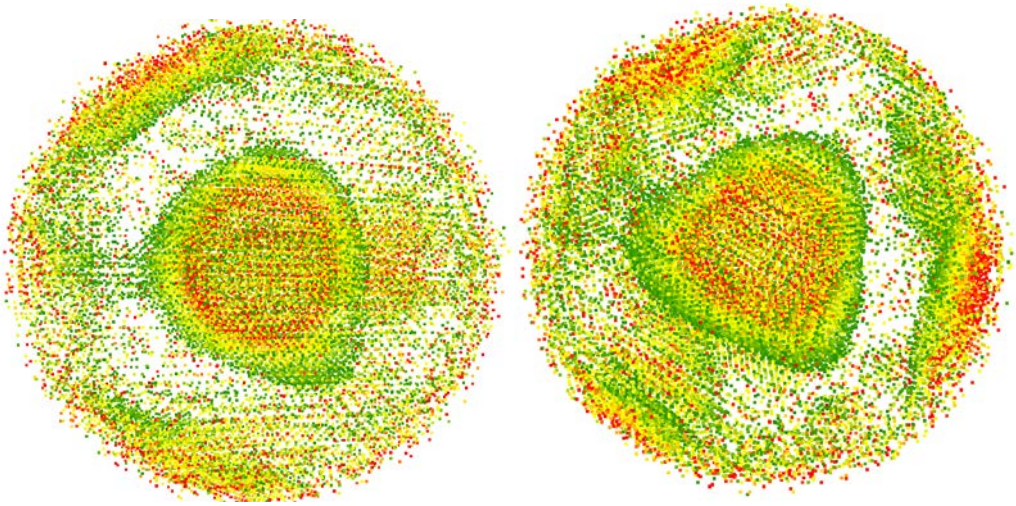

Figure 127: Filtered Sound Pressure RMS 3-3.1kHz Mode Shapes

Expanding the size of the band-pass window to 2.9-3.2kHz, the lobed mode-shape became more apparent, as seen in Figure 128. The impact surface was at the right side of the image and this suggested a mode shape with a bias in the direction of the axis through the ball and the point of first contact. The general mode shape, with high RMS at the surface and the centre may be considered to be two wavelengths across the diameter of the ball. Though the spherical form is undoubtedly more complex than a simple linear wave, the length of a wave at 3000Hz travelling at the speed of sound (343m/s) is 0.114 – remarkably close to half the diameter of a football.

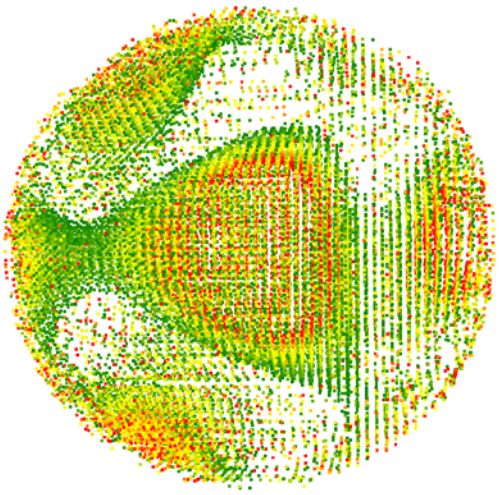

Figure 128: Filtered Sound Pressure RMS 2.9-3.2kHz Mode Shapes

The 2149-2549Hz frequency band was also selected as a useful region because of the content observed in lab tests. This lower frequency exhibited a completely different mode shape, though still with a potential bias toward the point of initial contact. Figure 129 shows the top 24% of RMS values on the left and the lowest 24% of RMS values on the right (colour RMS scales fitted

individually). The right image represents the node region and the left image represents an antinode, where pressure fluctuated most. At a lower frequency, the wavelength is greater (between 0.135 and 0.16) so complete waves cannot exist across the diameter in a linear sense.

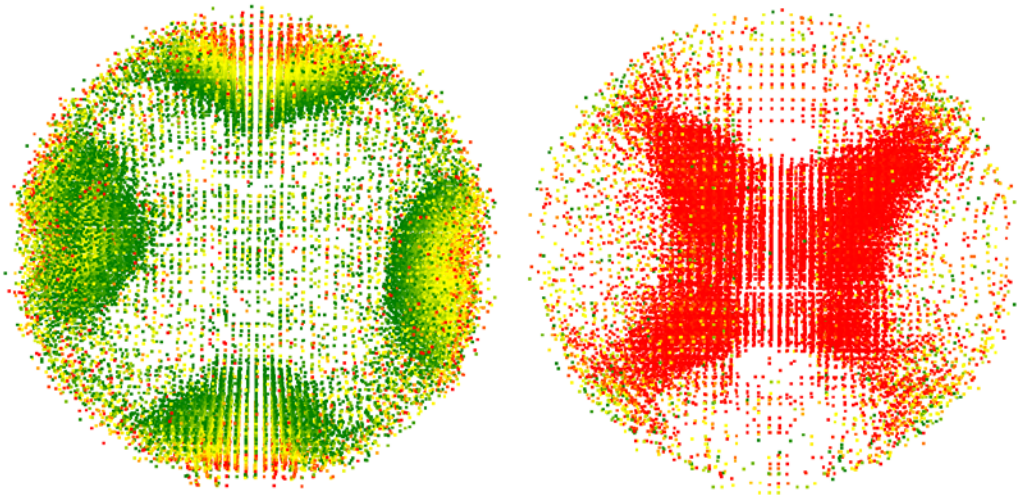

Figure 129: Filtered Sound Pressure RMS 2149-2549Hz, (high RMS left, low RMS right)

At higher frequencies, the modes were not as large and recognisable. Figure 130 shows the top 24% of RMS values and an oddly shaped centre phenomenon. The image at right of the figure is the irregular shape of the pressure fluctuation seen in the centre of the image at the left of the figure but without the surrounding nodes (filtered and removed by radius). Modes of vibration for the air within the cavity were expected to become more complicated at higher energy levels and frequencies and the somewhat disorganised result around 8kHz may be an indication of that.

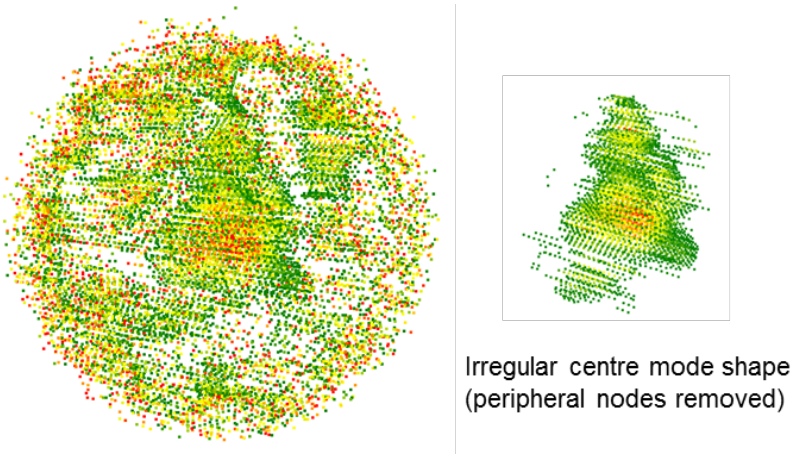

Figure 130: Filtered Sound Pressure RMS 7.9-8.2kHz

The simplicity of a mode shape appearance can also be attributed to the simplicity of the vibrating form – a centrally excited evenly supported disk will have cleaner mode shapes than an unevenly supported polygon with irregular edges. Deviations from symmetry have been shown to influence

the frequencies of spherical resonators (Mehl 1982) and following this logic, the dynamic asymmetries from post-impact oscillation may be responsible for disrupting standing waves. This could create an effect like irregular switches between constructive and destructive interference from the walls of the ball on the standing waves inside. The disruptive effect can be expected to be greater at higher frequencies because the wavelengths are shorter. In the football, the local diameter change (or change in wall location) due to structural vibrations had the potential to intercept a wave at a spot in the wavelength that led to an increased absorption or random dispersal of the wave's energy, effectively reflecting the wave at the wrong time. With lower frequencies and greater wavelengths, small structural vibrations had little effect on the standing waves so the waves and mode shapes were stronger and lasted longer within the cavity.

There was little available to compare the simulations of mode shapes within the football. Theoretical mode shapes for a basketball have been calculated (Russell 2010) and based on the FFTs of lab data collected earlier, the main frequencies present were largely shifted copies of what was seen in the football data. Though there were illustrated potential nodes in the literature, validation of the simulation was still challenging. Some bias toward the location of first impact could be assumed but orienting the ball properly to correctly position potential nodes was somewhat arbitrary. Furthermore, it was possible that multiple modes existed at one frequency, making it more difficult to identify precise node locations. Though exact connections or parallels between the simulation and published work could not be made, the trend of increasing mode n umber and complexity with increasing frequency seen in basketball research (Russell 2010) was also demonstrated with the football simulations. The general shapes could still be used to help understand the role of air pressure and acoustics within the ball. The effectiveness of the cylinder acoustic management foam, for example, can be explained as an artefact of the inner surface that, by virtue of its large inward dimension, is capable of interacting with and disrupting the noticeable longer-wavelength frequencies in much the same way shorter wavelength components of the pressure oscillation were sent into disarray by smaller structural oscillations.

7.6 Summary

The goal of this chapter was to understand the mechanisms responsible for different acoustic responses of footballs, especially the post-impact ringing sound. Lab-based tests of footballs and other pressurised sports balls helped to draw associations between physical properties of the ball and characteristics of the ringing sound. Simulation also confirmed and expanded on the lab tests to show that diameter was linked with dominant pitch, and mass and inner surface smoothness (or lack thereof) was linked with the ring duration. The ringing sound was determined to be a standing wave

or echo within the ball rather than structural oscillations resulting from deformation. A multi-physics approach was used to simulate the air within the ball and depict the pressures and acoustic standing waves in 3D space for the first time. The mode shapes at different frequency bands, though somewhat noisy (in a data-processing sense), backed up initial hypothesis on the simplified relationship between wavelength and ball diameter.

Diameter and mass are regulated by FIFA and cannot be changed enough to give an appreciable difference in acoustic response. The internal surface smoothness, however, has been demonstrated to have a noticeable effect and neither internal surface nor acoustics are regulated. Two types of inner surface disruption were tested strengthening the connection between inner surface and ring duration as well as providing practical methods of altering football acoustics.

8 Summary

8.1 Materials Testing and Characterisation

The tests on materials provided information for finite element analysis models, identified important considerations for testing football materials, and provided a basis for understanding some full-ball behaviour. Experiments on individual materials at multiple stages of processing from pre-assembly to the final ball configuration demonstrated the effect of assembly processes on mechanical properties. In the direction in-line with yarns, the fabric was stiffer after assembly but at a 45° angle to the yarns, it became more compliant. This was attributed to the pre-strain required to form flat panels onto a spherical contour – tensile yarn stiffness increased but the yarn-polymer matrix bond was weakened. The skin resulting from a mould surface when creating EVA panels stiffened the EVA compared to a sample cut from a sheet. Vacuum-formed TPU was more compliant than the plain sheet and the TPU with graphics was stiffer. In general, using only pre-processed materials resulted in a slightly stiffer virtual ball model than using materials taken from an assembled football.

A simple single-pull tensile test was demonstrated to be effective for characterising a material. In tensile tests of anisotropic materials, sample geometry had an influence but an in-plane shear test was able to provide reliable information. All materials tested stiffer at cold temperatures, especially the outer panel constituents EVA and TPU.

8.2 FEA Model Development

Multiple virtual models and methods were individually developed to address specific requirements of the research. A 2D mesh with composite shells inflated with a uniform pressure method was found to work nicely for general structural simulations but local deformation and compression of the foam required a 3D mesh in the region of interest. The simulations were designed to produce results including deformation, contact time, COR, and post-impact trajectory.

The standard structure was used as a starting point for developing a coupled Eulerian-Lagrangian simulation, replacing the uniform pressure method with an accurate representation of the fluid throughout the entire cavity. This model produced very similar results to the UPM model from a structural point of view but with the added benefit of detailed pressure information. Spatial pressure variation throughout time gave useful information for acoustic studies and the model was used to build upon acoustic lab testing.

8.3 Impact Behaviour

A deviation from a normal rebound to a normal impact was linked to a rotation induced by anisotropic deformation of the ball during contact. This effect, demonstrated with finite element analysis and the lab tests used to validate the simulations, was particularly noticeable in a patch carcass construction. Modifications were made to the patch carcass to alleviate the effects of anisotropy and the result saw an improvement in rebound consistency but a decrease in sphericity.

Using the information gathered in the study of the standard patch carcass, novel carcass prototype concepts were generated to address some of the undesirable effects of anisotropic materials on rebound consistency and sphericity. The prototypes were created following a unique system of "partial nets" with overlapping polygons on Platonic and Archimedean solids. This minimised the size of the anisotropic region while maintaining a consistent number of layers. The results for the novel prototype concepts showed great reduction in rebound deviation, supporting conclusions from the studies on the standard patch carcass.

Though the rebound characteristics depended greatly on the differing smaller regions of anisotropy, the size of the second body in the impact was shown to have little effect on the rebound trajectory compared to the size of the anisotropic regions on the ball.

8.4 Design of Experiments and Optimisation

Design of experiment and optimisation studies provided insight on the effect of yarn orientation on deformation characteristics and the individual contributions of different regions of the ball and individual materials to its overall performance. The regions in contact and opposite the contact surface were shown to be not as important to deformation and rebound as the region between, around the circumference. At high impact speeds, the effects of carcass stiffness had a greater effect on deformation than at lower impact speeds. Also at high impact speeds, the effect of EVA stiffness was greater on contact time than at low impact speeds. When the EVA foam was stiffer, the bladder stiffness had less of an effect on the maximum impact force than when the EVA foam was more compliant. These and other relationships were extracted from automated approximations fit to 400 simulations. The optimum yarn angle offset between two fabric layers was also determined to be 45° and this supported the panel arrangement seen in some of the novel carcass concepts.

8.5 Acoustics

The duration of the ring (conversely the ring decay) was demonstrated to be related to the mass of the ball and the smoothness of the inner surface. Trends in frequency content for spherical

pressurised balls were identified, and a correlation between diameter and dominant frequency was shown. Inner disruptions made of foam blocks or raised seam-like ridges decreased the ring duration. The standard outer foam panels of a football were found to remove some of the highest frequencies above 4kHz.

A variety of lab tests with different excitation methods revealed similar frequency profiles with differences only in amplitude so the emphasis was placed on frequency and ring decay relative to other balls. The dominant ringing sound of a football was around 3kHz, and there was a similar frequency spectral trace shifted higher and lower in the frequency spectrum for smaller and larger balls respectively.

In addition to the lab work, a finite element analysis model was developed to output air pressure at every point in a 3D mesh of the football cavity. Mapping the pressure oscillations allowed for visualisations of mode shapes within the ball that helped to explain the mechanism for the ring propagation. The RMS values for pressure oscillations at frequencies within specific frequency bands of interest highlighted the mode shapes within the cavity. At the typical dominant frequency around 3kHz, the antinodes appeared at the surface and centre. Furthermore, the high pressure variation at the surface may explain why inner surface disruptions are effective in decreasing the propagation of standing waves.

8.6 Recommendations for Future Work

8.6.1 Materials and Characterisation

With the fast pace of commercial sports equipment businesses, complete studies of material and processes can sometimes be cost-prohibitive because of a potential loss of return on invested time if materials are switched. That said, a more in-depth knowledge of the materials and how they are processed would advance football design and simulation. In particular, understanding the energy loss properties at different temperatures and the damage materials undergo during assembly and the first few games can help create more consistent footballs.

8.6.2 Model Creation

As computational power increases, it may be possible to create a single football model that combines many of the features used in individual models for this study. Fine contact pressures and local contact interactions require a fine 3D mesh and that can be very computationally expensive. Such detail may be necessary when exploring he interactions with the intricate laced and textured boot upper. Though high-speed impacts may be considered more important in a match and are

quicker to expose weaknesses in a football, the sheer quantity of low-speed impacts suggests that there is merit in investigating boot-ball contact in touch and controlling scenarios as well.

8.6.3 DOE and Optimisation

An interesting branch of these types of studies may be reverse-engineering football materials and construction based on desired properties. The current work could be used to suggest a carcass material stiffness that would preserve overall deformation if the outer foam were stiffer but this concept could be taken further beyond the current bladder-carcass-foam-skin construction to explore entirely different constructions and materials iteratively and automatically. An optimisation or DOE aimed at exploring the range of acoustic response possible within the confines of current structural requirements would also be an interesting study.

8.6.4 Acoustics

The sound of a football was a new area of exploration and there are many ways it can go from here. An important first step may be a perception study to clarify what is important to athletes both consciously and subconsciously. It would be interesting to look into possibilities of creating sectioned inner bladders that create different resonant chambers to modify the frequency response. There may also be merit in using acoustics as an investigative tool. For example, perhaps the post-impact ring decay can be used as an indicator of sphericity (or post-impact return to sphericity) for a given football.

The horizontal pulsing seen in the lab and simulation data must be explained if not for practical purposes but to complete the academic understanding of the data. It seems related to the structural deformation of the ball but more work is necessary to come to a conclusion.

9 Appendices

9.1 Pentagon Strain

These calculations show the mathematically expected strain required when a flat material takes on a spherical profile.

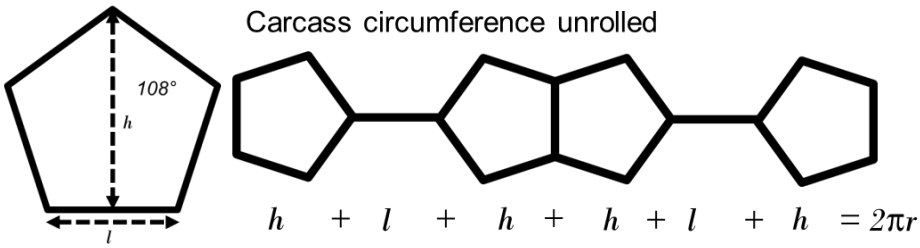

Calculating the area of the flat pentagon in terms of the edge length $\boldsymbol{l}$:

$$\frac{l^2\sqrt{25+10\sqrt{5}}}{4} = 1.72l^2 = A_{flat}$$

Determining the height of the flat pentagon in terms of edge length $\boldsymbol{l}$:

$$h = l\cos 18° + l\cos\frac{180°}{2}$$

$$h = 1.53l$$

Relating ball radius and edge length $\boldsymbol{l}$ and height $\mathbf{h}$ with radius $\mathbf{r}$:

$$4h + 2l = 2\pi r$$

$$8.15l = 2\pi r$$

$$r = \frac{8.15l}{2\pi}$$

Relating pentagon area (1/12 total ball area) with length $\boldsymbol{l}$:

$$A_{spherical} = \frac{4\pi\left(\frac{8.15l}{2\pi}\right)^2}{12}$$

$$A_{spherical} = 1.764l^2$$

The pentagon with a spherical contour (***$A_{spherical}$***) has 2.53% more area than the original flat pentagon (***A_{flat}***).

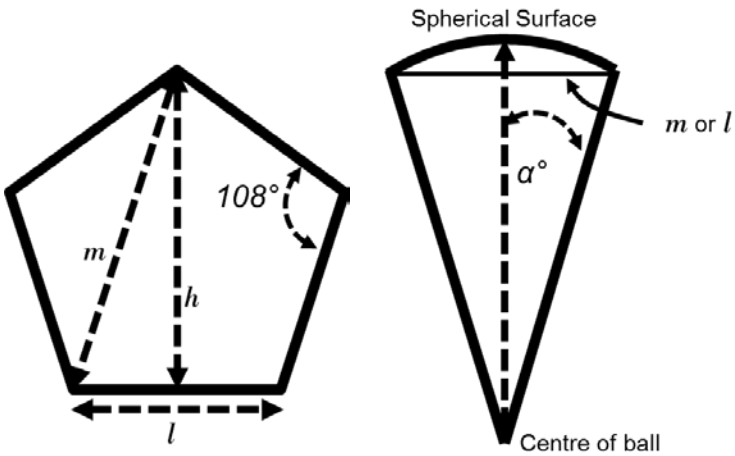

Length in terms of radius (from previous page):

$$l = 0.7709r$$

Longest flat distance through a pentagon m:

$$m = \sqrt{h^2 + \left(\frac{l}{2}\right)^2}$$

$$m = \sqrt{2.59l^2}$$

$$m = \sqrt{2.59(0.7709r^2)}$$

$$m = 1.24r$$

Spherical profile equivalent of $\boldsymbol{l}$:

$$l_{arc} = 2r\sin^{-1}\left(\frac{l}{2r}\right)$$

$$l_{arc} = 0.7914$$

Spherical profile equivalent of $\boldsymbol{m}$:

$$m_{arc} = 2r\sin^{-1}\left(\frac{\sqrt{1.53r^2}}{2r}\right)$$

$$m_{arc} = 1.33r$$

Length $\boldsymbol{l_{arc}}$ with a spherical profile is 2.7% greater than flat length $\boldsymbol{l}$.

Length $\boldsymbol{m_{arc}}$ with a spherical profile is 7.3% greater than flat length $\boldsymbol{m}$.

9.2 Supplemental Model Definition Data

9.2.1 Fluid Material Input Data

Uniform Point Method (UPM) air definition:

Molecular weight: 0.0298 $\frac{kg}{mol}$

Universal gas constant: 8.314 $\frac{J}{mol \cdot K}$

Specific heat capacity (polynomial representation, Shomate equation (Abaqus 2012)):

$$c_p = a + b(\theta - \theta^z) + c(\theta - \theta^z)^2 + d(\theta - \theta^z)^3 + \frac{e}{(\theta - \theta^z)^2}$$

a = 28.11

b = 1.96x10^{-3}

c = 4.802x10^{-6}

d = -1.966x10^{-9}

e = 0

Coupled Eulerian-Lagrangian (CEL) air definition, "Equation of State" (Abaqus 2012):

Density = 1.2$\frac{kg}{m^3}$

Equation of state, gas constant = 287 $\frac{J}{mol \cdot K}$

Specific Heat: 1012 $\frac{J}{K}$

Viscosity = 1.78x10^{-5} $\frac{Pa}{s}$

9.2.2 Solid Material Input Data

Butyl Bladder:

Density: 975$\frac{kg}{m^3}$

Poisson's ratio: 0.475

Hyperelasticity: Yeoh, n=2, uniaxial test data:

Strain	Stress (Pa)
0	0
0.04	150515
0.08	282147
0.12	397208
0.16	498011
0.2	586869
0.24	666093
0.28	737997
0.32	804894
0.36	869095
0.4	932914

Viscoelasticity, time domain:

Omega g* real	Omega g*imag	Omega k* real	Omega k*imag	Frequency
0.0432367	0	0.0432367	0	0.1
0.0536634	-0.0648148	0.0536634	-0.0648148	1
0.0712762	-0.148551	0.0712762	-0.148551	10
0.08281	-0.193438	0.08281	-0.193438	28
0.0897947	-0.216787	0.0897947	-0.216787	46
0.094686	-0.23128	0.094686	-0.23128	64
0.105475	-0.239332	0.105475	-0.239332	82

Patch Carcass Fabric

Density: 835 $\frac{kg}{m^3}$

Tensile Test Data:

Strain	Stress (Pa)
0	0
0.017	1695551.8
0.034	4479410.8
0.05	8185101.3
0.1	19614247
0.134	27930425
0.167	35398870
0.184	39330245
0.2	43170879

Shear Test Data:

Strain	Stress (Pa)
0	0
0.04	217550.39
0.08	439869.31
0.16	975612.76
0.36	3742420.7
0.72	20312693
0.84	31105950
0.92	40213298
1	51029320

TPU+EVA Outer foam and skin:

Density: $440\frac{kg}{m^3}$

Poisson's Ratio: 0.3

Hyperelasticity, Yeoh, n=3, uniaxial test data:

Strain	Stress (Pa)
0	0
0.017	82872.1
0.033	156888
0.05	225389
0.067	287981
0.1	397726
0.117	444560
0.15	527139
0.184	596039
0.2	625451
0.234	677971
0.25	700743
0.267	721918
0.284	741682
0.3	759971
0.334	793282
0.35	808632
0.367	823295
0.4	851010
0.417	864240
0.434	877141
0.467	902104
0.484	914199
0.5	926025
0.517	937556
0.55	959513
0.567	969787
0.584	979462
0.617	996507
0.634	1003580
0.65	1009450
0.667	1013940

Viscoelasticy, time domain

Omega g* real	Omega g*imag	Omega k* real	Omega k*imag	Frequency
0.1023	0	0.1023	0	0.1
0.1198	-0.1734	0.1198	-0.1734	1
0.2006	-0.389	0.2006	-0.389	10
0.7219	-0.2657	0.7219	-0.2657	100

TPU Skin:

Density: $700\frac{kg}{m^3}$

Poisson's Ratio: 0.475

Hyperelasticity, Yeoh, n=3, uniaxial test data:

Strain	Stress (Pa)
0	0
0.05	1685832
0.1	2860845
0.15	3654597
0.2	4178006
0.25	4523356
0.3	4764292
0.35	4955824
0.4	5134324

EVA Foam:

Density: $406\frac{kg}{m^3}$

Poisson's Ratio: 0.3

Hyperelastic, Yeoh, n=3, tensile test data:

Strain	Stress (Pa)
0	0
0.05	107749.99
0.1	200192.23
0.15	278997.35
0.25	402378.78
0.35	491259.41
0.45	559004.33
0.55	618978.66
0.7	723606.46

Latex Bladder:

Density: $567\frac{kg}{m^3}$
Poisson's Ratio: 0.475
Hyperelasticity, Yeoh, n=3, tensile test data:

Strain	Stress (Pa)
0	0
0.02	29579.78266
0.05	71294.74275
0.1	134153.912
0.15	189352.7693
0.22	255237.9431
0.36	355033.4642
0.47	412632.206
0.63	482026.9708

9.3 Notational Analysis

Notational analysis was pursued as a means of gathering information upon which to base boundary conditions and loading scenarios. The aim was to use information about the match to create a summary of what the football experiences. The elite, professional level was chosen because it represents the pinnacle of the sport and, due to the strength of the athletes, was most likely to exhibit the greatest range in loading scenarios. The intention was also to get information from a variety of clubs and leagues. Match tracking and notational analysis is often performed by or for the team for strategy and training purposes but that information is usually kept confidential.

With cooperation from the football notational analysis company Prozone Sports, information was obtained from a variety of clubs in the English Premier League and European Championships (16 matches of data in total). The Prozone data were captured using a semi-permanent camera system consisting of eight cameras (to cover each spot on the pitch twice). The captured datasets for each game also included the movements of individual players but this information was not made available. The available dataset included all ball-related events, primary and secondary players involved, the time of the event, and the XY coordinates of the event on the pitch (0,0 at the centre). The time of each event was recorded to the nearest 0.1s and independent assessment of the system comparing sprints against light gate measurement showed very strong correlations (0.999 for a 60m sprint (Di Salvo et al. 2006)). There is no available validation data tied directly to the way in which the data will be used in this study, but the accuracy of motion identification suggests that the positional accuracy is also acceptable.

The XY positions and times of adjacent events were used to calculate a distance and average speed for each event related to the ball. This allowed for an inspection of the game in terms of frequency of events by type as well as measurement (see Appendix section 0 for tables). Figure 131 shows that the most frequent events are slow and short. At this stage, only average speed can be presented, calculated with the XY position and temporal coordinates of each event. Of the 41633 events captured in the 16 matches, 20780 (49.9%) were touches (short, self-passes like dribbling) and only 356 (0.86%) were shots. Focusing testing on the most frequent usage scenario is not necessarily the best-practice in this instance. The various components of the ball respond differently for different impact severities (to be explored in greater detail later) and the importance of football behaviour can be said to increase with increasing speed and distance. The average for the average speed of a shot throughout the duration of the ball motion was 22.8m/s and the average shot distance was 16.1m. Shots were on average the fastest events recorded, followed by direct free kick crosses at 20.45m/s.

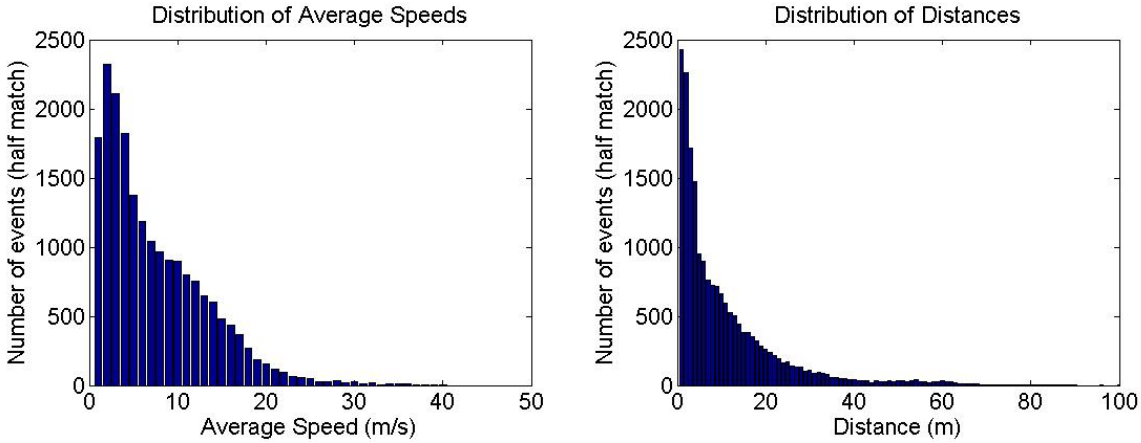

Figure 131: Distribution of Average Speeds (left) and Distances (right)

Distances and average velocities were indicative of the types of impacts experienced by a football in a match but more important for testing purposes is the initial velocity after impact, or, if possible, the speed of the boot. By supplementing the match data with information from other tests, the individual events could be better defined and consequently provide a better description of the impact scenario. Knowledge of rolling and aerodynamic resistance was used to suggest whether the ball was in flight or on the ground. A program was written in a MATLAB script (MathWorks, 2014, Mass., USA) and implemented to probe deeper into the results. The program organised the data by match, speed, distance and event type to view the data from different perspectives. In this study, some of the data was excluded, leaving only matches that used the football for which experimental aerodynamic data was available (see Appendix section 0).

In any given event, the football could either be on the ground, in the air, or a combination of the two. Using different sets of assumptions based on the likeliness of the ball to be rolling or flying, the motion, specifically the acceleration, could be inferred. With a known acceleration (linear or nonlinear) and known distance and time, the initial and final ball velocities could be calculated, providing more information about what the ball experienced in the match. Assumptions were necessary to begin the calculations but the event type, as well as the preceding and following events were known and these were used to provide context. For example, a very short 'touch' was likely to be on the ground and a corner kick to a header was likely to be in the air. Considering first the rolling case, knowing the football's linear acceleration compared to the expected acceleration on grass can suggest whether the ball was actually rolling.

The FIFA pitch standard was used to define rolling resistance. The standard is specified as a distance on the grass after rolling a football down a smooth 45° ramp from a height of 1m (FIFA 2010a). Approved pitches will let the ball roll between 4m and 8m. Converting potential energy at the top of

the ramp to velocity at the bottom (rotational energy is negligible in this case), the accelerations of the ball at the high and low end were -2.76m/s^2 and -1.38m/s^2, based on the speed at the bottom of the ramp and the distance by which the ball must stop. To compare with this range, and assuming a linear acceleration for the short distances of a rolling kick in this study, a necessary linear acceleration was calculated (a=2d/t). In Figure 132, the area under each line represents the distance covered. The distance and time for the event were known so the average speed represents the benchmark which all velocity profiles must meet. In the case where the roll-based deceleration was the same as the calculated deceleration, the ball rolled to a stop right before getting kicked again. If the deceleration calculated from the time and distance was less than the roll-based deceleration, the ball decelerated too slowly for the given information and it was intercepted before coming to a stop or the pitch was out of spec. If the ball seemed to decelerate faster than pitch should allow, the ball came to a stop and sat still before it was kicked again.

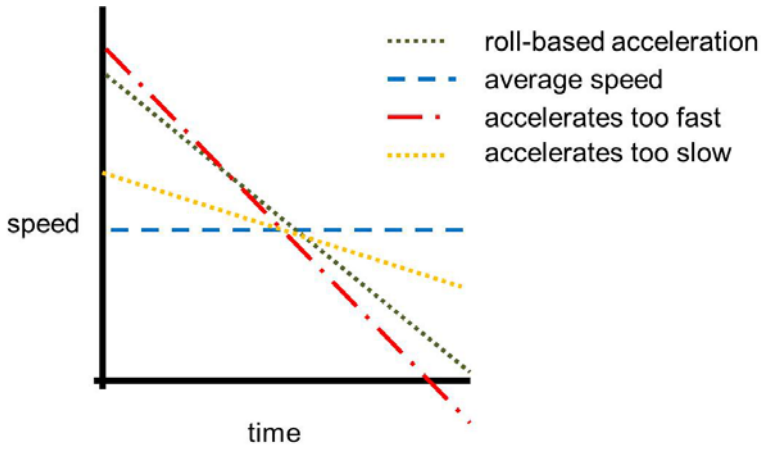

Figure 132: Rolling Resistance, Linear Accelerations as they compare to a theoretical average speed

Similar to the rolling condition, if a ball were known to be flying, the aerodynamic characteristics could shed light on the trajectory and initial velocity. Assuming constant (yet speed-dependent) aerodynamic properties (i.e. no spin), there could only be one trajectory (defined by launch angle, initial velocity, and velocity profile) that would allow the ball to be at both start and ending positions at the given times. The reverse has been done to experimentally determine (single) drag and lift coefficients (Bray & Kerwin 2003) but earlier studies have lacked the detailed information about velocity-dependent aerodynamic behaviour. Because the drag on a football is known to be nonlinear, the velocity degradation must be integrated across the flight path to accurately represent the forces at play. At higher ball airspeeds, the boundary layer cannot remain smooth (laminar), resulting in little pockets of turbulence and eddies. Practically speaking, this means a decrease in drag coefficient with higher velocity but there is also an abrupt change once the transition from laminar to turbulent flow occurs (Rogers 2011). For the 32 panel stitched football used in the wind

tunnel testing, the transition happens around 15m/s and well within the speeds seen in match play (Passmore et al. 2008). Due to the influence of specific football panel design on aerodynamic performance (Passmore et al. 2008), the trajectories could only be estimated for events from the three games that used the same ball as the wind tunnel testing. Drag coefficients for a ball in flight at a range of velocities (0.84-30.4m/s) were taken from wind tunnel testing conducted at Loughborough University (Passmore et al. 2011). These calculations assume that the ball was in flight for the entire event and become invalid if the ball bounces. To ensure that the calculations were applied appropriately, events can be selected based on the likeliness that the ball remained in the air. One such event was a corner-cross to a header.

A program was written in MATLAB to iterate through launch angles and velocities until the ball covered the specified distance and time according to a flight model developed for the study. Each potential trajectory was solved in 200 steps. Each step started with the velocity from the previous and calculated a drag force using experimentally determined drag coefficients (see Appendix 9.5). The vertical and horizontal distance was calculated using the duration of each step and the velocity (speed and flight angle) was modified with the drag force data and gravity acceleration. From the flight model, information for the XY (horizontal-vertical) trajectory was available, including where the ball would be after the given time. Velocity and launch angle were incremented by 0.01m/s and 0.01rad and put into the flight model to create potential trajectory iterations until a solution was discovered. The result was an estimated launch angle, initial velocity, and flight path.

Using the rolling resistance-based deceleration method on events less than 5 metres (7163 events), 11% ended with the ball rolling to a stop and 85% were intercepted while the ball was still in motion. The remaining 4% would have lost speed slower than is appropriate on a professional pitch.

Of the three datasets from matches that used a stitched 32-panel ball, 12 corner-cross to headers were found, ranging from 29-39m. The event chosen at random for this study had a distance of 33.4m and lasted 1.7s. From these parameters and the drag coefficients, the trajectory calculation script determined a launch angle of 25° and initial velocity of 24.3m/s in that direction. When it reached the end of its trajectory at 2.2m above the pitch, it was travelling at 19m/s. This was one of several possibilities, given a small range of vertical and horizontal (+/- 0.1m) positions. Figure 133(a) and (b) show drag and velocity broken into components and Fig. 3 (c) shows a graphical representation of the complete trajectory (X is horizontal, Y is vertical).

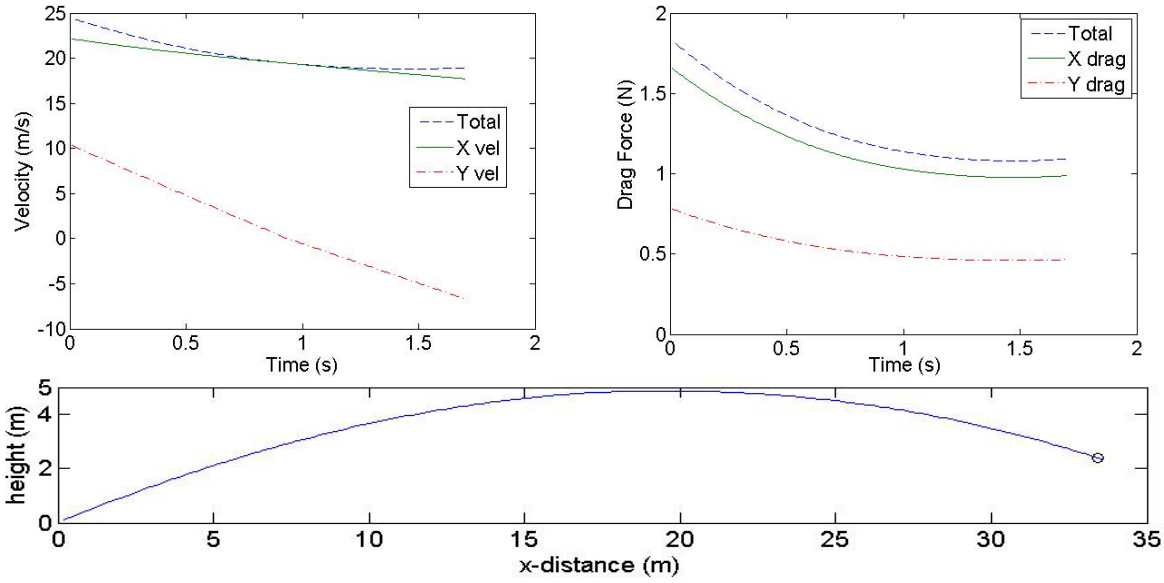

Figure 133: (a) Velocity Profile, (b) Drag Force, (c) Trajectory

The relationship between initial speed and impact conditions is not straightforward. A lossless ball-boot impact with a boot moving at a constant velocity *V* would move at *2V* at the end of contact: *1V* for the pushing motion of the boot, and *1V* for the energy stored and returned by the ball. The pushing motion has been identified as more than half of the release speed due to the losses that happen in the ball's energy storage and return. Starting at full deformation when the ball already carries the full speed of the boot, the dynamics between the ball's reformation and muscular contribution/opposition are complicated so the limb was more reliably simulated as a rigid object with a constant velocity (after full deformation). Based on measured foot velocity profiles, this was acceptable (Tsaousidis & Zatsiorsky 1996). Assuming the foot or impacter to be rigid simplifies the energy loss aspects of the scenario, attributing all losses to only the ball. Following this reasoning, a football with an initial speed of 24.3m/s must have been struck by something moving at *V* m/s, where *V* is related to the initial speed with the following equation:

$$initial\ velocity = V_1 + cor \times V_2$$

The first V_1 represents the pushing aspect of the kick and the V_2, related to the energy storage and release, is reduced by the coefficient of restitution. For a 24.3m/s kick, this suggests an initial impactor (flat plate for the purpose of easily identifying a COR) velocity of 13.1m/s for a ball with a COR of 0.85 (FIFA range is 0.82-0.88). In other words, to simulate the severity of impact that would produce a specific initial ball speed, the closing velocity between ball and plate (independent of which moves first) could be calculated using the COR and it will be noticeably less than the desired resulting initial speed. If the boot and ball are closing at a faster rate (for example, the ball is rolling

toward the boot) but the post-impact ball speed is the same, the impact is more severe. With these numbers in mind, 20m/s was selected as the standard impact speed for both lab tests and simulations. This velocity produced an impact in line with the most severe seen in match play and one that could be replicated with available equipment.

9.4 Notational Analysis Data

Average number of events per half-match. Three European Championship matches, ten English Premier League matches.

Event	English Premier League	European Championships	Totals
Touch	770.7	698.7	734.7
Pass	405.0	371.5	388.3
Header	62.3	42.3	52.3
Ball out of Play	34.5	33.0	33.8
Clearance	30.5	16.8	23.7
Tackle	25.7	20.2	22.9
Throw in	20.2	19.8	20.0
Block	14.2	14.2	14.2
Foul	11.3	16.3	13.8
Direct Free Kick Pass	10.5	13.8	12.2
Shot	10.0	9.5	9.8
Goal Kick	9.7	8.3	9.0
Goal Keeper Throw	5.0	6.8	5.9
Goal Keeper Pick Up	5.0	4.8	4.9
Dribble	1.2	6.8	4.0
Goal Keeper Catch	4.3	3.2	3.8
Corner Cross	4.2	3.2	3.7
Substitution	2.5	2.3	2.4
Indirect Free Kick Pass	2.3	2.2	2.3
Offside	2.3	2.2	2.3
Goal Keeper Save	1.5	2.0	1.8
Header Shot	1.7	1.7	1.7
Goal Keeper Save Catch	1.3	1.5	1.4
Goal	1.2	1.5	1.3
Yellow Card	1.2	1.2	1.2
Direct Free Kick Cross	0.7	1.3	1.0
Crosbar	0.2	0.3	0.3
Own Goal	0.2	0.0	0.1
Red Card	0.0	0.0	0.0

Average Distance and average speed for selected common events in the matches. A blank space indicates that there was no data available.

	Pass		Shot		Goal		Corner Cross		Indirect Free Kick Pass		Direct Free Kick Pass		Direct Free Kick Cross		Touch	
Game	Distance	Speed	Distance	Speed	Distance	Speed	Distance	Speed	Distance	Speed	Distance	Speed	Distance	Speed	Distance	Speed
Arsenal_v_Blackburn_1st_11FEB08.xlsx	16.133357	11.60345	18.48983	22.63207	52.75607	1.565462	33.95373	20.24009	37.9403555	14.74307805	27.67811	13.53546	36.0555599	20.0308666	3.288967	3.042074
Arsenal_v_Blackburn_2nd_11FEB08.xlsx	16.541353	11.31252	14.70774	23.17363	53.38353	0.854136	33.1177	21.71439	46.5103131	15.77597538	34.49792	14.37989			3.030146	2.864124
Arsenal_v_Liverpool_1st_05APR08.xlsx	17.362852	11.9145	22.61378	23.55597	53.27545	1.443779	31.81928	21.32197	11.6044345	12.89381611	26.00883	14.03048			3.191842	3.232328
Arsenal_v_Liverpool_2nd_05APR08.xlsx	18.1324	11.56545	13.65433	26.61889	52.97627	1.365368	31.97321	20.95903			28.20376	11.65774	34.2029531	19.0016406	3.474705	3.264177
Arsenal_v_ManU_1st_11Mar07.xlsx	16.566182	11.30869	18.92141	20.88557			36.0318	20.85313	16.2136007	9.500224049	24.26355	11.36814	25.7323271	21.669052	3.426524	3.55535
Arsenal_v_ManU_2nd_11Mar07.xlsx	17.093952	11.28837	19.32303	23.41753	53.02515	1.060864	33.45384	19.64912	33.872046	13.94785895	35.67881	13.214			3.593751	3.749106
Germany_v_Turkey_Euro_semi_1st_08.xlsx	17.375566	11.81731	14.29896	19.43506	53.00943	0.963204	32.01426	23.88282			28.4783	15.1011	28.1780056	16.5752974	3.636951	4.105594
Germany_v_Turkey_Euro_semi_2nd_08.xlsx	17.918287	10.91015	22.59629	26.14626	53.69467	0.880302	32.03933	26.95308			25.84536	12.21255			4.025694	4.297159
Russia_v_Spain_Euro_semi_1st_08.xlsx	16.266185	11.00414	17.5669	23.24104			35.73514	21.02067			18.1055	12.06021	22.0227155	20.0206505	3.837212	4.0324
Russia_v_Spain_Euro_semi_2nd_08.xlsx	15.998268	11.52682	15.13247	23.9139	53.68209	0.935336	28.26397	24.90987	28.7297081	14.17241405	16.95486	11.56073			3.691301	3.960128
Spain_v_Germany_Euro_final_1st_08.xlsx	16.348122	11.85545	15.92123	18.49437	54.08327	0.888067	36.74584	26.59472	14.8667003	7.576829865	15.51082	10.37768	31.3775178	19.7079344	3.39833	4.104314
Spain_v_Germany_Euro_final_2nd_08.xlsx	16.399839	11.61075	14.07087	23.67549			26.1725	20.1327	42.6498632	12.93799822	26.53216	12.91151	34.2125277	20.9074698	3.567256	4.02231
Arsenal_v_West_Brom_1.xlsx	16.192568	11.88007	10.30205	18.78363	52.45007	1.014778	27.13763	20.8751	55.3566731	15.12833983	25.76151	13.82542	33.9091389	22.6060926	3.311029	3.104989
Arsenal_v_West_Brom_2.xlsx	16.529925	11.68007	14.80444	21.56334	53.94736	1.135734	34.41966	20.23328	11.2444808	9.696379872	50.90245	16.11988	28.6224517	19.7212951	3.103068	3.133772
Aston_Villa_v_Norwich_City_1.xlsx	17.733304	12.02384	13.3665	24.11909	53.03772	1.012018	37.30262	19.69261	58.4374376	17.2001402	36.49353	16.07794	30.4137947	20.5352621	4.410155	4.470034
Aston_Villa_v_Norwich_City_2.xlsx	19.097815	11.35837	17.39124	21.79044	57.45637	1.463787	32.5084	19.72117	36.7024284	16.50093413	38.84768	13.97888	22.6775471	21.4812166	4.357428	4.989008
Blackburn_v_Chelsea_1.xlsx	17.364008	11.61296	24.68248	21.06327			37.07978	18.49774	26.1107667	10.88019424	28.37969	11.64902	37.309463	20.4414174	3.037078	3.130757
Blackburn_v_Chelsea_2.xlsx	17.957569	11.15539	14.92911	20.13173	53.4927	1.186091	29.79365	21.50343	64.3577689	15.51533301	33.57269	13.21459	32.3391589	24.8762761	3.452812	3.192048
Bolton_v_Stoke_City_1.xlsx	20.641377	11.59716	12.97529	18.23585	49.70742	1.143753	32.88219	20.76621	30.6397133	12.21767543	45.94561	15.39526	39.5957083	19.746291	3.489218	3.410367
Bolton_v_Stoke_City_2.xlsx	20.002002	11.5261	14.68292	25.59186	50.24882	1.029494	41.31712	17.47236	55.4155549	15.17887813	26.10906	13.16954	32.7696338	20.4810211	3.712766	3.453906
Fulham_v_Tottenham_1.xlsx	16.621712	11.40354	10.57033	26.60475	50.83118	1.082011	29.64205	22.66008	45.2291477	13.56775905	31.19198	11.34762	30.4484065	20.1293709	3.264581	2.979077
Fulham_v_Tottenham_2.xlsx	16.685398	11.82906	14.69416	26.09646	51.57039	1.011184	34.50707	18.83536			42.80751	16.91211	31.6281333	18.7160556	3.200334	3.173643
Liverpool_v_Swansea_City_1.xlsx	15.556182	11.60427	15.1898	26.92633			45.34523	17.09685	31.4425163	16.92676531	30.76606	14.77363	38.8021262	18.477203	3.411071	3.284052
Liverpool_v_Swansea_City_2.xlsx	17.067474	11.6417	15.24183	24.10965			31.96669	20.74696	19.1321998	10.34031851	33.11243	10.59493	29.4170663	21.7530925	3.63599	3.630629
Manchester_United_v_Sunderland_1.xlsx	16.824262	11.61247	20.76018	20.92126			32.79902	19.55279	39.7907402	13.56761996	38.89251	13.70221	26.3177758	19.9896877	3.315957	3.232231
Manchester_United_v_Sunderland_2.xlsx	18.015181	11.44862	14.15141	22.33793			33.62445	19.81527	57.1811407	16.33180288	39.8452	15.06844	19.6488804	24.5611005	3.475847	3.044936
Newcastle_United_v_Everton_1.xlsx	19.2769	12.38847	18.30508	25.06235	53.02358	1.40013	35.16395	22.95681	38.0694729	14.20929126	38.59417	14.49931	30.5234473	20.0391385	4.854995	5.434424
Newcastle_United_v_Everton_2.xlsx	19.713651	12.17288	18.54208	21.92284			37.37226	17.72833	38.6853838	10.64892133	39.54267	13.64401	35.9765453	18.7412631	4.918373	5.903699
Queens_park_v_Manchester_City_1.xlsx	17.49935	11.58803	11.90709	22.39127	50.01954	1.197507	39.2134	15.23997	60.6569971	17.33057061	42.69215	17.71875	35.2834976	20.7549986	3.121981	3.2997
Queens_park_v_Manchester_City_2.xlsx	16.558689	11.42333	19.07709	22.66048	54.03701	0.892791	38.39141	16.69192	18.7186867	10.37438481	36.80245	14.55335			3.084378	3.058796
Wolverhampton_v_Wigan_1.xlsx	17.40215	12.11413	12.68037	24.42691	52.94473	1.225188	35.87814	20.16476	50.2031641	15.55514216	35.18781	11.66165	30.7382319	19.2113949	3.393557	3.208187
Wolverhampton_v_Wigan_2.xlsx	17.774793	12.34497	13.75846	20.60404	52.22337	1.228801	44.63324	17.30109	38.0157188	14.78206502	37.55507	15.5458	29.1367094	21.6982804	3.726599	3.43004

9.5 Aerodynamic Data

Table 15: Velocity-Dependent Drag Coefficients

Lower Limit (m/s)	Upper Limit (m/s)	Drag Coefficient
0.84	5.04	0.3536
5.04	7.48	0.4399
7.48	10.03	0.3072
10.03	10.99	0.2659
10.99	12.02	0.2232
12.02	13.01	0.1657
13.01	13.98	0.149
13.98	15.00	0.1382
15.00	16.00	0.1436
16.00	16.99	0.154
16.99	18.02	0.1489
18.02	20.01	0.1486
20.01	24.99	0.1337
24.99	30.03	0.1523

9.6 Alternate Acoustic Excitation Methods

The hand-to-hand test was a short-distance open handed catch intended to simulate the experience of an athlete first touching and experiencing a new football. The slap test was an open handed slap sending the ball vertically about 1m. The test was chosen as a way to emphasise the type of sound created by squeezing air from between two bodies. In the flick test, the middle finger was restrained by the thumb and released explosively to contact the ball. This test was chosen for to represent a very light impact. The flick was the lightest, followed by the hand-to-hand and the slap in terms of severity and this was reflected in the spectrograms. The frequency peaks present in the flick were also seen in the hand-to-hand and slap but the more severe impacts showed additional frequencies as well.

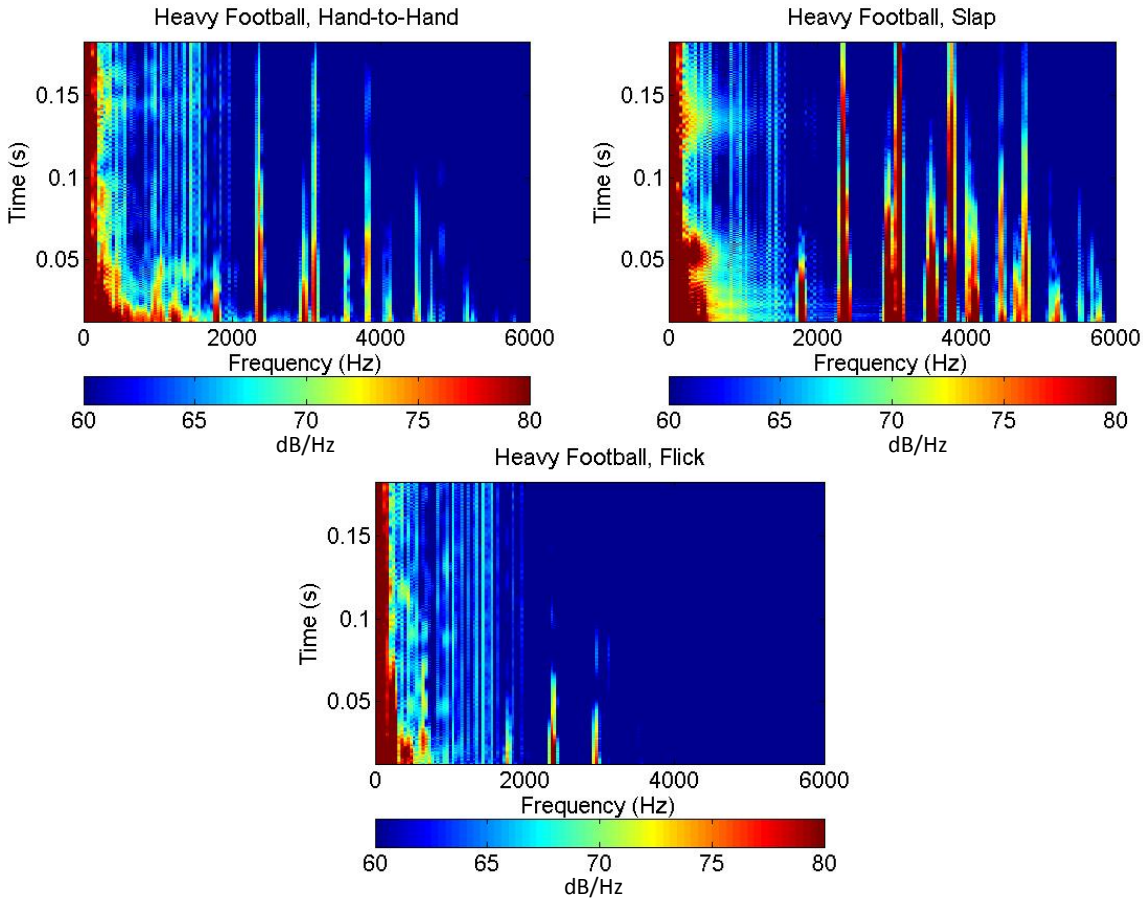

9.7 Acoustic Data

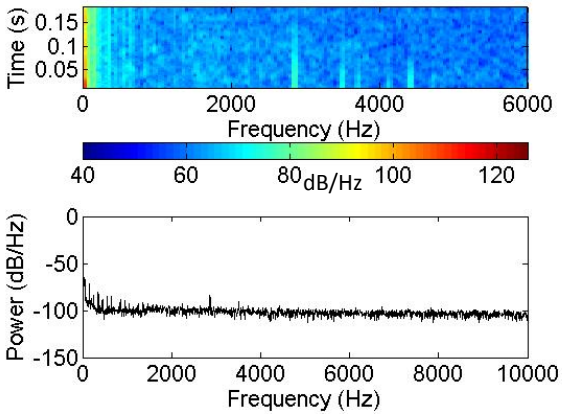

Figure 134: Cheap Football Spectrogram and FFT

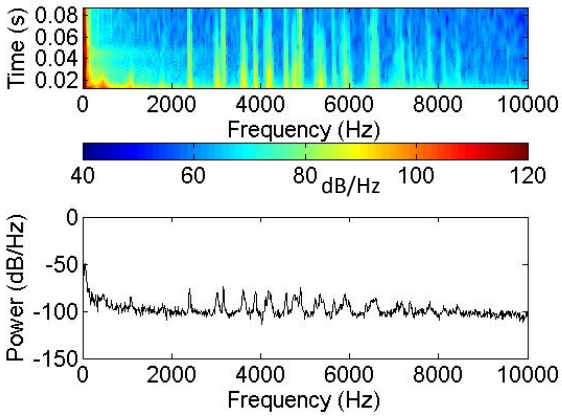

Figure 135: Volleyball Spectrogram

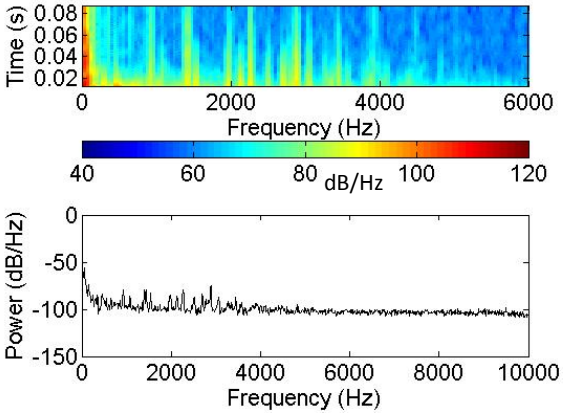

Figure 136: American Football Spectrogram and FFT

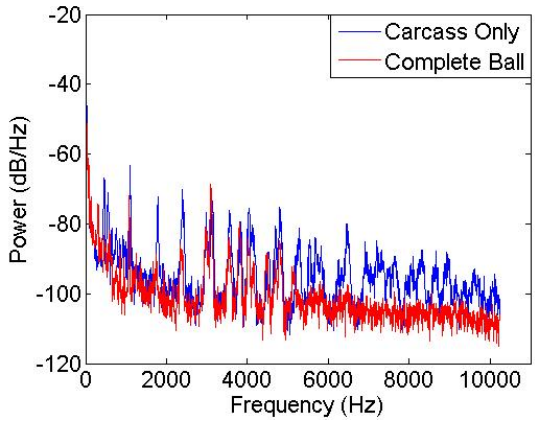

Figure 137: Complete Ball vs. Carcass (Dodecahedron)

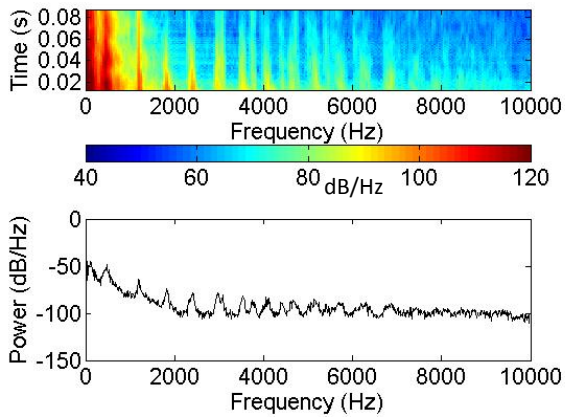

Figure 138: Latex Bladder Spectrogram and FFT

10 Works Cited

Abaqus, 2012. Abaqus Analysis User's Manual.

Abaqus, 2010. *Getting Started with Abaqus: Interactive Edition* 6.10 ed., Dassault Systems.

Abeyaratne, R. & Horgan, C.O., 1984. The pressurized hollow sphere problem in finite elastostatics for a class of compressible materials. *International Journal of Solids and Structures*, 20(8), pp.715–723. Available at: http://www.sciencedirect.com/science/article/B6VJS-482GM9N-14J/2/71dd09139f051aca2a2c075534eae9f0.

Aguiar, C.E. & Laudares, F., 2002. Listening to the coefficient of restitution and the gravitational acceleration of a bouncing ball. *American Journal of Physics*, 71(5), pp.499–501. Available at: http://link.aip.org/link/AJPIAS/v71/i5/p499/s1&Agg=doi [Accessed October 31, 2011].

Anderson, J.C. et al., 1985. *Materials Science* 3rd ed., Berkshire, England: Van Nostrand Reinhold (UK) Co. Ltd.

Arakawa, K. et al., 2009. Dynamic Deformation Behavior of a Golf Ball during Normal Impact. *Experimental Mechanics*, 49(4), pp.471–477. Available at: http://dx.doi.org/10.1007/s11340-008-9156-y.

Arruda, E.M. & Boyce, M.C., 1993. A THREE-DIMENSIONAL CONSTITUTIVE MODEL FOR THE LARGE STRETCH BEHAVIOR OF RUBBER ELASTIC MATERIALS. *Journal of Mechanics and Physics of Solids*, 41(2), pp.389–412.

Asai, T. et al., 2004. Computer Simulation of Ball Kicking Using the Finite Element Skeletal Foot Model. *Journal of Sport Sciences2*, 22(6), p.485.

Association, F., 2010. History of The FA. , (19.05.2010). Available at: http://www.thefa.com/TheFA/WhoWeAre/HistoryOfTheFA.

ASTM International, 2003. Standard Test Method for Tensile Properties of Plastics A. International, ed. *D638 - 03*.

ASTM International, 2008. Standard Test Methods for Vulcanized Rubber and Thermoplastic Elastomers - Tension A. International, ed. *D412-06a*.

Bartholomew, P., 2012. *The State of Current Practice in Engineering Design Optimisation*, NAFEMS.

Batra, R.C., 2008. Optilam Design of Functionally Graded Incompressible Linear Elastic Cylinders and Spheres. *American Institute of Aeronautics and Astronautics*, 46(8), pp.2050–2057.

Becker, A.A., 2004. *An Introductory Guide to Finite Element Analysis* R. C. Baker, ed., London, UK: Professional Engineering Publishing.

Blocken, B. et al., 2013. CFD simulations of the aerodynamic drag of two drafting cyclists. *Computers & Fluids*, 71, pp.435–445. Available at: http://linkinghub.elsevier.com/retrieve/pii/S0045793012004446 [Accessed April 11, 2013].

Bray, K. & Kerwin, D.G., 2003. Modelling the flight of a soccer ball in a direct free kick. / Modelisation de la trajectoire d ’ un ballon de football lors d ' un coup franc direct. *Journal of Sports Sciences*, 21(2), pp.75–85. Available at: http://articles.sirc.ca/search.cfm?id=S-864773.

British Standards, 1999. Textiles - Tensile properties of fabrics BSI, ed. *BS EN ISO 13934-1:1999*.

Burbank, S.D. & Smith, L. V., 2012. Dynamic characterization of rigid foam used in finite element sports ball simulations. *Proceedings of the Institution of Mechanical Engineers, Part P: Journal of Sports Engineering and Technology*. Available at: http://pip.sagepub.com/lookup/doi/10.1177/1754337112441112 [Accessed May 25, 2012].

Cairos_Technologies, 2013. Cairos Technologies AG. Available at: http://www.cairos.com/unternehmen/gltsystem.php.

Callister, W.D.J., 2000. *Materials Science and Engineering: An Introduction* 5th ed., New York: John Wiley & Sons, Inc.

Cantournet, S., Desmorat, R. & Besson, J., 2009. Mullins effect and cyclic stress softening of filled elastomers by internal sliding and friction thermodynamics model. *International Journal of Solids and Structures*, 46(11-12), pp.2255–2264. Available at: http://linkinghub.elsevier.com/retrieve/pii/S0020768309000080 [Accessed May 28, 2013].

Carre, M.J., Goodwill, S.R. & Haake, S.J., 2005. Understanding the effect of seams on the aerodynamics of an association football. *Proceedings of the Institution of Mechanical Engineers Part C-Journal of Mechanical Engineering Science*, 219(7), pp.657–666. Available at: <Go to ISI>://000231845500004.

Cech, P. & adidas, 2009. adidas Jabulani Video Release adidas, ed.

Cengel, Y.A. & Boles, M.A., 1989. *Thermodynamics: an engineering approach*, McGraw Hill.

Cooper, K., 2011. *adidas: the story as told by those who have lived and are living it*, Herzogenaurach: adidas AG.

Cotton, R. & Jones, R., 2007. Surface Interactions of Soccer Balls. *Mechanical and Manufacturing Engineering*, Doctor of , p.240.

Cox, R., Russell, D. & WVamplew, W., 2002. Encyclopedia of British Football.

Cross, R., 2000. The coefficient of restitution for collisions of happy balls, unhappy balls, and tennis balls. *American Journal of Physics*, 68(11), pp.1025–1031. Available at: http://link.aip.org/link/?AJP/68/1025/1.

Daish, C.B., 1972. *The Physics of Ball Games*, London: University Press Ltd.

Dargahi, J. & Najarian, S., 2004. Human tactile perception as a standard for artificial tactile sensing - a review. *International Journal of Medical Robotics and Computer Assisted Surgery*, 01(01), p.23. Available at: http://www.roboticpublications.com/index.php?page=abstract0101&id=3 [Accessed October 18, 2013].

Davies, W.J., 2010. The Acoustic Environment. In C. Plack, ed. *The Oxford Handboook of Auditory Science: Hearing*. Ne York: Oxford University Press, pp. 374–415.

Defraeye, T. et al., 2010. Aerodynamic study of different cyclist positions: CFD analysis and full-scale wind-tunnel tests. *Journal of biomechanics*, 43(7), pp.1262–8. Available at: http://www.ncbi.nlm.nih.gov/pubmed/20171640.

Diani, J., Brieu, M. & Gilormini, P., 2006. Observation and modeling of the anisotropic visco-hyperelastic behavior of a rubberlike material. *International Journal of Solids and Structures*, 43(10), pp.3044–3056. Available at: http://www.sciencedirect.com/science/article/B6VJS-4GWBF45-3/2/2e2e8c14425f672698b09736c8ba23f4.

Fahy, F.J. & Walker, J.G. eds., 1998. *Fundamentals of Noise and Vibration*, London: E & FN Spon.

Ferziger, J.H. & Peric, M., 1996. FURTHER DISCUSSION OF NUMERICAL ERRORS IN CFD. *International Journal for Numerical Methods in Fluids*, 23(November 1994), pp.1263–1274.

FIBA, 2010. Official Basketball Rules 2010, Basketball Equipment F. C. Board, ed.

FIFA, 2006. FIFA Big Count 2006. *FIFA Big Count*.

FIFA, 2013. FIFA Quality Concept. Available at: http://www.fifa.com/aboutfifa/organisation/marketing/qualityprogramme/goallinetechnology/index.html.

FIFA, 2010a. FIFA Quality Concept for Football Turf.

FIFA, 2010b. FIFA Quality Concept for Footballs F. I. de F. Association, ed.

FIFA, 2009. Laws of the Game F. I. de F. Association, ed. , p.140.

FIFA, 1996. Minutes of the 1996 Annual General Meeting of the International Football Association Board. In Rio De Janeiro, Brazil.

Fisher, S.R.A., 1971. *The Design of Experiments* 8th ed., New York: Hafner Publishing Company.

FIVB, 2009. Rules of the Game, Official Volleyball Rules FIVB, ed. , (19).

Gentot, L., Brieu, M. & Mesmacque, G., 2004. MODELING OF STRESS-SOFTENING FOR ELASTOMERIC MATERIALS. *Rubber Chemistry and Technology*, 77, pp.758–769.

Gingold, R.A. & Monaghn, J.J., 1977. Smoothed particle hydrodynamics: theory and application to non-spherical stars. *Royal Astronomical Society, Monthly Notices*, 181, pp.375–389.

Giulianotti, R., 1999. *Football: a sociology of the global game*, Malden: Polity Press and Blackwell Publishers Ltd.

Goodwill, S.R., Kirk, R. & Haake, S.J., 2005. Experimental and finite element analysis of a tennis ball impact on a rigid surface. *Sports Engineering*, 8(3), pp.145–158. Available at: http://www.springerlink.com/index/10.1007/BF02844015.

Gupta, V.K. & Khakhar, D. V, 1990. Formation of Integral Skin Polyurethane Foams. *Polymer Engineering & Science*, 39(7).

Harris, S., 2004. Heading for Danger. *Daily Mail*.

Harrison, P., Clifford, M.J. & Long, A.C., 2004. Shear characterisation of viscous woven textile composites: a comparison between picture frame and bias extension experiments. *Composites Science and Technology*, 64(10-11), pp.1453–1465. Available at: http://www.sciencedirect.com/science/article/B6TWT-4BBMTDS-2/2/58f56b9ca79fdd947b2ec02dd77dd462.

Hearle, J.W.S., 1967. The structural mechanics of fibers. *Journal of Polymer Science Part C: Polymer Symposia*, 20(1), pp.215–251. Available at: http://doi.wiley.com/10.1002/polc.5070200118.

Hearle, J.W.S., Potluri, P. & Thammandra, V.S., 2001. Modelling Fabric Mechanics. *Journal of Textile Industry*, 92(3), pp.53–69.

Hirth, A., Haufe, A. & Olovsson, L., 2007. Airbag Simulation with LS-DYNA Past – Present – Future. *Keynote - LS-DYNA User Forum, Frankenthal 2007*, pp.57–74.

Holmes, G. & Bell, M.J., 1985. The effect of football type and inflation pressure on rebound resilience. *Sports Turf Research Institute*, 61.

Hubbard, M. & Stronge, W.J., 2001. Bounce of hollow balls on flat surfaces. *Sports Engineering (International Sports Engineering Association)*, 4(2), pp.49–61. Available at: http://search.ebscohost.com/login.aspx?direct=true&db=s3h&AN=4937762&site=ehost-live.

ISO, 2012. Plastics - Determinatino of tensile properties - Part1: general principles (ISO 527-1:2012). *European Committee for Standardization*.

Jacobson, R.E., Ray, S.F. & Attridge, G.G., 1988. *The Manual of Photography* 8th ed., London: Focal Press.

Johannknecht, R., 1999. *The Physical Testing and Modelling of Hyperelastic Materials for Finite Element Analysis*, Duesseldorf: VDI Verlag GmbH.

Johnson, A. & Sherwin, K., 1996. *Foundations of Mechanical Engineering*, Boca Raton: Taylor & Francis Group.

Johnson, A.R., Quigley, C.J. & Freese, C.E., 1995. A viscohyperelastic finite element model for rubber. *Computer Methods in Applied Mechanics and Engineering*, 127(1-4), pp.163–180. Available at: http://www.sciencedirect.com/science/article/B6V29-3XY2KB3-P/2/ef7bf19b83b7487c06fde49a541040d6.

Johnson, W., Reid, S.R. & Trembaczowski-Ryder, R.E., 1973. The Impact , Rebound and Flight of a Well Inflated Pellicle as Exemplified in Association Football. In *Manchester Association of Engineers*.

Katz, J.I., 2010. Thump, ring: the sound of a bouncing ball. *European Journal of Physics*, 31(4), pp.849–856. Available at: http://stacks.iop.org/0143-

0807/31/i=4/a=014?key=crossref.35f917021652f7e5743a1b029d002a62 [Accessed November 24, 2011].

Lawrence, A., 1989. *Acoustics and the Built Environment*, New York: Elsevier Science Publishers Ltd.

Lee, E.-S. & Youn, S.-K., 2006. Finite element analysis of wrinkling membrane structures with large deformations. *Finite Elements in Analysis and Design*, 42(8-9), pp.780–791. Available at: http://linkinghub.elsevier.com/retrieve/pii/S0168874X06000151 [Accessed December 9, 2011].

Lees, A. & Nolan, L., 1998. The biomechanics of soccer: A review. *Journal of Sports Sciences*, 16(3), pp.211–234. Available at: http://www.informaworld.com/10.1080/026404198366740.

Lin, H. et al., 2009. Finite element modelling of fabric shear. *Modelling and Simulation in Materials Science and Engineering*, 17(1), p.015008. Available at: http://stacks.iop.org/0965-0393/17/i=1/a=015008?key=crossref.d1f3993ca07d121be6351b5fb577baeb [Accessed May 15, 2013].

Liu, I. & Tsiang, R.C., 2003. Tailoring Viscoelastic and Mechanical Properties of the foamed blends of EVA and various ethylene-styrene interpolymers. *Polymer Composites*, 24(3).

Lomov, S. V et al., 2006. Picture Frame Test of Woven Composite Reinforcements with a Full-Field Strain Registration. *Textile Research Journal*, 76(3), pp.243–252. Available at: http://trj.sagepub.com/content/76/3/243.abstract.

Luo, R.K., 2014. Mullins damage effect on rubber products with residual strain. *International Journal of Damage Mechanics*. Available at: http://ijd.sagepub.com/cgi/doi/10.1177/1056789514522504 [Accessed February 25, 2014].

Lyon, R.H., 2000. *Designing for Product Sound Quality*, New York: Marcel Dekker, Inc.

Maguire, J.A., Dunning, E. & Pearton, R.E., 1996. *The Sports Process: A Comparitive and Developmental Approach*, Human Kinetics Publishers.

Marinho, D. a et al., 2011. Three-dimensional CFD analysis of the hand and forearm in swimming. *Journal of applied biomechanics*, 27(1), pp.74–80. Available at: http://www.ncbi.nlm.nih.gov/pubmed/21451185.

Marklund, P.-O. & Nilsson, L., 2003. Optimization of airbag inflation parameters for the minimization of out of position occupant injury. *Computational Mechanics*, 31(6), pp.496–504. Available at: http://www.springerlink.com/Index/10.1007/s00466-003-0457-9 [Accessed September 18, 2011].

Marklund, P.-O. & Nilsson, L., 2002. Simulation of airbag inflation processes using a coupled fluid structure approach. *Computational Mechanics*, 29(4-5), pp.289–297. Available at: http://www.springerlink.com/openurl.asp?genre=article&id=doi:10.1007/s00466-002-0341-z [Accessed August 12, 2011].

Mather, G., 2009. *Foundations of Sensation and Perception* 2nd ed., New York: Psychology Press.

McCartney, J., Hinds, B.K. & Kelly, D., 2005. Modelling of anisotropic performance fabrics. *Journal of Materials Processing Technology*, 159(2), pp.181–190. Available at: http://linkinghub.elsevier.com/retrieve/pii/S0924013604007940 [Accessed May 15, 2013].

Mehl, J.B., 1982. Acoustic Resonance Frequencies of Deformed Spherical Resonators. *Acoustical Society of America*, 71(May), pp.1–5.

Mettler Toledo, 2005. sTAr Thermal Analysis System, operating instructions to the DMA?SDTA861e module.

Michaeli, W. et al., 2009. Analysis of the Impact Properties of Structural Foams. *Journal of Cellular Plastics*, 45(4), pp.321–351. Available at: http://cel.sagepub.com/cgi/doi/10.1177/0021955X09103945 [Accessed March 1, 2014].

Minetti, A.E., Machtsiras, G. & Masters, J.C., 2009. The optimum finger spacing in human swimming. *Journal of biomechanics*, 42(13), pp.2188–90. Available at: http://www.ncbi.nlm.nih.gov/pubmed/19651409 [Accessed March 15, 2013].

Morris, D., 1981. *The Soccer Tribe*, London: Jonathan Cape Ltd.

Mullins, L. & Tobin, N.R., 1947. Theoretical Model for the Elastic Behavior of Filler-Reinforced Vulcanized Rubbers. *Rubber Chemistry and Technology*, 30, pp.551–571.

Murray, B., 1994. *Football: a history of the world game*, Aldershot: Scholar Press.

NAFEMS, 1992. *A Finite Element Primer*, Glasgow: NAFEMS.

Neilson, P.J., 2003. The Dynamic Testing of Soccer Balls. *Mechanical and Manufacturing Engineering*, Doctor of , p.180.

Nike, 2010. Total 90 Tracer Ball Designed for Superior Performance. *Press Release*. Available at: http://nikeinc.com/t90/news/built-to-be-the-worlds-top-performing-football [Accessed August 15, 1BC].

Nunome, H. et al., 2002. Three-dimensional kinetic analysis of side-foot and instep soccer kicks. *Medicine & Science in Sports & Exercise*, 34(12), pp.2028–2036.

Ogden, R.W., 1972. Large Deformation Isotropic Elasticity - On the Correlation of Theory and Experiment for Incompressible Rubberlike Solids. *Proceedings of the Royal Society A: Mathematical, Physical and Engineering Sciences*, 326(1567), pp.565–584. Available at: http://rspa.royalsocietypublishing.org/cgi/doi/10.1098/rspa.1972.0026 [Accessed February 24, 2014].

Orejan, J., 2011. *Football/Soccer: History and Tactics*, Jefferson, North Carolina: McFarland & Company, Inc., Publishers.

Passmore, M. et al., 2011. The aerodynamic performance of a range of FIFA-approved footballs. *Proceedings of the Institution of Mechanical Engineers, Part P: Journal of Sports Engineering and Technology*. Available at: http://pip.sagepub.com/lookup/doi/10.1177/1754337111415768 [Accessed December 16, 2011].

Passmore, M.A. et al., 2008. Experimental studies of the aerodynamics of spinning and stationary footballs. *Proceedings of the Institution of Mechanical Engineers, Part C: Journal of Mechanical Engineering Science*, 222(2), pp.195–205.

PhaseVision, 2011. Phase Vision: Technology. Available at: www.phasevision.com/technology [Accessed November 14, 1BC].

Price, D.S. et al., 2008. Viscoelasticity of multi-layer textile reinforced polymer composites used in soccer balls. *Journal of Materials Science*, 43(8), pp.2833–2843.

Price, D.S., Harland, A. & Jones, R., 2005. *Advanced Modelling of Soccer Balls*. Loughborough: Loughborough University.

Price, D.S., Jones, R. & Harland, A.R., 2006. Soccer ball anisotropy modelling. *Materials Science and Engineering: A*, 420(1-2), pp.100–108. Available at: http://www.sciencedirect.com/science/article/B6TXD-4JHMY3C-5/2/a0b24d97d268d667fa6c3c25d41172ed.

Pytel, A. & Kiusalaas, J., 2003. *Mechanics of Materials*, Pacific Crove, California: Thomson Brooks/Cole.

Rezaei, A. et al., 2011. Finite element modelling and experimental study of oblique soccer ball bounce. *Journal of sports sciences*, 29(11), pp.1201–13. Available at: http://www.ncbi.nlm.nih.gov/pubmed/21777166 [Accessed November 24, 2011].

Roberts, J. et al., 2001. Human perceptions of sports equipment under playing conditions. *Journal of Sport Sciences*, 19(7), pp.485–497.

Roberts, J.R. et al., 2005. Evaluation of impact sound on the feel of a golf shot. *Journal of Sound and Vibration*, 287(4-5), pp.651–666. Available at: http://www.sciencedirect.com/science/article/B6WM3-4FCRFFS-2/2/307e13f9bc6a935db24b90e09b607b8f.

Roberts, J.R. et al., 2005. Evaluation of vibrotactile sensations in the “feel” of a golf shot. *Journal of Sound and Vibration*, 285(1-2), pp.303–319. Available at: http://linkinghub.elsevier.com/retrieve/pii/S0022460X04007151 [Accessed March 25, 2012].

Roberts, J.R., Jones, R. & Rothberg, S.J., 2001. Measurement of contact time in short duration sports ball impacts: an experimental method and correlation with the perceptions of elite golfers. *Sports Engineering*, 4, pp.191–203.

Rogers, D., 2011. *A Study of the Relationship Between Surface Features and the In-Flight Performance of Footballs*. Loughborough University.

Ronkainen, J. & Harland, A., 2007. Soccer ball modal analysis using a scanning laser doppler vibrometer (SLDV). *Sports Engineering*, 11(1), pp.49–54.

Russell, D. a., 2010. Basketballs as spherical acoustic cavities. *American Journal of Physics*, 78(6), p.549. Available at: http://link.aip.org/link/AJPIAS/v78/i6/p549/s1&Agg=doi [Accessed August 25, 2011].

Di Salvo, V. et al., 2006. Validation of a new performance analysis system in Football. *International Journal of Performance Analysis in Sport*, 6(1), pp.108–119.

Schneider, K. & Zernicke, R.F., 1988. Computer Simulation of Head Impact : Estimation of Head-Injury Risk During Soccer Heading. *International Journal of Sport Biomechanics*, 4, pp.358–371.

Serban, D.A. et al., 2012. Viscoelastic Properties of Semi-Crystalline Thermoplastic Polymers: Dynamic Analysis and Creep. *Solid State Phenomena*, 188, pp.211–218. Available at: http://www.scientific.net/SSP.188.211 [Accessed May 14, 2013].

Shim, V.P.W. et al., 2004. A visco-hyperelastic constitutive model to characterize both tensile and compressive behavior of rubber. *Journal of Applied Polymer Science*, 92(1), pp.523–531. Available at: http://dx.doi.org/10.1002/app.20029.

Shinkai, H. et al., 2009. *Ball Impact Dynamics of Instep Soccer Kicking*, Medicine & Science in Sports & Exercise April 2009;41(4):889-897.

Shinkai, H. et al., 2007. Ball-foot interaction in impact phase of instep in soccer kick. *Journal of Sport Science and Medicine*, Suppl. 10, p.26.

Shishido, H., Doi, S. & Okimura, Y., 2004. Ball for ball game.

Simulia, 2012. Abaqus Keywords Reference Manual.

Simulia, 2011a. *Abaqus Technology Brief Simulation of Airbag Deployment Using the Coupled Eulerian-Lagrangian Method in Abaqus / Explicit*,

Simulia, 2011b. *Isight 5.6 User's Guide* 5.7 ed., Paris: Dassault Systems.

Sinz, W. & Hermann, S., 2008. The development of a 3D-Navier–Stokes code for the simulation of an airbag inflation. *Simulation Modelling Practice and Theory*, 16(8), pp.885–899. Available at: http://linkinghub.elsevier.com/retrieve/pii/S1569190X08000609 [Accessed August 12, 2011].

Smith, L. V & Duris, J.G., 2009. Progress and challenges in numerically modelling solid sports balls with application to softballs. *Journal of Sports Sciences*, 27(4), pp.353–360. Available at: http://www.informaworld.com/10.1080/02640410802641392.

Sondergaard, R., Chaney, K. & Brennen, C.E., 1990. Measurements of Solid Spheres Bouncing Off Flat Plates. *Journal of Applied Mechanics*, 112(3), pp.694–699.

Stronge, W.J. & Ashcroft, A.D.C., 2007. Oblique impact of inflated balls at large deflections. *International Journal of Impact Engineering*, 34(6), pp.1003–1019. Available at: <Go to ISI>://000244631700001.

Tanaka, K. et al., 2012. Construction of a finite element model for collisions of a golf ball with a club during swing. *Proceedings of the Institution of Mechanical Engineers, Part P: Journal of Sports Engineering and Technology*. Available at: http://pip.sagepub.com/lookup/doi/10.1177/1754337112442619 [Accessed May 25, 2012].

TexGen, 2013. TexGen. Available at: http://texgen.sourceforge.net/index.php/Main_Page.

TheFA.com, 2010. Favouring football's human side. , (19MAY10).

Tsaousidis, N. & Zatsiorsky, V., 1996. Two types of ball-effector interaction and their relative contribution to soccer kicking. *Human Movement Science*, 15(6), pp.861–876. Available at: http://linkinghub.elsevier.com/retrieve/pii/S0167945796000279.

Tuplin, S. et al., 2012. The application of simulation to the understanding of football flight. *Proceedings of the Institution of Mechanical Engineers, Part P: Journal of Sports Engineering and Technology*. Available at: http://pip.sagepub.com/lookup/doi/10.1177/1754337112444402 [Accessed May 25, 2012].

Udeshi, A., 2010. Advanced Characterisation of Sports Balls.

Wade, S., 2012. Table Tennis Doping: Pingpong's Version of "Doping" Has Different Twist. *Huffington Post*. Available at: http://www.huffingtonpost.com/2012/08/04/table-tennis-doping-olympics_n_1741894.html.

Walker, P.J. et al., 2010. Design of a force acquisition system for high-energy short-duration impacts. *Proceedings of the Institution of Mechanical Engineers, Part P: Journal of Sports Engineering and Technology*, 224(2), pp.129–139. Available at: http://dx.doi.org/10.1243/17543371JSET65.

Wei, W. & Xingwen, D., 2009. The Analytical Model of Shear Properties of the Pre-impregnated Woven Fabric Composite. *Journal of Elastomers and Plastics*, 41(2), pp.105–117. Available at: http://jep.sagepub.com/cgi/doi/10.1177/0095244308088877 [Accessed April 20, 2014].

Wesson, J., 2002. *The Science of Soccer*, London: Taylor and Francis.

Wiart, N. et al., 2011. Effect of temperature on the dynamic properties of soccer balls. *Proceedings of the Institution of Mechanical Engineers, Part P: Journal of Sports Engineering and Technology*, 225(4), pp.189–198. Available at: http://pip.sagepub.com/lookup/doi/10.1177/1754337111411644 [Accessed April 19, 2013].

Wilson, J., 2008. *Inverting the Pyramid*, London: Orion Books Ltd.

Yeoh, O.H., 1993. Some forms of the strain energy function for rubber. *Rubber Chemistry and TEchnology*, 66(5), pp.754–771.

Zouari, R., Amar, S.B. & Dogui, A., 2008. Experimental and numerical analyses of fabric off-axes tensile test. *Journal of the Textile Institute*, 101(1), pp.58–68. Available at: http://www.informaworld.com/10.1080/00405000802231341.